ON THE COMPARISON OF COMPUTATIONAL METHODS FOR ANALYZING LONGITUDINALLY SKEWED STEEL I-GIRDER BRIDGES

by

Christopher Jason Stull

B.S., Purdue University, 2004

Submitted to the Graduate Faculty of

School of Engineering in partial fulfillment

of the requirements for the degree of

Master of Science

University of Pittsburgh

2006

UNIVERSITY OF PITTSBURGH

SCHOOL OF ENGINEERING

This thesis was presented

by

Christopher Jason Stull

It was defended on

June 30th, 2006

and approved by

Dr. J.S. Lin, Associate Professor, Civil and Environmental Engineering

Dr. K.A Harries, Assistant Professor, Civil and Environmental Engineering

Thesis Advisor: Dr. C.J. Earls, Associate Professor, Civil and Environmental Engineering

ON THE COMPARISON OF COMPUTATIONAL METHODS FOR ANALYZING LONGITUDINALLY SKEWED STEEL I-GIRDER BRIDGES

Christopher Jason Stull, M.S.

University of Pittsburgh, 2006

With the myriad of commercially available finite element analysis (FEA) software packages in industry, solutions to relatively complex problems have become more readily attainable for the engineer; making way for the realization of many of the innovative structures seen throughout today's infrastructure. While it may be assumed that most commercially available FEA software packages will arrive at an accurate solution for a given, well posed linear-elastic small displacement problem, an assumption which cannot be made is that the user of the software will always construct an appropriate model for the given analysis context. That being said, concern has been expressed with regard to the applicability and accuracy of a more simplistic grillage analysis technique (current industry standard) when compared with a full three-dimensional shell finite element analysis. Employing the aforementioned modeling approaches to a longitudinally skewed, steel I-girder bridge, analyses of these models are carried out using the commercially available FEA software package, ADINA. Comparisons are then made between the modeling approaches; the results of which follow in this thesis.

TABLE OF CONTENTS

LIST OF TABLES

LIST OF FIGURES

ACKNOWLEDGEMENTS

First of all, I would like to thank my wife, Carol; without her, I would never have begun my graduate career. Her support has been unwavering throughout, and I can't thank her enough for that. I must thank my parents who instilled in me the value of education and gave me the tools to further my life with it. To my advisor, Dr. Earls: I have yet to regret my decision to attend Pitt, and I am honored to be continuing as your Ph.D. student at Cornell. Thanks are also extended to Tom Howell, my office mate for the better part of a year; he is far more of a resource than he will ever admit. Finally, I would like to thank my friends, family, and professors. Clearly, I could not have accomplished all that I have in my life without your help. Thank you all.

1.0 INTRODUCTION

The question of which modeling technique is appropriate for a given structure is typically answered by first considering the objectives of the analysis (e.g. is the salient behavior in question more global or local in nature, etc.?). Understanding that irregularities in the global behavior of a structure lead one to investigate the behavior in a more localized fashion, the initial question is all but answered; the desired modeling technique must accurately predict both global *and* local behaviors with sufficient accuracy in order to carry out the design.

While this conclusion is intuitive, it is the discovery and implementation of this multi-scale analysis paradigm which poses a challenge to the engineer. Two critical (and often competing) interests within the framework of the multi-scale analysis are: a desired level of accuracy in results and the time-efficiency of the analysis. As it is that solution accuracy and time-efficiency are often competing interests, the decision on which desired aspect receives more consideration is a direct function of the economy behind the project, as well as the requirements of the project's owner(s). The willingness of said owner(s) to accept certain inefficiencies in the design in order to retain capital determines the final solution to the problem of choosing a modeling technique.

That being said, it is still often cost effective for the engineer to simplify the modeling approach employed in order to estimate the structural response of the components within the structure. It is frequently assumed that the application of a simplified analysis methodology,

within well understood bounds, will lead to a conservative design; understanding when such an assumption does not apply, however, is of paramount importance to the engineer. In other words, the analysis methodology may be well understood and known as conservative within a certain analysis context. However, once a structural system is assembled from combinations of simplified models, global behavior may arise that is inconsistent with the assumptions made during the simplification occurring in each seemingly conservative model. The net result of this misapprehension may be an un-conservative strength prediction. Another concern comes from the "comfort" associated with a conservative design; "a conservative design is a safe design," but this thought-process leads to both an inefficient use of material and it hampers innovation in the industry. Albert Einstein said it best when he noted "things should be made as simple as possible, but no simpler."

These simplified approaches can take on a variety of forms: the discretization of slabs (or plates) into an assembly of beams (see Section 1.1), the smoothing of geometric irregularities within the design (non-prismatic members being approximated as prismatic sections), the idealization of boundary conditions, etc. The question of how far the engineer can take a given simplification is a question which is frequently asked but rarely answered; as such an answer would require the construction of a more complex (and subsequently more accurate) model. This, however, defeats the purpose of simplifying the model in the first place. In the following work, one such simplification (the grillage analysis technique) is tested to its limit and then compared against two more refined finite element models; at issue is the response of longitudinally skewed, steel I-girder bridges.

1.1 GRILLAGE ANALYSIS

Grillage analysis refers to a modeling technique, typically employed in the analysis of concrete slabs, whereby the slab is reduced to an equivalent skeleton or "grillage" of representative beam members. Composing this assembly are both longitudinal and transverse grillage members, each of which represents the stiffness of the concrete slab in its component direction. In spite of ever increasing computational power over the past decade (leading to an expanded implementation of the finite element method of analysis), the grillage analysis technique remains popular with designers as a tool for the approximation of the slab behavior for a number of configurations [Hambly, 1991; O'Brien and Keogh, 1999].

1.1.1 Guidelines for usage

While the application of the grillage analysis technique lends itself to interpretation with regard to both the mesh density and constitutive properties of longitudinal and transverse members, general recommendations for its usage can be found in the literature. Those which are most applicable to the scope of this work in this thesis are described below.

The frequency of longitudinal grillage members is essentially governed by the width of the slab; for a relatively narrow slab, a single member would sufficiently represent the one-way response of the slab in its entirety. Conversely, a wide slab would require the use of multiple longitudinal members with the suggestion that these members not be placed closer than 2 to 3 times the slab thickness (doing so complicates the model with an insignificant gain in accuracy) [Hambly, 1991]. With respect to these members' section properties, the moment of inertia, I, and the torsional constant, J, are computed by way of Equations (1.1) and (1.2), respectively:

$$I = \frac{bd^3}{12} \tag{1.1}$$

$$J = \frac{bd^3}{6}, \tag{1.2}$$

where b is the tributary width of slab represented by the grillage member and d is the depth of the slab. Note that these equations take into account the concrete cross-section only and should be adjusted as necessary to account for the inclusion of reinforcing steel in the design (e.g. apply transformed section properties, etc).

The subsequent grillage mesh should be proportioned such that the appropriate transverse grillage members closely represent the spacing of the longitudinal grillage members; this insures the proper *global* distribution of the applied loading through the slab. That being said, however, a significantly relaxed guideline of 1 to 3 times the longitudinal grillage member spacing also exists based on the fact that the transverse grillage members will often carry a lesser bending moment than their longitudinal counterparts [O'Brien and Keogh, 1999]. It is further recommended that transverse grillage members are oriented at right angles with respect to the longitudinal members; an exception to this is found in the case of longitudinally skewed slab configurations where the transverse stiffness of the slab follows the skew angle [Hambly, 1991]. Section properties are again calculated as per Equations (1.1) and (1.2), keeping in mind that alterations should be made for anisotropic slab configurations.

With regard to the boundary conditions of grillage models, it is important to note that the location of longitudinal members should closely align with the support locations of the actual slab being modeled [O'Brien and Keogh, 1999]. Additional economic benefits of the grillage analysis technique are realized when analyzing a longitudinally skewed slab configuration where it has been shown that simply supported slabs with skew angles of less than 20° can be modeled

with right angle support conditions [Hambly, 1991]. In other words, a mildly skewed slab may be modeled as a square slab without a significant loss in accuracy. It should be noted that this does not apply to a slab which is continuous at an intermediate support region.

A noteworthy exception to these guidelines follows from the treatment of concentrated loads (which can take the form of either applied loads or reactions from the imposed boundary conditions), where it is intuitively recommended that a finer grillage mesh is employed at, and near, these regions. The rationale behind this recommendation follows from the fact that typical concentrated loads are actually distributed over an area of the slab; increasing the mesh density at these locations therefore allows for a more representative load application (see Figure 1.1).

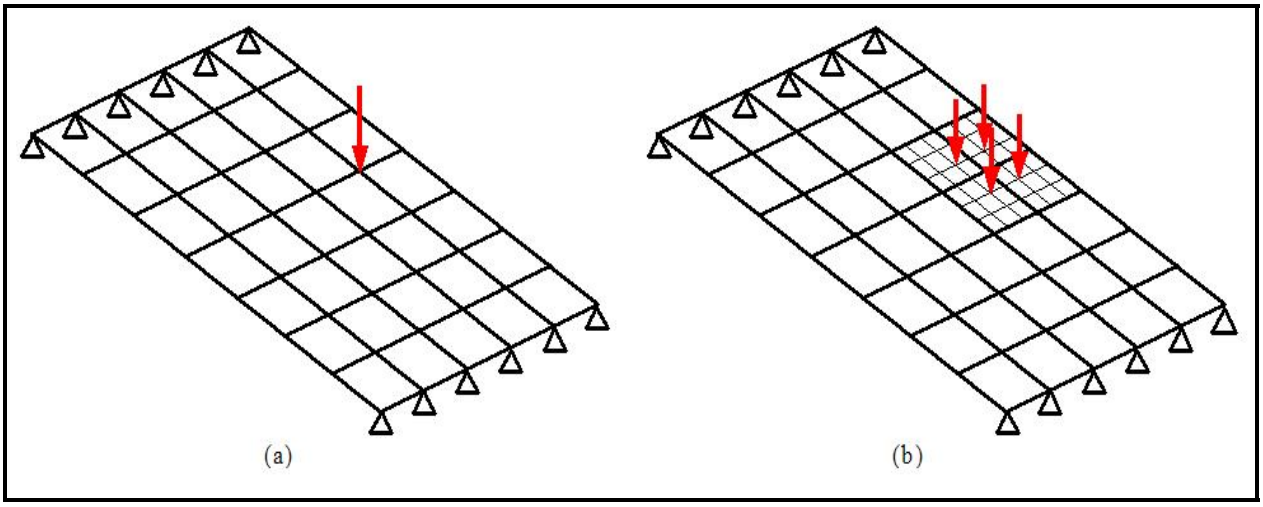

Figure 1.1 Typical grillage meshes: (a) coarse mesh; (b) incorporation of localized fine mesh.

While following these guidelines may result in a reasonable representation of the concrete slab in question, it is important to understand that this technique provides only an *approximation* to the actual slab behavior. The availability of continuum (commonly referred to as an 8-node "brick"), plate, and shell finite element formulations provides for more accurate

results. However, the time required for the *proper* construction of models using these more sophisticated finite elements is greater; as well as the computational demand required for analysis. Recognizing these dramatic increases in demand, the application of the grillage analysis technique to steel I-girder bridges is sometimes viewed as an advantageous option in practice; versus the complications of developing a three-dimensional shell finite element model.

1.1.2 Application to steel I-girder bridges

As stated above, the application of a grillage analysis to concrete slab applications does leave some room for interpretation; however, its application to steel I-girder bridges is even more vague; which leads to a situation where a "reliable method" quickly becomes unreliable due to a lack of discipline in its use. Generally, longitudinal grillage members should be coincident with the location of longitudinal girders in the actual bridge. Section properties for these members should be computed about the centroid of a transformed section which is accomplished through the transformation of concrete into steel or vice versa by way of the applicable modular ratio, n:

$$n = \frac{E_c}{E_s} \text{ ; for converting concrete into steel} \tag{1.3}$$

$$n = \frac{E_s}{E_c} \text{ ; for converting steel into concrete (less common)} \tag{1.4}$$

By applying this technique of transformed sections, it must be recognized that the concrete component is assumed to act *elastically* which means that the concrete must be neglected within an appropriate region adjacent to supports (the bounds of this region of course shift with moving loads on the bridge). Furthermore, the incorrect application of the effective slab width can lead to additional errors in the model by over- or underestimating the equivalent stiffness of the member in question [Kostem, 1986].

As with the longitudinal members, transverse grillage members should be placed coincident with the locations of the diaphragms and / or cross-frames. An effective slab width is then computed as $b_w + 0.3s$, where b_w is the width of the diaphragm and s is the transverse spacing of the longitudinal girders [Hambly, 1991]. Section properties, while taking into account both the diaphragm and the concrete slab above, are based upon the addition of each component acting about it's own centroid; in other words, $I_{total} = I_{diaphragm} + I_{slab}$ (i.e. composite action is assumed not to apply in the transverse members).

Between these primary members, "secondary" members which represent the transverse stiffness component of only the concrete slab may be included by applying the aforementioned guideline of 1 to 3 times the spacing of the longitudinal members. This guideline could of course result in the secondary members either having a considerable spacing (relative to the span length) or being completely eliminated due to the location of the primary members. It is stated however, that the spacing indicated by this guideline may be exceeded "without significant loss of accuracy" [O'Brien and Keogh, 1999]; the implications of this statement are examined in the following work.

A final recommendation as to the application of grillage analysis to steel I-girder bridges comes from the treatment of loads on the structure. While the use of tributary areas for load application does result in the correct *statical* distribution of loads when considering only longitudinal girders, it is easily seen that this methodology is incorrect from the perspective of localized structural response; as the presence of a concrete slab would also impose a couple at the girder-slab intersection. Figure 1.2 illustrates a solution to this problem which involves the inclusion of "auxiliary" longitudinal members positioned between the primary longitudinal

members; the section properties of the primary longitudinal members are then adjusted appropriately [Hambly, 1991].

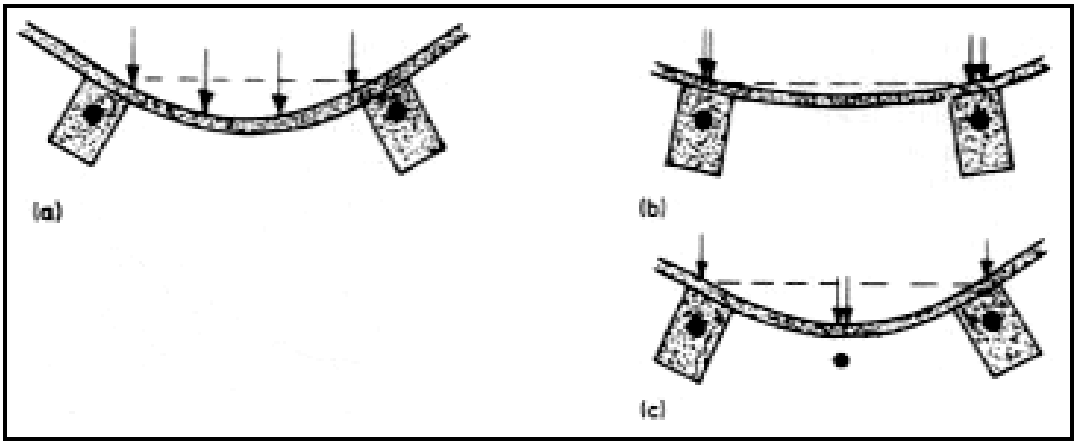

Figure 1.2 Errors due to statical distributions of loading: (a) loading; (b) erroneous statical redistribution; (c) improved statical redistribution with auxiliary member [Hambly, 1991].

The grillage analysis technique, though providing a reasonably accurate solution to a wide range of problems involving concrete slabs, has been shown here to involve a fair bit of engineering judgment on the part of the analyst in order to properly capture "real-world" response. Unfortunately, this type of situation may lead to an inaccuracy in the solution arising out of a misinterpretation of key structural characteristics and errors in engineering judgment. Examining the common practice of idealizing a steel I-girder bridge structure as an assembly of beam finite elements (similar in nature to grillage analysis technique as discussed previously) will provide some information as to the limits of such a simplification.

1.2 LITERATURE REVIEW

As previously mentioned, the grillage analysis technique has proven to be an effective technique for the approximation of slab behavior. However, the focus of the current work involves the applicability of this method to longitudinally skewed, steel I-girder bridges. In order to contextualize the current work, previous related work from the literature is discussed below.

The first such work reported on the results from grillage models of two simple span bridges. Each of these bridges consisted of eight pre-stressed concrete I-girders with a constant transverse spacing of 6'-0"; this resulted in a total bridge width of 44'-6". The specified thickness of the reinforced concrete slab was 7.5 inches. The only differences between the bridges was with respect to their span lengths (50'-0" for "Bridge 1" versus 78'-0" for "Bridge 2") which resulted in differing sizes of the pre-stressed concrete I-girders employed: PennDOT 20/33 and PennDOT 24/48, respectively [Kostem, 1986]. It should be noted that the concluding remarks in this work generalized the results into those pertaining to "short" spans and those pertaining to "medium-to-long" span bridges. However, beyond the short span designation being associated with approach spans, physical dimensions of these categorical descriptions were not explicitly stated in the referenced work.

With respect to the loaded girders only, it was found that the mid-span moments and deflections fell within 15% of a "detailed finite element analysis," erring on the conservative side [Kostem, 1986]. This result, however, only applies to medium-to-long span bridges with short spans producing conservative values within 5%. Structural reactions for the loaded girders were reported as being underestimated by 10% (these results were not categorized with regard to the span length). This particular result was surprising given that the load distribution mechanism in a grillage model is expected to be less effective when compared with a more refined finite

element model (which explicitly includes a model of the concrete deck). It is therefore expected that the reactions in a grillage model would be higher in the loaded girders and subsequently lower in the unloaded girders.

A description of the aforementioned "detailed finite element analysis" was not included in the referenced work; however, it is assumed by way of examining the included references that such a finite element analysis may have employed "plate bending elements with membrane stiffness properties" to model both the pre-stressed concrete beams as well as the concrete deck.

A later work by the same author included a parametric study of the structural response parameters from grillage models of six steel I-girder bridges [Kostem and Ragazzo, 1993]. Each of these bridges consisted of five girders with a transverse spacing of 8'-8" resulting in a 44'-0" total bridge width. In this case, the reinforced concrete deck was specified as 8 inches thick. Again, the bridges differed in span lengths and subsequently in girder designations. The first three bridges employed "rolled girders with cover plates" with span lengths of 50'-0", 70'-0" and 90'-0" with the remaining three bridges employing "welded plate girders" with span lengths of 90'-0", 140'-0", and 170'-0" [Kostem and Ragazzo, 1993]. As was the case in the previous work, results were generalized into span length designations; however, there is more guidance provided in this case: "short-to-medium" span bridges consisted of 50 to 90 foot spans lengths with "long" span bridges defined as 140 feet in length.

With regard to the mid-span moments, a reverse trend is found (as compared with the previously reported results [Kostem, 1986]), where the average error for short-to-medium span bridges is 10%; while that associated with long span bridges is termed as "acceptable" [Kostem and Ragazzo, 1993]; whether these results are conservative or non-conservative was not indicated. This trend, however, is again reversed when considering *maximum* moments and

deflections. In the case of the maximum moments, the performance of the grillage analysis improves with decreasing span length; while in the case of the maximum deflections, an *underestimation* of the true response is reported. As before, the finite element model to which the above grillage analysis results are compared is not explicitly described in the work; it is only reported as being "meticulously modeled by finite element tools" [Kostem and Ragazzo, 1993].

In a more recent, unrelated work, a general assessment of modeling techniques, as they apply to a curved steel I-girder bridge system, compares the results from a "conventional" grillage model to those from an experimental test of a subject bridge [Chang, et al, 2005]. Upon reviewing the approach taken in constructing this conventional grillage model, it is noted that the guidelines specified in Sub-Sections 1.1.1 and 1.1.2 are closely followed throughout. Salient features of the subject bridge employed in this work follow below.

The subject bridge, a steel curved I-girder configuration, consisted of only three girders with top flanges imbedded in an 8 inch concrete deck; this corresponds to fully composite action between these super-structure components. It is noted that of the three girders, only results from the center and exterior girders, designated as "G2" and "G3," respectively, were reported upon. Radial spacing of these girders was 8'-9" with the center girder having a radius of curvature of 200'-0". Rounding out the description, it is noted that the span length of the center girder was 90'-0", which lies between the generalized span dimensions defined in the previously discussed works.

With regard to results reported, the three parameters discussed in the previous works are again the focal point of this work. Mid-span vertical deflections for G2 and G3 were reported with non-conservative errors of 27% and 39%, respectively; this non-conservative trend continues with a 17% error reported for G2 and a 4% error reported for G3 when considering

maximum longitudinal bending stresses [Chang, et al, 2005]. It is further reported that reactions are actually both conservative (G2) and non-conservative (G3) in nature, with 17% and 3% errors, respectively.

The obvious conclusion from the consideration of these published findings is that there is no discernable general trend between long and short span bridges, with regard to grillage analysis conservatism. Furthermore, the results from the latter two works beg a question: was the finite element model to which the results were compared in the 1986 work identical (in the sense of accuracy measures) to that used in the 1993 work? It seems unlikely that the two models would be identical since significant advances in computational technology would have allowed for a more refined finite element modeling in the latter work. However, even a refined finite element model would not explain a reversal in trends as is seen when comparing the results from the two works. Overall, these results lead to a troubling hypothesis: grillage analysis results may not universally be viewed as being conservative. This hypothesis has enormous and pervasive implications for a design approach predicated on the application of engineering judgment to guarantee conservatism.

1.3 SCOPE OF WORK

It is the intent of the author to provide the reader with information regarding the advantages, disadvantages, and limitations inherent in applying a simplified modeling approach to a bridge (in particular, a longitudinally skewed, steel I-girder bridge). This will be carried out through the examination of the results from two distinct modeling approaches. The first approach, designated as the “grillage finite element” model, employs beam elements to represent the

longitudinal / transverse steel members individually; with the inclusion of the concrete deck being accomplished through the application of transformed / combined section properties. This model is intended to push the limits of applicability of the grillage analysis technique as it applies to steel I-girder bridges.

The second model, called the "shell finite element" model, is constructed with shell elements being placed at the mid-surface of the constituent cross-sectional plate components, and extending along the longitudinal girders. Beam and shell elements, representing the diaphragms, and either continuum elements or shell elements, representing the concrete deck are also employed in this more refined modeling approach.

Considered structural responses include: reactions, vertical deflections, and longitudinal bending stresses (only the longitudinal girders are considered in this work). The examination of vertical deflections and longitudinal bending stresses will be carried out through the comparison of maximum values; as well as profiles taken along the length of the bridge. Through this examination, conclusions will be drawn as to the applicability of the grillage modeling approach.

1.4 THESIS ORGANIZATION

Chapter 2 provides a discussion of the subject bridge chosen for this work, including the reasoning behind the thirteen chosen load cases which are to be applied to the three finite element models. Chapters 3 and 4 examine the modeling strategies employed in this work with Chapter 3 outlining the grillage modeling approach and Chapter 4 outlining each of the two shell finite element modeling approaches employed. A presentation and discussion of the results from the analysis of select load cases follows in Chapter 5. Chapter 6 subsequently completes the

main body of this work by discussing the conclusions drawn from the results analysis. Appendices A through E are reserved for the presentation of the results omitted from the main body of this thesis; in other words, results from the load cases not selected for presentation in Chapter 5. Finally, Appendix F provides sample input files so that the reader may employ and / or improve on; with regard to the modeling strategies discussed in Chapter 4.

2.0 SUBJECT BRIDGE

The subject bridge chosen for this work actually consists of two adjacent steel I-girder bridges serving as overpasses at the intersection of Interstate 70 and Pennsylvania State Route 519 in Washington County, Pennsylvania. Due to similarities between the two structures, a model of only one of these bridges is developed (the northernmost, six-girder bridge). This bridge was selected as a result the author's involvement in another research investigation; the details of which can be found in the references [Stull, et al, 2006]. The development of the shell finite element model of the subject structure, as reported in the current thesis, was a direct aid to this, as well as the other research program. However, inexperience with more sophisticated modeling approaches led to the initial development of the grillage model; as discussed Chapter 3.

2.1 DESCRIPTION

The subject bridge consists of a three-span continuous steel I-girder super-structure with a 30° longitudinally configured skew angle oriented from northwest to southeast (see Figure 2.1); it should be noted that interior piers are parallel to this skew angle as well. The primary components of the super-structure are W24x76 steel I-girders with top flanges imbedded in a 7.5 inch concrete deck. As a result of this embedment, it is assumed that the steel girders and deck

experience fully composite action. The lengths of the three spans are 27 feet, 50 feet, and 27 feet, respectively (later designated as Span 1, Span 2, and Span 3, respectively).

Transverse diaphragms consist of two typical sections: W16x36 and C15x33.9. The various locations of these members are depicted in Figure 2.1.

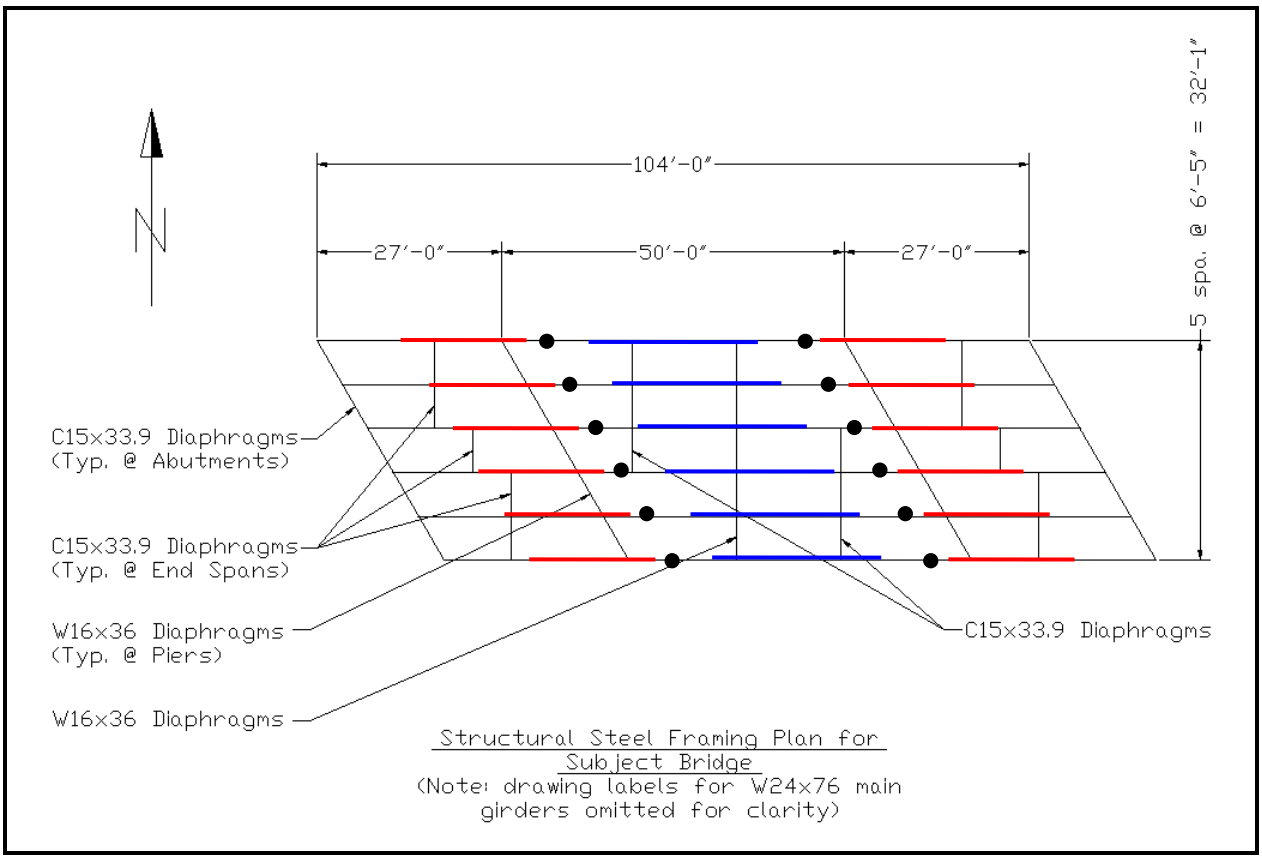

Figure 2.1 Plan view of steel framing plan for the subject bridge.

Other important structural features include the presence three sets of top and bottom flange cover plates located on each longitudinal steel girder; the thicknesses of all cover plates are 0.6875 inches. One set, indicated by the blue lines in Figure 2.1, consists of 26 foot cover plates, positioned over the longitudinal centerline of the bridge. Each of the other two sets, indicated by the red lines in Figure 2.1, consist of 20 foot cover plates, located at a 5 foot outward offset from

each pier (away from the center of the bridge). Finally, each of the six girders also has two splice locations which are offset 7.5 feet inward from each pier (toward the center of the bridge); these are indicated by black circles in Figure 2.1.

Bearing conditions consist of genuine pinned connections at the west end of the bridge, (Abutment 1) and rocker-type bearings at each of the two piers and the east end abutment (Pier 1, Pier 2, and Abutment 2, respectively). Typical concrete abutment details, as well as hammerhead-style concrete piers, describe the exposed components of the sub-structure. As it is the steel super-structure that forms the primary focus of the work discussed herein, these components from the sub-structure are of little significance to the current thesis, and thus will not be discussed further.

Finally, the design drawings provided for the subject bridge are dated in the late 1950's which subsequently governs the following material specifications. ASTM A7 steel (minimum yield strength of 30 kips per square inch (ksi)) is specified for all structural steel, and the *deck* concrete is referred to as "PennDOT Class A" for which the minimum design compressive strength is 3,000 pounds per square inch (psi).

2.2 LOADING CASES

Thirteen loading cases are chosen for consideration within the current work; each of which consists of two (or three) of the following components: concentrated loads from a "design truck" and / or a "design tandem," and uniformly distributed "design lane load." The magnitudes and configurations of each of these components are obtained from the 2004 AASHTO LRFD Bridge Design Specifications (Articles 3.6.1.2.2, 3.6.1.2.3, and 3.6.1.2.4, respectively); the design truck

is employed with a constant 14’-0” axle spacing for each of the applicable loading cases (see Figure 2.2). This stems from the desire to arrange the applied loading such that the mid-span moments and deflections will be maximized in the center span; recall that this span is 50 feet long. Furthermore, it is important to note that the concentrated loads from each axle are applied *at right angles* to the longitudinal members (i.e. axles are not aligned with the skew angle of the bridge).

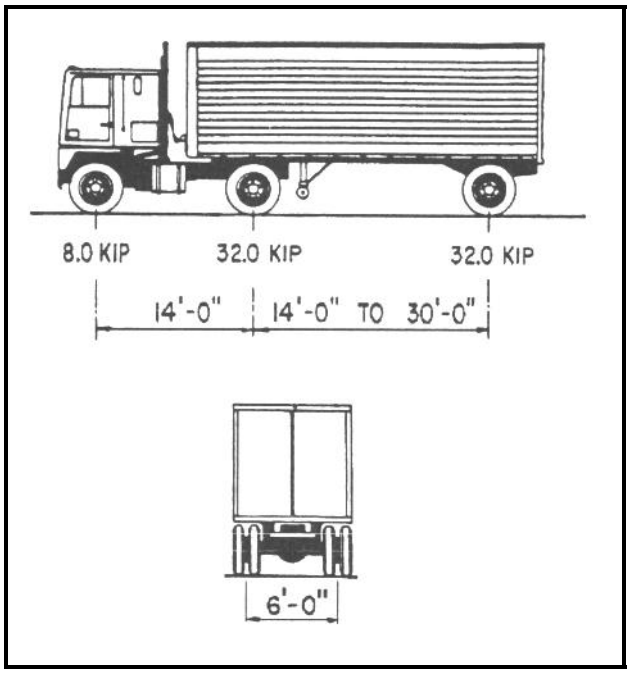

Figure 2.2 Geometric Proportions of the design truck [AASHTO, 2004: Figure 3.6.1.2.2-1].

2.2.1 Loading Cases 1 and 2

Loading Cases 1 and 2 involve the loading of Spans 1 and 2, respectively; per Article 3.6.1.1.1 [AASHTO, 2004], two design lanes were imposed upon the structure for loading cases of this type. Figures 2.3 and 2.4 depict these loading cases; the shaded portion of the deck indicates the aforementioned uniformly distributed lane load (typical for Figures 2.3 through 2.15). Keep in

mind that these figures (and those following in this section) are only representative of the loading cases utilized for this work; adjustments are made for the grillage model, in order to attempt a more representative distribution of the loads (see Sub-Section 3.2.3).

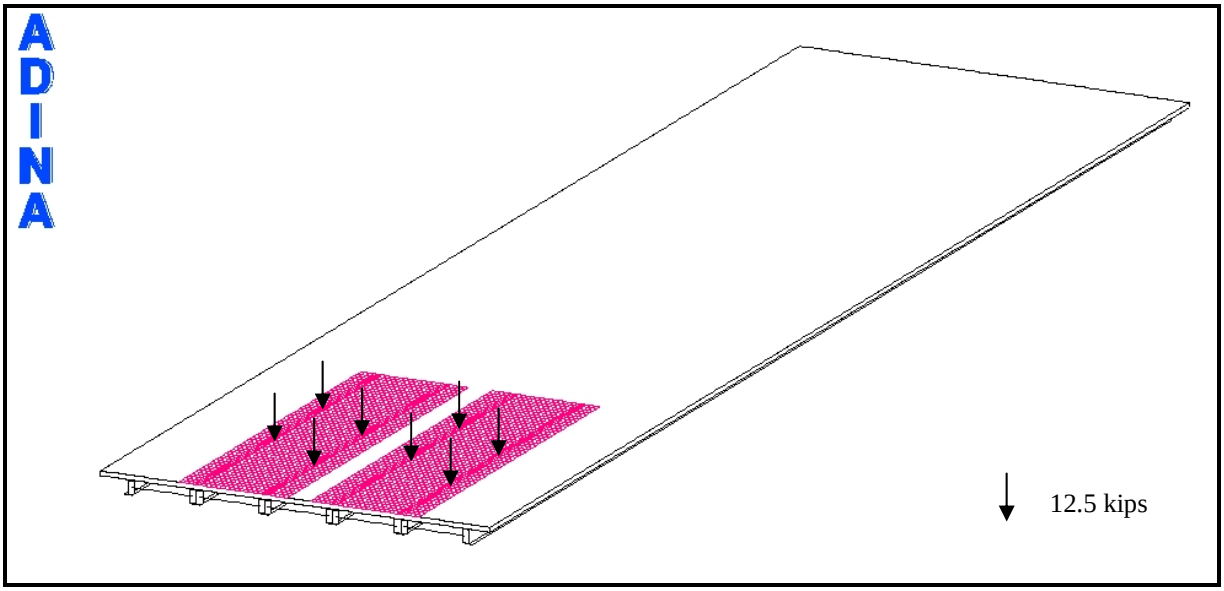

Figure 2.3 Isometric view of Loading Case 1.

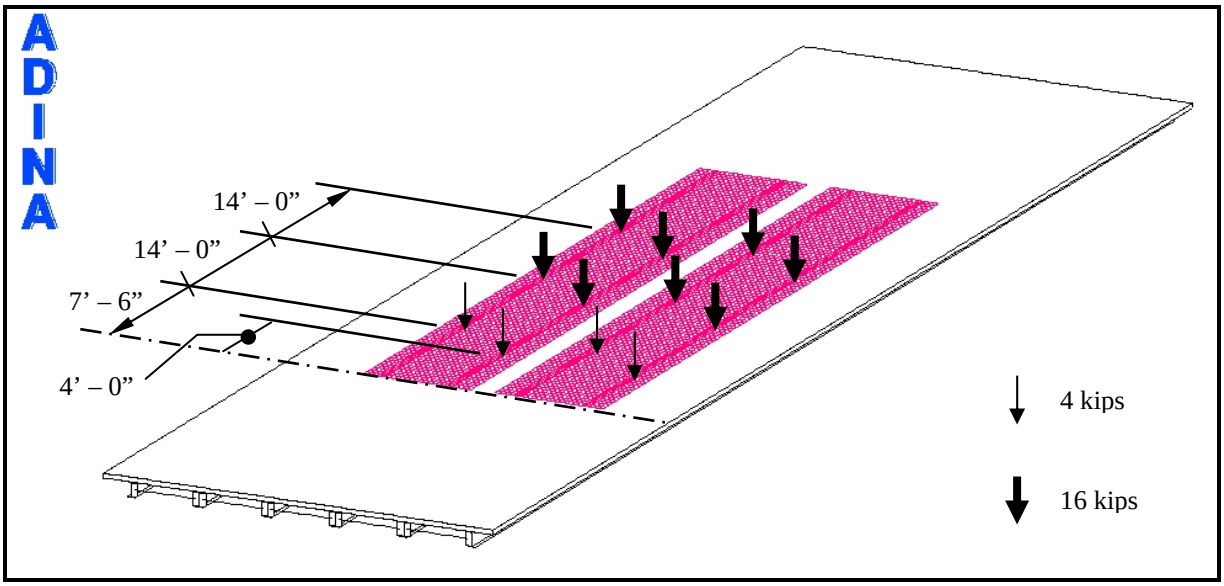

Figure 2.4 Isometric view of Loading Case 2 (dimensions typical for loading cases involving design truck).

2.2.2 Loading Case 12

Loading Case 12 is a combination of Loading Cases 1 and 2 to create a maximum negative moment condition at Pier 1, shown below in Figure 2.5.

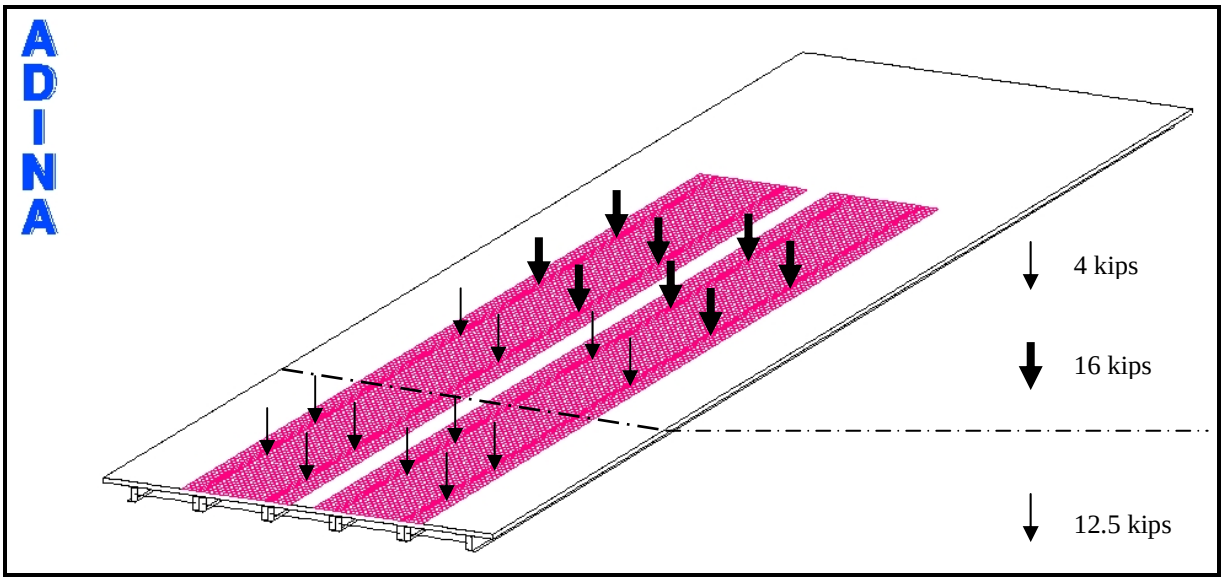

Figure 2.5 Isometric view of Loading Case 12.

2.2.3 Loading Cases 3 though 8

Loading Cases 3 through 8 involve loading the exterior girders individually for each of the three spans; Loading Cases 3 through 5 apply to the northernmost girders, Girders 1 and 2, and Loading Cases 6 through 8 apply to the southernmost girders, Girders 5 and 6. These loading cases were primarily motivated by the aforementioned research program where the behaviors of the exterior girders of the structure are of primary interest.

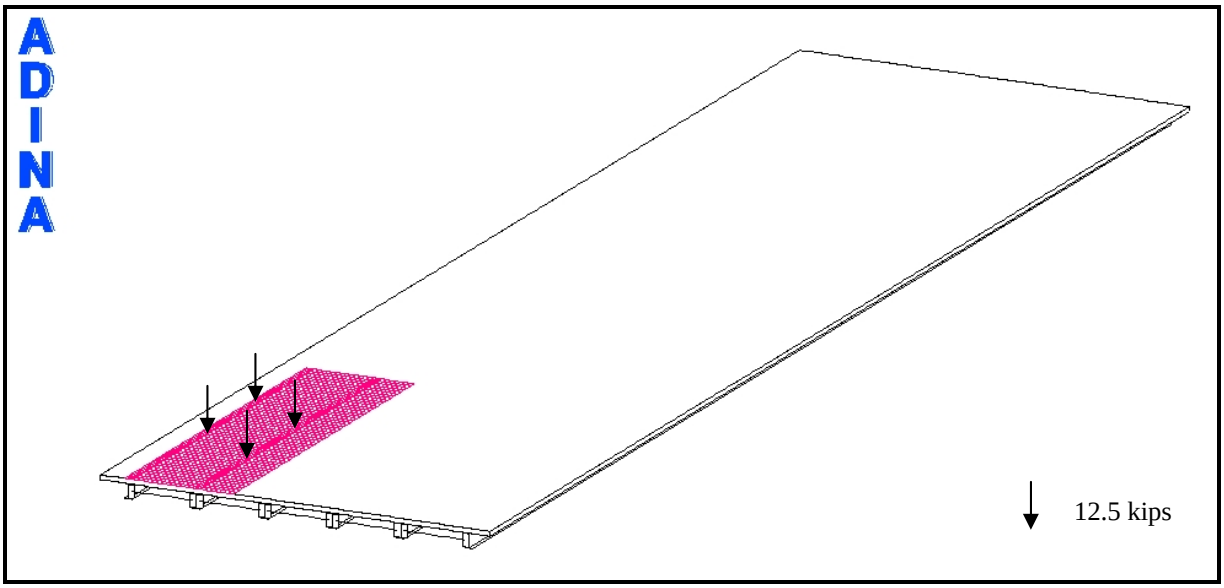

Figure 2.6 Isometric view of Loading Case 3.

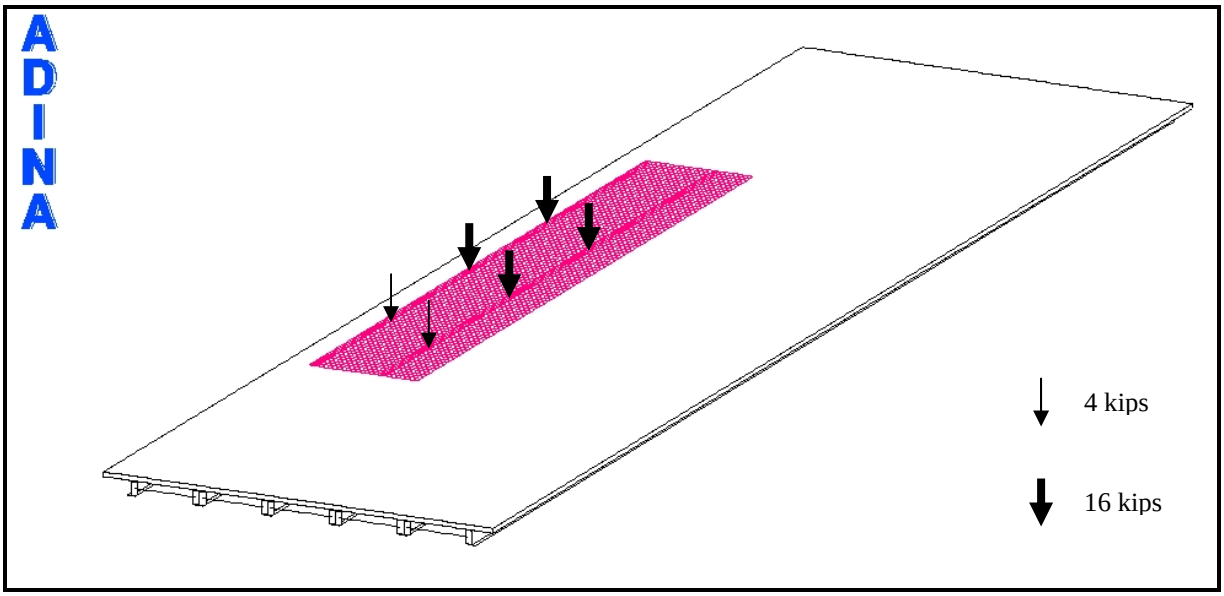

Figure 2.7 Isometric view of Loading Case 4.

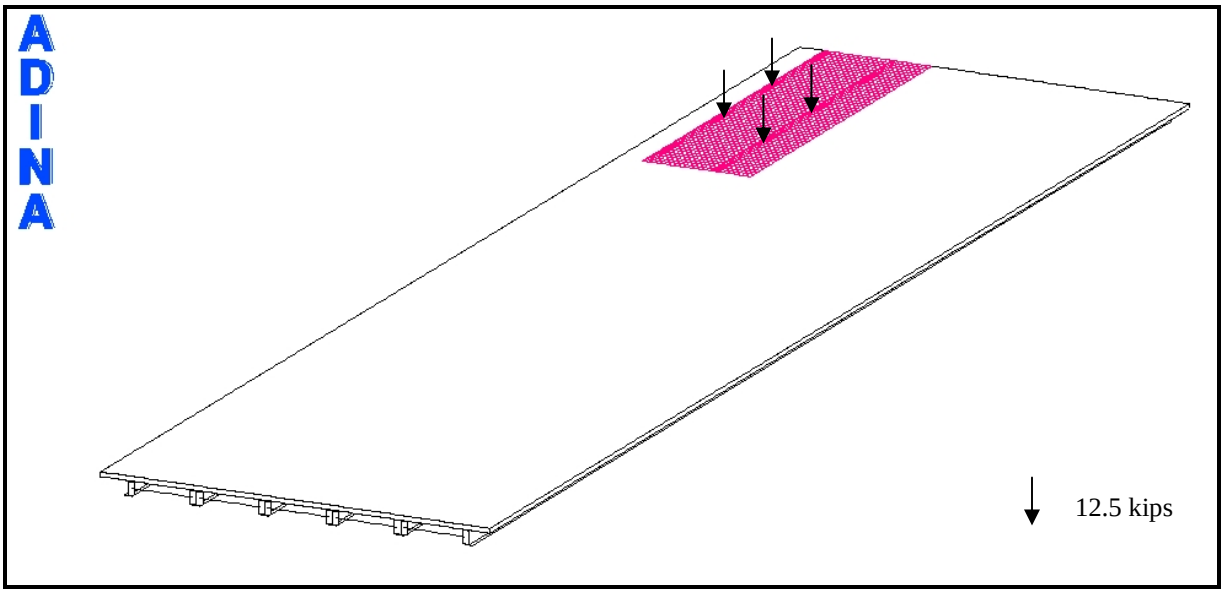

Figure 2.8 Isometric view of Loading Case 5.

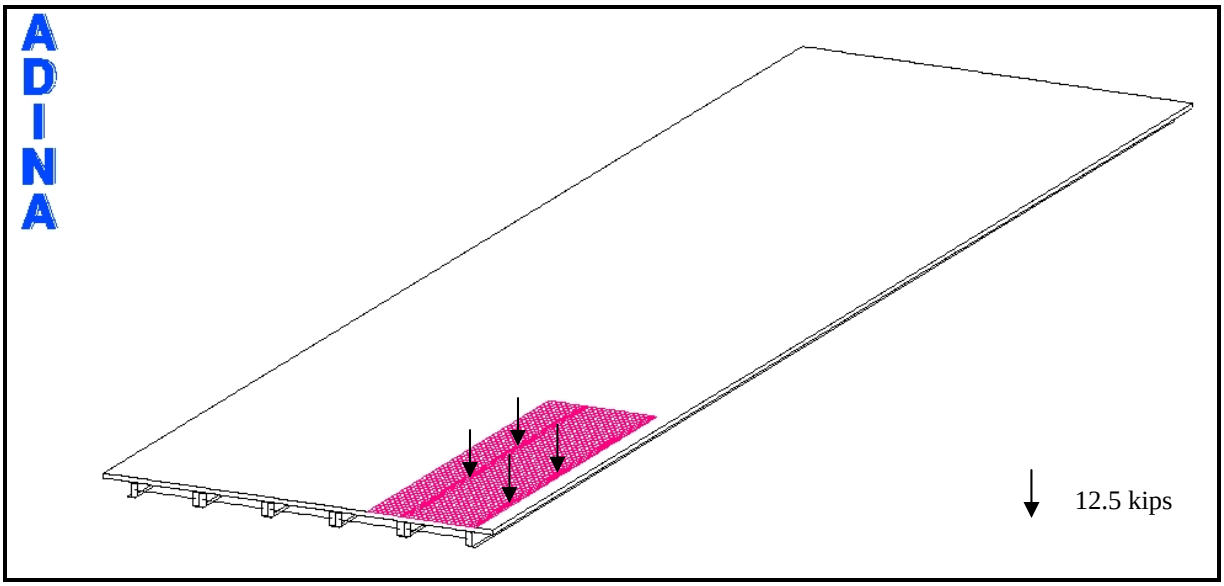

Figure 2.9 Isometric view of Loading Case 6.

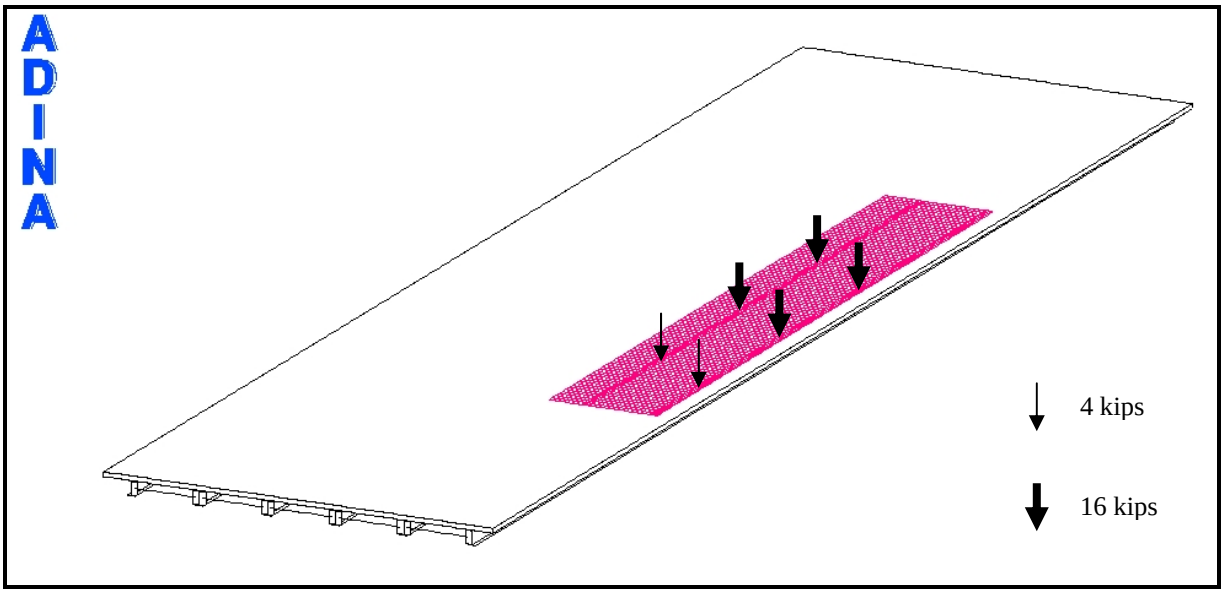

Figure 2.10 Isometric view of Loading Case 7.

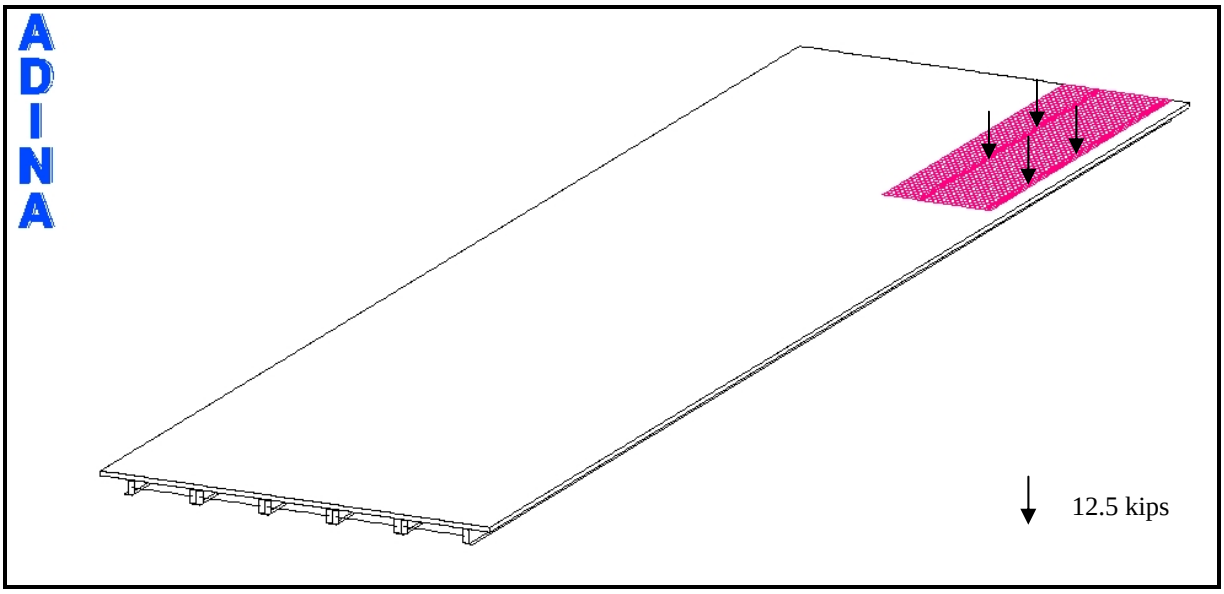

Figure 2.11 Isometric view of Loading Case 8.

2.2.4 Loading Cases 9 through 11

The primary motivation behind Loading Cases 9 through 11 is to examine vertical reaction distributions with applied loads at and near the structural supports. With regard to Loading Case 9, the structural supports are those associated with Pier 1; Loading Cases 10 and 11 are associated with the structural supports at Abutment 1. Noting the locations of the loads (as depicted in Figures 2.12 through 2.14), only the reactions are examined for these loading cases.

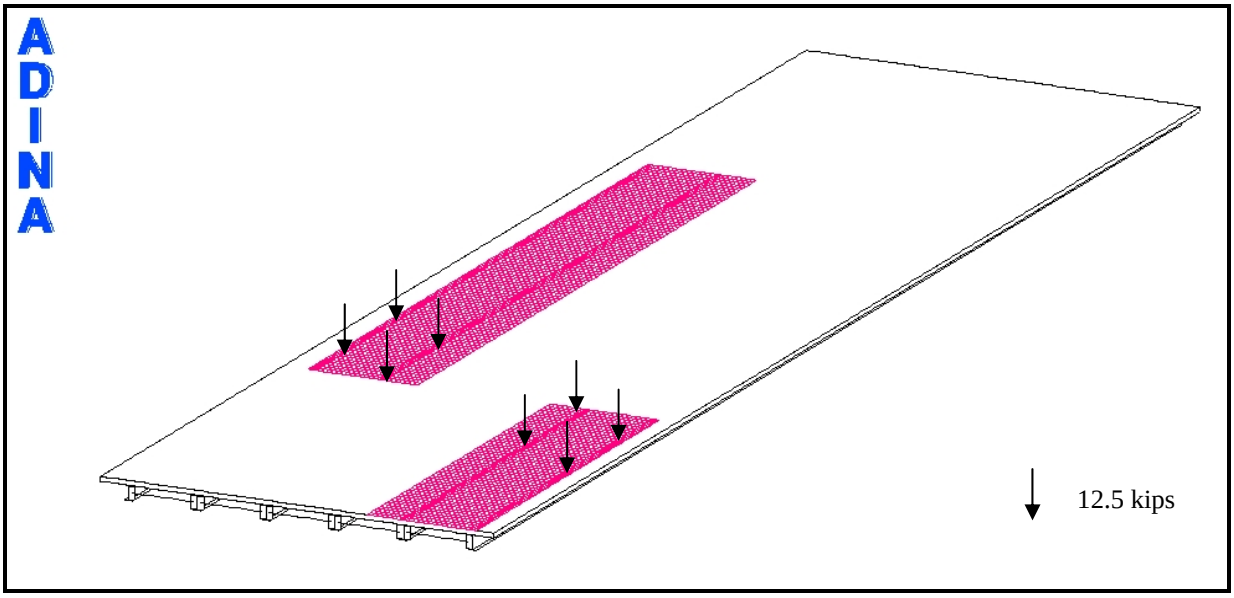

Figure 2.12 Isometric view of Loading Case 9.

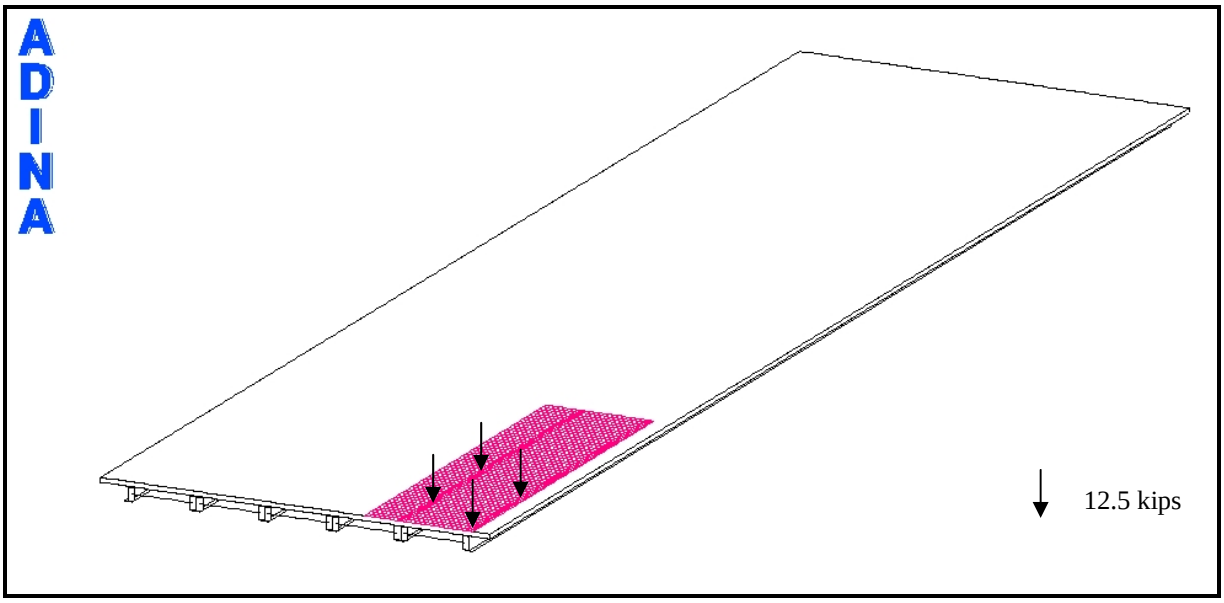

Figure 2.13 Isometric view of Loading Case 10.

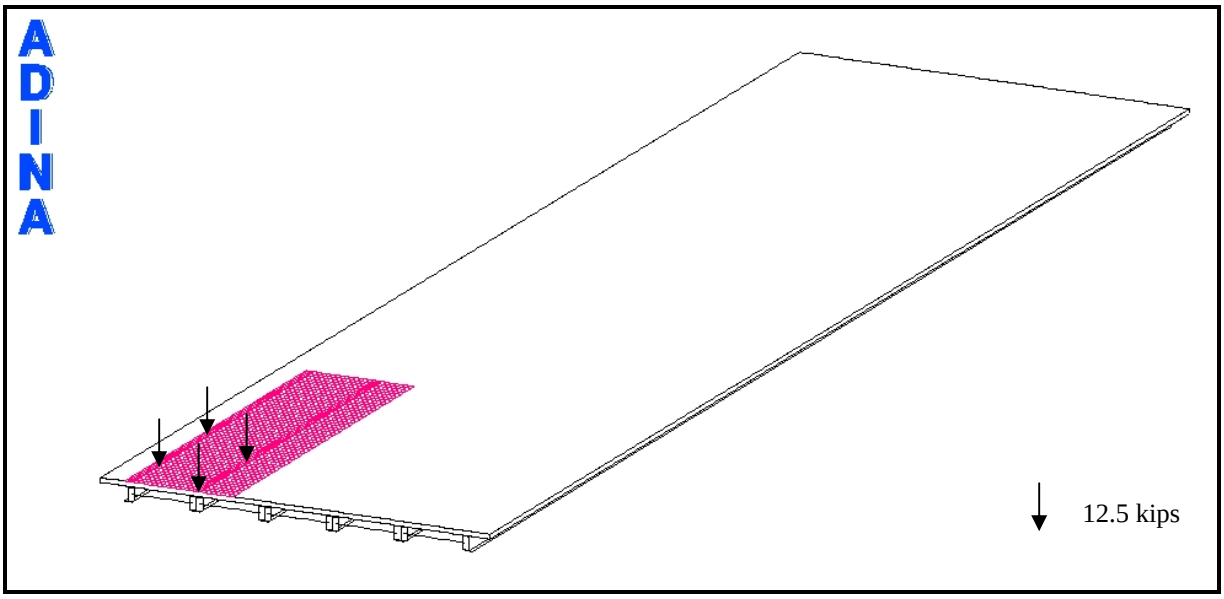

Figure 2.14 Isometric view of Loading Case 11.

2.2.5 Loading Case 13

Finally, Loading Case 13 is designed to induce a global torsion in the bridge in order to maximize warping torsional effects in the longitudinal members (effects of warping torsion within the individual beam elements within the grillage model are not overtly considered in the element formulation).

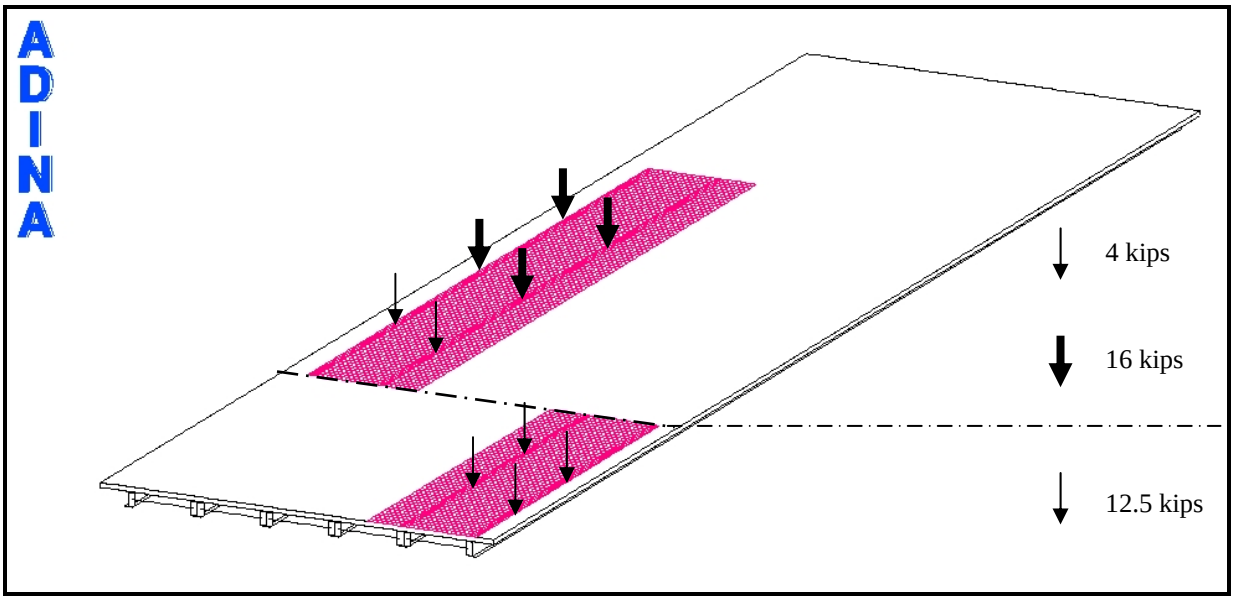

Figure 2.15 Isometric view of Loading Case 13.

3.0 GRILLAGE FINITE ELEMENT MODEL

The behavior and accuracy of the grillage finite element model, as compared with a shell finite element model, forms the primary focus of this work. With this in mind, it is imperative that an accurate description of this model be presented in order that this work will not be confused (or combined) with a similar work considering a more (or less) accurate modeling strategy than that presented herein. Following is a brief outline of the finite element formulation employed in the beam finite element used in the grillage modeling reported on herein. In addition, a description of the grillage finite element model itself is also provided.

3.1 FINITE ELEMENT MODEL FORMULATION

The grillage finite element model employs 2-node "Hermitian" beam elements based upon Bernoulli-Euler beam theory; six degrees of freedom exist at each of the two nodes: three represent nodal displacements with the remaining three representing nodal rotations [Przemieniecki, 1968]. The characterization of Hermitian beam elements credits the French mathematician, Hermite, for his work with the interpolation polynomials: in the present case, a cubic interpolation is used to model transverse nodal displacements [Felippa, 2004]; all remaining degrees of freedom follow a linear interpolation [ADINA, 2003].

Continuing the formulation, individual element stiffness matrices are obtained through the closed form evaluation of the following volume integral (i.e. numerical integration is not used for the integration of the stiffness matrix):

$$\underline{K}^{(m)} = \int_{V^{(m)}} \underline{B}^{(m)T} \underline{C}^{(m)} \underline{B}^{(m)} dV^{(m)}, \tag{3.1}$$

where the $\underline{B}^{(m)}$ is the element strain-displacement matrix (evaluated by differentiating the interpolation matrix), and $\underline{C}^{(m)}$ is the element stress-strain material matrix [Bathe, 1996]. The superscript *(m)* simply indicates the element for which the stiffness matrix is being evaluated. Individual, local element stiffness matrices are then assembled through the direct stiffness method; and one may subsequently arrive at an expression for the *global* stiffness matrix of the structure (a transformation of local to global coordinates is also implied in this step). It is therefore of paramount importance that the local orientation of the individual elements in the structure be defined correctly. In ADINA, this orientation is performed through the definition of an auxiliary node; which orients the element cross-section as depicted in Figure 3.1 (an I-section is shown for clarity of the concept).

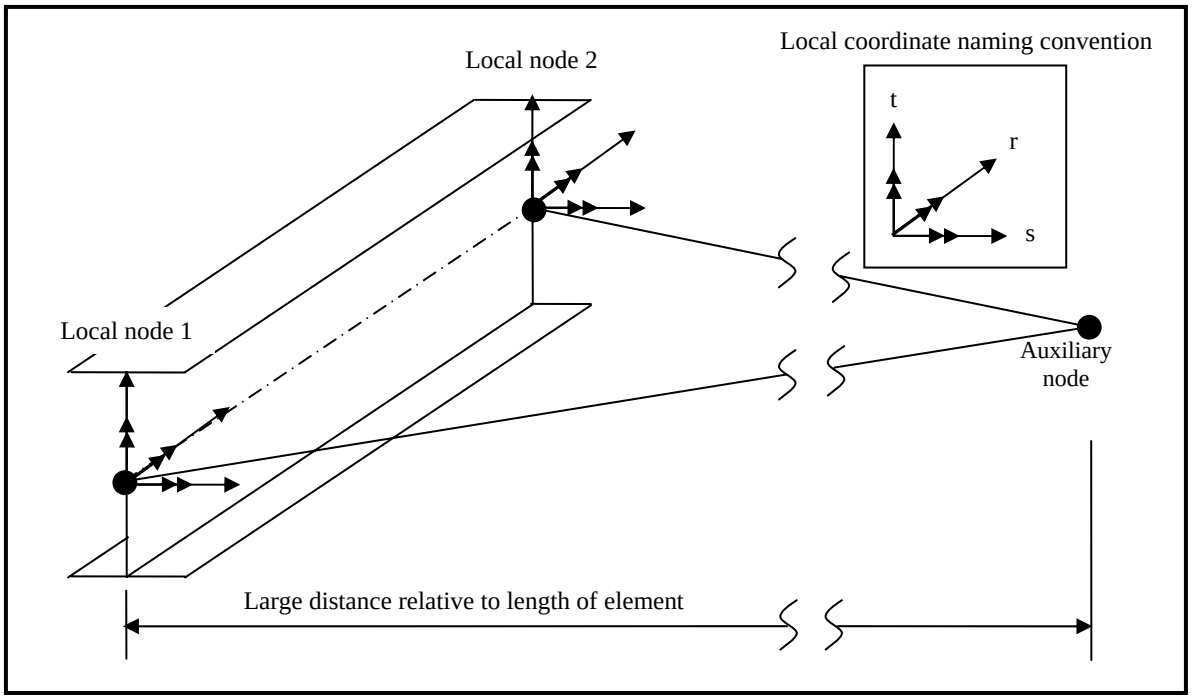

Figure 3.1 Definition of local element coordinates through auxiliary node.

Finally, completing the formulation, the global stiffness matrix is then modified using the imposed boundary conditions, and a solution to the problem is obtained through the evaluation of the following general equation of equilibrium:

$$\underline{K}\,\underline{U} = \underline{R}\,. \tag{3.2}$$

Here, $\underline{K}$ is the global structural stiffness matrix, $\underline{U}$ is the vector of nodal displacements, and $\underline{R}$ is the vector of applied nodal forces [Bathe, 1996]. As it is that nodal displacements are the primary modeling unknowns within the classical direct stiffness approach, information regarding the stresses / strains in the individual elements can be subsequently arrived at through the a priori knowledge of the cross-sectional properties assigned to the element in question.

Typical of most numerical analysis techniques, it must be understood that the solution obtained using this method, regardless of the mesh refinement, may be approximate, and must be

taken as such. While increasing the number of elements in a given model will increase the accuracy, there is a trade-off with the computational power necessary to complete the analysis.

3.2 MODEL CONSTRUCTION

Now that a brief explanation of the formulation employed for the grillage finite element model has been given, the remainder of the chapter will be devoted to a physical description of the model. Keeping in mind the plan view of the subject bridge previously presented in Figure 2.1, Figure 3.2 depicts an isometric view of the grillage finite element model developed for this work.

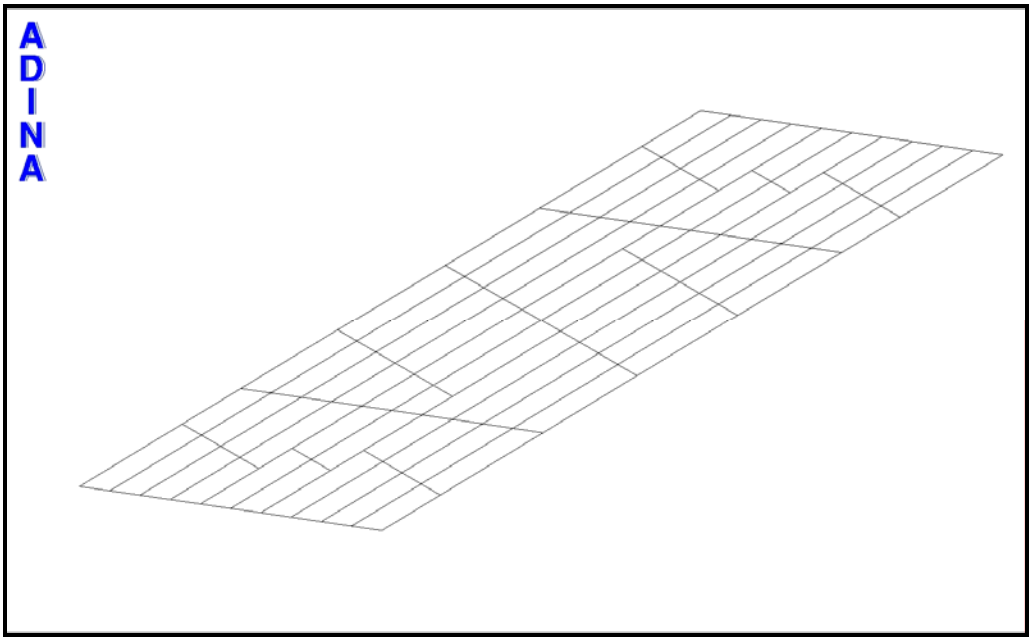

Figure 3.2 Isometric view of grillage finite element model.

Note that the primary difference between the two figures can be seen with the presence of the so-called auxiliary members in the grillage finite element model (Figure 3.2). These auxiliary

members account for the load application issue encountered with grillage analysis of steel I-girder bridges as discussed in Sub-Section 1.1.2; thus these auxiliary members represent only a width of the concrete deck (one-half of the transverse spacing of the longitudinal girders). Comparatively, they offer little to the longitudinal stiffness of the model as they contribute a flexural stiffness representing only a small portion of the concrete deck.

The locations of the remaining members shown in Figure 3.2 are approximately coincident with the locations of the main *steel* super-structure members in the structure (longitudinal steel girders and transverse steel diaphragms). In order to locate the transverse components of the model as closely as possible, to that given in Figure 2.1, a six inch subdivision (i.e. element spacing) within the longitudinal components is employed; subsequently, the transverse components are also subdivided at this length. In other words, the element spacing for all components of this model is roughly six inches long resulting in 2,821 elements (approximately 16,500 degrees of freedom). Given this highly refined mesh density, it can also be expected that the results obtained from subsequent analyses will be of *relatively* high accuracy, insuring that this modeling approach is sufficiently represented (i.e. a better than "conventional" grillage model is used in the current research).

3.2.1 Transformed cross-sections

An important concern in constructing this model emanates from the assignment of cross-sectional properties to the elements. This assignment is undertaken using a two-step process: transforming the effective concrete cross-section into an equivalent steel cross-section, and subsequent computation of the transformed section properties for input into ADINA. When transforming a concrete cross-section into an equivalent cross-section of steel, there are two

items which must be attended to: the width of concrete to be considered (i.e. the effective slab width) and the preservation of the neutral axis location from the initial composite cross-section to the final transformed cross-section.

Per Article 4.6.2.6.1 [AASHTO, 2004] the effective slab width for the interior longitudinal members was taken to be the least of the following three values:

1) One-quarter of the effective span length;
2) 12.0 times the slab thickness, plus the greater of either the web thickness or one-half of the width of the top flange of the girder; or
3) The average transverse spacing of adjacent beams.

For the exterior longitudinal members, the above values were adjusted to be one-half of the effective width of the adjacent interior beam (which was constant for this bridge) plus the least of the following:

1) One-eighth of the effective span length;
2) 6.0 times the slab thickness, plus the greater of either one-half of the web thickness or one-quarter of the width of the top flange of the girder; or
3) The width of the overhang.

Without prior knowledge of the behavior of the structure, the effective span length is calculated by applying a uniformly distributed load to a three-span continuous beam and then analyzing this structure through application of the moment-distribution approach. The effective span length is then taken as the distance between points of zero moment in the main span, or 32.88'. Employing this information within the foregoing AASHTO specified effective width prescriptions, it is found that condition 3) controls for both the interior and exterior longitudinal members: with effective widths of 77 inches and 68.5 inches, respectively. Having arrived at an

effective slab width, preservation of the neutral axis in the transformed cross-section is achieved by applying the modular ratio to the *width*; as opposed to the thickness of the slab.

Computation of the transformed section properties is then performed by standard means; i.e. the bending moments of inertia are computed about the neutral axis using Equation (1.1) with the addition of the term Ad^2 (as an application of the Parallel Axis Theorem); A corresponds to the cross-sectional area of the component being considered with d being its distance from the overall cross-sectional neutral axis to the centroid of the component in question.. Similarly, torsional properties are computed based on Equation (1.2) where a summation of the torsional constants of the two cross-sectional components (the transformed effective slab width and the steel cross-section) gives a single torsional constant to be employed in the model. That being said, it is noted that half of the effective slab width is omitted from the main longitudinal members' cross-sections in order to account for the presence of the auxiliary members imposed on the model.

Furthermore, variability in the main longitudinal members' cross-sections (through the cover plates and splice plates present in the subject bridge) is accounted for by varying the cross-sectional properties in the model. Table 3.1 presents the computed values for this model (an explanation of this table follows).

Table 3.1 Cross-sectional properties for grillage finite element model.

Cross Section	J (in^4)	I_x (in^4)	I_y (in^4)	A (in^2)
1	321	4337	125	53
2	323	6390	183	64
3	322	7034	176	81
4	410	4666	171	62
5	412	6815	230	73
6	411	7580	222	90
7	96	491	26	20
8	192	534	34	29
9	192	401	17	28
10	278	143	42	31

Cross-sections 1, 2, and 3 represent the transformed sections of the basic interior longitudinal I-section, the basic interior longitudinal I- section with top and bottom cover plates, and the basic interior longitudinal I-section with splice plates, respectively. Cross-sections 4 through 6 follow a similar arrangement for the exterior girders. Cross-sections 7 through 9 represent the abutment I-section, the pier I-section, and the C-section transverse members, respectively; computation of these properties is described in more detail below. Finally, cross-section 10 refers to the auxiliary longitudinal member; recall that these members are employed to facilitate the correct statical redistribution of the applied loads.

Rounding out the discussion of member section properties, the transverse members are computed in a similar fashion with the exception that the bending moments of inertia are simply

summed versus the inclusion of the Ad^2 term as with the longitudinal members (i.e. no composite action is assumed for the transverse structural members). The effective width of concrete for these members was taken to be the suggested value of $b_w + 0.3s$, as previously described in Sub-Section 1.1.2. Finally, having transformed the various effective concrete slabs into equivalent steel cross-sections, a linear elastic material model is employed in the analysis of this finite element assemblage corresponding to steel (*E=29,500 ksi*, *v=0.3*).

3.2.2 Boundary conditions

As previously discussed, a typical pin-roller boundary condition arrangement is present in the subject bridge. In dealing with longitudinally skewed bridge models, it is expedient to ensure that the local and global coordinate systems coincide: this precludes the need for the separate definition of a local coordinate system at each boundary condition location. It is therefore pointed out that the boundary conditions imposed in this model are as indicated in Table 3.2 ("x" indicates fixity of the respective degree of freedom). Fixities indicated in this table are only applied to the primary longitudinal members (e.g. auxiliary members are not restrained at the piers).

Table 3.2 Fixity of degrees of freedom at boundary condition locations.

Location	**Degree of Freedom**					
	u_x	u_y	u_z	θ_x	θ_y	θ_z
Abut. (Span 1)	x	x	x	-	-	-
Pier 1	-	x	x	-	-	-
Pier 2	-	x	x	-	-	-
Abut. (Span 3)	-	x	x	-	-	-

3.2.3 Method of load application

Given the coarse arrangement of the members in this model, loads are applied at interior locations (Loading Cases 1, 2, and 12) wherein rigid body statics is used to reckon the portion of an applied loading imposed on the deck in between the longitudinal members in order that a statically equivalent loading may be assigned to adjacent members in the grillage model. In this research, such distributions were obtained from simplified modeling of longitudinal girders and auxiliary members within a slice of bridge cross-section in order that their reactions may be used to define the equivalent member loads in the grillage model. Figures 3.3 and 3.4 display the simplified bridge cross-sections considered when arriving at the loading distributions used in the present work. Regarding loads applied at exterior locations (Loading Cases 3 through 11 and 13), the arrangement of loads depicted in Figure 3.5 is also considered.

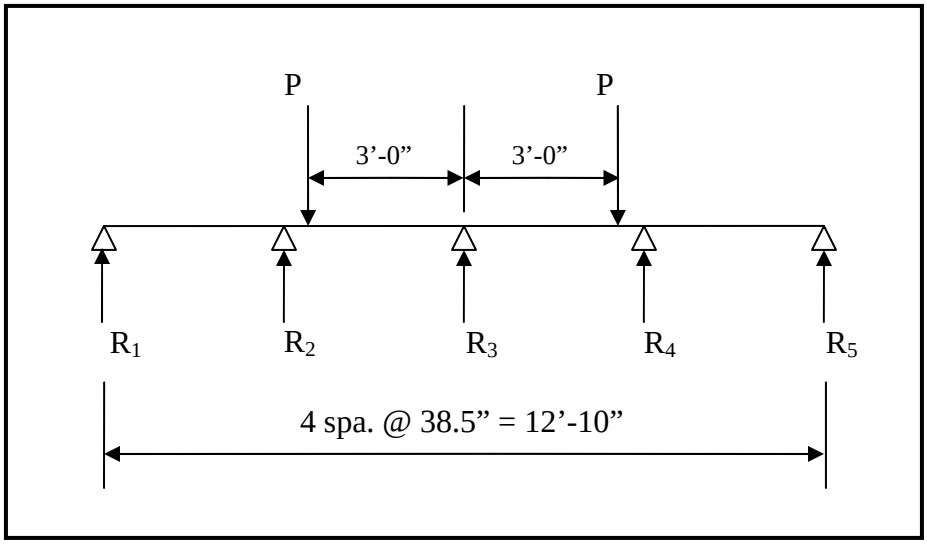

Figure 3.3 Concentrated load configuration for loads at interior locations.

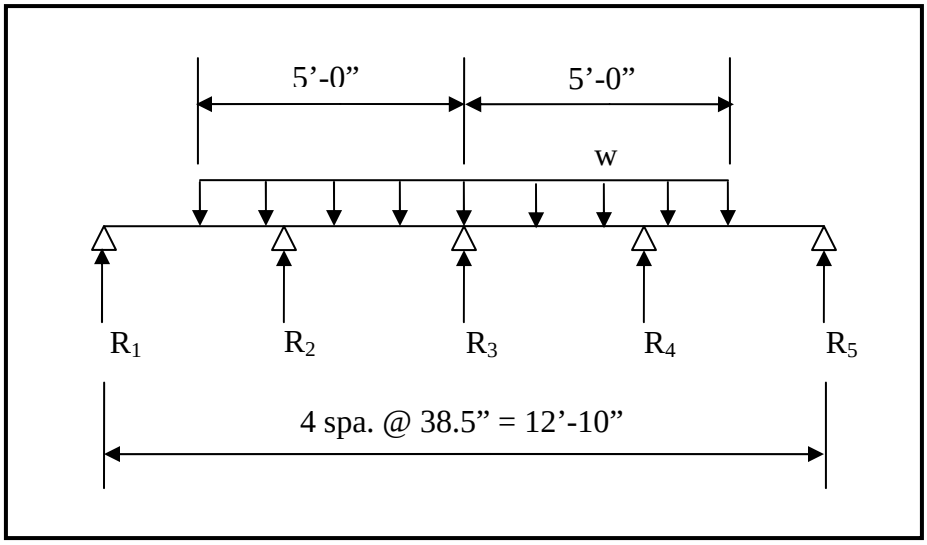

Figure 3.4 Uniformly distributed load configuration for loads at interior locations.

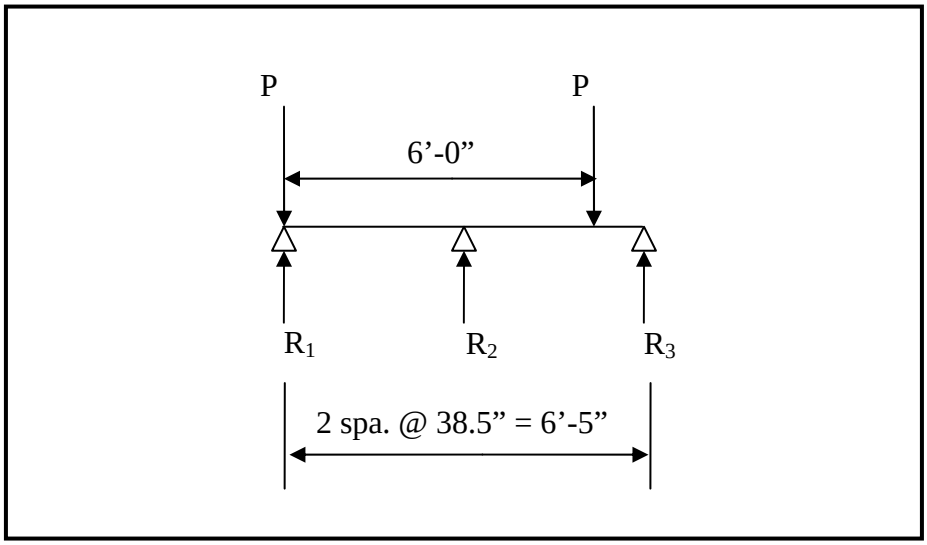

Figure 3.5 Concentrated load configuration for loads at exterior locations.

A discussion of these loading depictions now follows. First, noting the dimensions in the figures, one can see how these directly apply to the grillage finite element model. The 38.5 inch dimension is one-half of the transverse spacing of the longitudinal steel girders (the spacing at

which the longitudinal components of the model are located). The thought is that the applied loads will statically distribute to the respective members based on the reaction distributions from the depicted load configurations. In applying this concept, it is assumed that loads applied to the bridge interior are distributed to *five* longitudinal members (steel girders and auxiliary members) and loads applied to the bridge exterior are applied to *three* of these longitudinal members; this was based on a detailed mapping of the bridge deck geometry.

It then follows that in Figures 3.3 and 3.4, R_1, R_3, and R_5 represent loads to be applied to two of the four main *interior* longitudinal members while R_2 and R_4 represent loads to be applied to the auxiliary members. In Figure 3.5, R_1 and R_3 represent loads to be applied to the main *exterior* longitudinal members and R_2 again represents the load to be applied to the auxiliary counterpart. The concentrated loads applied in Figures 3.3 and 3.5 represent a axle load of 20 kips while a uniformly distributed lane load of 1 kip per inch is depicted in Figure 3.4. Reaction distributions were then computed based on an analysis of these structures; percentages of the indicated loads are given in Table 3.3. For example, for a bridge interior load case, 48.2 % of the total axle load and 31.5 % of the lane load is applied to the two main girders as a concentrated load and a uniformly distributed load, respectively.

Table 3.3 Distribution of reactions for Figures 3.3 through 3.5.

Reaction	Bridge Interior		Bridge Exterior	
	Load Distribution		Load Distribution	
	Axle Loads	Lane Load	Axle Loads	Lane Load
R_1	-1.2 %	2.4 %	48.5 %	16.7 %
R_2	48.2 %	31.5 %	9.6 %	33.3 %
R_3	6.0 %	32.2 %	41.9 %	33.3 %
R_4	48.2 %	31.5 %	0 %	16.7 %
R_5	-1.2 %	2.4 %	0 %	0 %

Note that the lane load for the exterior case has no figure associated with it; this is primarily due to the location of this lane load resulting approximately in a uniform distribution over the four exterior longitudinal members. Therefore, it is assumed that the reaction distribution to R_1 through R_4 is one-sixth, one-third, one-third, and one-sixth, respectively. This concludes the description of the grillage finite element model; following is a description of the shell finite element model to which the former will be compared.

4.0 SHELL FINITE ELEMENT MODELS

As indicated in Section 1.3, two shell finite element models establish the basis for assessing the results obtained from the grillage finite element model. The motivation behind the development of *two* shell finite element models comes from the need to address computational limitations present during the initial stages of this work. When employing shell elements for both major bridge components (i.e. the longitudinal steel girders and concrete deck), it is estimated that the model consists of approximately two million degrees of freedom. By replacing the shell elements composing the concrete deck with 8-node continuum finite elements, the model is reduced to approximately one million degrees of freedom (mesh density is also modified). Furthermore, the need for rigid connections between the girder top flange and the concrete deck is eliminated (see Sub-Section 4.2.3).

While the initial motivation for the use of continuum finite elements is to decrease the required computational demand, additional benefits come from the further comparison of the two separate shell finite element modeling approaches. From this comparison, a decision may then be made as to the choice of one modeling approach over the other (i.e. is the computational demand required by modeling the concrete deck with shell finite elements warranted?). Furthermore, the use of continuum elements to model the concrete deck allows for the future implementation of a concrete material model [Bathe, et al, 1989]; for this thesis, a linear-elastic material model for the concrete deck is employed (see Sub-Section 4.2.4).

As the shell finite element models briefly described above form the basis against which the results of the grillage finite element model will be compared, it is imperative that a thorough discussion of the salient features of these models be included in this thesis. For the readers' benefit, it must be understood that if one eliminates this type of discussion from any scholarly work, questions similar to those posed in Section 1.3 arise; in this case, such questions would result in only a partial fulfillment of the goals set forth by the author. Following, therefore, is a detailed discussion of each of the two shell finite element models as well as a discussion of the finite element formulations employed throughout.

4.1 FINITE ELEMENT FORMULATIONS

4.1.1 Isoparametric finite element formulation

Beyond the 2-node Hermitian beam finite elements employed in the grillage finite element model, the shell finite element model also employs two "isoparametric" finite element formulations: the 8-node continuum and the "MITC4" shell finite elements (see Sub-Section 4.1.2). The term isoparametric refers to the specification of "interpolation functions," defined within in a "natural coordinate system," that are employed to compute *both* element coordinates and element displacements [Bathe, 1996]. Figure 4.1, Tables 4.1 and 4.2, as well as the explanation that follows, serve to illustrate the basic concepts of the isoparametric formulation.

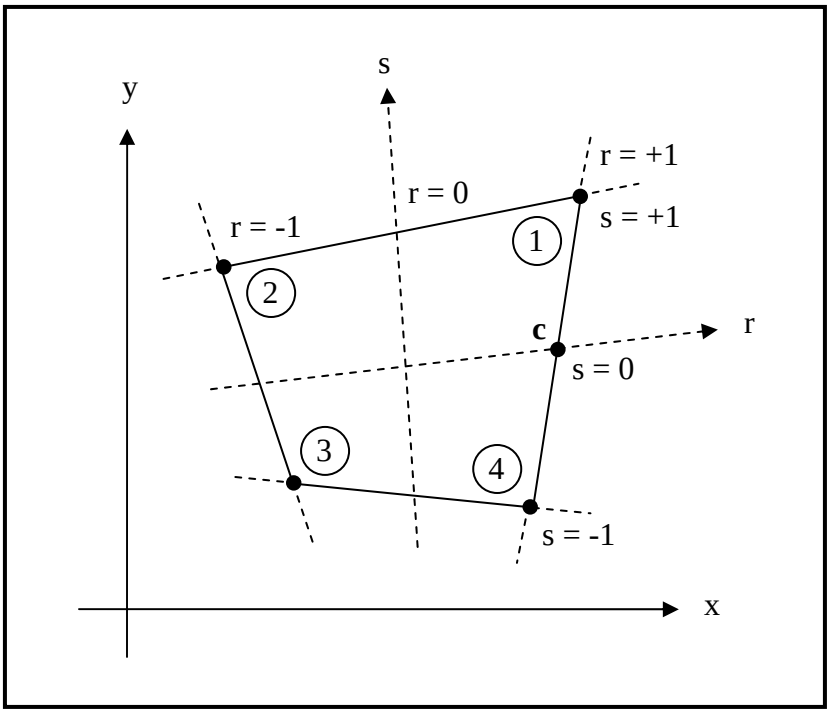

Figure 4.1 Two-dimensional element defined within global and natural coordinate systems.

Table 4.1 Nodal coordinates (global and natural).

Node	Global Coordinates (x , y)	Natural Coordinates (r , s)
1	(7 , 7)	(1 , 1)
2	(1 , 6)	(-1 , 1)
3	(2.5 , 2)	(-1 , -1)
4	(6 , 1.5)	(1 , -1)

Table 4.2 Element interpolation functions for element in Figure 4.1.

Node	Element Interpolation Function
1	$h_1 = ¼ (1 + r) (1 + s)$
2	$h_2 = ¼ (1 - r) (1 + s)$
3	$h_3 = ¼ (1 - r) (1 - s)$
4	$h_4 = ¼ (1 + r) (1 - s)$

Figure 4.1 illustrates a two-dimensional quadrilateral element with four assigned nodes: one to each corner. The global coordinate system is defined with the standard "x" and "y" axes while the natural coordinate system is defined with the "r" and "s" axes; the limits of the associated natural coordinate variables (*r* and *s*) are +/- 1 and are used to define the element edges (in the case of Figure 4.1). These two coordinate systems then relate to each other through the use of interpolation polynomials and discrete nodal coordinates; as subsequently discussed. For the two-dimensional quadrilateral element depicted in Figure 4.1, the definition of element coordinates in the global reference frame is obtained from the following two equations:

$$x = \sum_{i=1}^{N} h_i x_i \tag{4.1}$$

$$y = \sum_{i=1}^{N} h_i y_i \ , \tag{4.2}$$

where x and y are the global coordinate variables at any point on the element, h_i are the interpolation functions defined in Table 4.1 using natural coordinates, and x_i and y_i are the global nodal coordinates.

As mentioned above, the isoparametric formulation is employed such that the element coordinates *and* the element displacements are determined using the same interpolation functions. Equations (4.3) and (4.4), which analogously describe the displacements u and v at any point on the element (u and v correspond to the displacements in the x and y directions, respectively), follow from the previous statement:

$$u = \sum_{i=1}^{N} h_i u_i \tag{4.3}$$

$$v = \sum_{i=1}^{N} h_i v_i \ , \tag{4.4}$$

where h_i is as above and u_i and v_i are the individual nodal displacements in the global coordinate system.

Clearly, the purpose behind the interpolation functions referenced above is simply to interpolate the values of the desired global coordinate variables (or global displacements), at any point on the element, given the a priori knowledge of the global nodal coordinates (or global nodal displacements). For clarity of this concept, consider a point, "c," on the right edge of the element in Figure 4.1, centered between nodes 1 and 4: (r , s) = (+1 , 0). In order to determine the value of the x-coordinate for this point, x_c, one applies Equation (4.1) which yields the following expression (the "¼" term from the interpolation functions is factored out):

$$x_c = h_1 x_1 + h_2 x_2 + h_2 x_2 + h_2 x_2 = \frac{1}{4}\left[(2)(1)(7) + (0)(1)(1) + (0)(1)(2.5) + (2)(1)(6)\right] = \frac{1}{2}(7+6) = 6.5\,.$$

As expected, this value is exactly equal to the average of the values at the endpoints of the line on which the point resides (with respect to the *x* direction).

While the above result appears trivial, it is the intent of the author to provide the reader with a basic understanding of the implementation of interpolation functions as they apply to the isoparametric finite element formulation. Analogous procedures may be employed for the same two-dimensional element in which 9 or 16 nodes are assigned (versus 4 as in Figure 4.1). Configurations such as this would result in a quadratic or cubic interpolation of the coordinate values, respectively (i.e. the edges of the element would then be defined by a curve; versus a straight line used in the four node element). These higher-order formulations subsequently allow for more complex geometries and displacement fields, but result in increased computational demands on a per element basis.

Continuing the formulation, individual element stiffness matrices must now be determined. As a first step, it is necessary to formulate the corresponding strain-displacement matrix, $\underline{B}^{(m)}$. Recall that the strain-displacement matrix is evaluated through calculating the derivatives of the interpolation matrix. However, in the case of the isoparametric finite element

formulation, it is recognized that the interpolation matrix is a function of the *natural* coordinate variables. Therefore, a transformation is required such that the computed strain-displacement matrix is expressed in terms of the global coordinate variables. This transformation occurs through the implementation of the Jacobian operator, $\underline{J}$, defined as follows (for a two-dimensional element):

$$\begin{bmatrix} \frac{\partial}{\partial r} \\ \frac{\partial}{\partial s} \end{bmatrix} = \begin{bmatrix} \frac{\partial x}{\partial r} & \frac{\partial y}{\partial r} \\ \frac{\partial x}{\partial s} & \frac{\partial y}{\partial s} \end{bmatrix} \begin{bmatrix} \frac{\partial}{\partial x} \\ \frac{\partial}{\partial y} \end{bmatrix} = \underline{J} \begin{bmatrix} \frac{\partial}{\partial x} \\ \frac{\partial}{\partial y} \end{bmatrix} \tag{4.5}$$

Having related the derivatives of the natural coordinate system to those of the global coordinate system, the construction of the individual element stiffness matrices may commence. While the evaluation of the volume integral specified in Equation (3.1) would result in the correct formulation of the element stiffness matrices, it is recognized that this integral, previously evaluated over the global coordinate volume, is now evaluated over the *natural* coordinate volume; thus a transformation of the limits of integration is achieved by including the determinant of the Jacobian operator as part of the integrand. In evaluating these types of integrals, ADINA employs a Gauss numerical integration scheme, which produces a consistent numerical framework for the evaluation of the volume integral to a function [ADINA, 2003]. Further details of both the Gauss numerical integration scheme as well as its implementation in the finite element method may be found in the references [Bathe, 1996; Logan, 2001].

Given an understanding of the isoparametric formulation in two dimensions, one can easily extend the formulation to three dimensions, thus yielding the formulation of the 8-node continuum element used in this thesis.

4.1.2 Treatment of element locking phenomenon

Specific to the MITC4 shell finite elements, it is important to note that a "mixed" formulation is employed (versus the "displacement-based" formulation described above) in order to correctly account for the inclusion of shear deformations within the element. When considering only a displacement-based formulation, a the situation can arise (e.g. in shear-deformable shell finite elements made to be thin) in which the contribution to the element stiffness due to the transverse and membrane shear strains erroneously dominates the contribution from the other components (e.g. bending, etc.). Depending on the magnitude of this error, this can result in a condition known as "element locking;" characterized by the element being overly stiff (i.e. element deformations are significantly lower than theoretical values).

By employing a mixed interpolation scheme where transverse strains are assumed to be derivable from nodal displacements (rather than solely by nodal rotations), the possibility of element locking is eliminated from the formulation; in the case of the MITC4 shell finite element formulation, the shear strain components are interpolated independently and then linked to the previously defined interpolation functions [Bathe, 1996]. Through this link, the Gauss numerical integration scheme employed above for the displacement-based interpolation scheme remains a valid approach in the determination of the element stiffness matrices. This concludes the discussion of the finite element formulations employed in the shell finite element models developed for this thesis; following is a physical description of the shell finite element models.

4.2 MODEL CONSTRUCTION

The three primary components of the subject bridge which must be modeled are: (1) the longitudinal steel girders, (2) the transverse steel diaphragms, and (3) the concrete deck. The previously discussed grillage finite element model requires that *combined* section properties be computed in order to model the individual grillage members. However, when considering a three-dimensional shell finite element model (with or without continuum elements to represent the concrete deck), this step is eliminated since actual the cross-sectional geometries define the finite element mesh for each component. Therefore, the primary task in the development of these shell finite models lies in the regulation of the finite element mesh configuration and the implementation of constraints in order to more accurately represent structural response.

A note before proceeding: two shell finite element models are being discussed in this section; recall that one model employs continuum finite elements to represent the concrete deck with the second model employing shell finite elements with "rigid links" (see Sub-Section 4.2.3). For clarity, these models will henceforth be referred to as the "continuum deck" and the "shell deck" models, respectively.

4.2.1 Longitudinal steel girders

In both the continuum deck and shell deck models, the longitudinal steel girder meshes are composed of MITC4 shell finite elements defined along the mid-plane of each of the constituent cross-sectional plate components. There are four cross-sectional geometries used to represent the cross-sectional variations encountered in the subject bridge (see Section 2.1 for locations of these variations); these cross-sections are illustrated in Figures 4.2, 4.3 and 4.4.

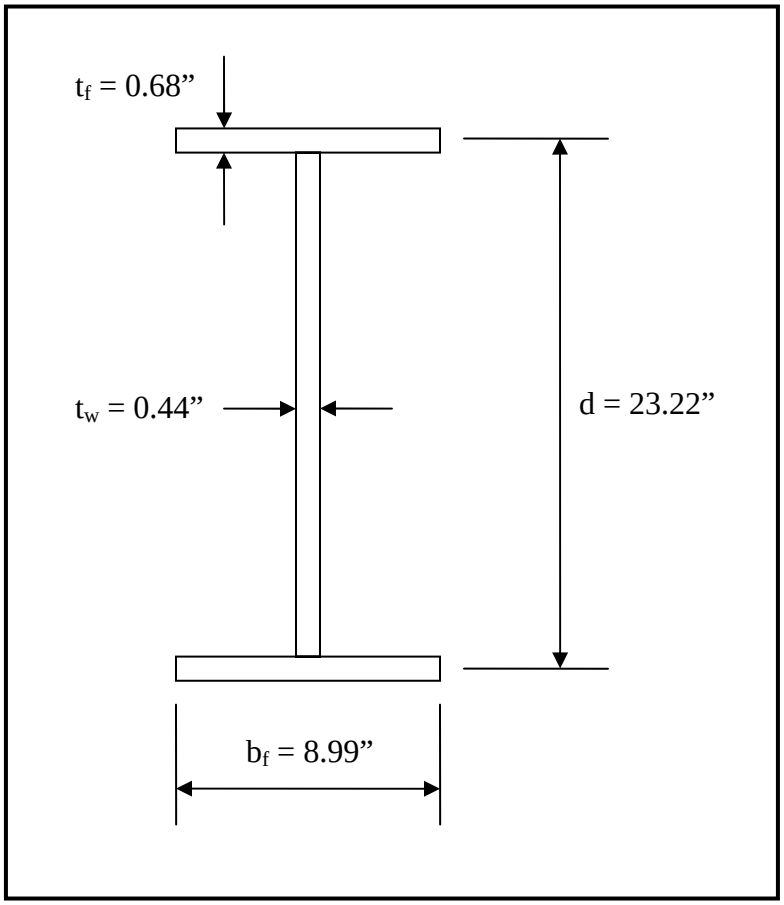

Figure 4.2 Cross-sectional geometry of basic W24x76 girder [AISC, 2004].

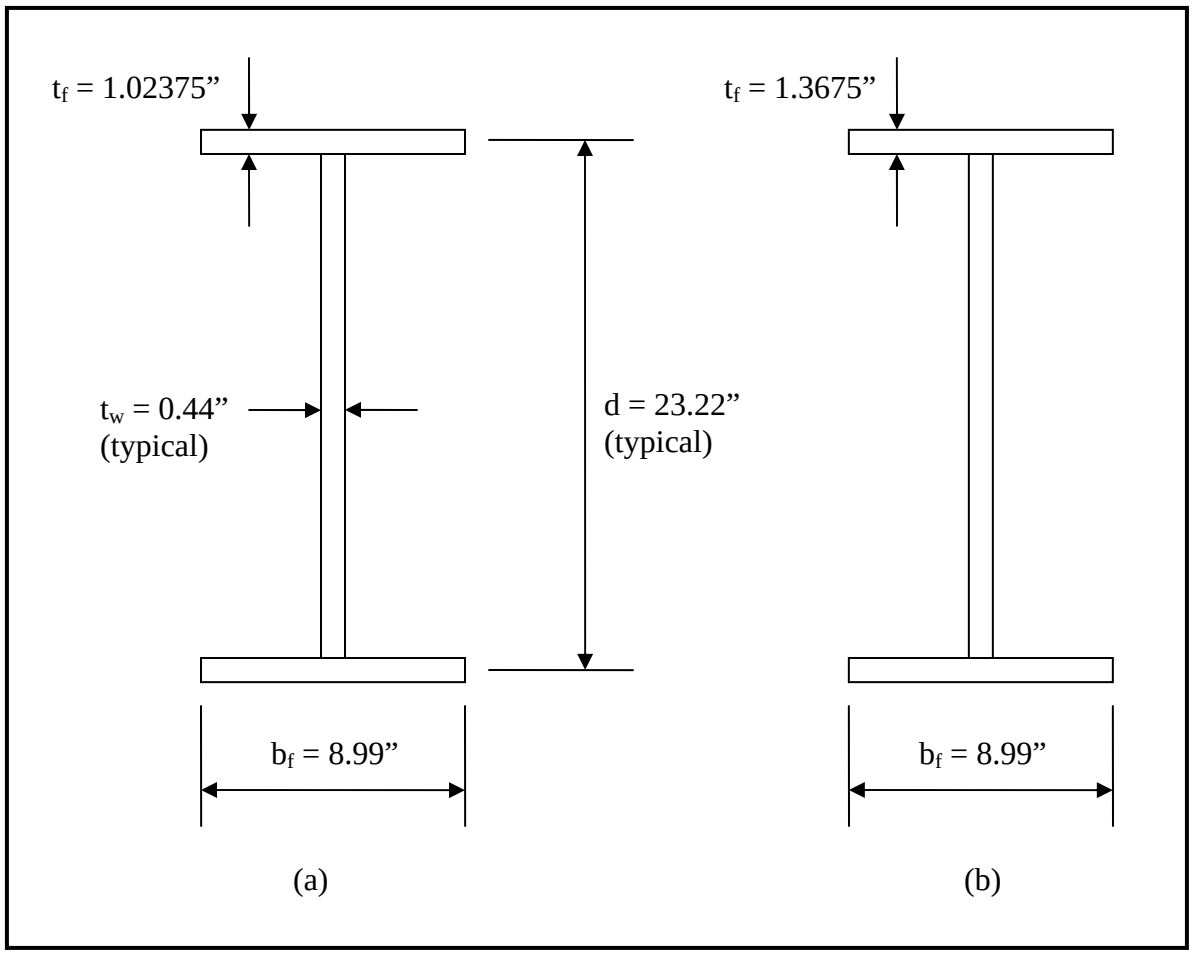

Figure 4.3 Cross-sectional geometry of basic W24x76 girder with cover plates: (a) half ; (b) full.

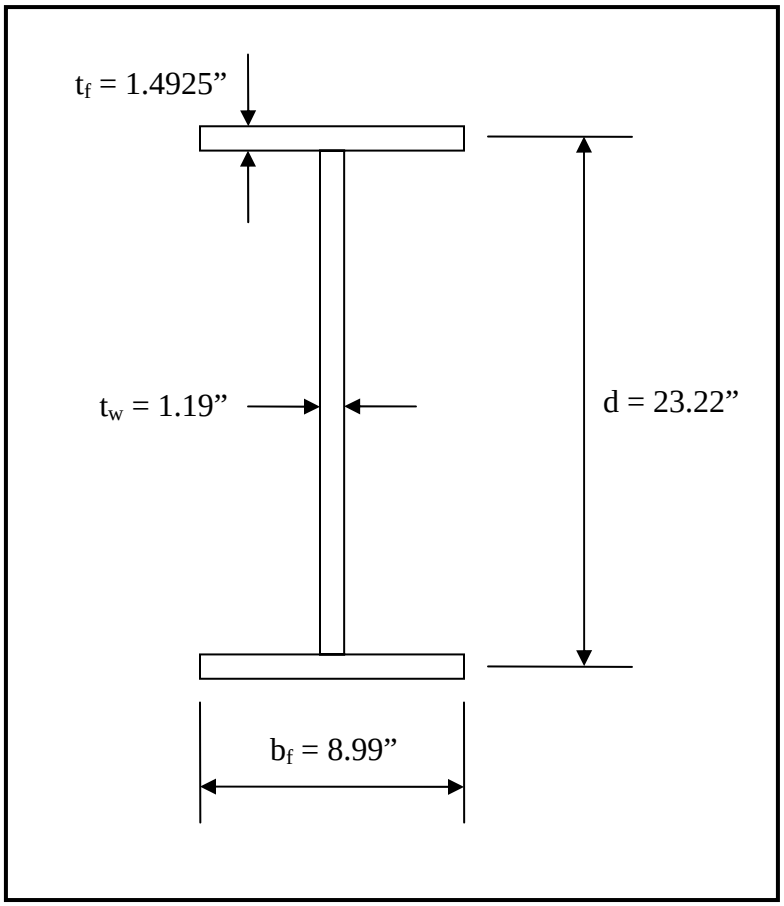

Figure 4.4 Cross-sectional geometry of basic W24x76 girder with splice plates.

The partitioning of Figure 4.3 into two parts is a result of a cover plate transition section present in the subject bridge. These transition sections are typically employed by designers to mitigate the effect of stress raisers encountered when varying cross-sectional geometry in a structural component.

The shell mesh density varies between the top and bottom flanges in order to accommodate the concrete deck mesh described in Sub-Section 4.2.3. Considering the significant contribution of the longitudinal steel members to the overall system response, it is important that the characteristics of these differing mesh configurations be thoroughly

understood before any comparisons between the modeling approaches may be made. Figures 4.5 and 4.6 illustrate the shell finite element mesh configurations employed in the longitudinal steel girders for the continuum deck and shell deck models, respectively.

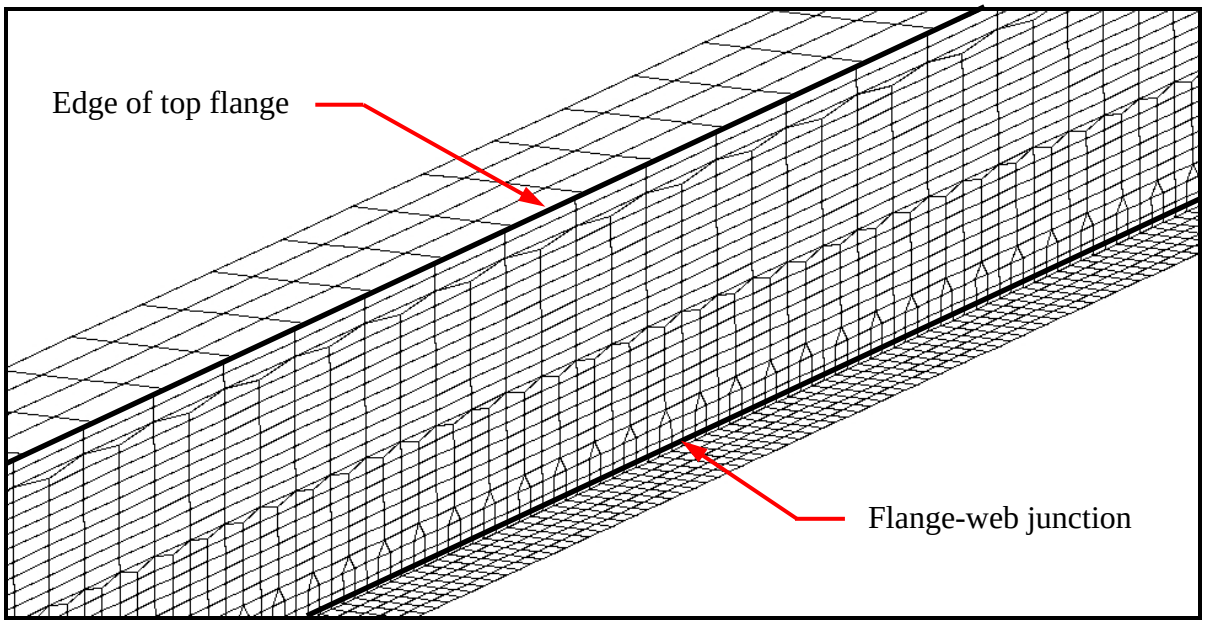

Figure 4.5 Longitudinal steel girder finite element mesh configuration (continuum deck model).

Important features to note in Figure 4.5 include the significant difference in individual element dimensions between the top and bottom flanges. For the top flange, each element is 6 inches long by approximately 2.5 inches wide, resulting in an aspect ratio of 2.4; elements in the bottom flange are 1 inch by 1 inch with an aspect ratio of 1.0. This difference results from the following two assertions: (1) that a relatively fine mesh density is employed in the tensile flange of the girder and (2) that a minimum of four elements compose the top flange; as needed for a somewhat accurate representation of the anticipated flange stress distribution. Assertion (2) is additionally constrained by the desire to reduce the size of the shell deck model (as a result of

computational hardware limitations); it is for this reason that the specified minimum number of elements are chosen for modeling the top flange in this approach.

Despite the differences in the respective lengths of these flange elements, connectivity at the flange-web junctions is achieved by grading the web element sizes from 6 inches long by 1 inch wide at the top flange-web junction, to 1 inch by 1 inch at the bottom flange-web junction. It is noted that relatively high aspect ratios exist for the elements in the top half of the web, with values ranging from 4.0 in the middle to 6.0 at the top. Aspect ratios in this range approach the upper bound of acceptable values for analysis. However, it will be shown in the following chapters that the results from the continuum deck analyses closely parallel those from the shell deck analyses; which subsequently employs a denser, more uniform mesh in the web (see Figure 4.6).

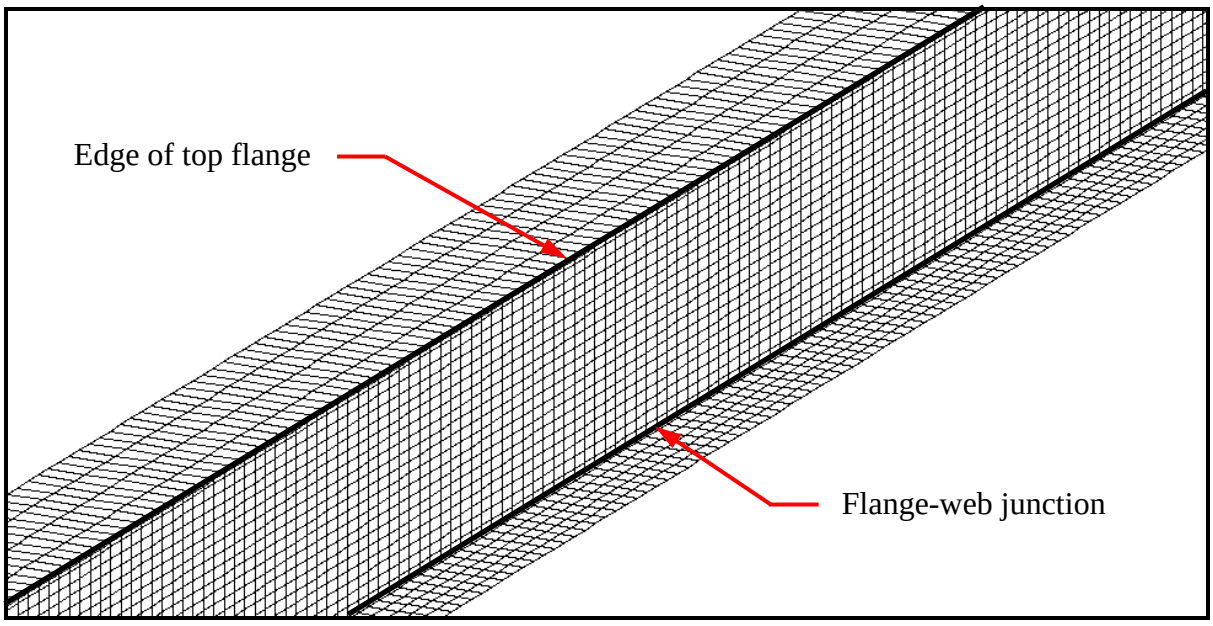

Figure 4.6 Longitudinal steel girder finite element mesh configuration (shell deck model).

As mentioned above, it is seen that the mesh density for the shell deck modeling approach is much finer than that used in the continuum deck model, as depicted in Figure 4.5 (recall that this approach also results in a significant increase in computational demand). Both the bottom flange and the web are composed of 1 inch by 1 inch elements, with the top flange consisting of elements that are 1 inch long by approximately 2.5 inches long. Assertion (2) is again the grounds for the flange element dimensions.

Note that the aspect ratios of the top flange elements for the continuum deck and shell deck models are nearly equal in magnitude (~2.5), but orthogonal in orientation (i.e. the element's long side is parallel to the longitudinal girder in the continuum deck model and perpendicular in the shell deck model). Considering the benefit of comparing and contrasting results from these two modeling approaches, this difference in top flange mesh configuration may be seen as a source of discrepancy between the two models. However, due to the presence of the concrete deck (bracing the top flange against local buckling), it is reasonable to assume that the effects on the accuracy of the solution will be negligible (regardless of the element orientation) [Logan, 2001].

4.2.2 Transverse steel diaphragms and connector plates

Transverse steel diaphragms are accounted for through 2-node Hermitian beam elements [Przemieniecki, 1968] *rigidly* attached to MITC4 shell finite element connector plates. In ADINA, this rigid diaphragm-to-plate connection is achieved through the use of node-to-node rigid links; the configuration of a typical diaphragm-to-girder connection is illustrated in Figure 4.7. When assigning rigid links between nodes, a constraint is imposed on the applicable degrees of freedom of a "slave" node such that this node behaves in a kinematically appropriate manner

in relation to the displacements of a “master” node. It follows therefore that the configuration of rigid links imposed at the diaphragm connector plates shown in Figure 4.7 is actually twofold in purpose.

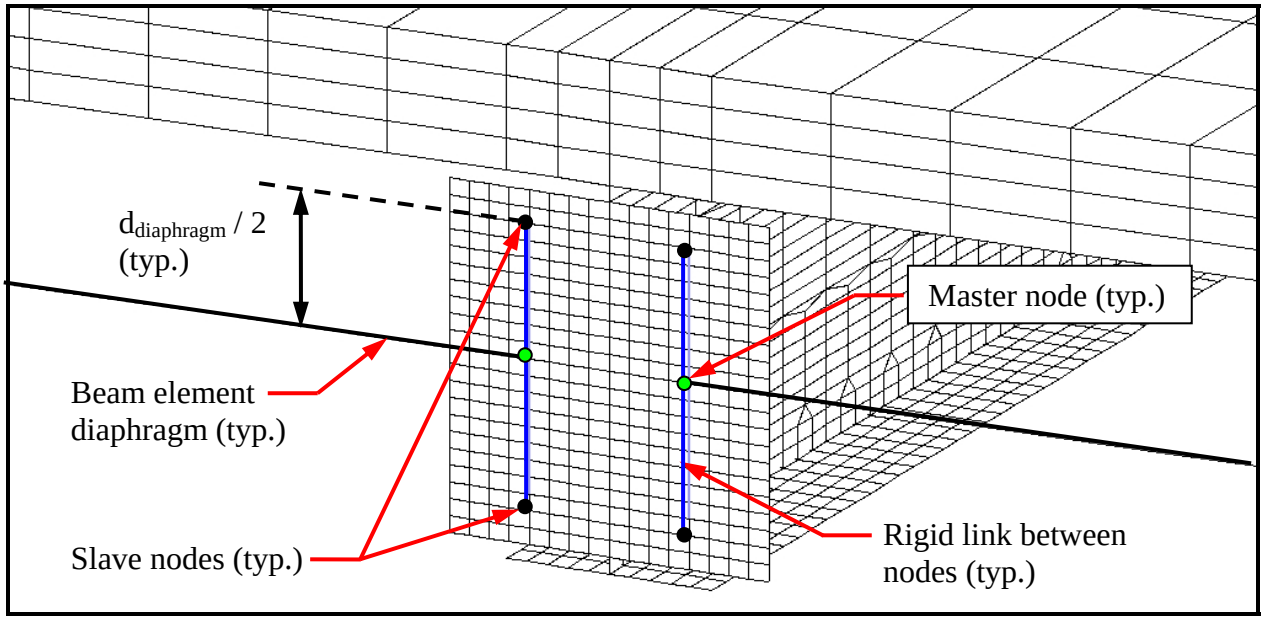

Figure 4.7 Diaphragm-to-girder connection.

First, the full depth of the diaphragm cross-section is attached to the connector plates which allows for a more representative transference of moment from the diaphragms to the girders; this connection is modeled as a fixed connection, versus a shear connection only, based on the design drawings of the subject bridge. Second, due to the fact that the beam elements representing the diaphragms are actually attached to three nodes (versus only one node at the beam / plate intersection), there is a more even distribution of diaphragm forces into the connector plates, and subsequently into the longitudinal girders. The actual transverse steel diaphragms are either rolled channels or I-sections connected to the longitudinal steel girder webs using plates that extend over a portion of these webs (i.e. some moment transfer is

provided). Since one-dimensional beam elements are employed as analogs for the transverse steel diaphragms, the rigid links permit the proper kinematic interaction between these one-dimensional beam ends and the three-dimensional shell finite element model employed at the connector plates.

The finite element mesh configuration for each transverse steel diaphragm connection is identical throughout the entire model (only the cross-section assignments vary as per Figure 2.1); this is of great benefit with respect to time requirements for modeling (see Section 4.4). Diaphragms are subdivided into 10, 2-node beam elements, which results in an element length of approximately 7 inches; this element length is nearly coincident with beam element lengths imposed throughout the grillage finite element model. The connector plates consist of 1 inch by 1 inch shell elements aligned along vertical element boundaries in the webs of the longitudinal steel girders; this allows for complete plate-to-web connectivity without the use of additional constraint equations (see Section 4.4). Furthermore, it should be noted that the connections are identical for both the continuum and shell deck models as the shell elements in the web employ identical lengths in the vertical direction (of 1 inch).

4.2.3 Concrete deck

Up to this point in the shell model description, the primary difference between the continuum deck and shell deck models has come from the respective finite element mesh configurations imposed in each model. These mesh configurations, as previously mentioned, are primarily a result of the employed modeling approaches emanating from hardware limitations, etc.

4.2.3.1 Continuum deck model – As the name implies, this model makes use of 8-node continuum finite elements to model the concrete deck. Figure 4.8 illustrates a representative cross-section of the continuum finite element mesh configuration for this model.

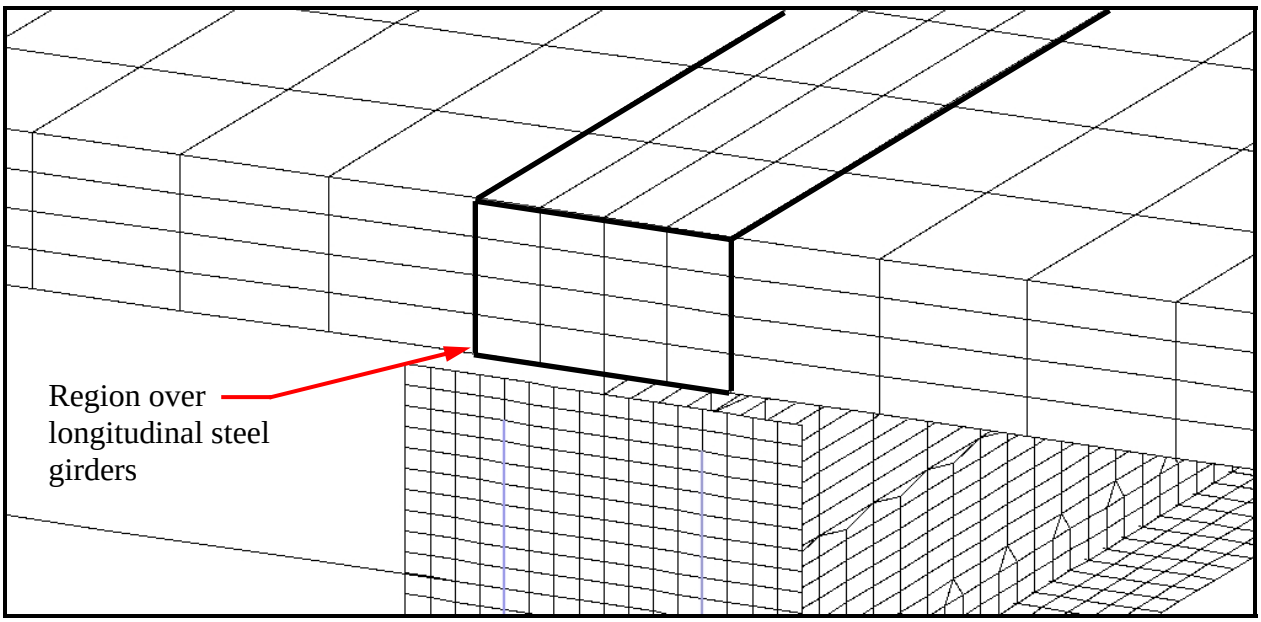

Figure 4.8 Representative cross-section of continuum finite element concrete deck model.

As discussed in Sub-Section 4.2.1, the top flanges of the longitudinal steel girders are modeled with four elements in the transverse direction (two per outstand leg) which subsequently imposes the same constraint on the continuum finite elements directly above the girders. However, due to the desire to reduce the computational demand required by the continuum deck model, a standard longitudinal length of 6 inches is imposed throughout; which results in the aforementioned 6 inch long by approximately 2.5 inch wide element dimensions (with respect to the x-y plane).

Along these lines, continuum finite elements not positioned directly over the longitudinal steel girders are assigned a length in the transverse direction of approximately 6 inches which

results in a roughly square finite element mesh configuration in the regions between the longitudinal steel girders (again, in the x-y plane). In order to allow for a reasonably accurate distribution of internal stresses *through* the deck, the thickness of the 7.5 inch concrete deck is subdivided into four elements. This results in the complete element dimensions as follows: for the continuum finite elements directly over the longitudinal girders, 6 inches long by approximately 2.5 inches wide by 1.88 inches deep and for those between the longitudinal girders, 6 inches long by approximately 6 inches wide by 1.88 inches deep.

It is pointed out that by employing identical longitudinal element lengths in both the top flange of the girders and the concrete deck, node-to-node connectivity is automatically achieved; thus eliminating the need to impose additional constraint equations (see Figure 4.9).

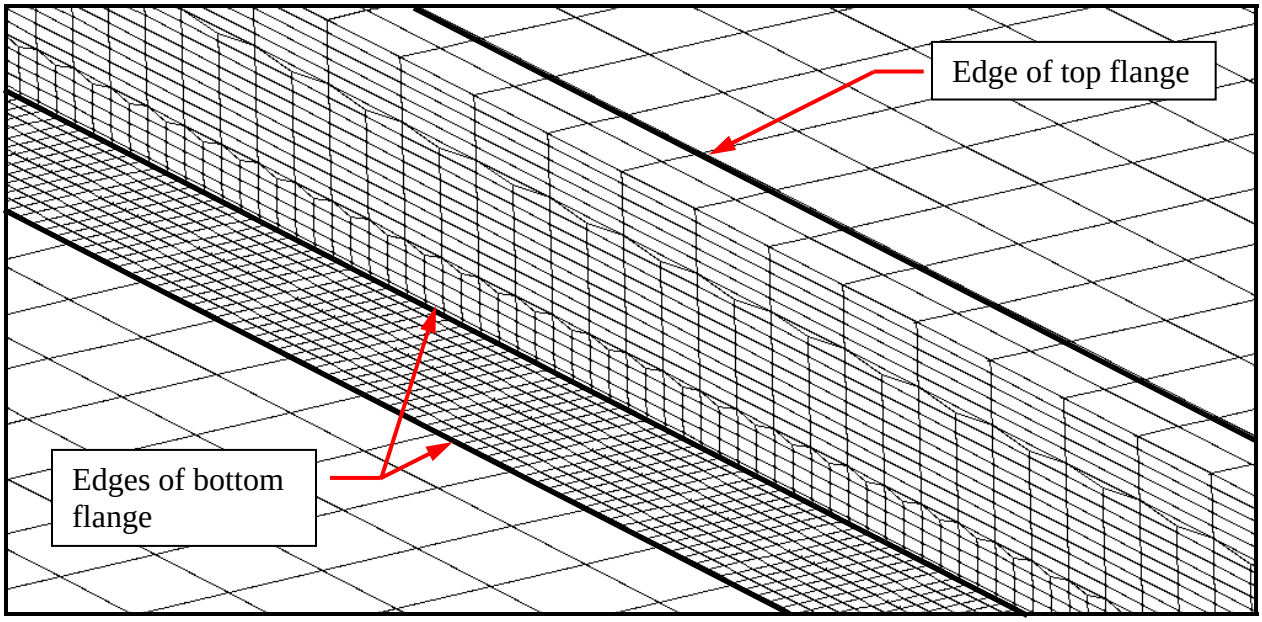

Figure 4.9 Underside of continuum deck shell finite element model.

4.2.3.2 Shell deck model – The shell deck model employs MITC4 shell finite elements which are connected to the longitudinal steel girders by way of the node-to-node rigid links. Figure 4.10 illustrates a representative cross-section of this finite element configuration.

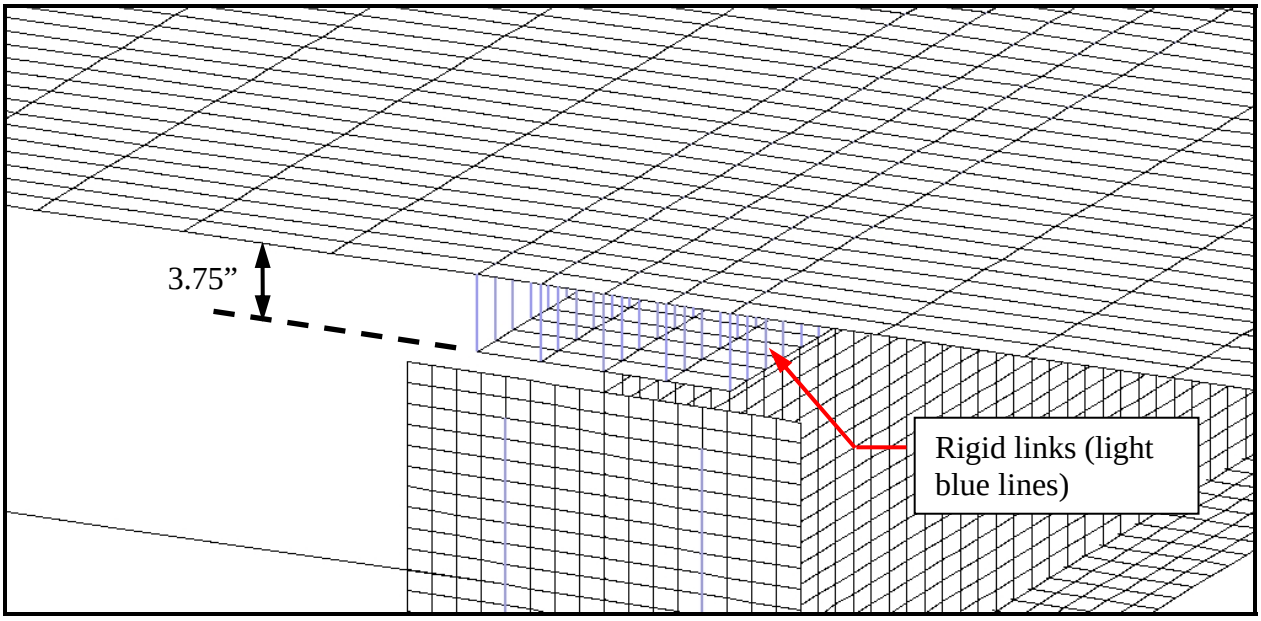

Figure 4.10 Representative cross-section of shell finite element concrete deck model.

As illustrated in the figure, the shell finite elements which represent the concrete deck are offset from the top flange of the longitudinal steel girders by a distance of 3.75 inches (half the depth of the concrete deck). This offset, acting in congress with the imposed rigid links, sets these elements in the correct vertical position (i.e. section properties of the composite section are preserved). The thicknesses assigned to these elements are subsequently made to be equal to the actual depth of the concrete deck: 7.5 inches.

The physical dimensions of the resulting finite element mesh configuration are then as follows: for the shell finite elements directly over the longitudinal girders, 1 inch long by approximately 2.5 inches wide, and for those between the longitudinal girders, 1 inch long by

approximately 6 inches wide. In light of these deck element dimensions, it is noted that the concrete deck element aspect ratios are relatively high as compared with those used to model the longitudinal steel girders. However, in spite of these aspect ratios, it is expected that the characteristic of interest in the concrete deck, that of it being a load distribution mechanism for the applied loads to reach the adjacent longitudinal steel girders, will be preserved. Furthermore, it will again be shown in the proceeding chapters that these aspect ratios have little effect on the structural response measures being considered.

4.2.4 Material models

Three material models are employed in both the continuum deck, and shell deck models: a multi-linear inelastic model representing the characteristics of ASTM A7 steel in uniaxial tension and compression, a linear-elastic steel model, and a linear-elastic concrete model.

The multi-linear inelastic material model is applied to all MITC4 shell finite elements which represent steel cross-sections (longitudinal steel girders and diaphragm connector plates). Figure 4.11 illustrates the stress-strain curve of this material model; additionally, the typical material properties of steel also apply (*E=29,500 ksi*, *v=0.3*). Note in Figure 4.11 that the strain measure depicted is "logarithmic" strain; this measure of strain is also referred to as "true" strain, and is defined by the following integral describing the specialized case of uniaxial stress in a rod:

$$e = \int_{\ell_0}^{\ell} \frac{d\ell}{\ell} = \ln\left(\frac{\ell}{\ell_0}\right), \tag{4.6}$$

where ℓ_0 is the initial length of the rod and ℓ is the length of the rod in the deformed configuration.

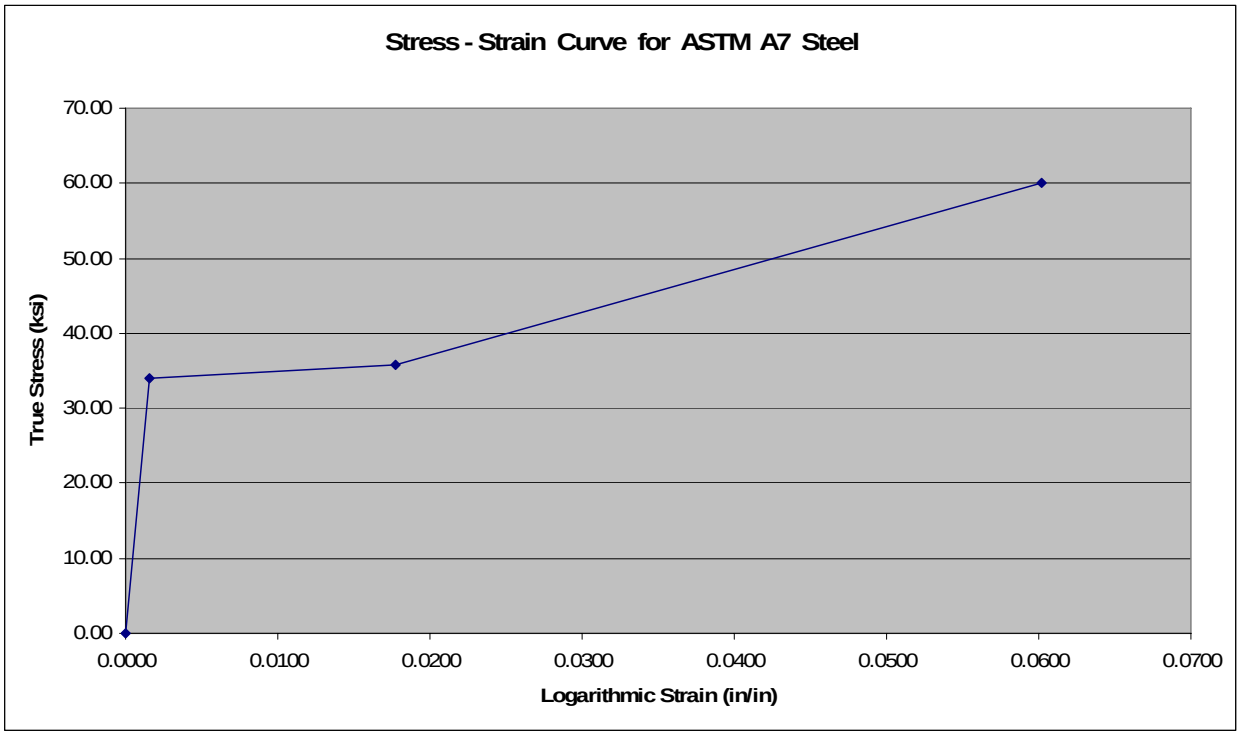

Figure 4.11 Multi-linear inelastic stress-strain curve for ASTM A7 steel.

All transverse steel diaphragms (only those portions which are represented by 2-node Hermitian beam elements) employ the linear-elastic steel material model. Finally, the material model chosen for the concrete deck (regardless of whether the continuum deck or shell deck model is being considered) is a linear-elastic concrete model with *E=3,122 ksi*, *v=0.17*. The value for the modulus of elasticity, E_c, was computed based upon the recommended value in ACI 318-02, Section 8.5:

$$E_c = 33 w_c^{1.5} \sqrt{f_c^{'}} \approx 57{,}000 \sqrt{f_c^{'}}\,, \qquad (4.7)$$

where w_c is the unit weight of concrete taken as approximately 145 pounds per cubic foot (pcf), and $f_c^{'}$ is the compressive strength of concrete, specified as 3,000 psi (see Section 2.1).

While a material model which considers the actual behavioral characteristics of concrete (e.g. high compressive capacity with little to no tensile capacity) would seem more realistic, such

a material model is more appropriate when the ultimate capacity of the structure is sought. Since it is that the previously discussed loading cases (see Section 2.2) induce minimal stresses in the concrete deck, the need to consider the effects of concrete crushing and / or cracking is eliminated with respect to the scope of this work; thus eliminating any concomitant increase in computational expense emanating from the more complex material model.

4.2.5 Boundary conditions

Boundary conditions are applied to the continuum and shell deck finite element models in a nearly identical fashion to those in the grillage finite element model; the primary difference lies in the fact that the reaction interface is now a line of nodes along a transverse shell element boundary versus a single node as in the grillage model.

4.2.6 Method of load application

The methods employed to apply loads to the shell finite element models are relatively simplistic, in that the loads are directly applied to the concrete deck portion of the model as pressures representing the effects of design vehicle(s) and lane loadings; as set forth in the 2004 AASHTO LRFD Bridge Design Specifications and arranged as per the descriptions given in Section 2.2.

It should be noted, however that the tire patches were taken as 20 inches *long* by 10 inches *wide* which is actually orthogonal to the orientation specified by Article 3.6.1.2.5 [AASHTO, 2004]. Having recognized this error *after* the results for this thesis were compiled, it was decided that such an error would have little effect on the structural response measures in question; the centroid of this incorrect tire patch is only 4 inches away from that of the correct tire patch.

4.3 NONLINEAR FINITE ELEMENT ANALYSIS PROCEDURE

In contrast to the grillage finite element model, both of the shell finite element models employ a nonlinear material model to represent the material properties of the longitudinal steel girders and diaphragm connector plates. As previously discussed, the loading cases considered in this thesis are not sufficient to cause *global* yielding in any of the structural components. However, local yielding is possible at locations directly over supports. A brief explanation of the primary characteristics of a nonlinear finite element analysis approach, based on that found in the references, is presented in the following to assist the reader in understanding the nature of the loading protocol adopted in the shell finite element modeling approach [Bathe, 1996].

First, consider the simplified structural behaviors illustrated in Figure 4.12 where *R* is the applied load and *U* is the displacement corresponding to this load.

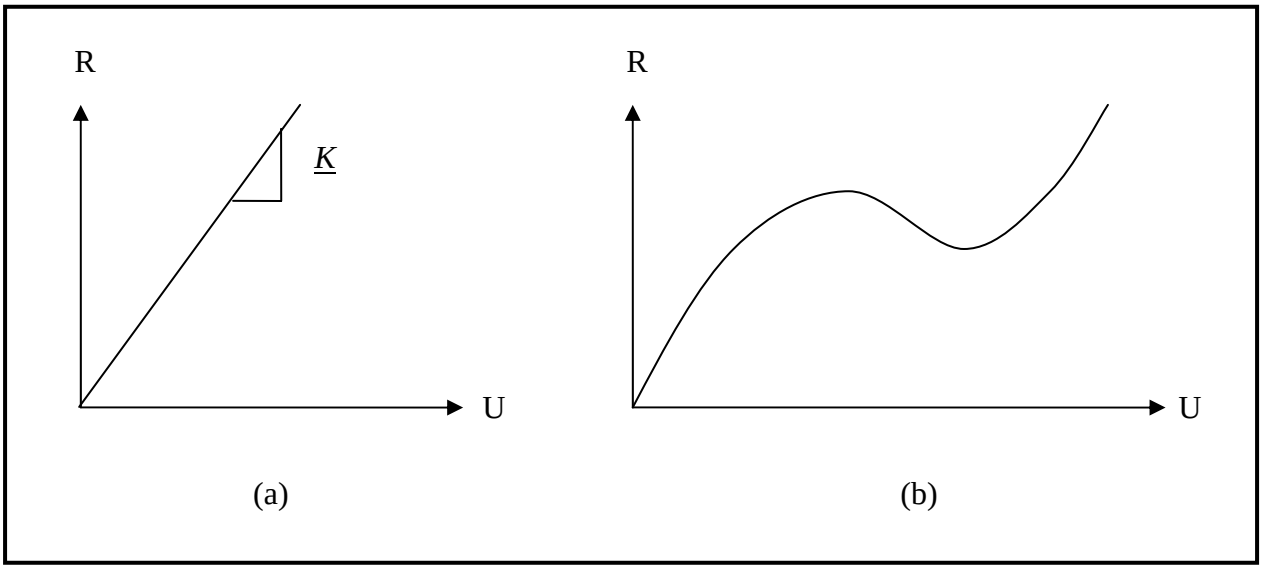

Figure 4.12 Load-displacement curve for an example single degree of freedom system depicting: (a) linear; and (b) nonlinear behavior.

Previously, in Section 3.1, Equation (3.2) was presented as the condition necessary to satisfy equilibrium in a loaded structure. While not explicitly stated in the previous discussion, the application of this equation was predicated on a linear relationship between the applied loads and the resulting structural displacements; this relationship takes the form of the global structural stiffness matrix, $\underline{K}$, and is illustrated in Figure 4.12(a).

When considering a problem for which this linear relationship does not apply (as is the case in Figure 4.12(b)) an alternative approach must be employed. This alternative approach is based on the incremental solution of linearized equilibrium expressions formulated in force-displacement space. In adapting this incremental approach, the equilibrium condition specified in Equation (3.2) is then reduced to the following:

$$ {}^{t+\Delta t}\underline{R} - {}^{t+\Delta t}\underline{F} = \underline{0}, \tag{4.8} $$

where t represents the "time" for which the solution is known, Δt represents the additional increment in "time" at which a solution is desired, ${}^{t+\Delta t}\underline{R}$ are the applied loads for which equilibrium is desired and ${}^{t+\Delta t}\underline{F}$ are the nodal point forces corresponding to the element stresses in the equilibrium configuration being sought. Here, time is used only for convenience in notation (i.e. we are focusing on a static problem, and this time is used for book-keeping with regard to the evolution of the applied load during the incremental solution process). Figure 4.13 illustrates this incremental approach in a more detailed way for the same single degree of freedom system, depicted in Figure 4.12(b).

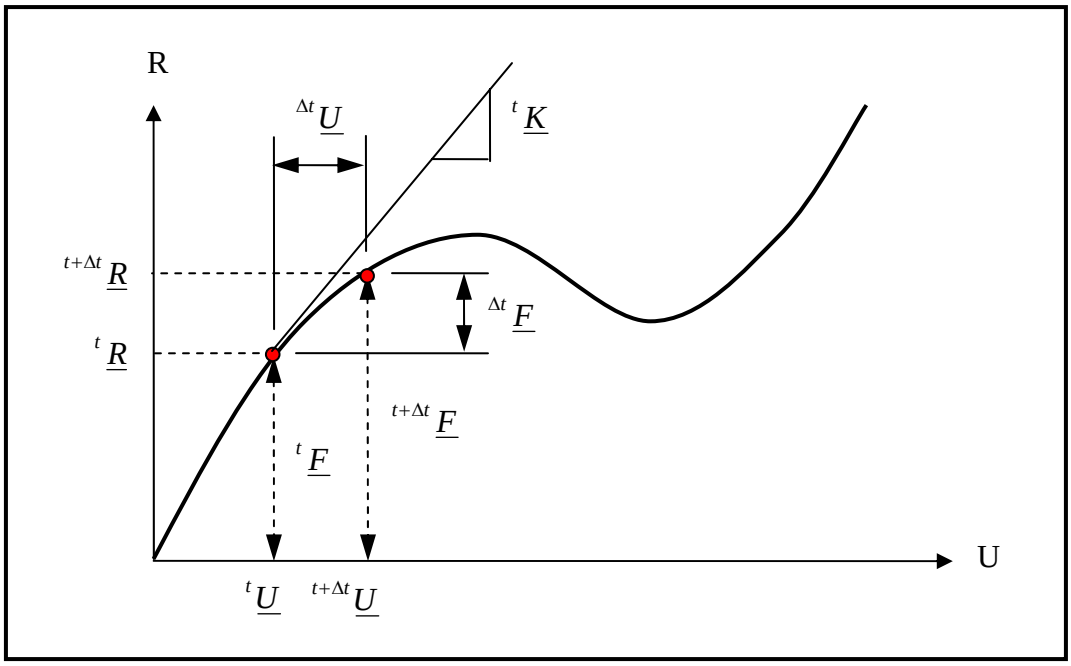

Figure 4.13 Conceptual illustration of a nonlinear finite element analysis approach.

Arriving at this unknown solution on the equilibrium path, by referencing the last known solution, is achieved through an approximation of the incremental system response, as follows:

$$^{\Delta t}\underline{F} = {}^{t}\underline{K}\,{}^{\Delta t}\underline{U}\,, \tag{4.9}$$

where $^{\Delta t}\underline{F}$ are the reactive nodal point forces balancing the externally applied load ($^{t+\Delta t}\underline{R}$), $^{\Delta t}\underline{U}$ are the incremental nodal displacements, and $^{t}\underline{K}$ is the "tangent stiffness matrix." As is clear from Figure 4.13, the tangent stiffness matrix is the derivative of the nodal point forces with respect to the nodal point displacements at the known solution time (i.e. the Taylor series expansion of the equilibrium response about last known equilibrium configuration).

Substituting Equation (4.9) into Equation (4.8), one arrives at an equilibrium condition which more closely represents that of Equation (3.2):

$$^{t}\underline{K}\,{}^{\Delta t}\underline{U} = {}^{t+\Delta t}\underline{R} - {}^{t}\underline{F}\,. \tag{4.10}$$

The nodal displacements with respect to the unknown solution, ${}^{t+\Delta t}\underline{U}$, are then obtained through the addition of the incremental nodal displacements obtained from Equation (4.10) and the nodal displacements from the known solution at time *t*.

A formalization of the foregoing is embodied within the so-called "Newton-Raphson" solution strategy. The Newton-Raphson technique for iteratively solving for a nonlinear equilibrium path is one of the more common ways to treat material as well as geometric nonlinearity within a finite element framework.

4.3.1 Newton-Raphson iteration scheme

The Newton-Raphson iteration scheme is best explained through the presentation of two equations and a figure which illustrates how these equations are related. Equations (4.10) through (4.12) may be employed in conjunction with Figure 4.14 to illustrate this technique:

$${}^{t+\Delta t}\underline{K}^{(i-1)}\,\underline{\Delta U}^{(i)} = {}^{t+\Delta t}\underline{R} - {}^{t+\Delta t}\underline{F}^{(i-1)}, \quad i = 1, 2, 3, \ldots, \text{n (iterations)} \tag{4.11}$$

$${}^{t+\Delta t}\underline{U}^{(i)} = {}^{t+\Delta t}\underline{U}^{(i-1)} + \underline{\Delta U}^{(i)}, \quad i = 1, 2, 3, \ldots, \text{n (iterations)} \tag{4.12}$$

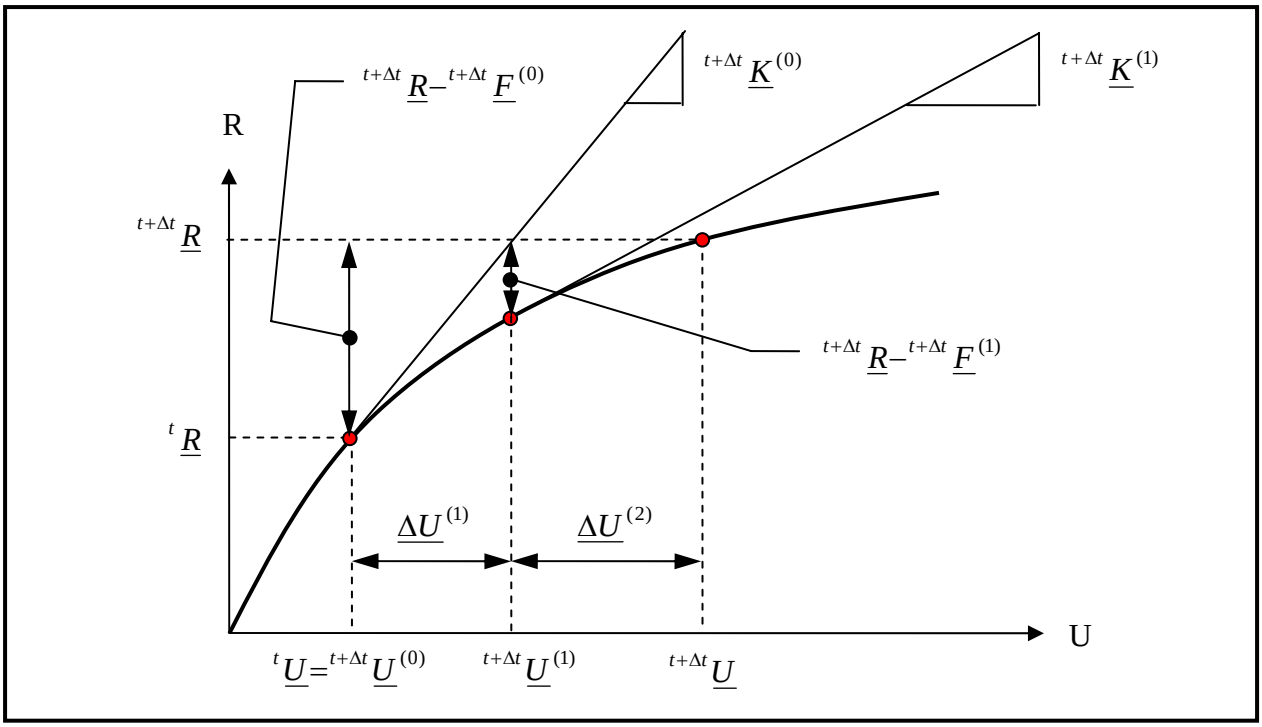

Figure 4.14 Conceptual illustration of Newton-Raphson iteration scheme.

Beyond the explanation provided by Figure 4.14, it is noted that convergence in this iterative strategy is measured by a quantity known as the "residual:" $^{t+\Delta t}\underline{R}-{}^{t+\Delta t}\underline{F}^{(i-1)}$, where the ideal solution would result in this expression equating to the zero vector [Bathe, 1996]. It is often sufficient to impose a threshold value to which this expression is compared, after each iteration. Upon satisfaction of this threshold criterion, the solution is deemed accurate, and the analysis may continue (if so desired) to the next load increment. It is important to keep in mind that this threshold is model-specific in nature, and therefore should be adjusted as necessary to arrive at a reasonably accurate solution, in the most computationally effective manner possible.

4.4 MODEL BUILDING STRATEGIES

The proceeding chapters are dedicated to the presentation and discussion of the results obtained from the finite element models discussed in the forgoing, and while this forms the primary focus of the current work, it is of significant benefit to the reader that the model building strategies employed throughout also be reported upon. Considering the author had little prior experience with ADINA or any other FEA software package, trial and error forms the primary source of information with regard to the development of these model building strategies. Furthermore, it should be understood that the model building strategies discussed herein most efficiently apply to the following situations: models which exhibit some amount of component recurrence and / or what can be termed as "trial models."

Component recurrence refers to situations which involve the modeling of entire structures where the repetitious nature of adding components to the model lends itself to the development of an automated procedure to perform these activities. Trial models are those which may not be finalized with regard to mesh density, geometrical properties, etc.; where modification of these properties becomes increasingly difficult with the increasing complexity of the model. This again would lend itself to an automated procedure where modifying a few key parameters would update the entire model; precluding the need to pour through each component individually.

The primary means of this automation is through the development of input files (.IN). These are typically ASCII-text files which house the program-specific commands necessary to construct a model (i.e. they act as scripts for ADINA-AUI to build the models); eliminating the need to interact with the often cumbersome graphical user interface (GUI). While the program-specific commands discussed herein apply directly to the commercially available FEA software

package, ADINA, it is the *strategy* which is being emphasized; upon understanding the key points of this strategy, one can easily apply it to similar software packages.

A final note which should be made before continuing is that the modeling strategies discussed herein apply to models constructed through the use of geometry tools (as opposed to the direct input of finite element mesh data). This essentially breaks the construction into two phases: the development of the model's physical geometry and the application of a finite element mesh to this geometry. While the generation of finite element meshes by manually defining all nodes, elements, etc. allows more control over element designations, locations, etc.; this modeling approach assumes a number of known parameters which are not always available prior to construction.

By utilizing the available geometry tools, the "auto-mesh" features available in ADINA may be employed which allow for the rapid generation of the associated finite element meshes on top of assigned geometric entities. Furthermore, the development of the physical geometry serves as an aid to visualize the model in its entirety prior to the application of the finite element mesh. What follows is a description of the advantages, as well as recommendations for improvement, with regard to the associated geometry tool commands which, when combined, make up the main part of the input file (.IN). Appendix F of this thesis contains samples of these files for use as learning tools and / or methods to construct similar finite element models. As the use of these geometry tools does have its drawbacks when compared with the direct input of the finite element mesh topology, Sub-Section 4.4.2 is included to elucidate these drawbacks.

4.4.1 Important aspects of input file generation

The most important part of developing an input file is organization. Keep in mind that the purpose behind this approach is to automate the replication or modification of various components in the model; without keeping track of the thousands of command lines in a typical file, one quickly defeats this purpose. The most effective means of organization employed by the author was the subdivision of individual operations into separate worksheets in an Excel workbook. For example, one section might apply to the construction of cross-sectional geometry while another section might apply to the generation of the finite element mesh, etc. The separation of these operations provides both a systematic approach to the construction of the model and an avenue by which problems with this construction can be quickly diagnosed. Figure 4.15 provides a sample of the operation subdivisions employed in the construction of the shell finite element model.

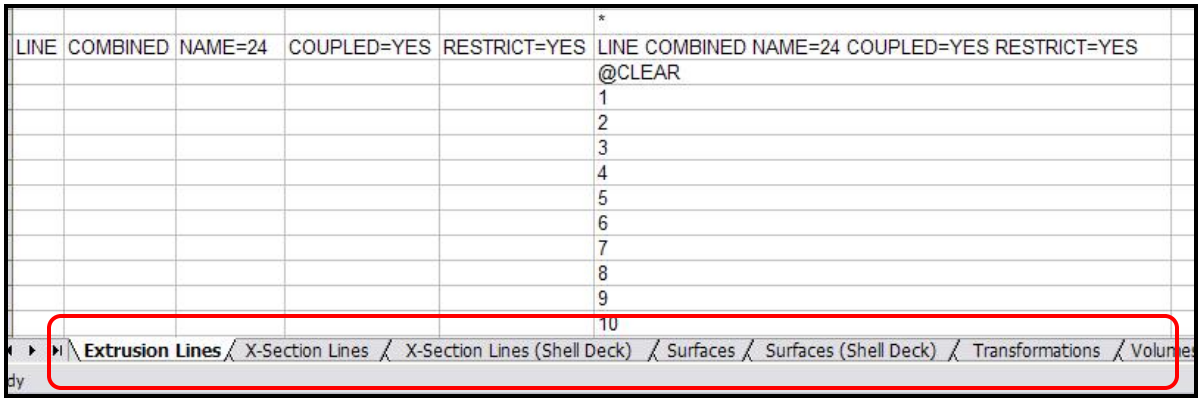

Figure 4.15 Example of subdividing tasks in model construction.

Having stressed the organization aspect of this approach, the following contains an overview of the procedures which save the most significant amount of time in constructing a

finite element model. The most basic, but least trivial of these procedures involves the designation of initial points throughout the model. Discipline taken with both the location of these points *and* the adopted numbering scheme allows for the most automated model construction. Furthermore, it is likely that a single point can be utilized for a number of operations throughout the model. When properly understood, this sort of repetitious use can directly apply to resolving mesh discontinuity issues which may arise as a result of using the geometry tools.

Another useful command in ADINA is the "transformation" command. While this command is used in a number of operations in ADINA, the copy (or "translation") function within this command is of significant importance to the user. Using a point-to-point translation, one can simply copy repetitious components to specified locations throughout the model. For example, in a bridge finite element model, it is likely that a number of cross-frame connector plates need to be included to properly model the cross-frame action in the bridge. While one could create each of these plates individually, it is far more efficient to construct only one plate at a single point and then copy this plate to the appropriate locations (previously defined points). The creation of these individual point-to-point transformations can also be automated which again emphasizes the need to incorporate a regular numbering scheme when assigning point coordinates. An example of this is given in Figure 4.16, where it is important to note the regularity in the numbering of Column H.

	A	B	C	D	E	F	G	H	I
1	TRANSFORMATI	TRANSLATION	NAME=1	MODE=POINTS	P1=	373	P2=	372	TRANSFORMATI TRANSLATION NAME=1 MODE=POINTS P1=373 P2=372
2									*
3	TRANSFORMATI	TRANSLATION	NAME=2	MODE=POINTS	P1=	373	P2=	398	TRANSFORMATI TRANSLATION NAME=2 MODE=POINTS P1=373 P2=398
4									*
5	TRANSFORMATI	TRANSLATION	NAME=3	MODE=POINTS	P1=	373	P2=	399	TRANSFORMATI TRANSLATION NAME=3 MODE=POINTS P1=373 P2=399
6									*
7	TRANSFORMATI	TRANSLATION	NAME=4	MODE=POINTS	P1=	373	P2=	400	TRANSFORMATI TRANSLATION NAME=4 MODE=POINTS P1=373 P2=400
8									*
9	TRANSFORMATI	TRANSLATION	NAME=5	MODE=POINTS	P1=	373	P2=	401	TRANSFORMATI TRANSLATION NAME=5 MODE=POINTS P1=373 P2=401
10									*
11	TRANSFORMATI	TRANSLATION	NAME=6	MODE=POINTS	P1=	373	P2=	402	TRANSFORMATI TRANSLATION NAME=6 MODE=POINTS P1=373 P2=402
12									*
13	TRANSFORMATI	TRANSLATION	NAME=7	MODE=POINTS	P1=	373	P2=	403	TRANSFORMATI TRANSLATION NAME=7 MODE=POINTS P1=373 P2=403

Figure 4.16 Transformation commands for point-to-point translation.

Figure 4.16 gives an example of another useful tool in the creation of input files: the "concatenate" function in Excel. Most are familiar with the drag-and-fill or drag-and-copy features in Excel, and while these are convenient functions for individual line items, it is unlikely that entire lines of ADINA commands will behave as desired. By splitting up the various components of the command, modifying the key variable components (names, point numbers, etc.), and then concatenating them, one saves the time required to modify each line of code in the file. Again, it becomes apparent that by maintaining an efficient numbering scheme, one could also eliminate the need to drag rows of data by imbedding equations to update entire columns (which are associated with multiple lines of code) by changing a single number.

Similar steps may be applied to most any command utilized in the construction of a finite element model, e.g. the creation of lines, surfaces, etc. As with points, it is also important to apply a disciplined numbering scheme when creating lines, surfaces, volumes, etc. Doing so allows for a continued ease of automation when merging the command structure of ADINA with the drag-and-fill options available in Excel.

A final group of functions particular to the construction of shell finite element models stems from the creation of the girders (and deck, if so desired) in ADINA; of which "extrude" is the overriding function. The extrude function is not a standalone command, but is rather an

option available to the user when creating individual geometric components in the model (lines, surfaces, etc.). For example, the extrusion of a point will yield a line; the extrusion of a line will yield a surface, etc. By using this function, one eliminates the need to create a multitude of lines and subsequent surfaces in order to construct an individual beam. Instead, one creates a single cross-section of the beam by connecting predefined points with lines and then extruding this group of lines along a vector or a previously created "extrusion line."

Where a vector is only a magnitude in a single direction, the advantage of an extrusion line lies in the option of defining it as a series of combined lines. Essentially, an extrusion line is a further automation of the extrude function. While these lines can govern the direction of an extrusion, they can also be designed to provide "breaks" in the extrusion. These breaks are achieved by defining the extrusion line as a combination of two or more lines where the common endpoints create the aforementioned break. Breaks essentially provide a "joint" in the finite element mesh where nodal connectivity may be insured. Such joints are useful when considering girder to cross-frame connections where coincident nodes would preclude the need to define individual constraint equations for each connection. Figures 4.17 and 4.18 illustrate such a case.

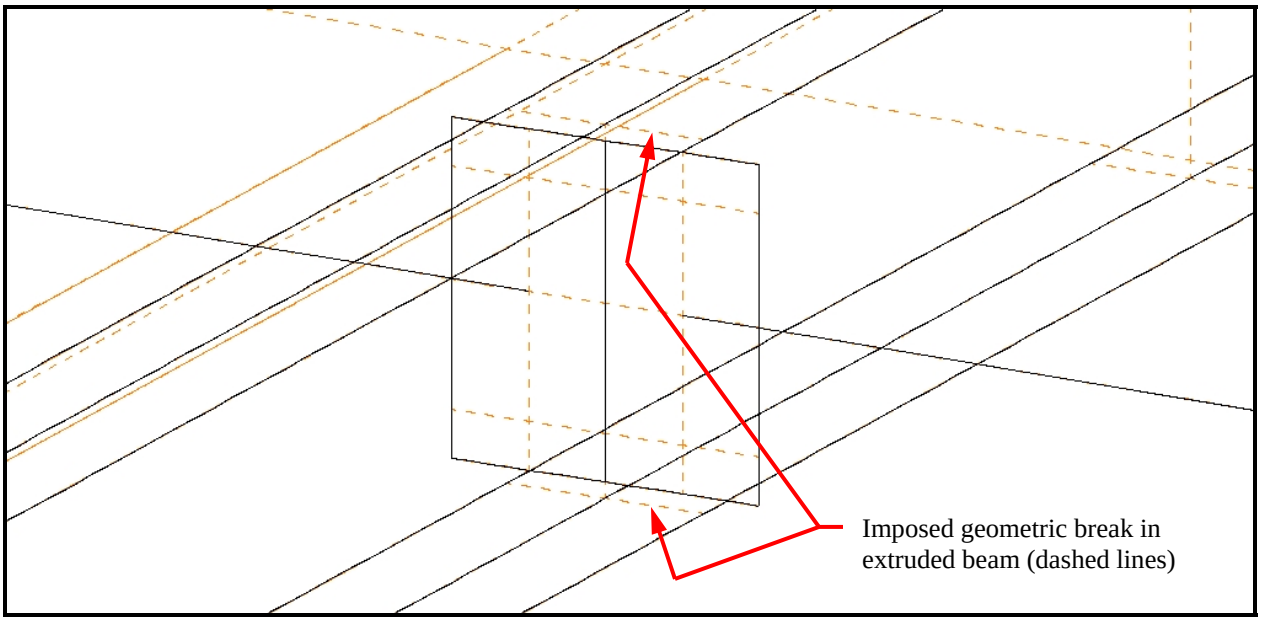

Figure 4.17 Geometry showing break in beam at cross-frame connection.

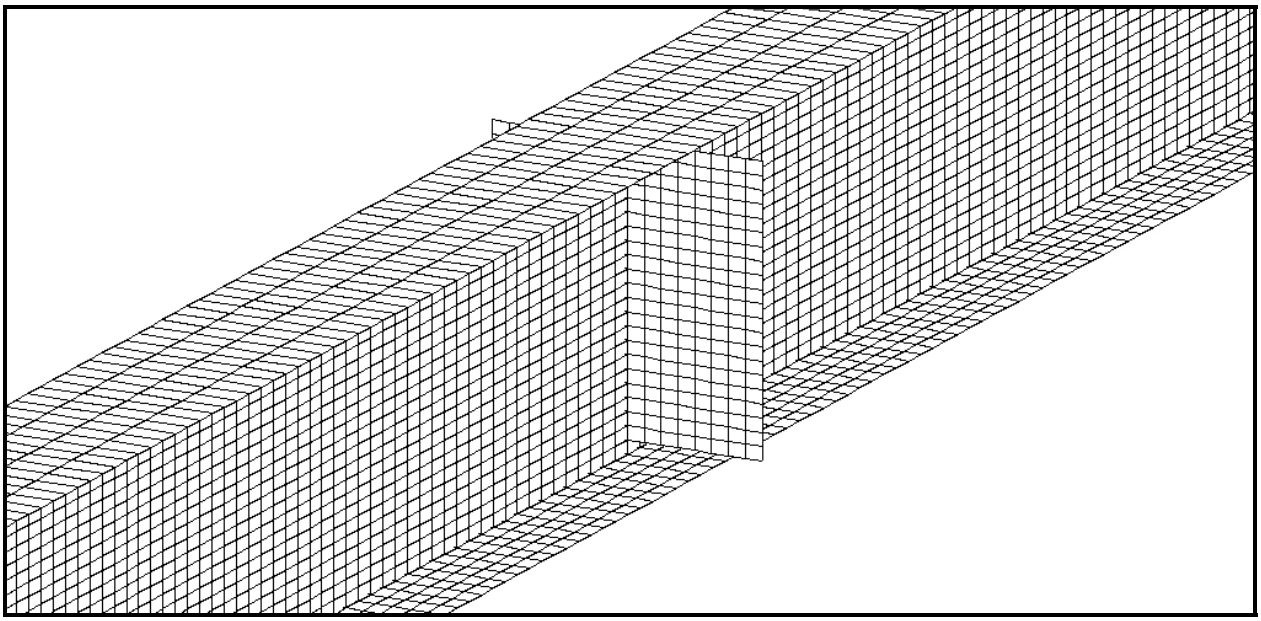

Figure 4.18 Resulting *auto-generated* finite element mesh.

Another notable advantage extrusion lines provide comes from the imposed breaks being used as a method to vary shell thickness properties in non-prismatic members (cover plates, splice plates, etc.).

Thus far, the input file has been implied as a tool to construct a finite element model in its entirety. However, it is probably the automation of individual operations which is of the most benefit. Consider the combination of commands utilized to modify the mesh density of a given shell finite element model. Through the GUI, one would be required to first discern which geometric components require modification; these groups of elements would then be deleted. Following deletion, these components would then be re-subdivided and then re-meshed. Consider now, the application of these steps to a complicated model, and one can quickly appreciate the automation afforded through the use of the input file. Understanding where the geometric components lie enables the user to execute all of these steps automatically.

4.4.2 Drawbacks of the modeling approach

While one gains a significant potential for the automatic creation of a finite element model by employing the available geometry tools, there is a major disadvantage to using these tools: irregular node and element numbering. When considering a relatively simple model such as a portal frame, this is of little consequence. It is situations involving shell finite element models with a myriad of components for which this is a major problem; moreover, it is the use of the aforementioned extrusion lines which cause the majority of this problem.

As previously discussed, extrusion lines are most advantageous when employed to create breaks in the extrusions. These breaks, however, impose that a single extruded geometric entity is actually a series of interconnected geometric components, which has an ADINA-assigned

numbering scheme. The key to solving this problem lies in the recognition of the pattern used by ADINA for this numbering scheme. Upon understanding this pattern, one can quickly apply a similar methodology to the node and element numbering schemes. The subsequent definition of "zones" within the finite element model facilitates this process by allowing the user to decipher only portions of the model as required; as opposed to attempting the difficult task of "mapping" the *entire* finite element mesh.

The final drawback associated with this modeling approach relates to the upfront time required to develop a typical input file. This is primarily due to the trial and error method of understanding the command syntax; each commercially available F.E.A. software package will have its own syntax. Keep in mind that one of the incentives to building an input file is that manually executed commands of a repetitious nature can be made automatic. Therefore, the syntax for a command (or function within a command) need only be ascertained once; replication and modification in Excel using the previously prescribed methods then follows.

With regard to ADINA, however, it is the intent of the author to partially eliminate this problem by providing the reader with sample input files utilized in the construction of the shell finite element model employed in this work. Found in Appendix F are select lines of code which the reader may use directly or modify as required to develop the desired model. Keep in mind that the sample input files given are only a small portion of that utilized to construct the entire model. Typical input files developed by the author have exceeded ten thousand lines of code; however, by using the tools available in Excel, the generation of these files is made with relative ease.

5.0 PRESENTATION AND DISCUSSION OF RESULTS

Following a detailed analysis of the results from all thirteen loading cases, it is deemed sufficient that the results from only six of these are presented in Chapter 5 so as not to convolute the main body of the thesis: these are Loading Cases 1 through 4, 10, and 13 (see Section 2.2); the remainder appear in the Appendices. In considering Loading Cases 1 and 2, maximum vertical deflections and longitudinal bending moments are examined in Spans 1 and 2, respectively. Load Cases 3 and 4 provide insight into the nature of the transverse distribution of deck loads to adjacent members. Results from Loading Case 10 allow for the examination of vertical reaction distributions in situations where applied loads occur at, and near, the structural supports. Finally, Loading Case 13, which induces a global torsion in the bridge, serves to demonstrate how the applied loads interact transversely within the model; warping torsional effects in the longitudinal members are not directly considered in this thesis. In addition to the presentation and discussion of these six loading cases, the reader is directed to Appendices A through E, for the results from the remaining seven loading cases are presented.

Conventions in notation that are employed within the current chapter are subsequently described. In the figures, modeling approaches are referred to as follows: “Grillage” - representing the grillage finite element model, “Continuum” - representing the continuum deck finite element model, and “Shell” - representing the shell deck finite element model. As briefly noted in Section 2.1, vertical reactions are obtained for: Abutment 1 (west end abutment), Pier 1

(the westernmost pier), Pier 2 (the easternmost pier), and Abutment 2 (the east end abutment); Figure 5.1 is provided for clarity.

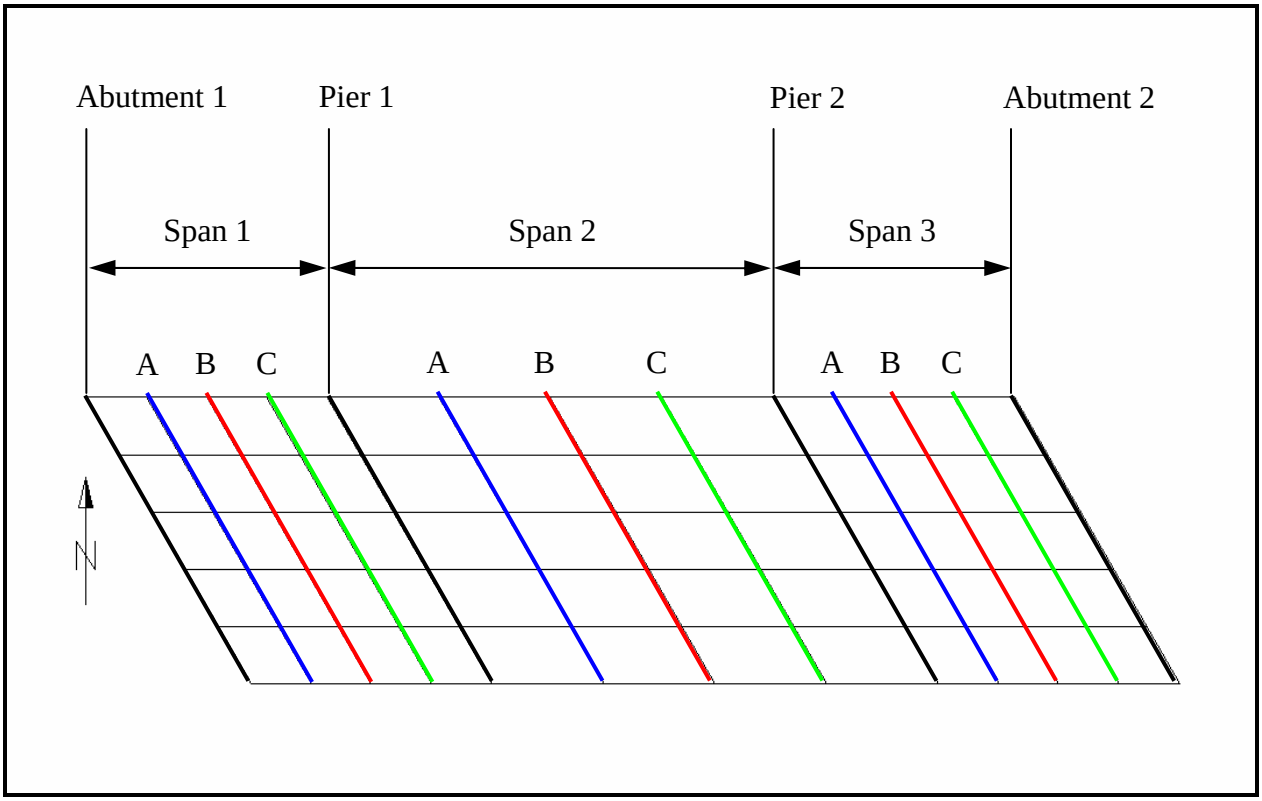

Figure 5.1 Referenced locations throughout bridge.

Vertical deflection and longitudinal bending stress profiles are obtained at the following locations: “Span X-A”, “Span X-B”, or “Span X-C” where “X” indicates the span number and “A,” “B,” or “C” indicate the longitudinal quarter-point at which the data are taken (see Figure 5.1).

Also within the figures, girders are referenced by “G” followed by a number with Girder 1 (G1) being the northernmost girder, and so on. “LC” followed by a number, “X” indicates Loading Case “X” (e.g. LC1 refers to Loading Case 1). Units employed throughout are as

follows: reactions are measured in kips, deflections are measured in inches, and stresses are measured in ksi.

5.1 VERTICAL REACTIONS

Vertical reactions for the grillage finite element model are obtained directly; as it is that boundary conditions in this model are applied to individual nodes at the appropriate locations along each girder. As discussed in Section 4.2.5, however, vertical reactions for the shell finite element models are computed by summing the 9 individual nodal reactions which compose the transverse shell element boundary line to which the boundary condition is applied. The figures in the following sub-sections illustrate vertical reaction distributions for the grillage and shell finite element models with respect to each of the six loading cases; a discussion then follows each set of figures. As noted previously, results from the omitted loading cases may be found in Appendix A.

5.1.1 Loading Case 1

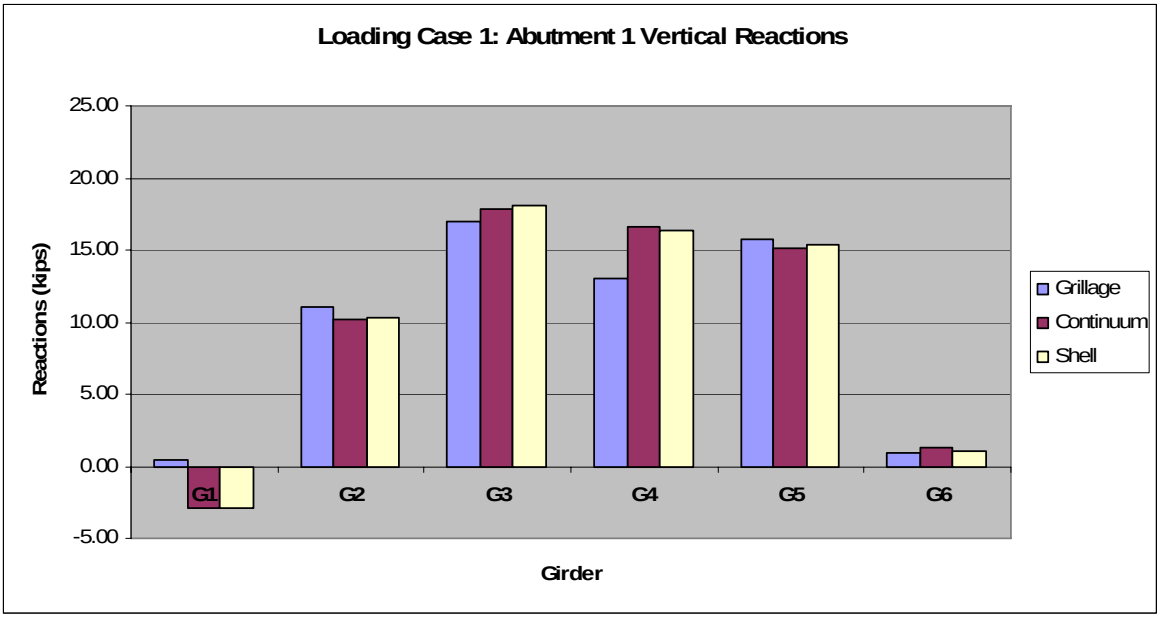

Figure 5.2 Loading Case 1: Abutment 1 vertical reactions.

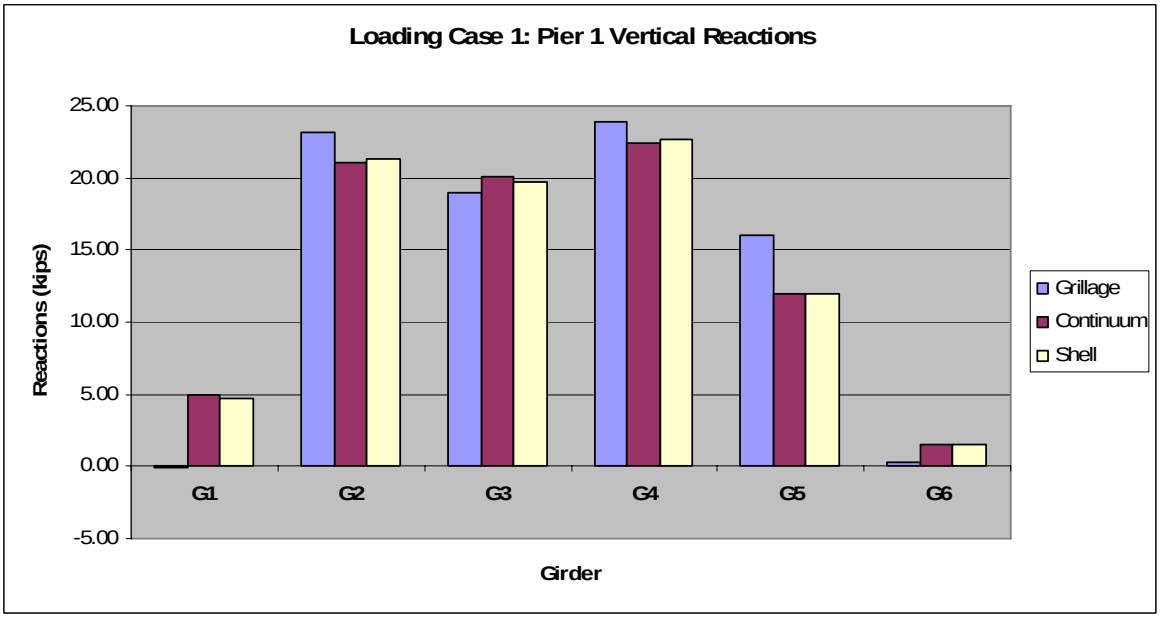

Figure 5.3 Loading Case 1: Pier 1 vertical reactions.

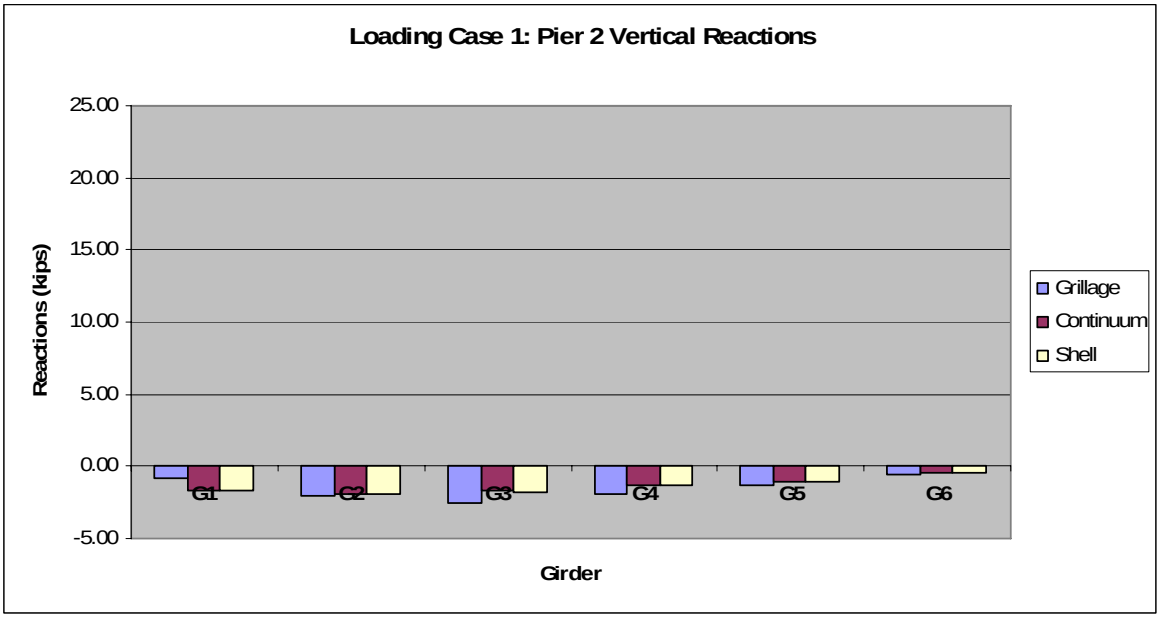

Figure 5.4 Loading Case 1: Pier 2 vertical reactions.

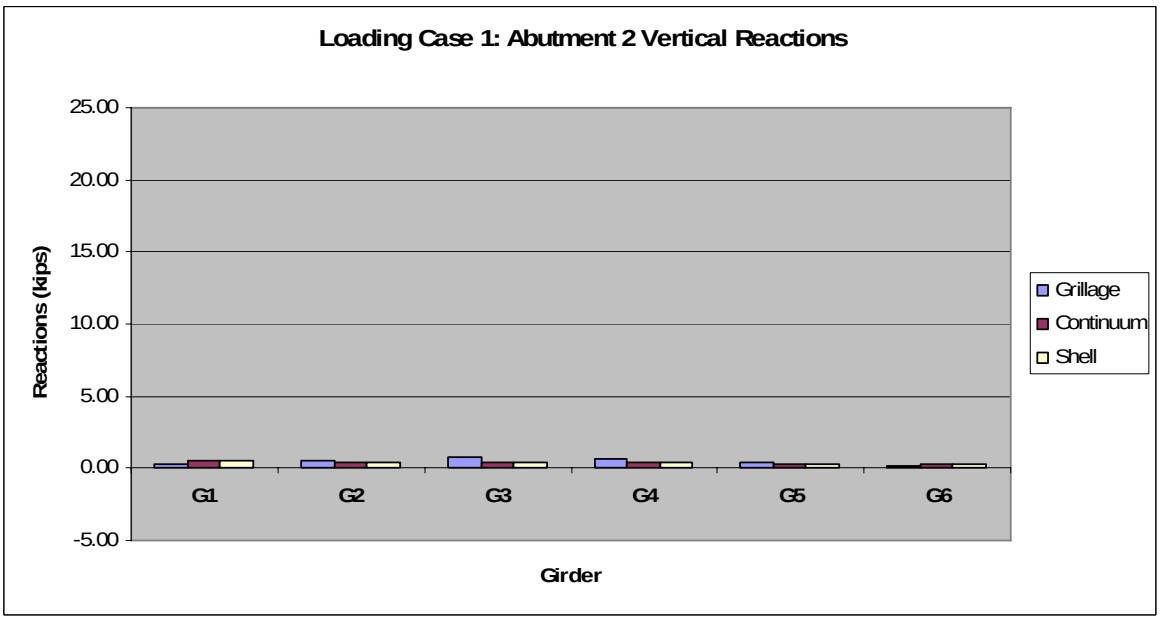

Figure 5.5 Loading Case 1: Abutment 2 vertical reactions.

Referring to Figures 5.2 and 5.3, the vertical reactions at G1 and G6 for the grillage finite element model are typically lesser in magnitude than those in the shell finite element models. It

is believed that behavior arises out of the grillage model lacking the more complete load distribution mechanism provided by the inclusion of the slab in the shell finite element models. Also evident in these figures are the discrepancies between the reactions in G2 through G5. In order to understand these discrepancies, it is necessary to explore the flow of forces through the various grillage members as well as the relative stiffnesses of regions within the longitudinal members; Figure 5.6 provides elucidation of these parameters.

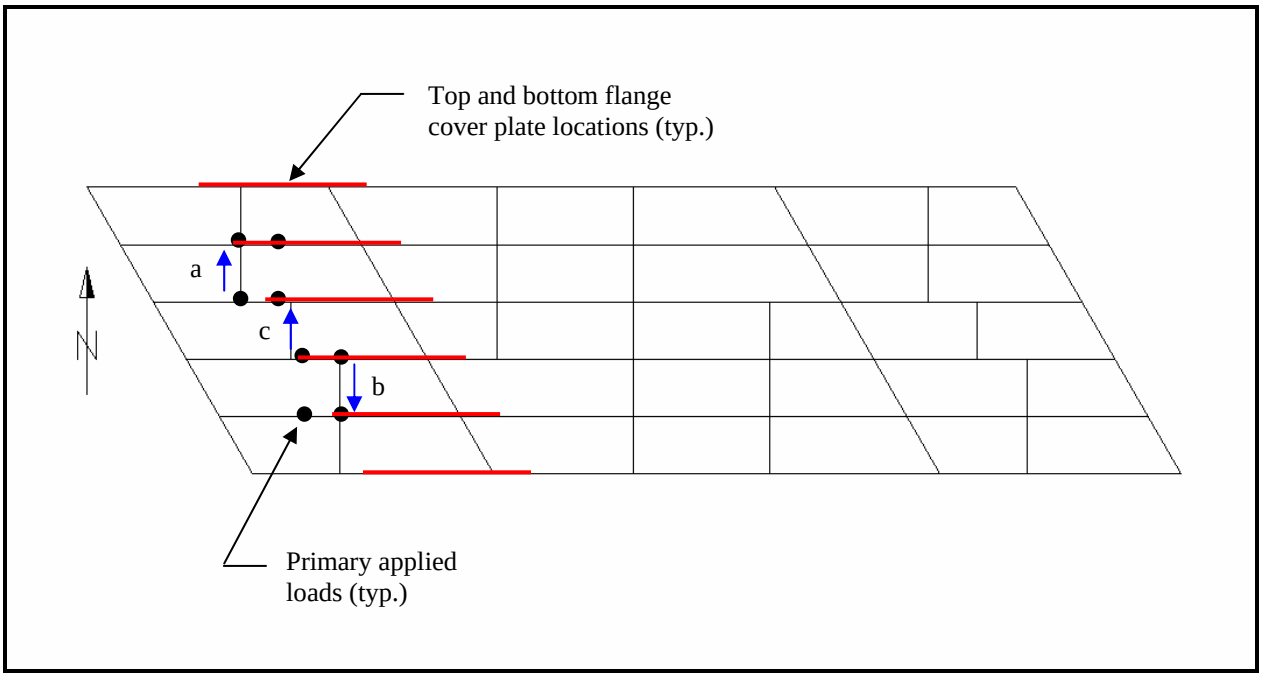

Figure 5.6 Load transfer mechanism exhibited in Span 1.

Due to the relative locations of the applied loads on G2 and G5, larger vertical reactions will be occur in Pier 1 and Abutment 1, respectively; this behavior is less pronounced in G5 due to the lower stiffness of the "bare" cross-section (i.e. the cross-section without cover plates). Furthermore, due to the transverse members at points "a" and "b" in Figure 5.6, a portion of the applied loads from G3 and G4 will transfer to G2 and G5, respectively. Considering the relative

locations of these transverse members, additional vertical forces must be equilibrated in G2 and G5 which is directly seen in Figures 5.2 and 5.3; again, due to the lower stiffness of the bare cross-section, G2 exhibits this behavior to a lesser degree.

The most interesting behavioral characteristic of the grillage finite element model for this loading case, however, comes from the transverse member at point "c" in Figure 5.6. Due to the relative stiffnesses of G3 and G4 at the respective intersections with this transverse member, more applied load is transferred to G3 than is transferred to G4. This is indicated in Figure 5.2 by the reduced reaction in G4 at Abutment 1; the increased reaction at Pier 1 is due to the location of the easternmost applied load. However, it happens that G3 exhibits little discrepancy between the shell finite element models; this occurs as a result of applied loads being transferred *to* G2 and *from* G4 which leads to an approximate zero net effect on G3.

5.1.2 Loading Case 2

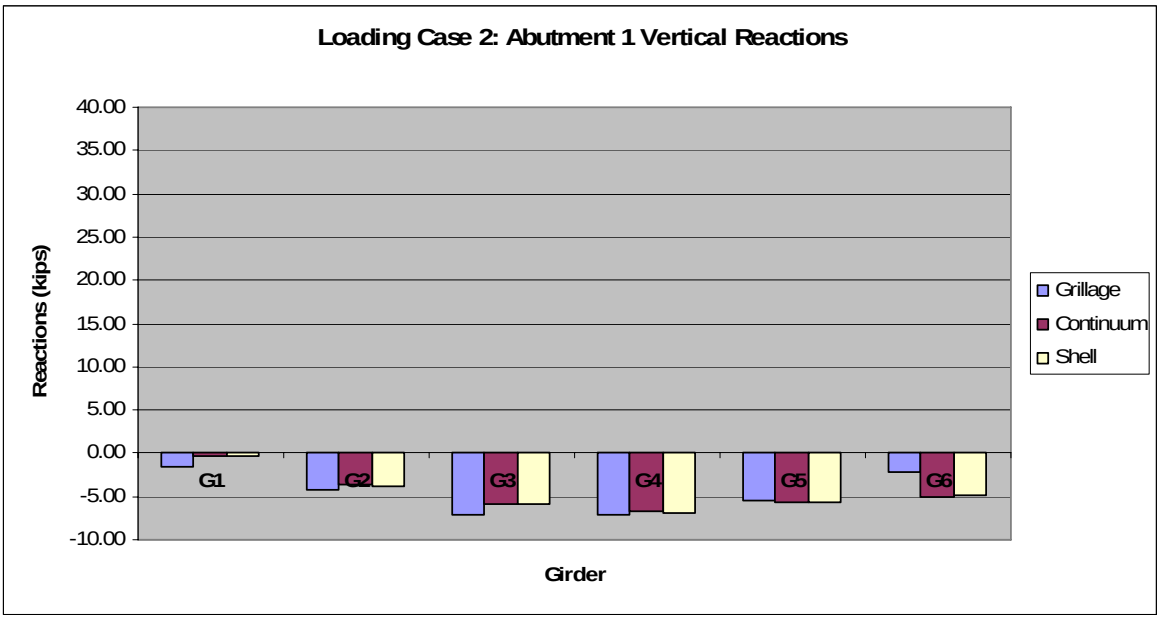

Figure 5.7 Loading Case 2: Abutment 1 vertical reactions.

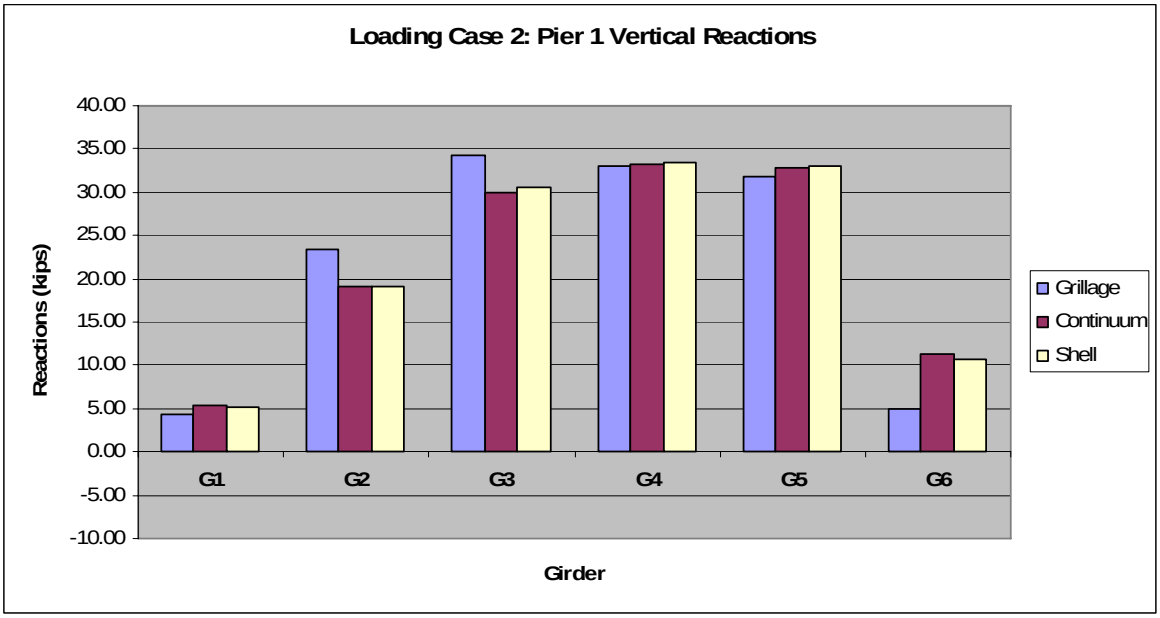

Figure 5.8 Loading Case 2: Pier 1 vertical reactions.

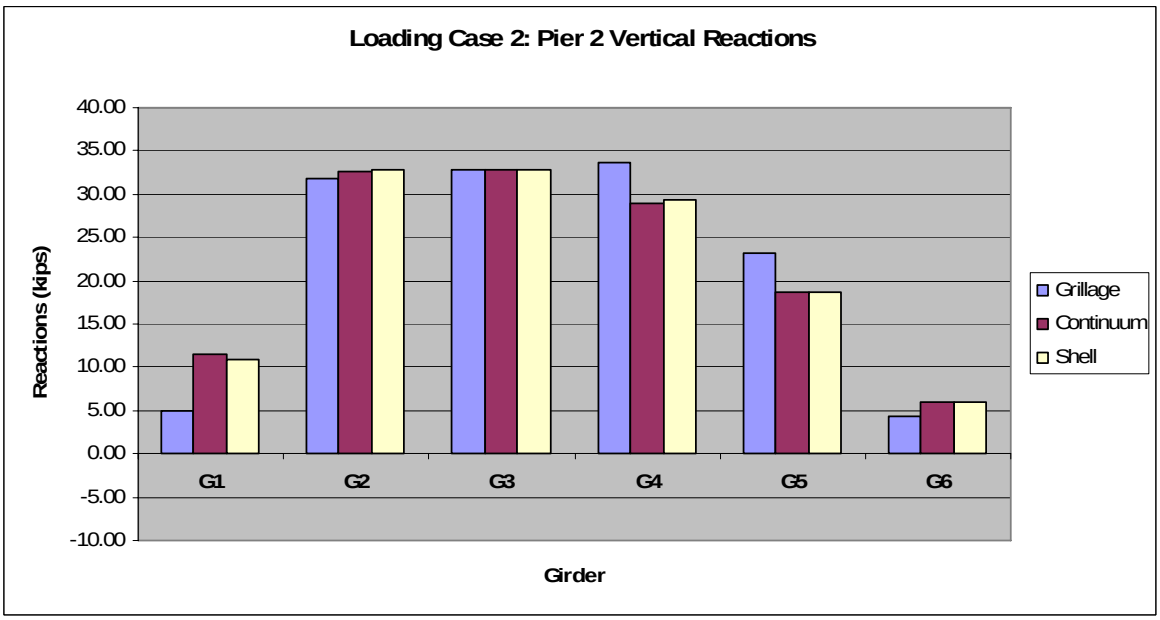

Figure 5.9 Loading Case 2: Pier 2 vertical reactions.

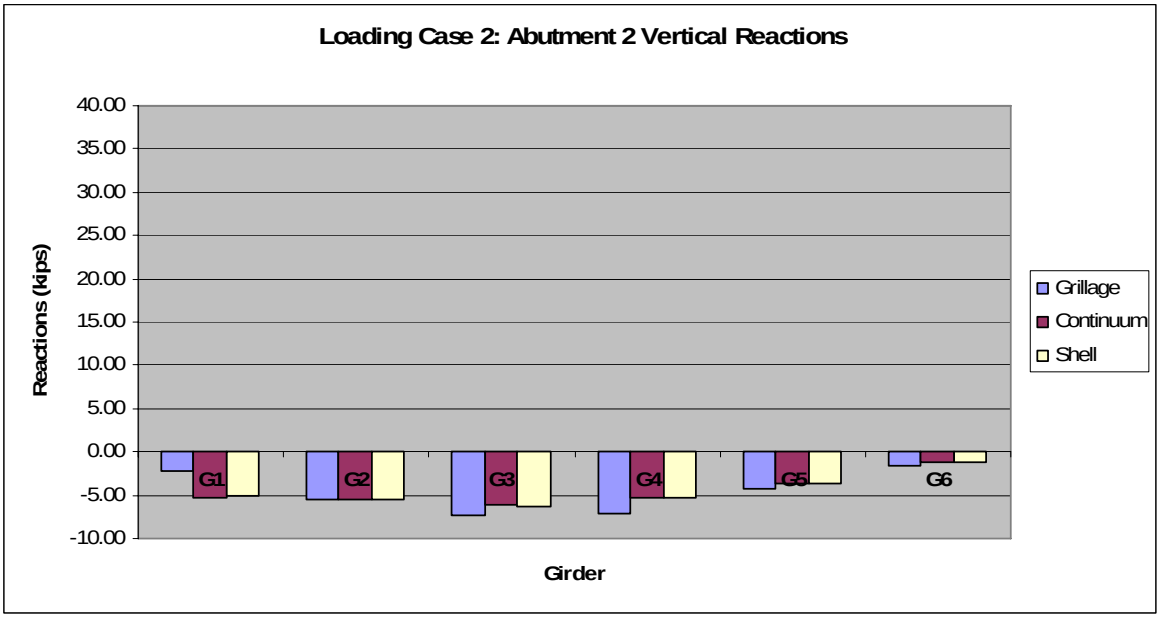

Figure 5.10 Loading Case 2: Abutment 2 vertical reactions.

In Loading Case 2, the discrepancies between the G2 / G3 vertical reactions at Pier 1 and the G4 / G5 vertical reactions at Pier 2 are of primary interest. Given that the longitudinal members in Span 2 are symmetrical with respect to the transverse bridge centerline, it is clear that the asymmetric configuration of the transverse members in this span results in the error in the grillage model. Essentially, the transverse members closest to the piers create a condition where the stiffnesses of the longitudinal members at the Pier 1 end are greater than those at the Pier 2 end for G2 / G3, and vice versa for G4 / G5; this is due to the added stiffnesses from the adjacent longitudinal members which is overestimated by the transverse members in the grillage finite element model.

Closer inspection of Figures 5.8 and 5.9 additionally reveals that the *relative* errors between the vertical reactions for G2 and G3 are *not* the same (i.e. the percentage increase as a function of the vertical reactions in the shell finite element models is not equal for G2 and G3).

However, as in Loading Case 1, G2 and G3 intersect the westernmost transverse members with and without cover plates, respectively (see Figure 2.1). This translates to the greater percentage of error found in G2 than in G3. Of course, the reverse of this condition applies to G4 and G5.

5.1.3 Loading Cases 3 and 4

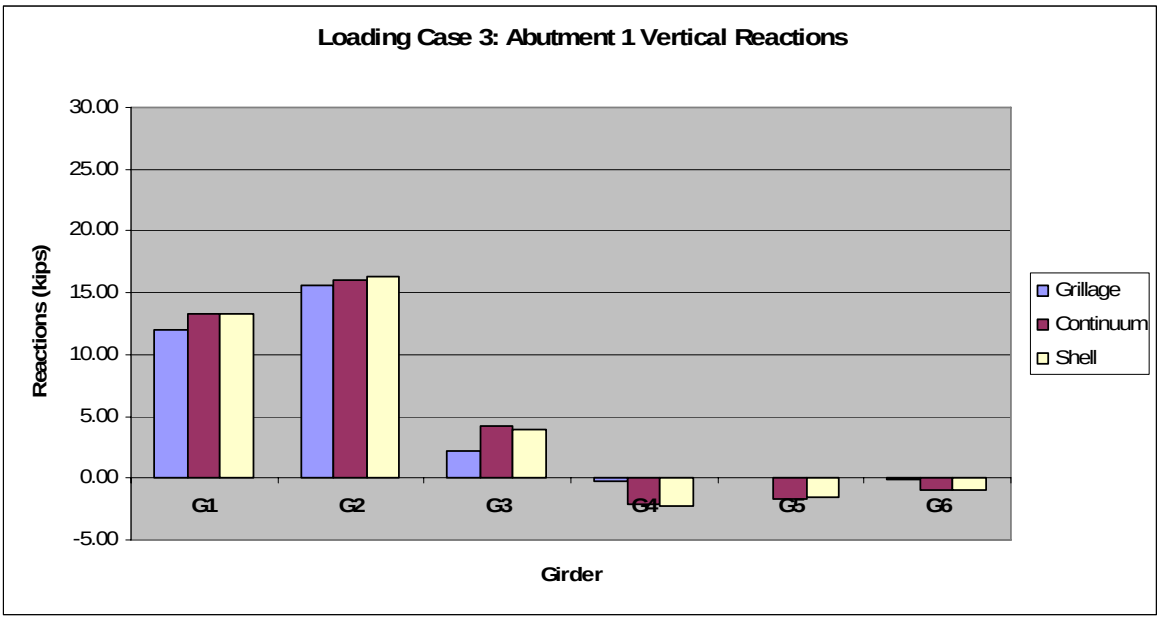

Figure 5.11 Loading Case 3: Abutment 1 vertical reactions.

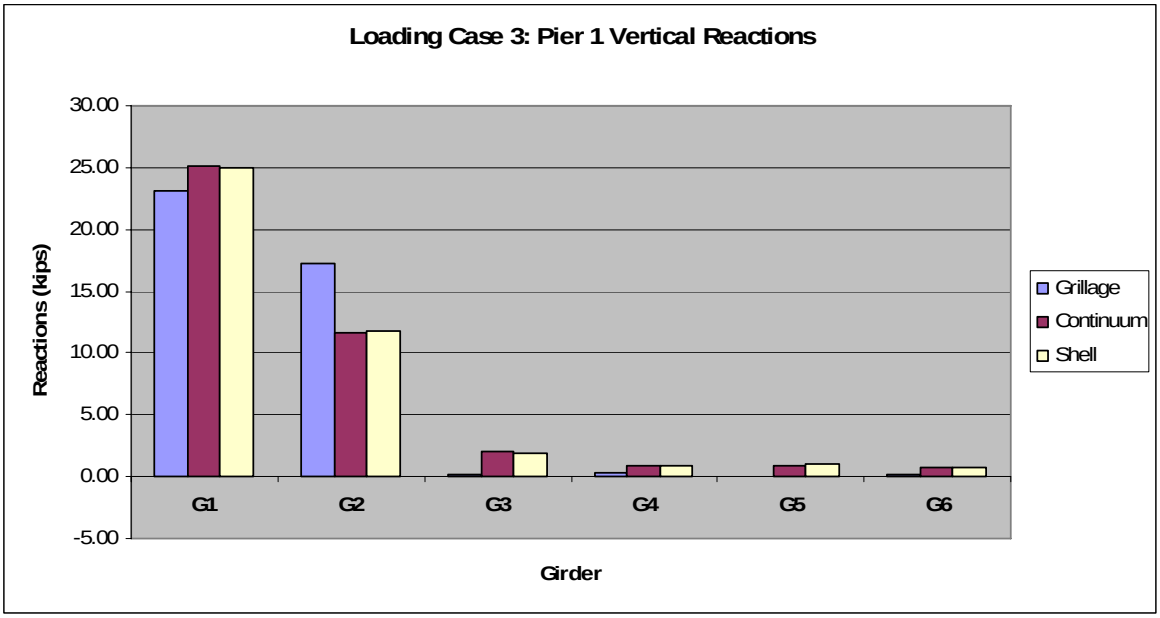

Figure 5.12 Loading Case 3: Pier 1 vertical reactions.

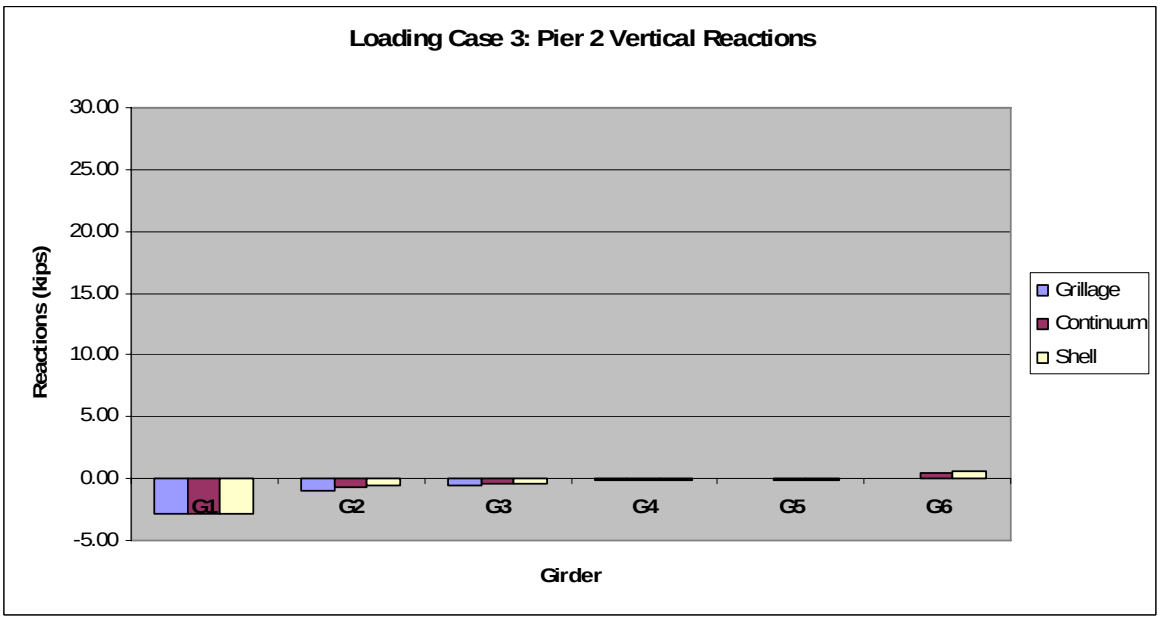

Figure 5.13 Loading Case 3: Pier 2 vertical reactions.

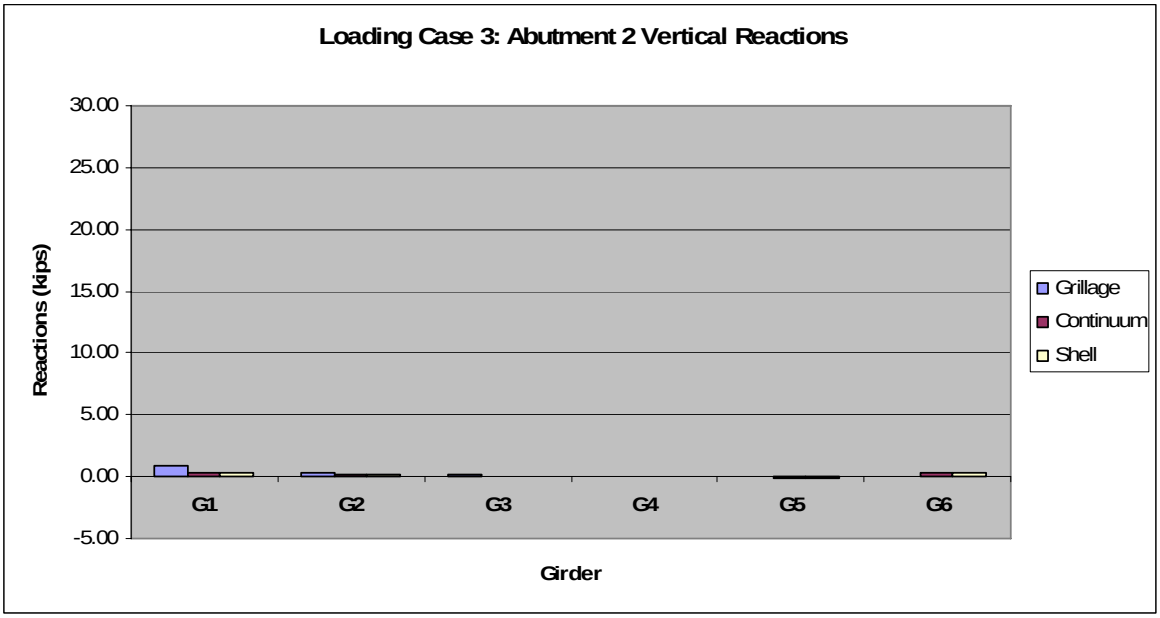

Figure 5.14 Loading Case 3: Abutment 2 vertical reactions.

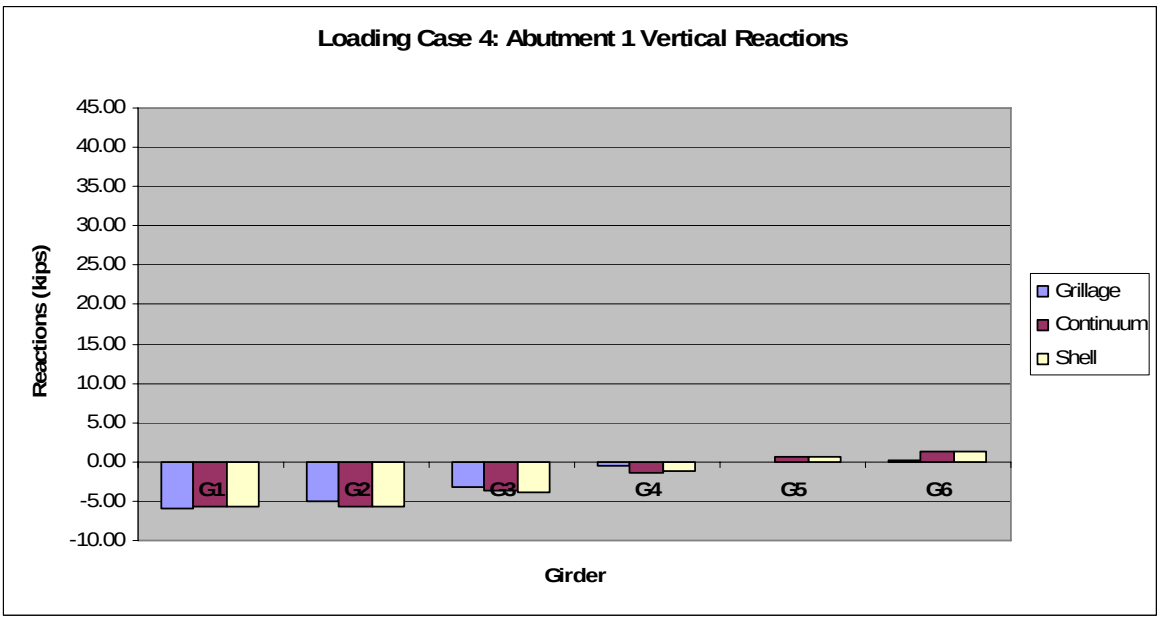

Figure 5.15 Loading Case 4: Abutment 1 vertical reactions.

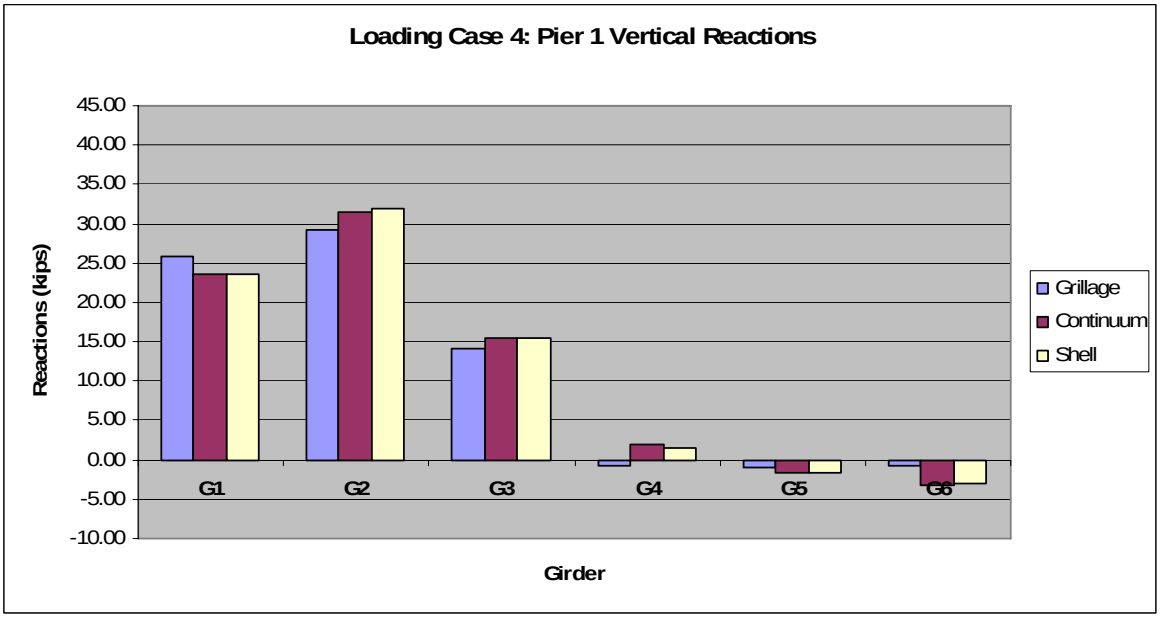

Figure 5.16 Loading Case 4: Pier 1 vertical reactions.

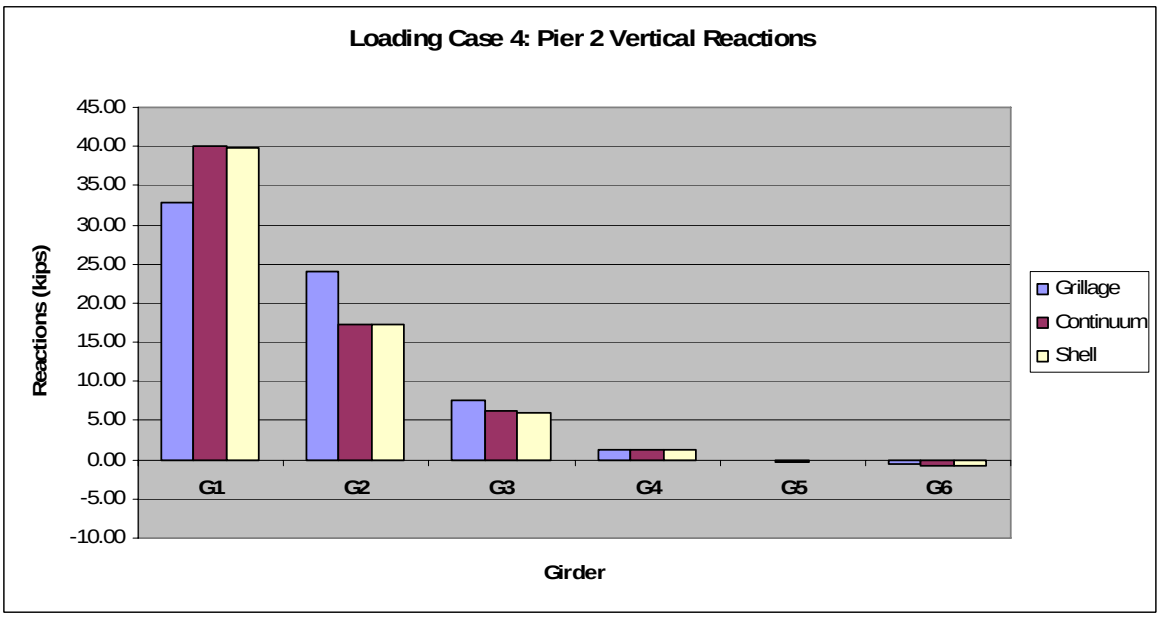

Figure 5.17 Loading Case 4: Pier 2 vertical reactions.

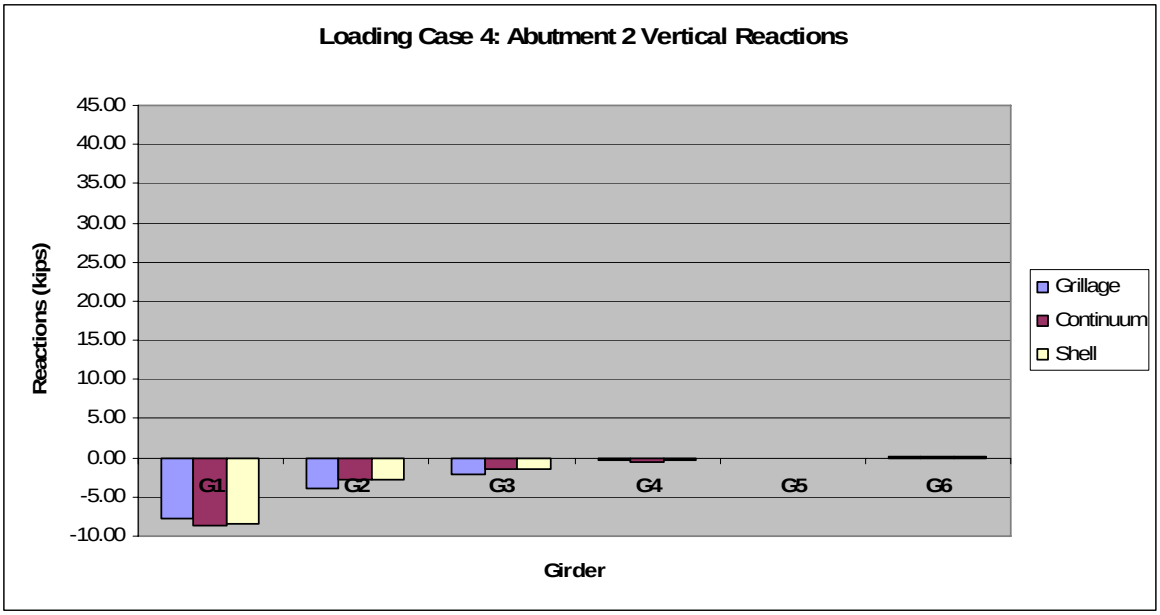

Figure 5.18 Loading Case 4: Abutment 2 vertical reactions.

Loading Cases 3 and 4 help to highlight the primary deficiency of the grillage finite element modeling approach as compared with the shell finite element models: the correct development of a transverse load distribution mechanism. In Figures 5.13 and 5.18, it is seen that the applied loads on G1 are actually distributed *to* G2; it is expected that the grillage model will err on the side of *not* distributing load to an adjacent member. However, the results presented herein show that errors in the load distribution mechanism for the grillage finite element model can actually be traced to two distinct behavioral characteristics: one which is more localized in nature and one which affects global structural system response.

The first of these is with regard to applied loads which are located at or near transverse member intersections. As noted above, these applied loads will tend to distribute *to* adjacent longitudinal members in the grillage. However, as compared with the shell finite element models, it is clear that the contributions from the transverse members are overestimated significantly in this case. The opposite behavior is of course seen when applied loads are located

away from transverse member intersections. Clearly, loads such as these are not sufficiently transferred to adjacent members which causes the vertical reactions located away from the applied loading to be lower in magnitude (as noted in Sub-Sections 5.1.1 and 5.1.2).

This type of behavior is of significant importance to the engineer for two reasons. In the first case, it is clear that due to the local transference of loads to adjacent members, internal forces within these adjacent members will be overestimated while the internal forces will be underestimated in the loaded girder. The reverse is true when considering the second case in which loads are not properly distributed to adjacent members. However, the consequences resulting from the latter case are of greater significance as the underestimation in response leads to a non-conservative design.

5.1.4 Loading Case 10

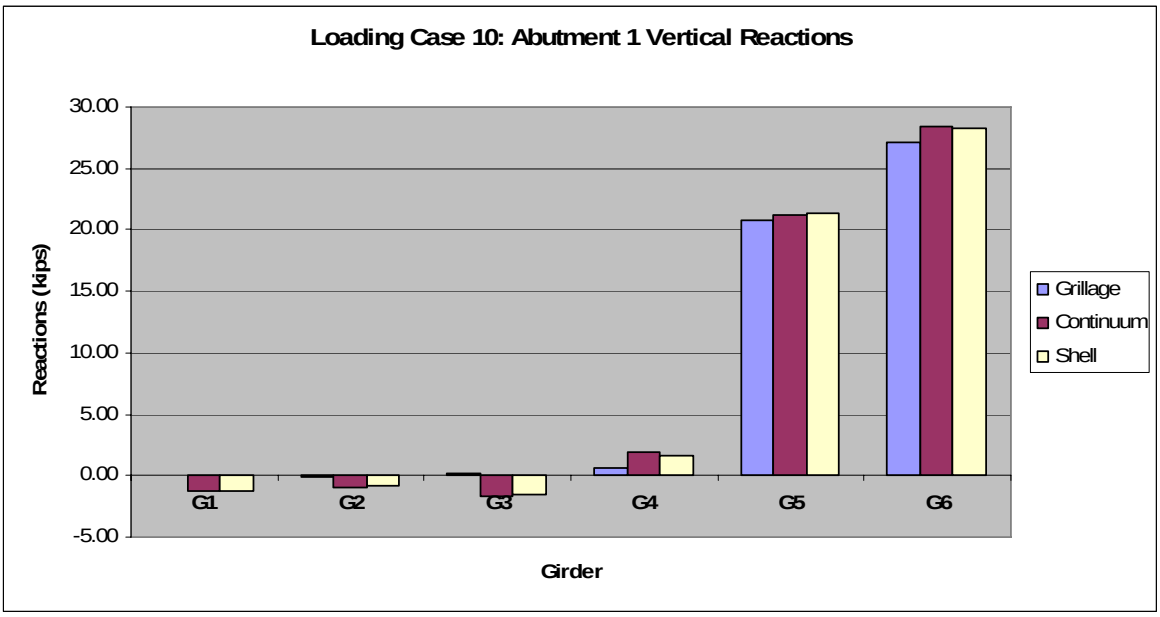

Figure 5.19 Loading Case 10: Abutment 1 vertical reactions.

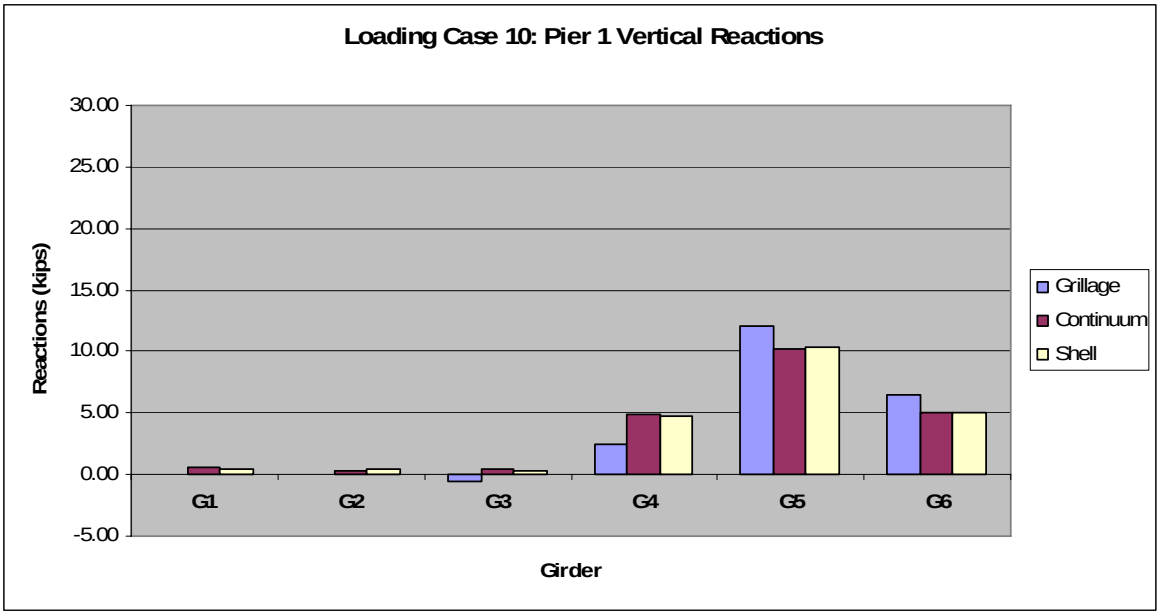

Figure 5.20 Loading Case 10: Pier 1 vertical reactions.

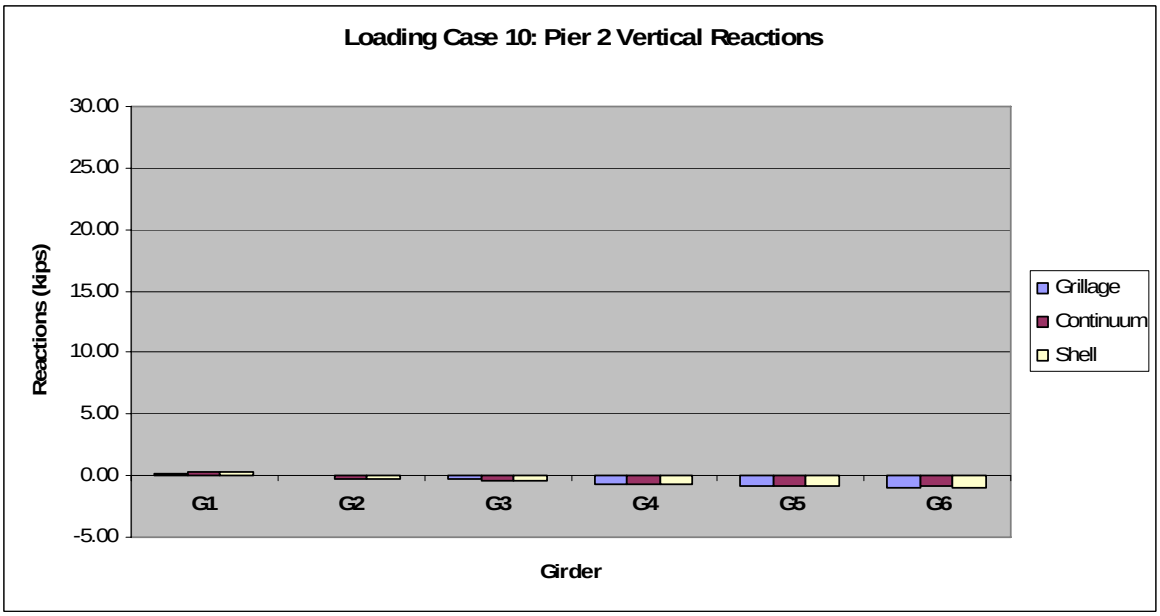

Figure 5.21 Loading Case 10: Pier 2 vertical reactions.

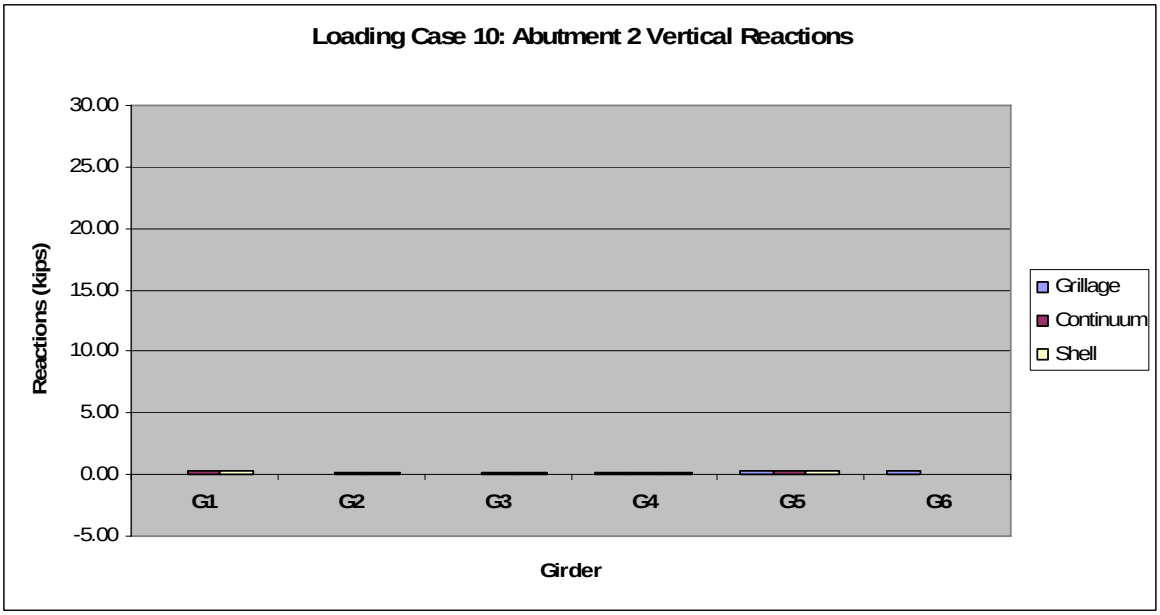

Figure 5.22 Loading Case 10: Abutment 2 vertical reactions.

Despite the fact that the applied loads are located a short distance from the structural supports (with respect to the span length), there are still significant discrepancies which emerge in Loading Case 10. It is apparent from the reaction distribution in Figures 5.19 and 5.20 that the single transverse member provided between the loaded girders, G5 and G6, and G4 in the grillage finite element model is not sufficient to generate the level of distribution exhibited by the shell models for this loading case.

5.1.5 Loading Case 13

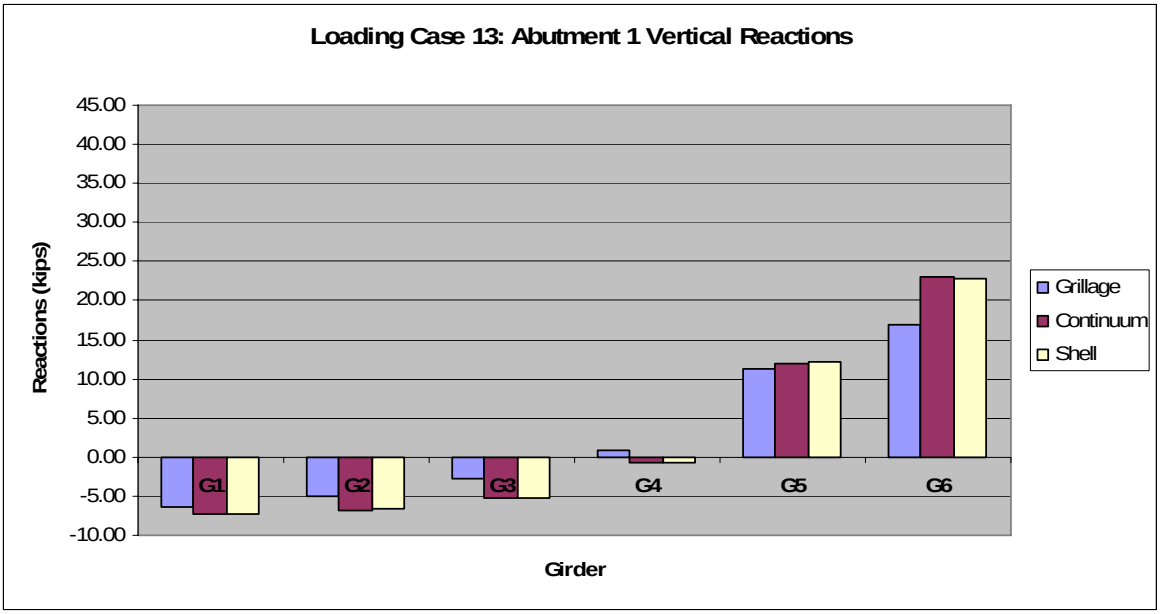

Figure 5.23 Loading Case 13: Abutment 1 vertical reactions.

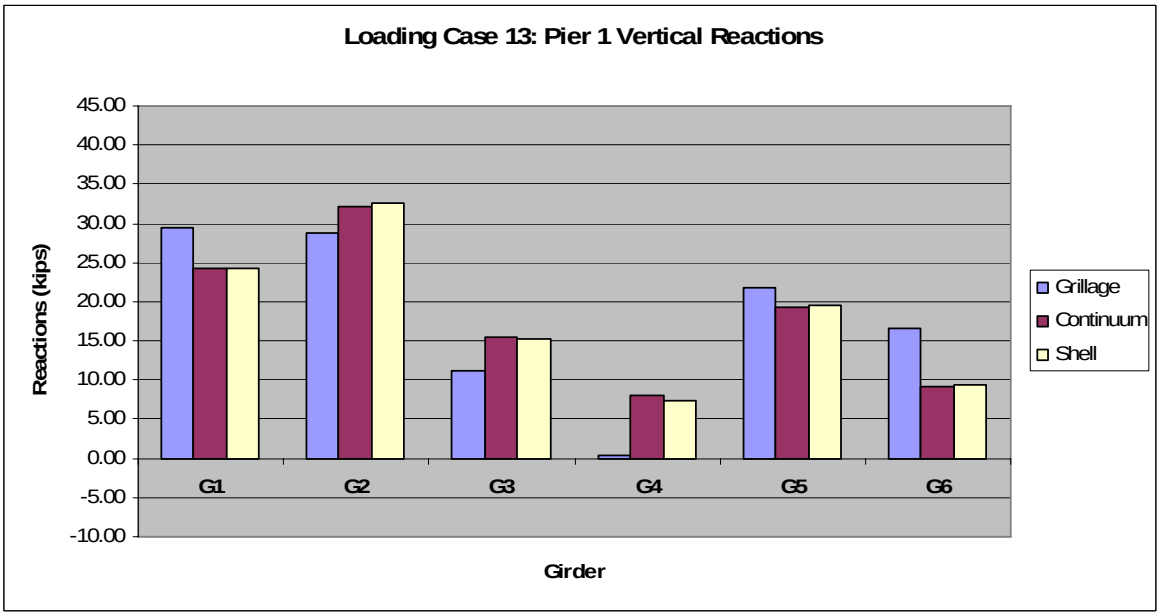

Figure 5.24 Loading Case 13: Pier 1 vertical reactions.

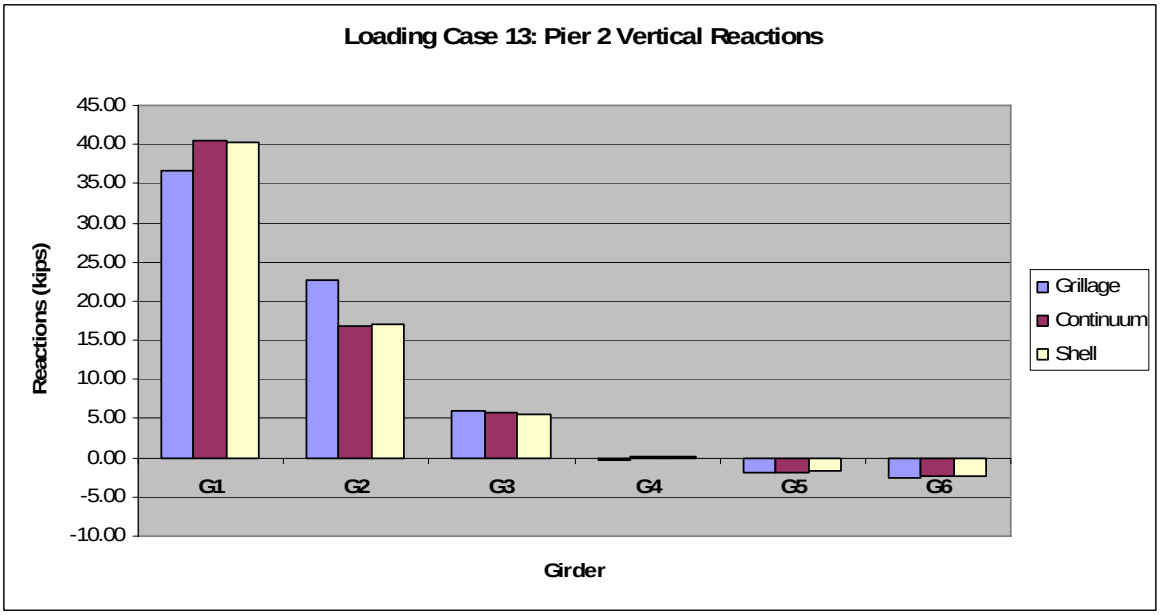

Figure 5.25 Loading Case 13: Pier 2 vertical reactions.

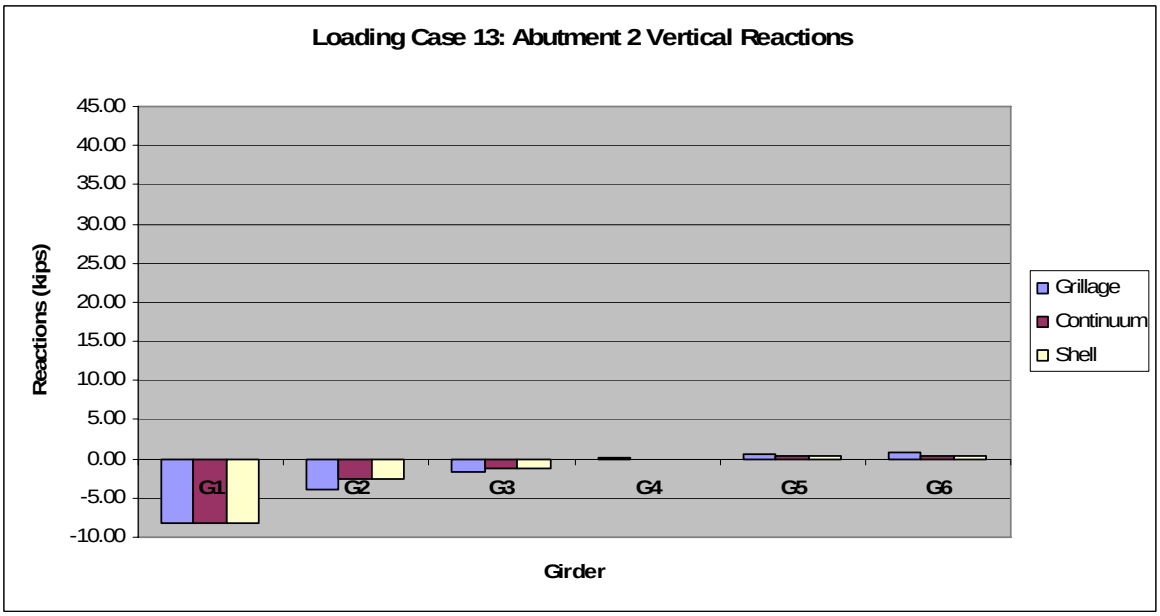

Figure 5.26 Loading Case 13: Abutment 2 vertical reactions.

Loading Case 13 provides a broader picture of the bridge behavior as the applied loads are located in adjacent spans as well as at opposite transverse ends of the bridge (see Figure 2.15).

In Figures 5.23, 5.25, and 5.26, the behavior of the grillage finite element model is shown to accurately predict the vertical reactions for a number of girders. However, it is important to keep in mind that over- and underestimations in structural responses are inherent to the grillage modeling approach employed herein (see Sub-Section 5.1.4). Therefore, it is deduced that the apparent accuracies in the grillage finite element model, as seen in the above figures, are actually illusions resulting from the interaction of applied loadings (i.e. overestimations in response due to one applied loading combine with underestimations in a second applied loading).

5.2 MAXIMUM VERTICAL DEFLECTIONS

The comparison of maximum vertical deflections is accomplished by first obtaining the magnitudes and locations of this parameter for the shell finite element models (locations were identical for both the shell finite element models); the magnitudes of this parameter are then obtained from the grillage finite element model at the *same* location. Therefore, it is possible that the values reported for the grillage finite element model are not the actual maximum vertical deflections for this modeling approach; however, it is noted that global system structural behavior was relatively equivalent across each of the three models.

Data for only the girders deemed “critical” (i.e. those located directly underneath the applied loading) were collected; this statement also applies to Section 5.4. As it is that the primary motivation behind Loading Case 10 was to examine vertical reaction distributions (see Sub-Section 2.2.4), further results (i.e. vertical deflections and longitudinal bending stresses) are

not reported on in this thesis. Results from the remaining loading cases are found in Appendix B.

5.2.1 Loading Case Comparisons

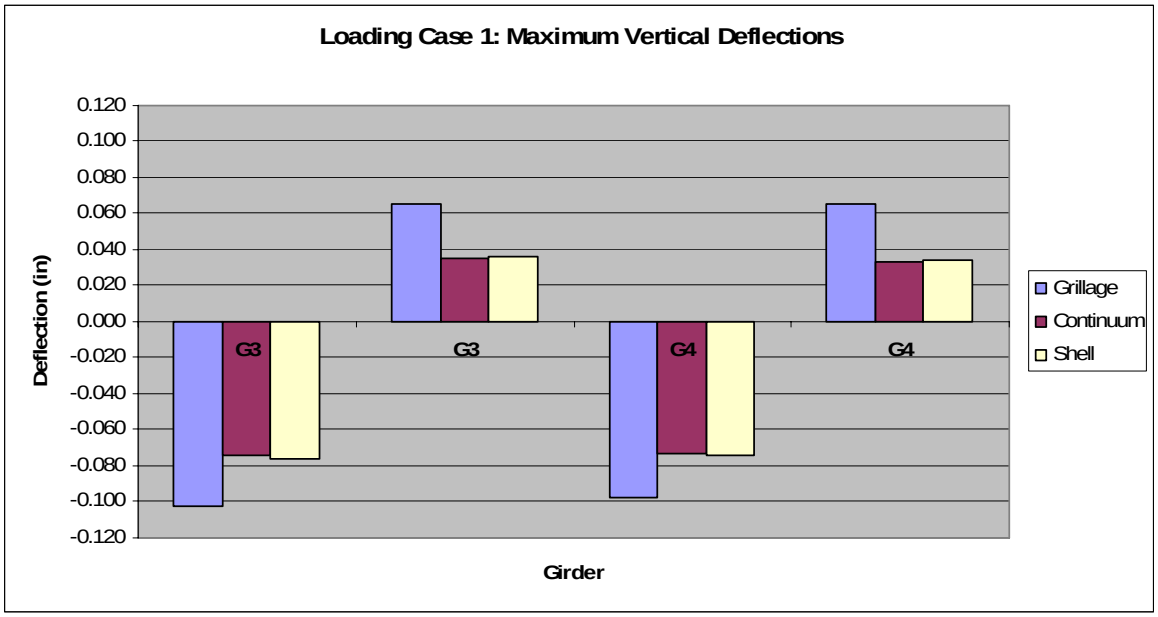

Figure 5.27 Loading Case 1: maximum vertical deflections.

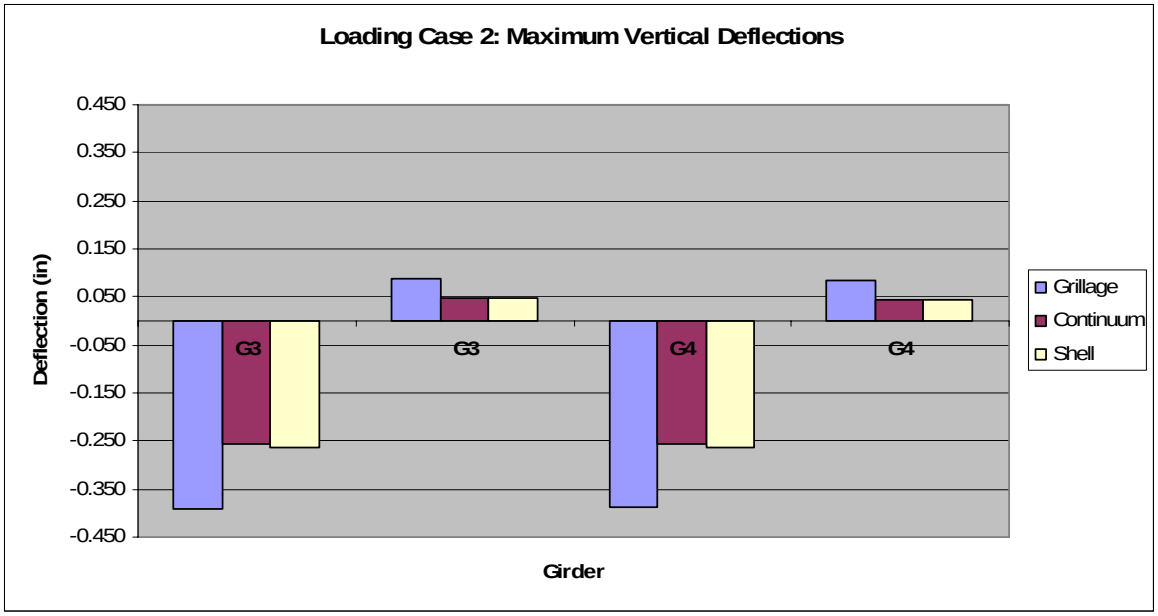

Figure 5.28 Loading Case 2: maximum vertical deflections.

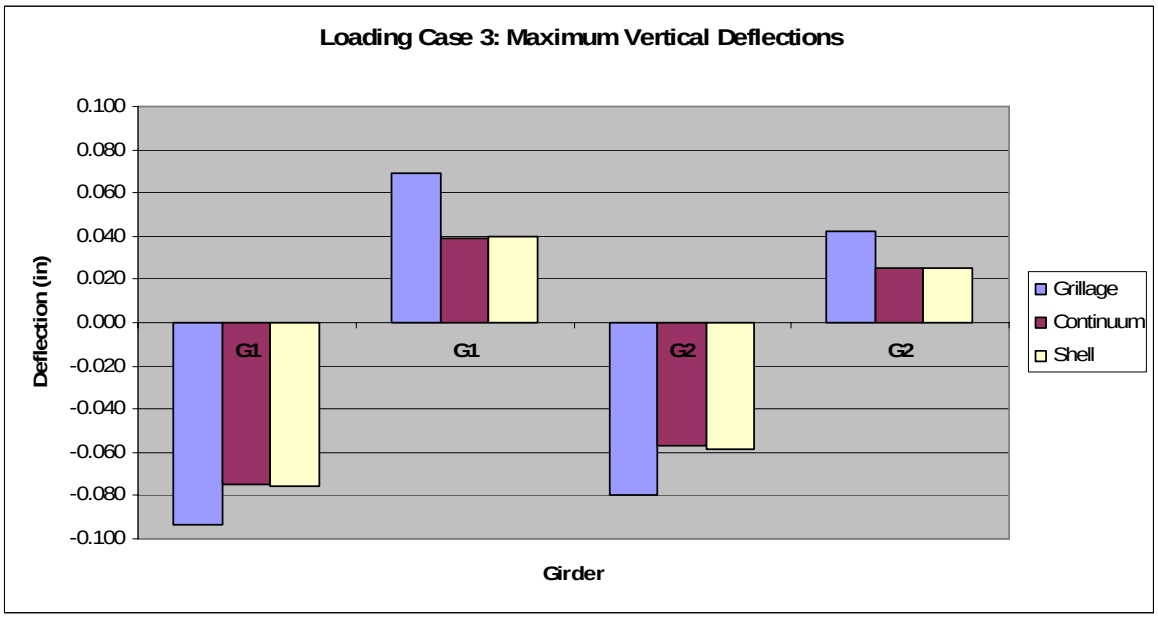

Figure 5.29 Loading Case 3: maximum vertical deflections.

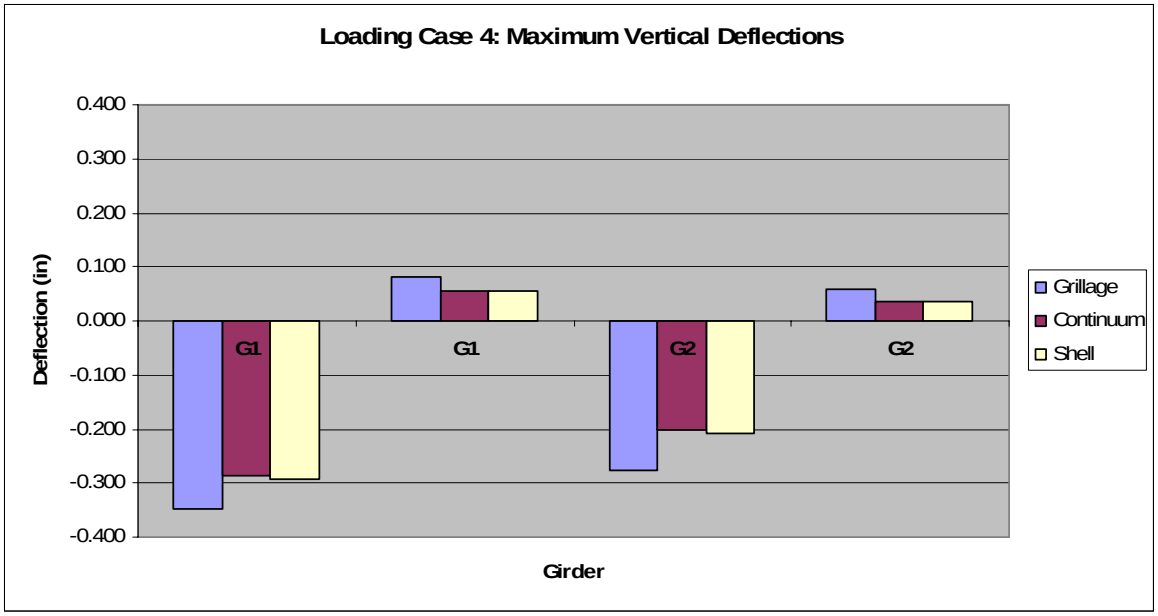

Figure 5.30 Loading Case 4: maximum vertical deflections.

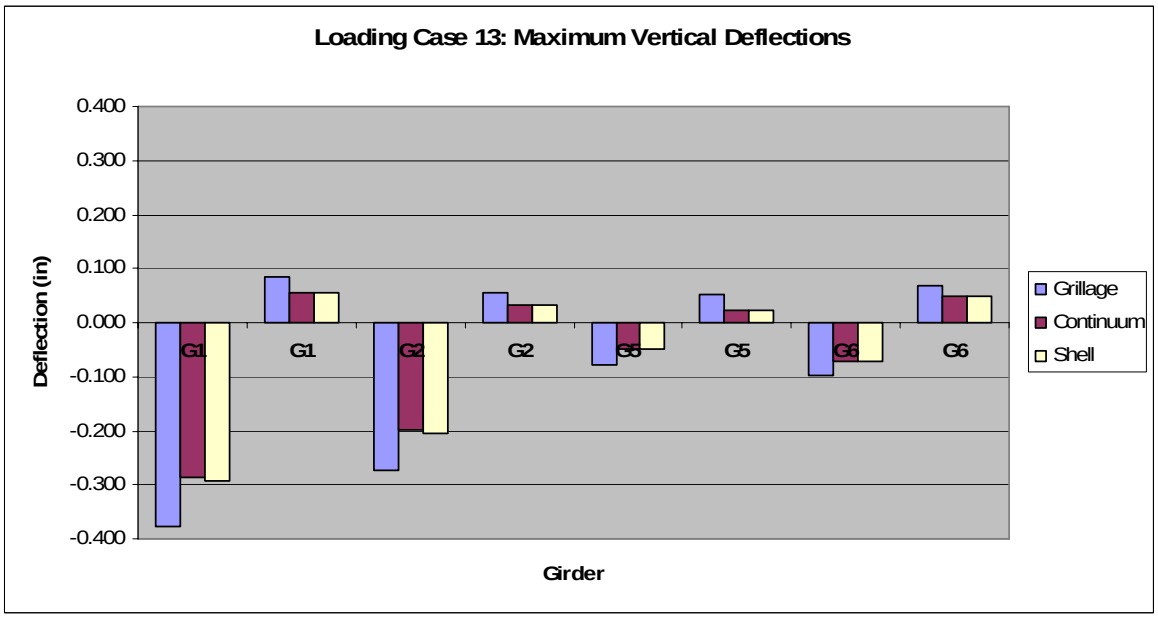

Figure 5.31 Loading Case 13: maximum vertical deflections.

A cursory examination of Figures 5.27 to 5.31 clearly indicates the following: maximum vertical deflections are overestimated in the grillage finite element model as compared to the shell finite

element models. By expanding the examination to all of the load cases, it is seen that this trend is consistent, regardless of the loading case employed. This is not a surprising conclusion, however, as the global behavior made apparent in Section 5.1 would dictate that loads are not globally distributed throughout the grillage; the critical girders carry the majority of the applied loading which results in greater deflections (this trend is also evident in Section 5.4).

5.2.2 Modeling approach comparisons

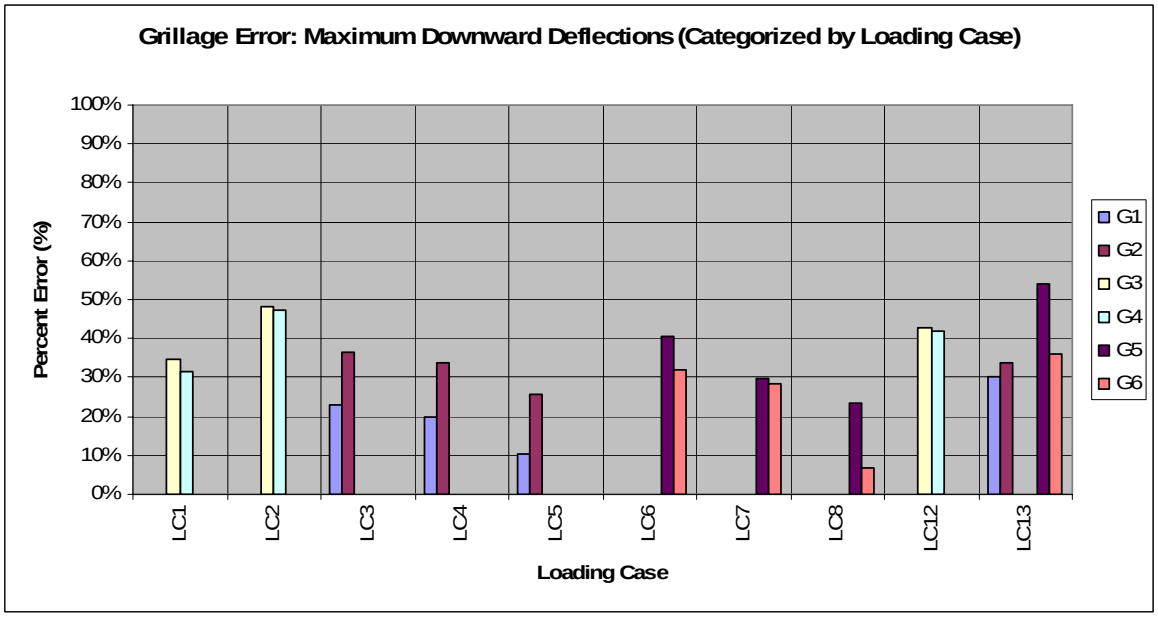

Figure 5.32 Grillage error: maximum downward deflections (categorized by loading case).

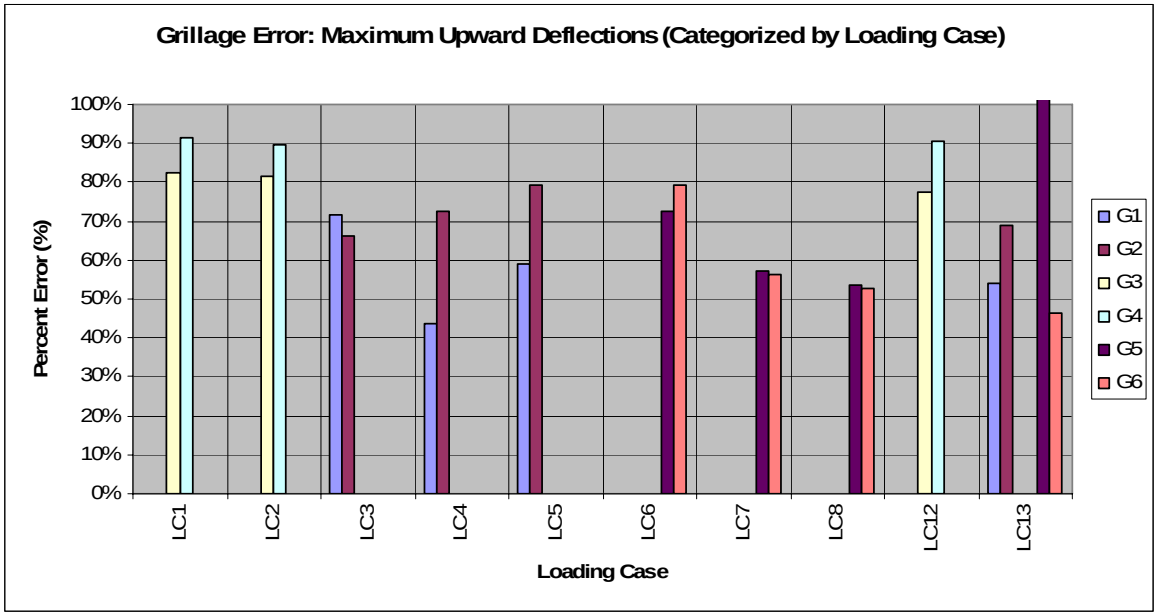

Figure 5.33 Grillage error: maximum upward deflections (categorized by loading case).

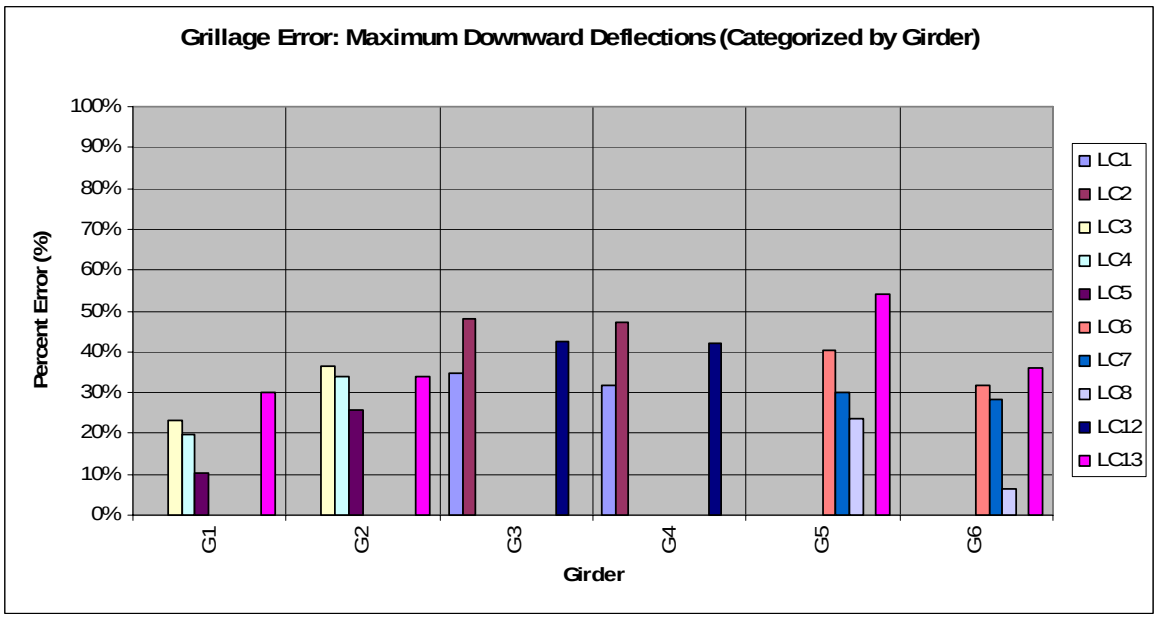

Figure 5.34 Grillage error: maximum downward deflections (categorized by girder).

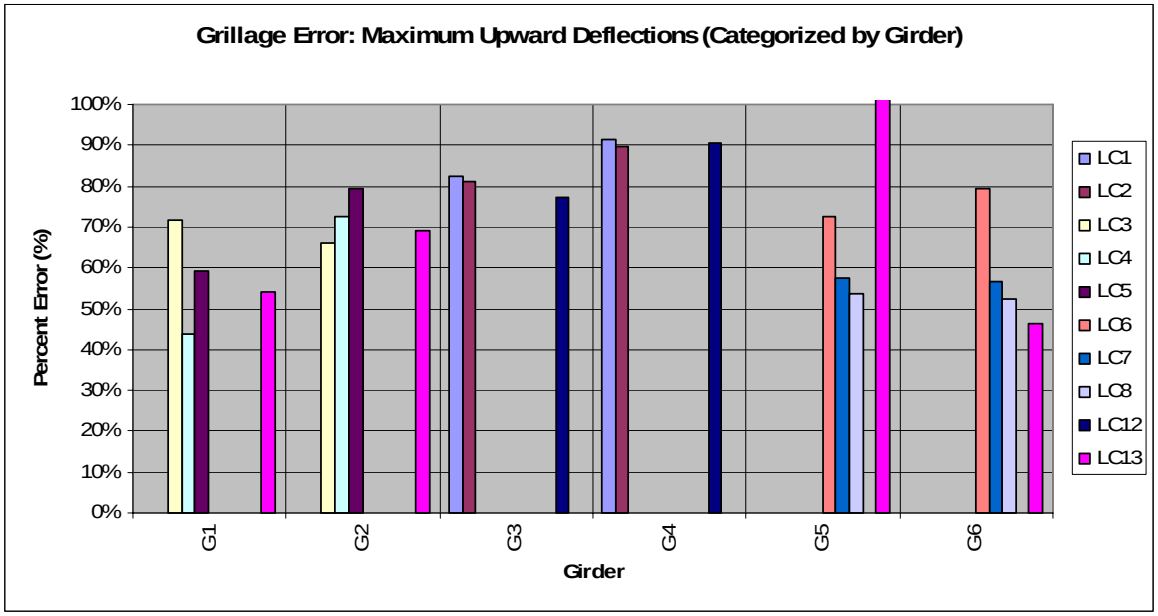

Figure 5.35 Grillage error: maximum upward deflections (categorized by girder).

While establishing the general trend that maximum vertical deflections are overestimated in the grillage modeling approach; insight into the specific weaknesses of the grillage finite element model itself may be gained through a categorization of the error magnitudes. This is performed in Figures 5.32 through 5.35 where grillage error percentages (as compared with the shell deck model) are categorized by loading case and by girder line, respectively. It is clear from these figures that the errors with respect to maximum *downward* deflections (i.e. errors associated with loaded spans) are significantly less in magnitude than those with respect to maximum *upward* deflections (i.e. errors associated with unloaded spans). Therefore, the above hypothesis that errors will increase in magnitude at locations away from the applied loading is reinforced.

5.3 VERTICAL DEFLECTION PROFILES

The vertical deflection profiles given below are obtained by extracting vertical deflections from each girder at a specified bridge cross-section located at a discrete point along the length of the bridge; locations of these cross-sections are found in Figure 5.1. Note that a single profile cross-section is taken as parallel to the skew angle. For each loading case, profiles were obtained from the loaded span and the adjacent unloaded span; for loading cases in which the applied loading is located in Span 2, Span 3 data were used for the unloaded span. Upon examining the data, it is found that the trends noted in Loading Case 2 are roughly identical to those in Loading Case 1. This is also the case for Loading Cases 3 and 4. Therefore, only Loading Cases 1, 3 and 13 are presented in the main body of the thesis; results from the remaining loading cases are found in Appendix C.

5.3.1 Loading Case 1

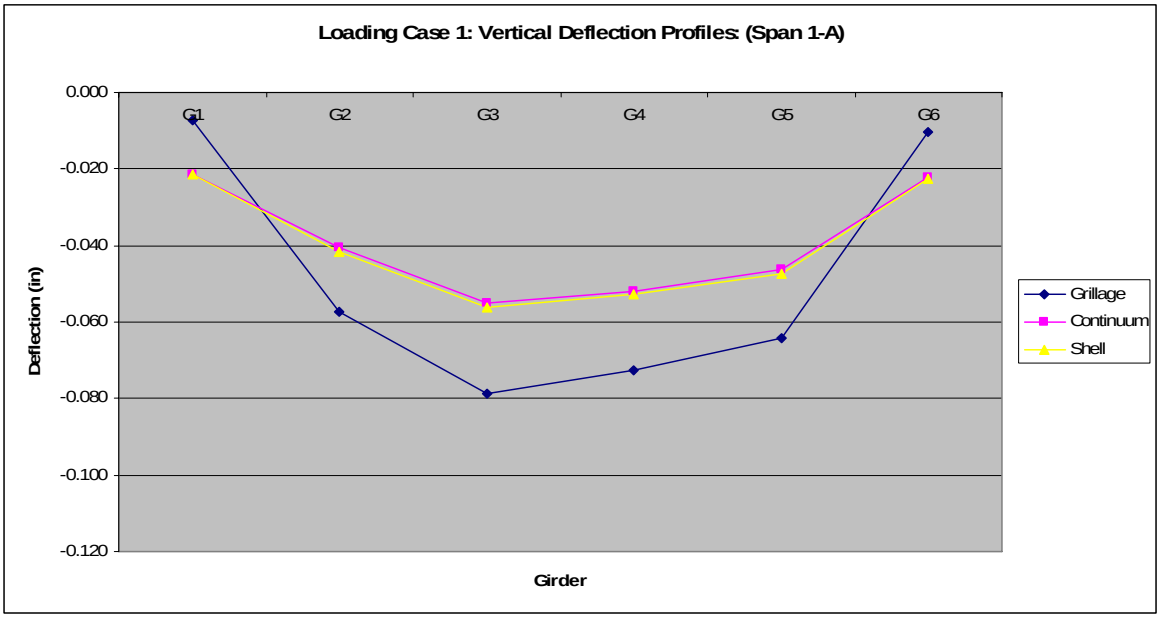

Figure 5.36 Loading Case 1: vertical deflection profiles (Span 1-A).

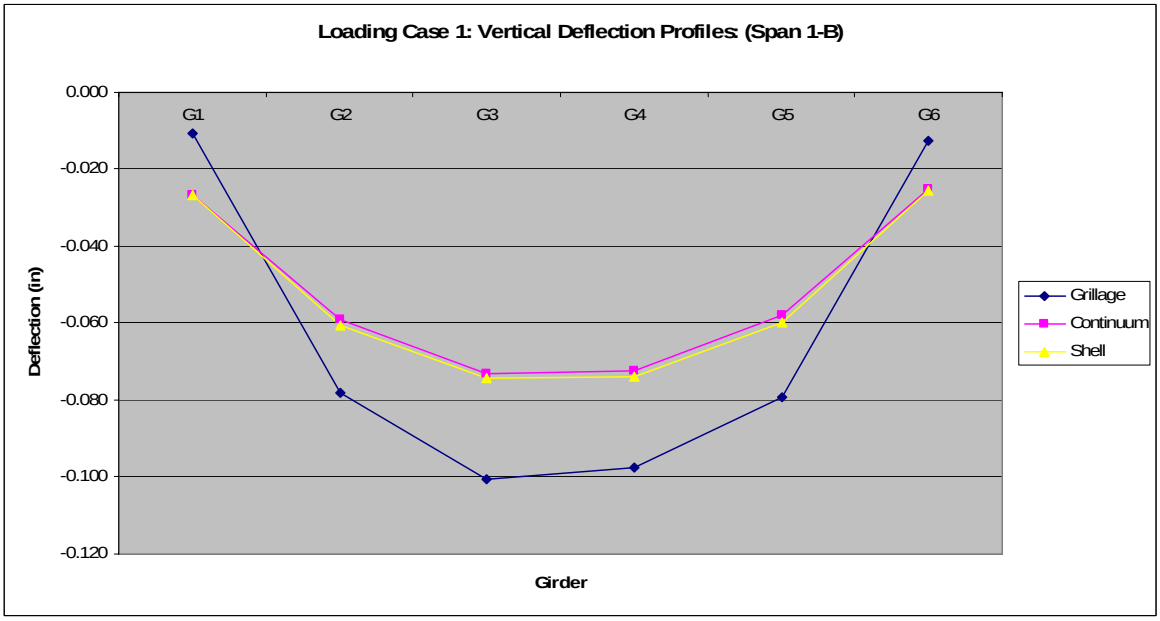

Figure 5.37 Loading Case 1: vertical deflection profiles (Span 1-B).

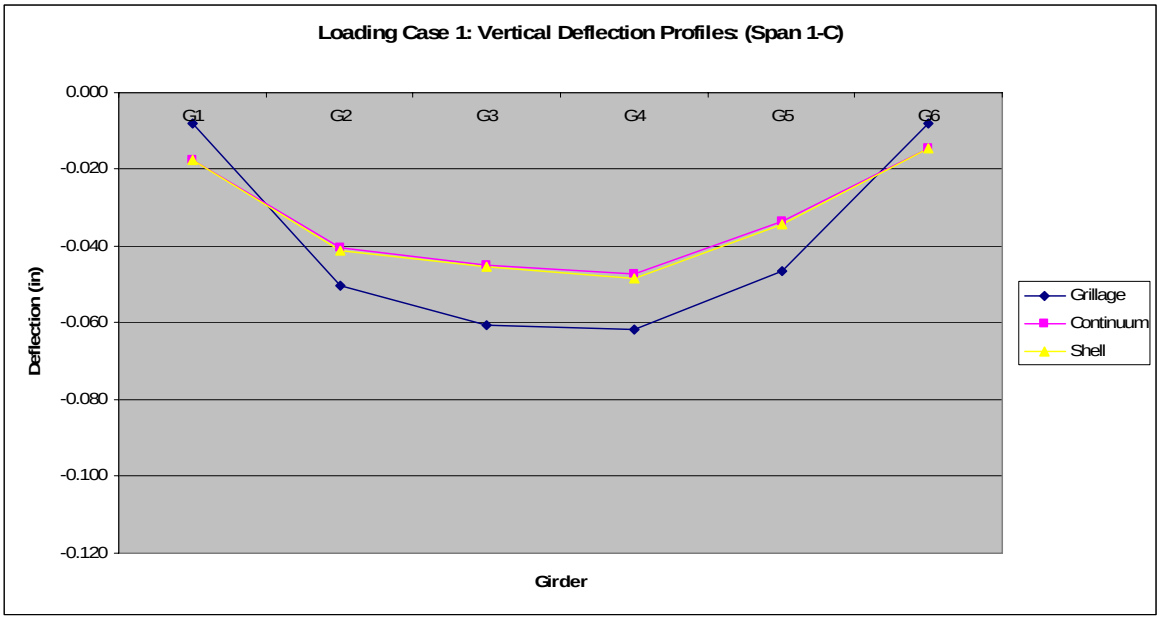

Figure 5.38 Loading Case 1: vertical deflection profiles (Span 1-C).

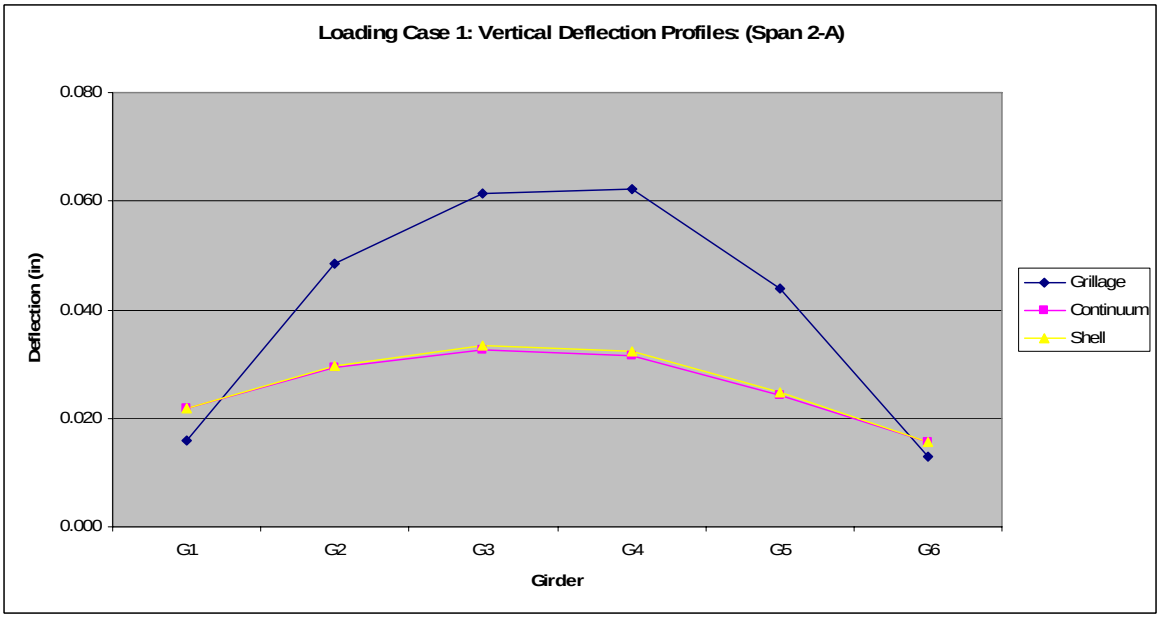

Figure 5.39 Loading Case 1: vertical deflection profiles (Span 2-A).

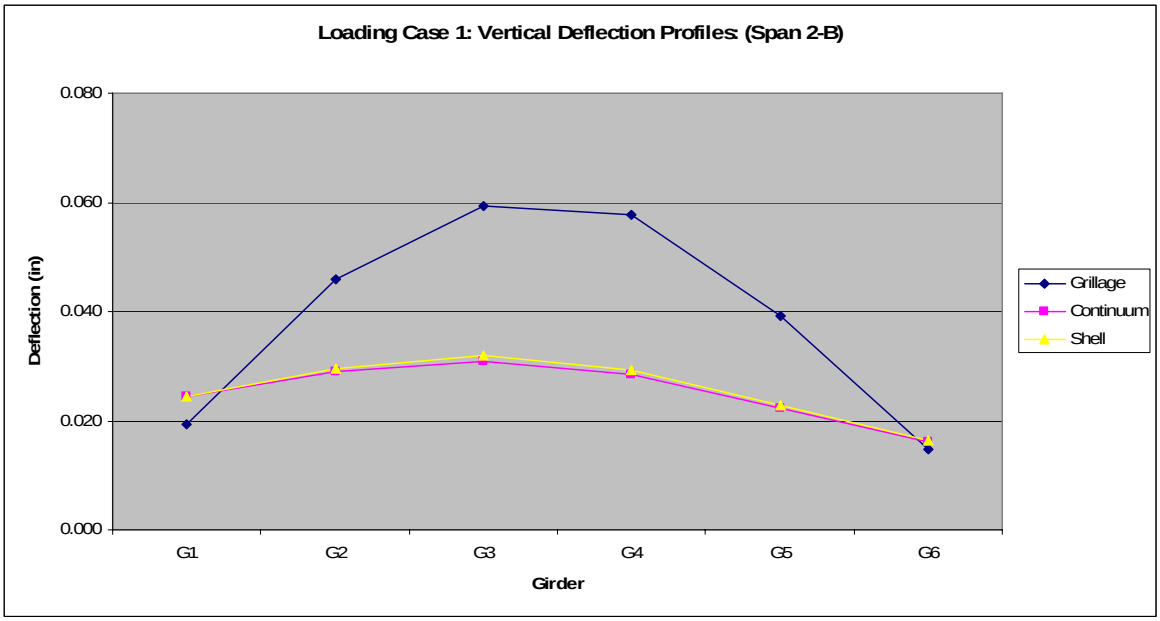

Figure 5.40 Loading Case 1: vertical deflection profiles (Span 2-B).

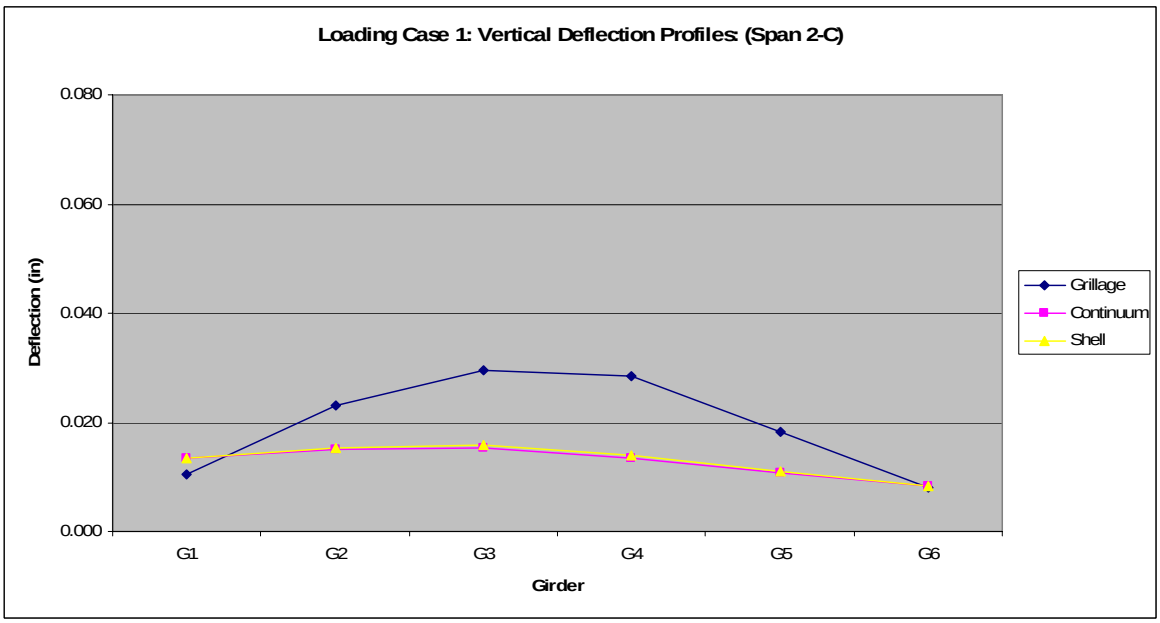

Figure 5.41 Loading Case 1: vertical deflection profiles (Span 2-C).

Upon examining Figures 5.36 through 5.41, it is seen that the trends established in Section 5.2 are consistent along the length of the bridge. For example, the vertical displacements for G1 and

G6, in all but one case, are less in magnitude for the grillage finite element model as compered with those for the shell finite element models. This is expected as the resultant of the applied loading for Loading Case 1 falls on the transverse centerline of the bridge (i.e. at locations away from the applied loading, response is underestimated). Furthermore, when comparing Figures 5.36 through 5.38 to Figures 5.39 through 5.41, the trend in which the unloaded span exhibits significantly larger relative errors, as discussed in Sub-Section 5.2.2, is reinforced.

5.3.2 Loading Case 3

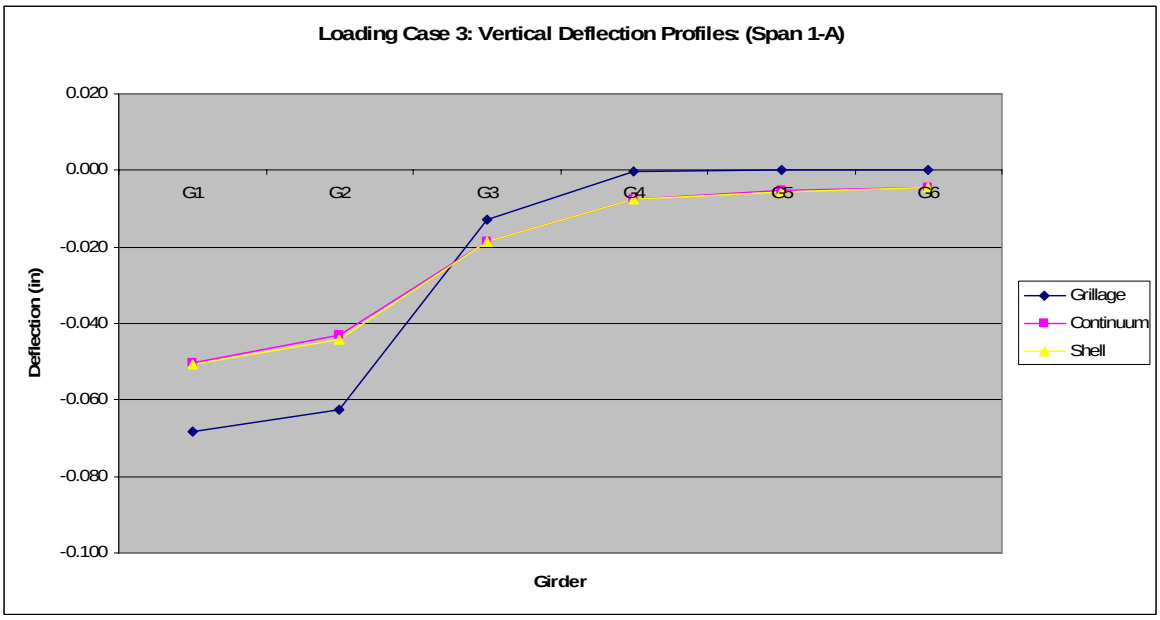

Figure 5.42 Loading Case 3: vertical deflection profiles (Span 1-A).

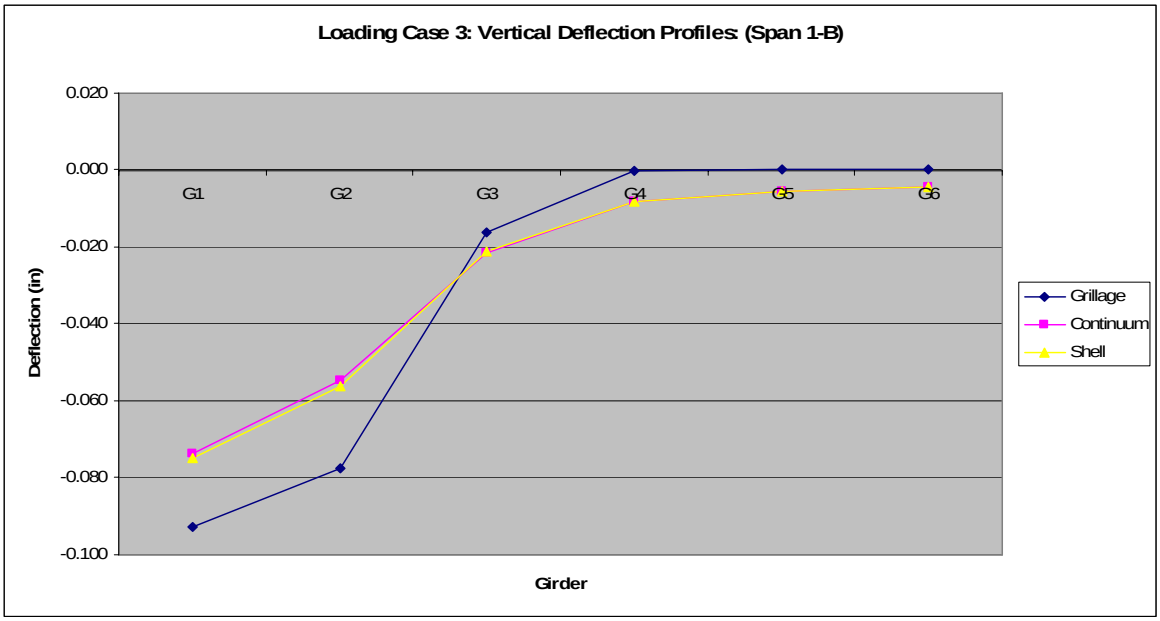

Figure 5.43 Loading Case 3: vertical deflection profiles (Span 1-B).

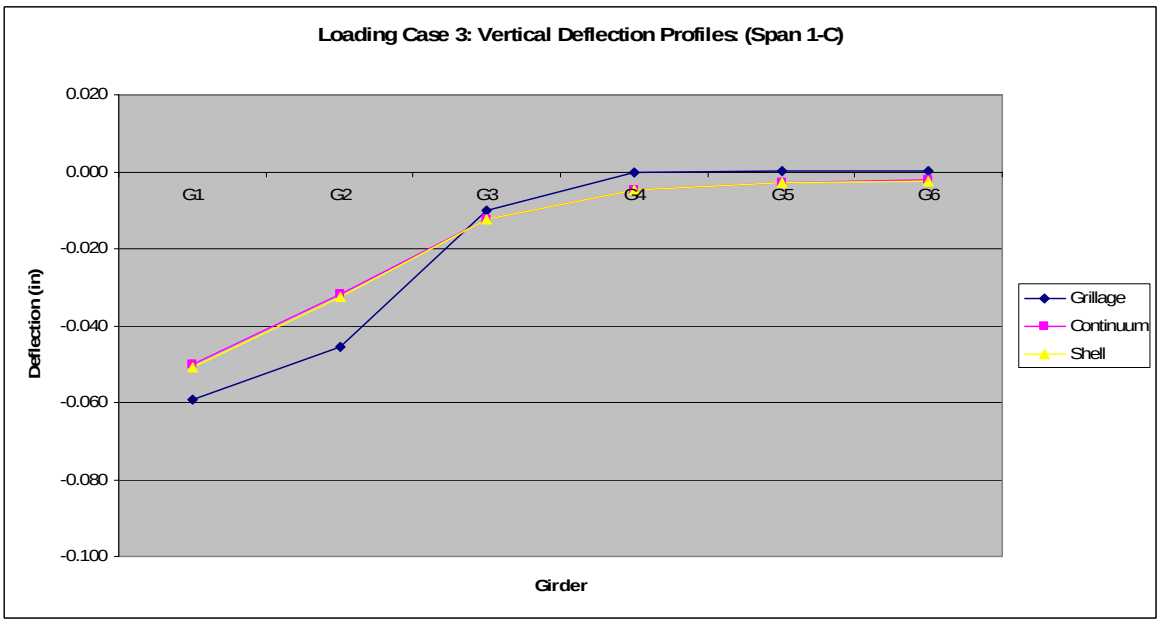

Figure 5.44 Loading Case 3: vertical deflection profiles (Span 1-C).

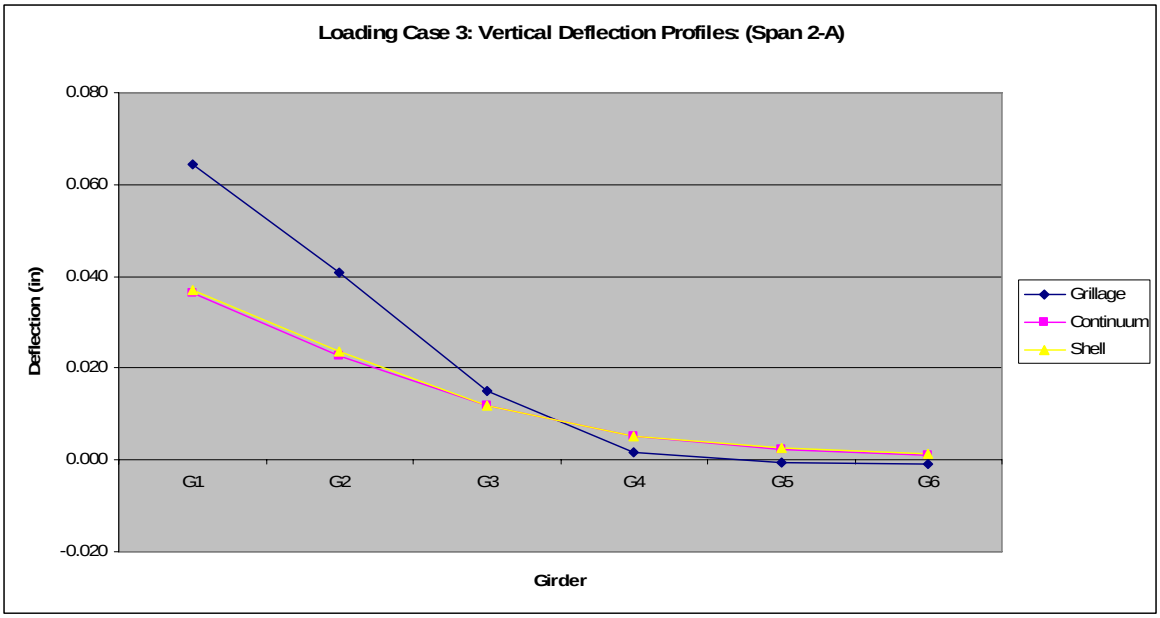

Figure 5.45 Loading Case 3: vertical deflection profiles (Span 2-A).

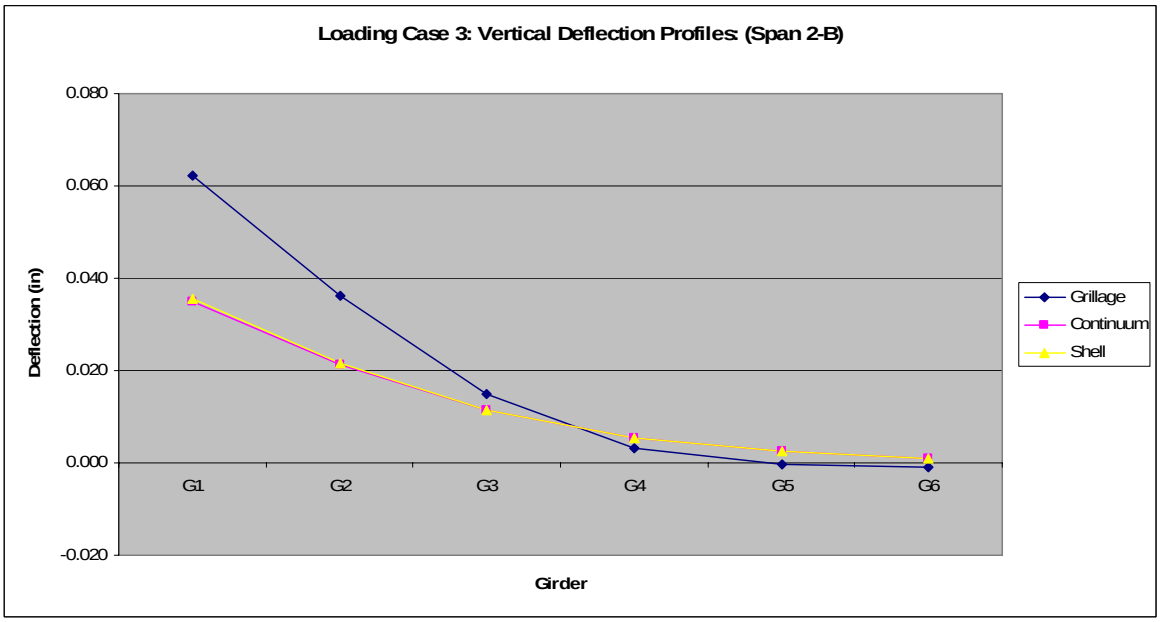

Figure 5.46 Loading Case 3: vertical deflection profiles (Span 2-B).

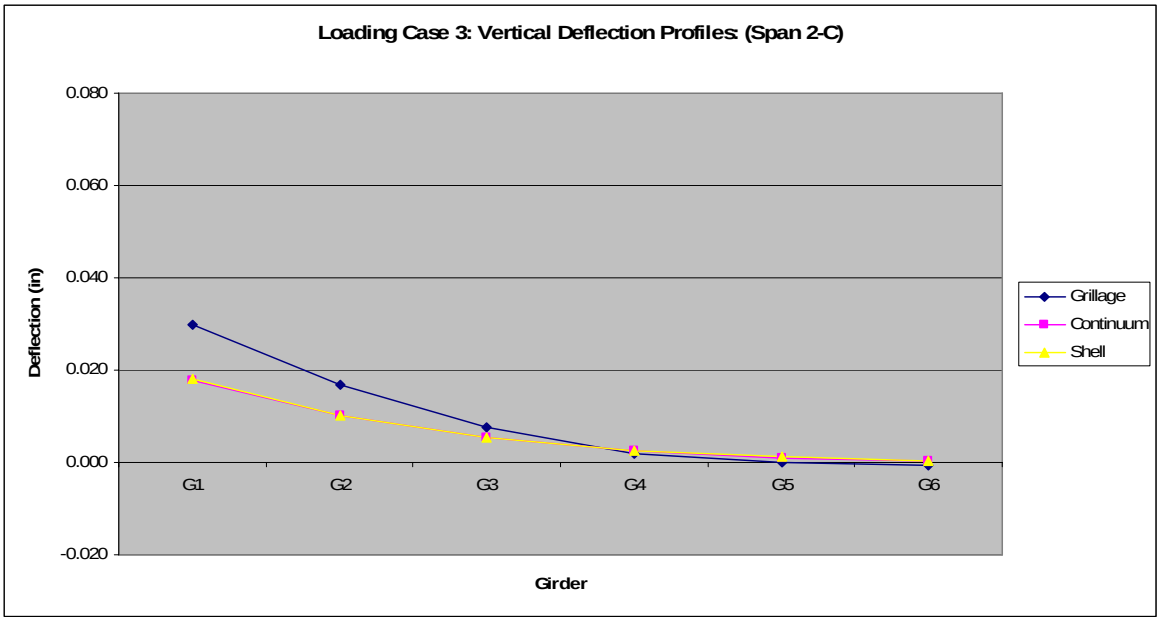

Figure 5.47 Loading Case 3: vertical deflection profiles (Span 2-C).

The vertical deflection profiles for Loading Case 3 demonstrate the expected trends as well: overestimated vertical deflections at and near the applied loading, and underestimated vertical deflections away from the applied loading. It is noted, however, due to the location of the applied loads, there occurs a point in each profile in which the deflections are accurately predicted by the grillage finite element model. Keep in mind that this is not in fact due to the accuracy of the model, but instead due to the combined effect of the errors noted above.

5.3.3 Loading Case 13

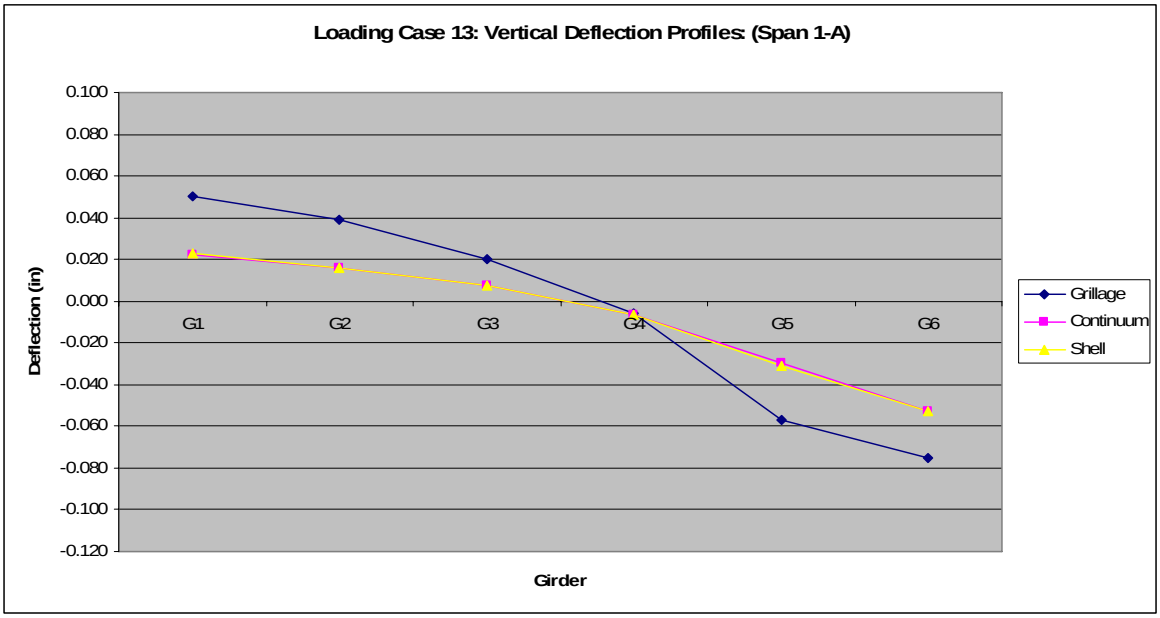

Figure 5.48 Loading Case 13: vertical deflection profiles (Span 1-A).

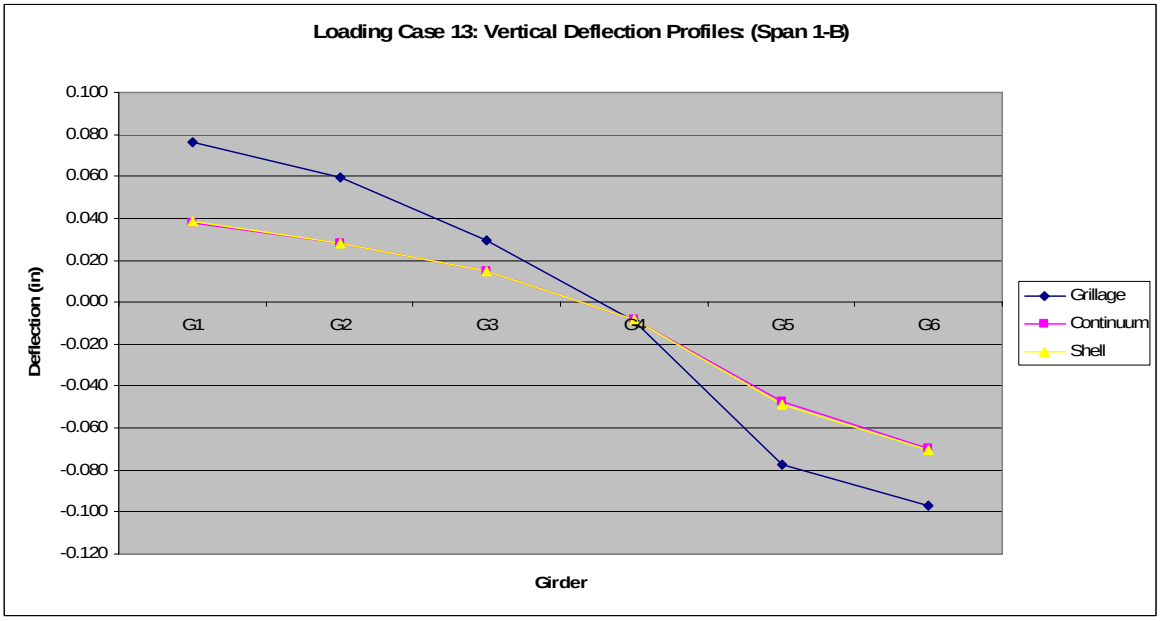

Figure 5.49 Loading Case 13: vertical deflection profiles (Span 1-B).

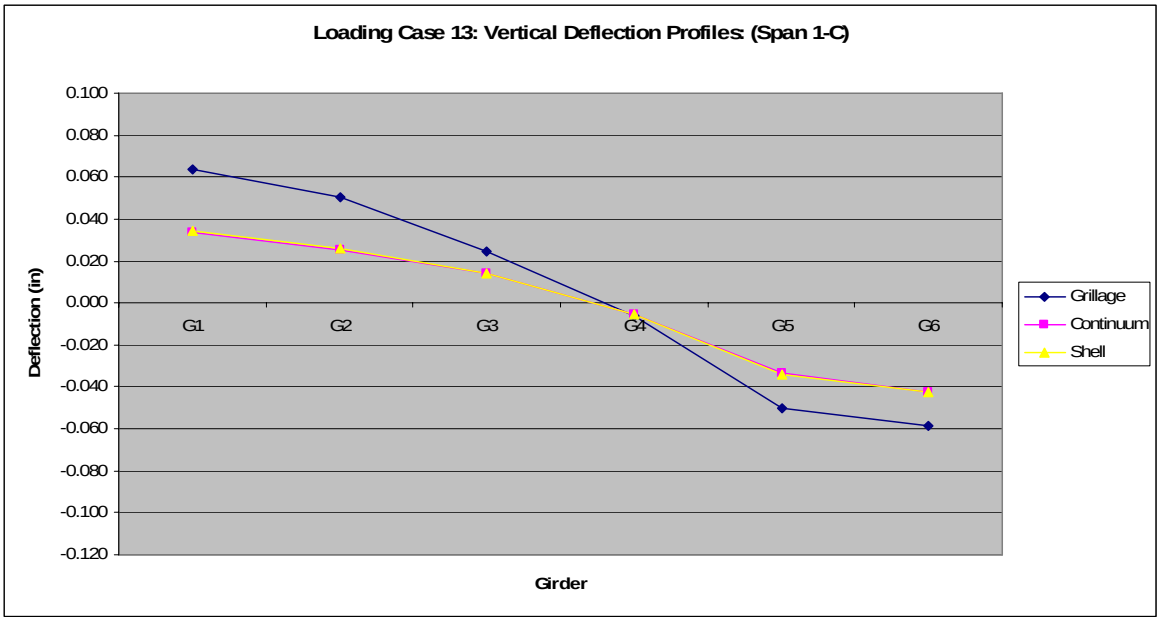

Figure 5.50 Loading Case 13: vertical deflection profiles (Span 1-C).

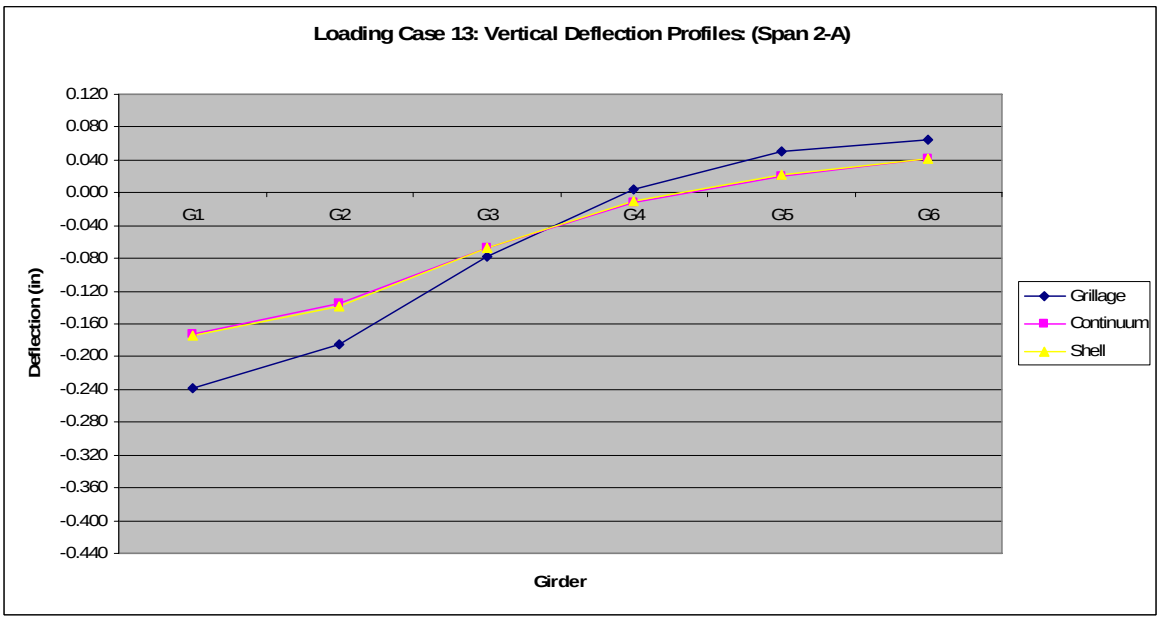

Figure 5.51 Loading Case 13: vertical deflection profiles (Span 2-A).

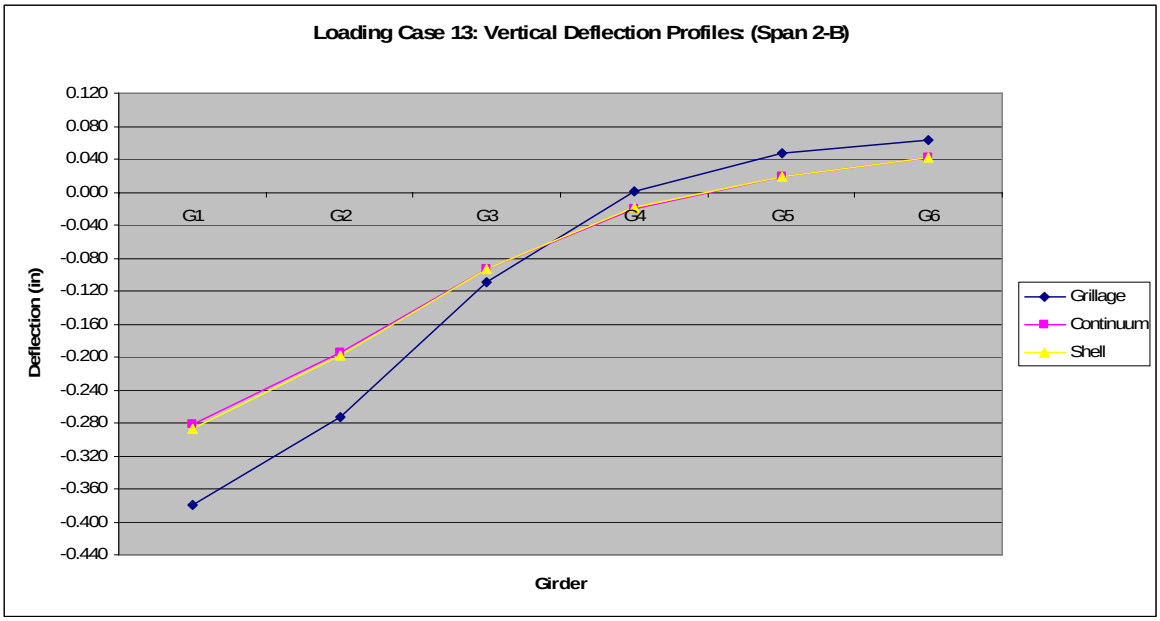

Figure 5.52 Loading Case 13: vertical deflection profiles (Span 2-B).

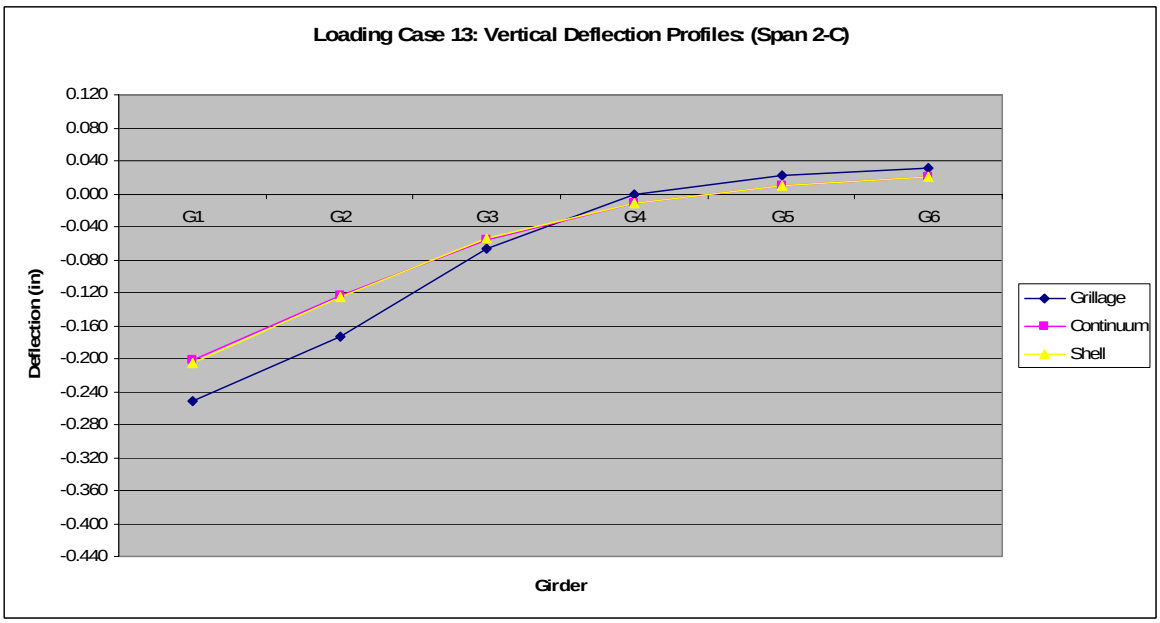

Figure 5.53 Loading Case 13: vertical deflection profiles (Span 2-C).

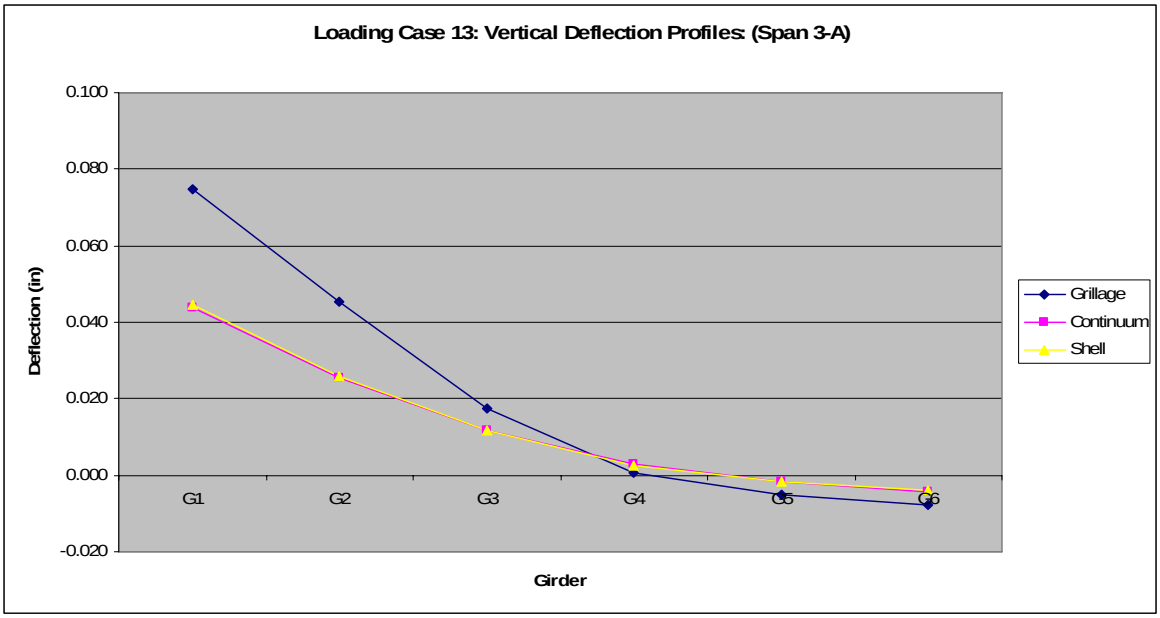

Figure 5.54 Loading Case 13: vertical deflection profiles (Span 3-A).

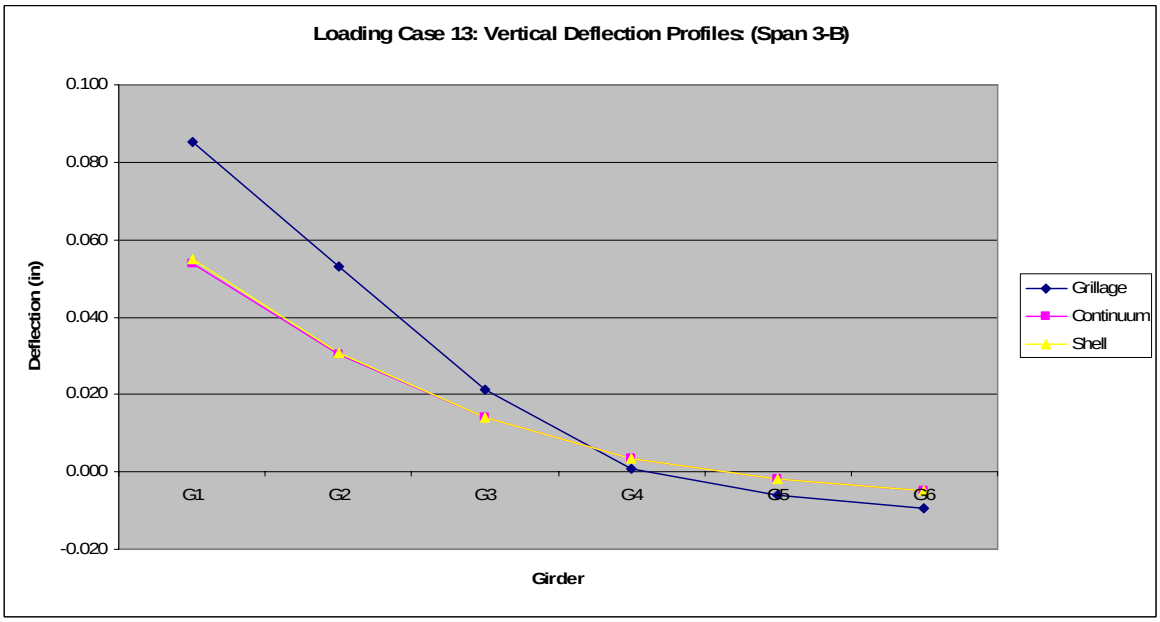

Figure 5.55 Loading Case 13: vertical deflection profiles (Span 3-B).

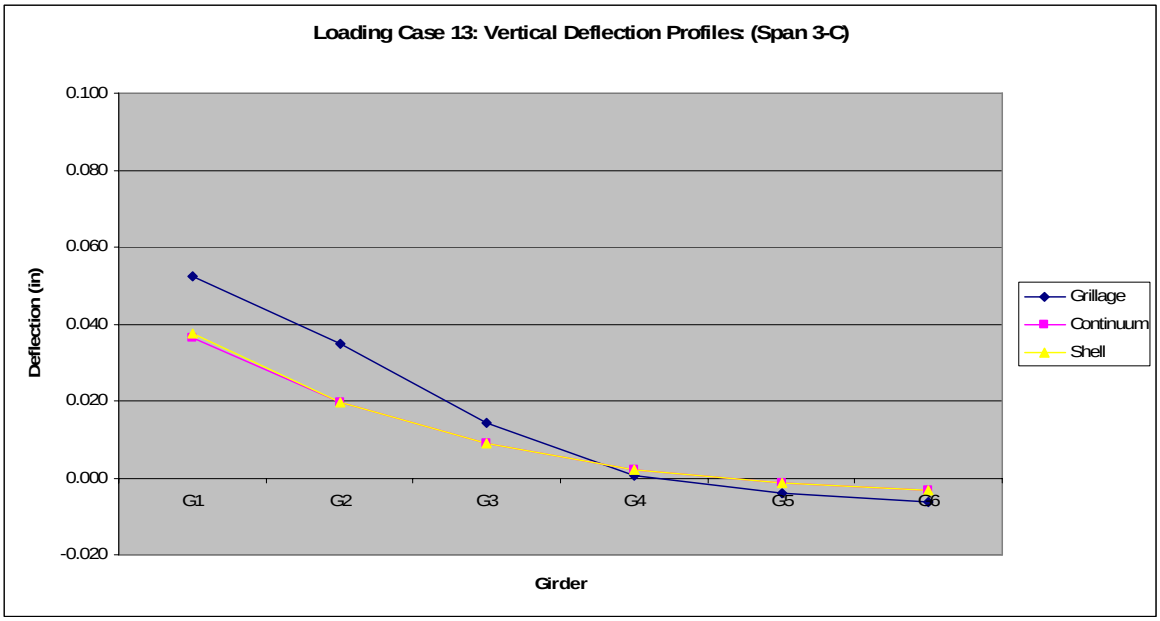

Figure 5.56 Loading Case 13: vertical deflection profiles (Span 3-C).

When considering the discussion in Sub-Section 5.1.5, it is expected that the vertical deflection profiles obtained for Loading Case 13 will actually exhibit a more accurate behavior. For example, it could be hypothesized that the underestimation of Span 2 vertical deflections for G5 and G6 will result from the Span 2 applied loading, while overestimations of these vertical deflections will results from the Span 1 applied loading. The conclusion emanating from this hypothesis is that the Span 2 vertical deflections for G5 and G6 will balance the errors and reflect values which are approximately accurate with respect to the shell finite element models.

By examining Figures 5.51 through 5.53, this hypothesis is proven incorrect; the error magnitudes follow the same trends as noted in Sub-Section 5.3.2. In fact, a rather unexpected behavior is discovered upon examination of Loading Cases 4, 5, 7, and 8 (Appendix C): the typical underestimation of response at locations away from the applied loading is not present. This, of course, has some bearing on the discussion of Loading Case 13 as this loading case is a

combination of two other loading cases; leading to the conclusion that such a hypothesis as that posed above, while valid for vertical reaction distributions, is not universally so for vertical deflection profiles.

Furthermore, as it is that Loading Cases 4, 5, 7, and 8 encompass the loading of exterior girders on Spans 2 and 3, it is apparent that the performance of the load distribution mechanism in the grillage model varies; despite the relatively uniform configuration of transverse members in each span (e.g. Spans 1 and 3 employ *identical* configurations). This implies that the grillage modeling approach assumed herein is highly dependent on the imposed boundary conditions (i.e. Span 1 is restrained from longitudinal movement at Abutment 1 where Spans 2 and 3 are only restrained in this direction *through* Span 1); and therefore, a direct application of the idealized boundary conditions is not applicable for this model.

5.4 MAXIMUM LONGITUDINAL BENDING STRESSES

As with the maximum vertical deflections, the maximum longitudinal bending stresses are obtained by first considering the response of the bottom flanges of the shell finite element models (i.e. the tensile flanges), and then obtaining the longitudinal bending moment from the same location in the grillage finite element model. The stresses corresponding to these moments are then computed through the following equation:

$$\sigma_b = \frac{M_b c}{I}. \tag{4.11}$$

where *c* is the distance from the neutral axis to the bottom flange and *I* is the longitudinal bending moment of inertia. The values of c and I are based on the section properties derived in Sub-Section 3.2.1. Appendix D is reserved for the loading cases not presented in this section.

5.4.1 Loading Case Comparisons

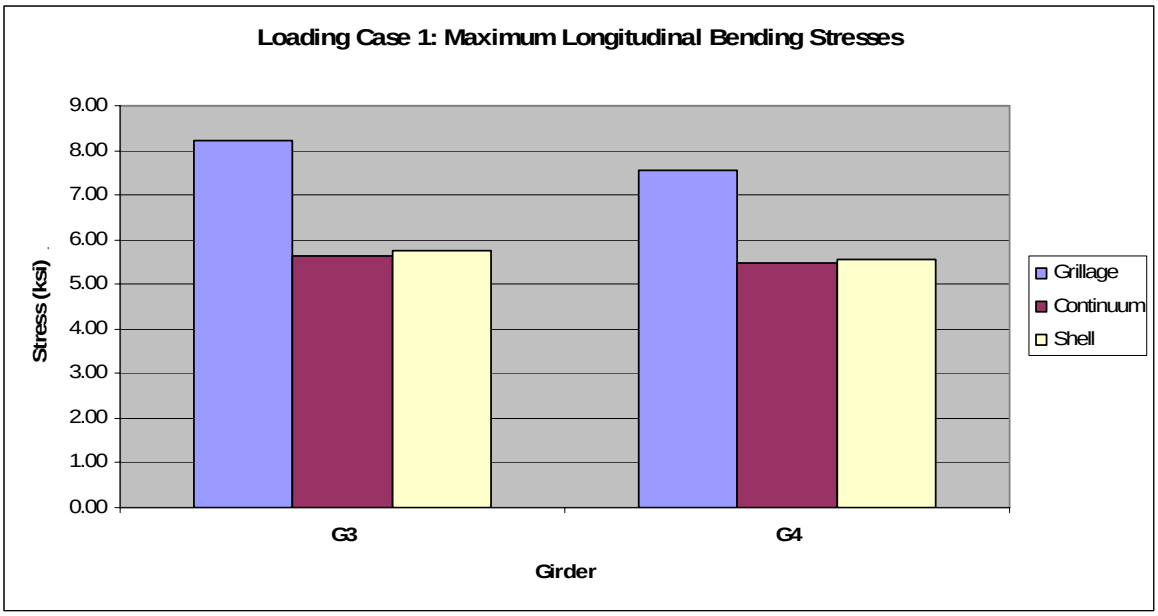

Figure 5.57 Loading Case 1: maximum longitudinal bending stresses.

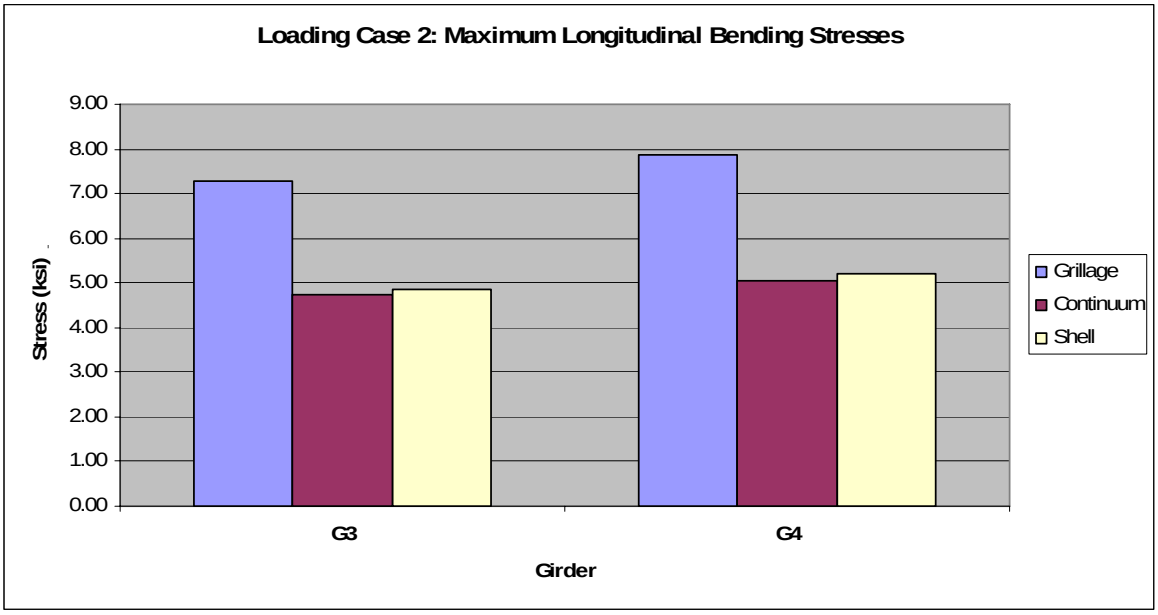

Figure 5.58 Loading Case 2: maximum longitudinal bending stresses.

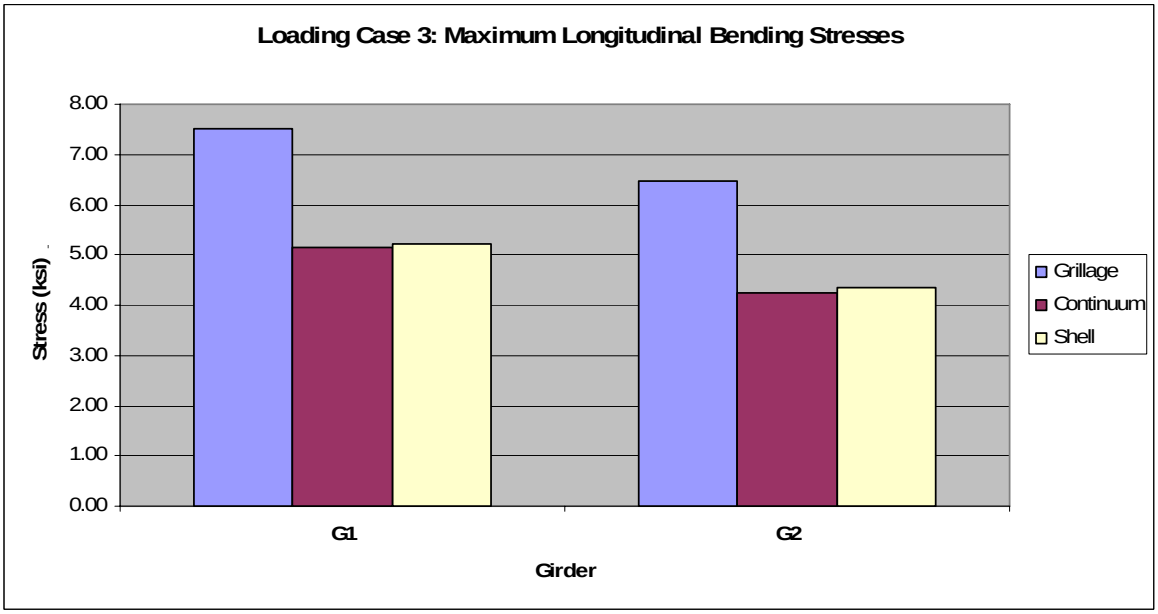

Figure 5.59 Loading Case 3: maximum longitudinal bending stresses.

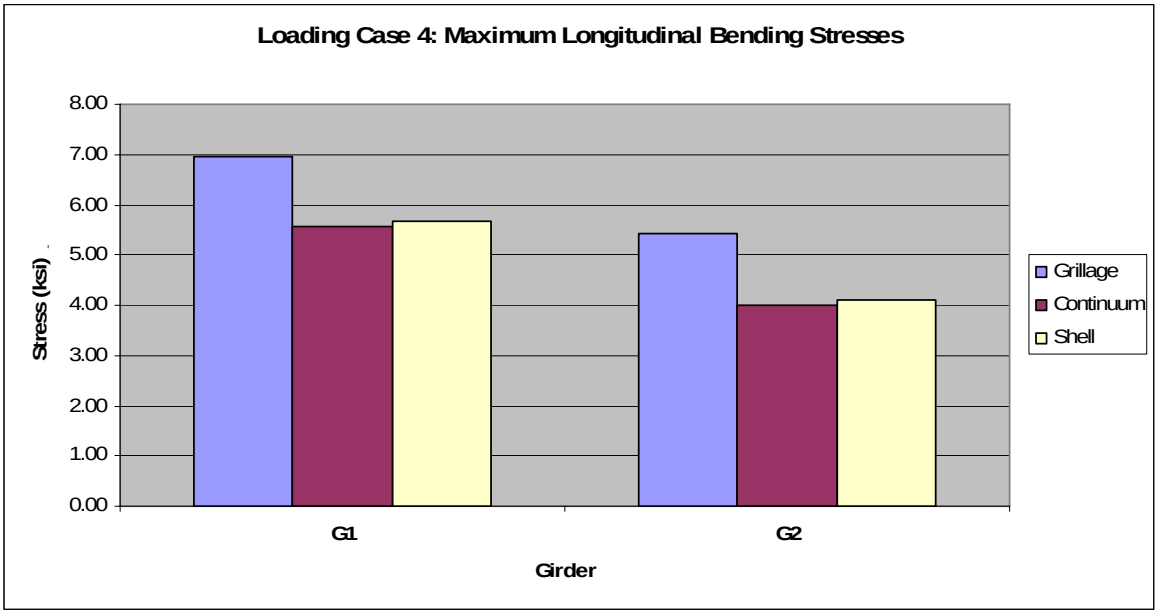

Figure 5.60 Loading Case 4: maximum longitudinal bending stresses.

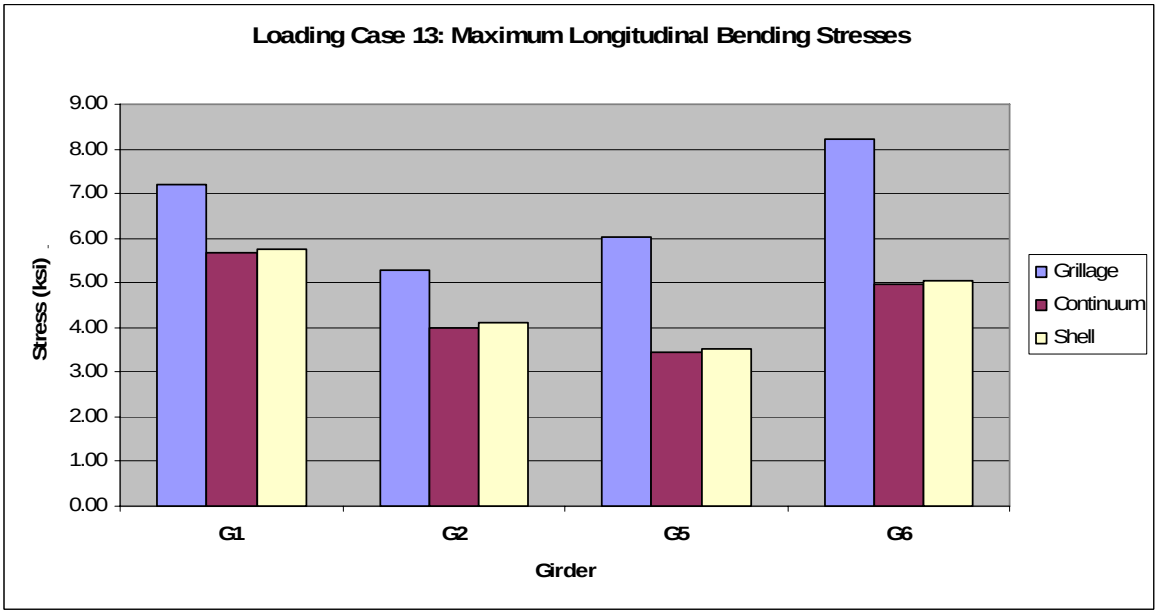

Figure 5.61 Loading Case 13: maximum longitudinal bending stresses.

Considering the discussion in Sub-Section 5.2.1, there is little need for further examination of Figures 5.57 through 5.61. While the error magnitudes are slightly different, the general trend

exhibited in these figures is identical to that shown previously through examination of the maximum vertical deflections.

5.4.2 Modeling approach comparisons

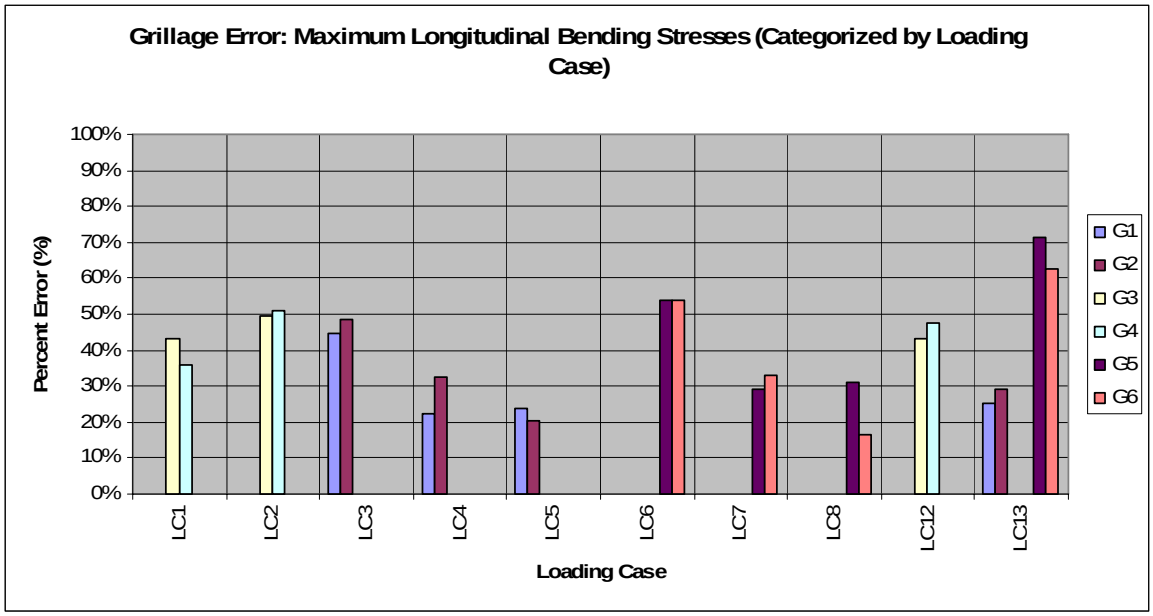

Figure 5.62 Grillage error: maximum longitudinal bending stresses (categorized by loading case).

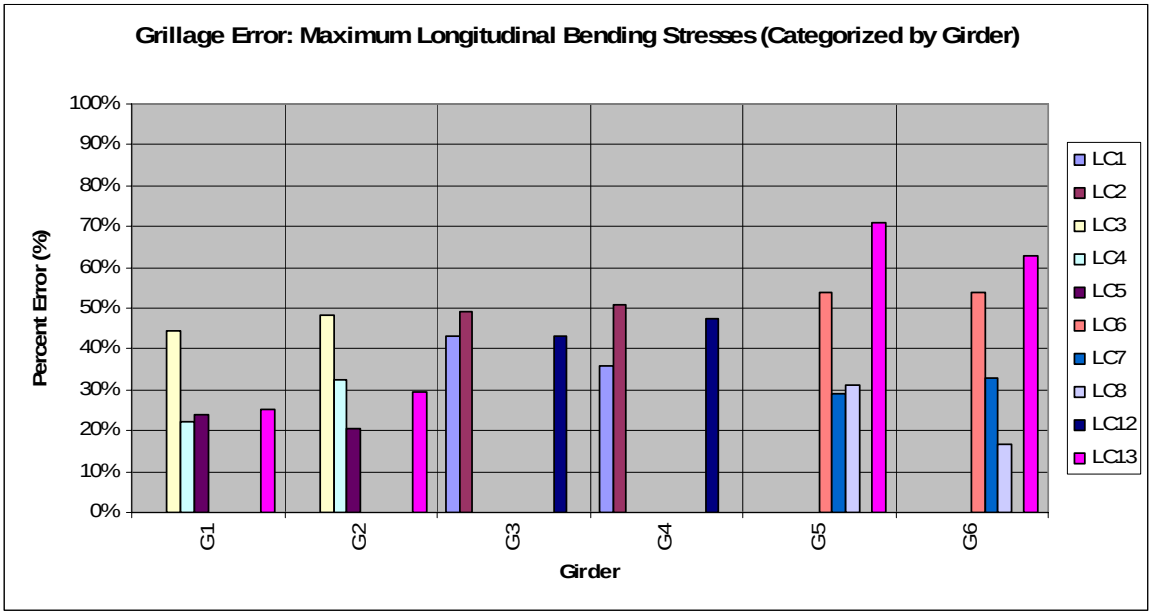

Figure 5.63 Grillage error: maximum longitudinal bending stresses (categorized by girder).

The major conclusion that is drawn from the examination of Figures 5.62 and 5.63 is that which was pointed out in Sub-Section 5.3.3: in cases where an applied loading is located over the exterior girders in Spans 2 and 3, the grillage finite element model produces errors which are smaller in magnitude than those corresponding to like cases in Span 1. Loading Case 13, in particular demonstrates this behavior as it is seen in Figure 5.62 that the errors obtained from G1 and G2, which correspond to Span 2, are approximately 25%; those obtained from G5 and G6, which correspond to Span 1, are 2 to 3 times this. It is apparent that the assumed boundary conditions in the grillage finite element model are incorrect and require further consideration if improvements are to be made in this modeling approach.

5.5 LONGITUDINAL BENDING STRESS PROFILES

Longitudinal bending stress profiles were obtained through identical means as the vertical deflection profiles in Section 5.3. Again, it is noted that stresses are obtained directly from the shell finite element models, while a calculation based on the derived section properties is required of the grillage finite element model. It follows that many of the behavioral characteristics seen in Section 5.3 are again demonstrated in this section; therefore, only Loading Cases 3 and 13 are discussed with additional comments made on characteristics seen in the other loading cases. Results from these loading are available in Appendix E.

5.5.1 Loading Case 3

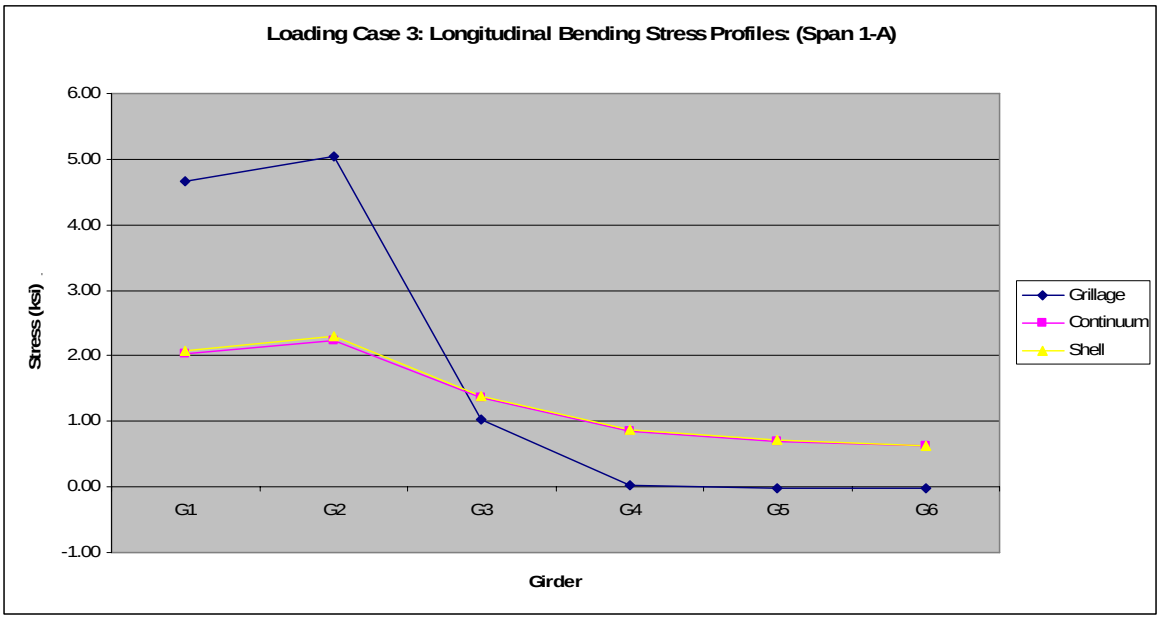

Figure 5.64 Loading Case 3: longitudinal bending stress profiles (Span 1-A).

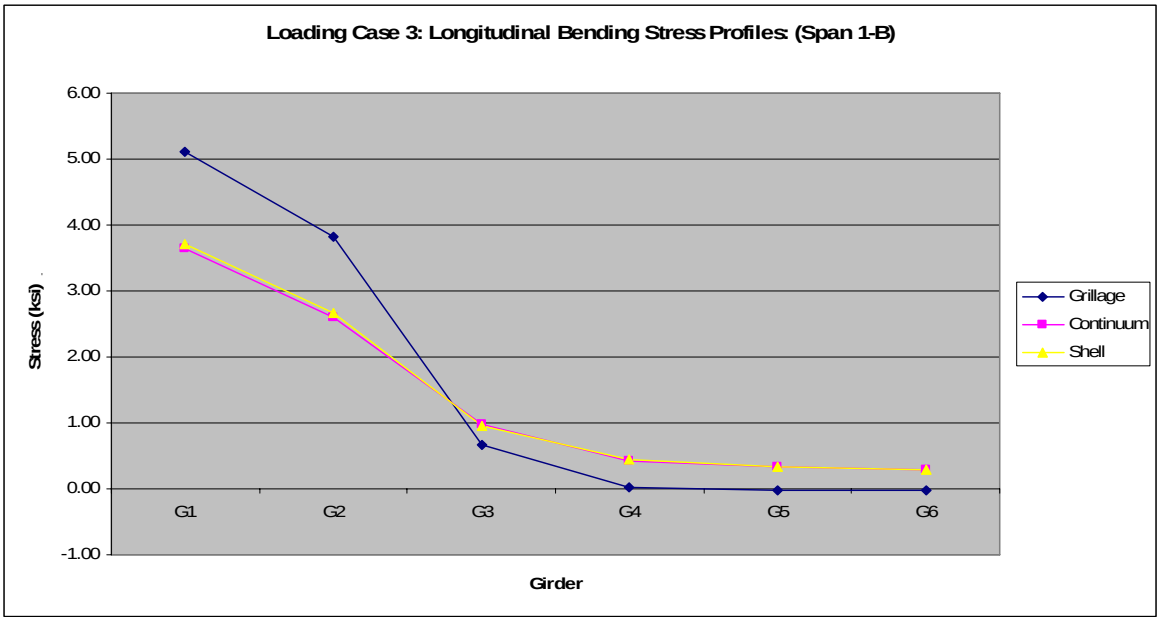

Figure 5.65 Loading Case 3: longitudinal bending stress profiles (Span 1-B).

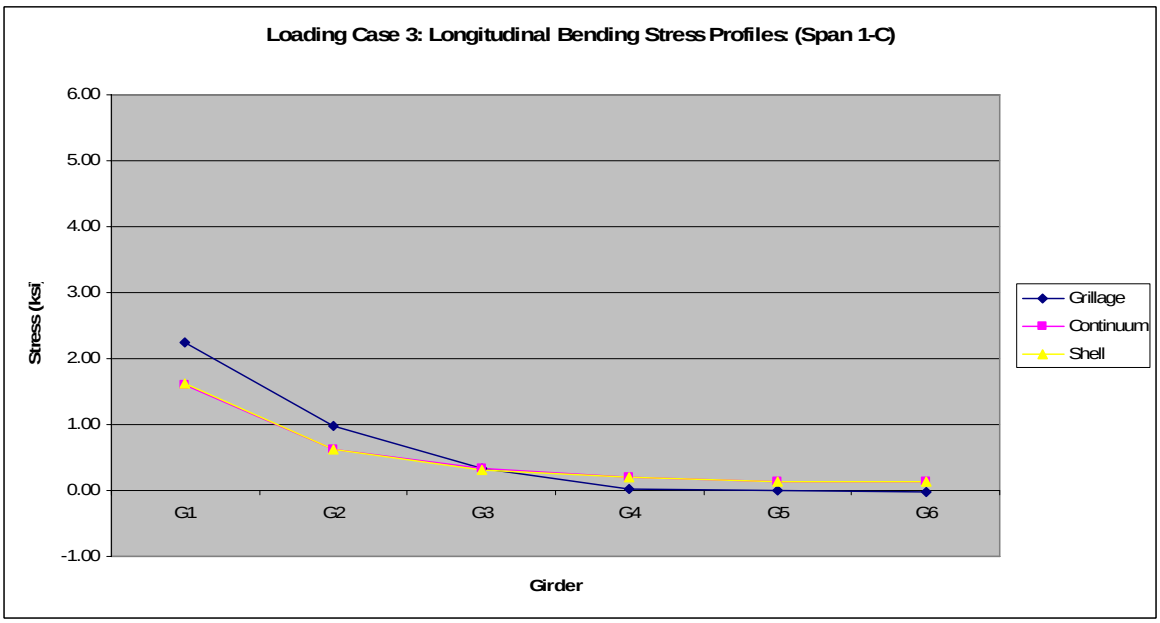

Figure 5.66 Loading Case 3: longitudinal bending stress profiles (Span 1-C).

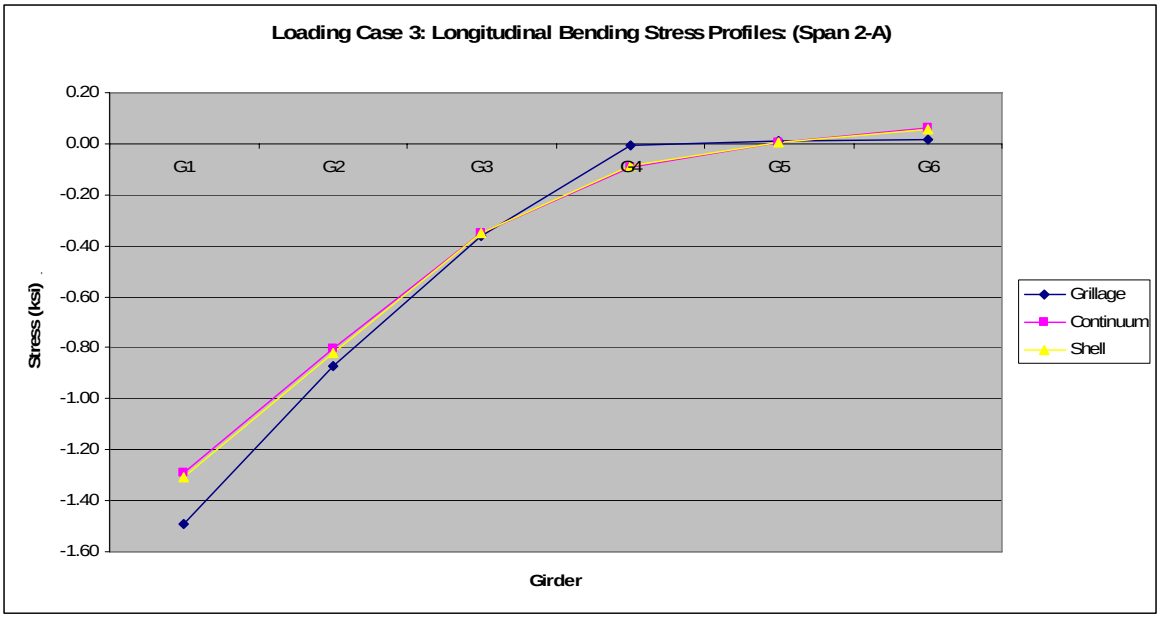

Figure 5.67 Loading Case 3: longitudinal bending stress profiles (Span 2-A).

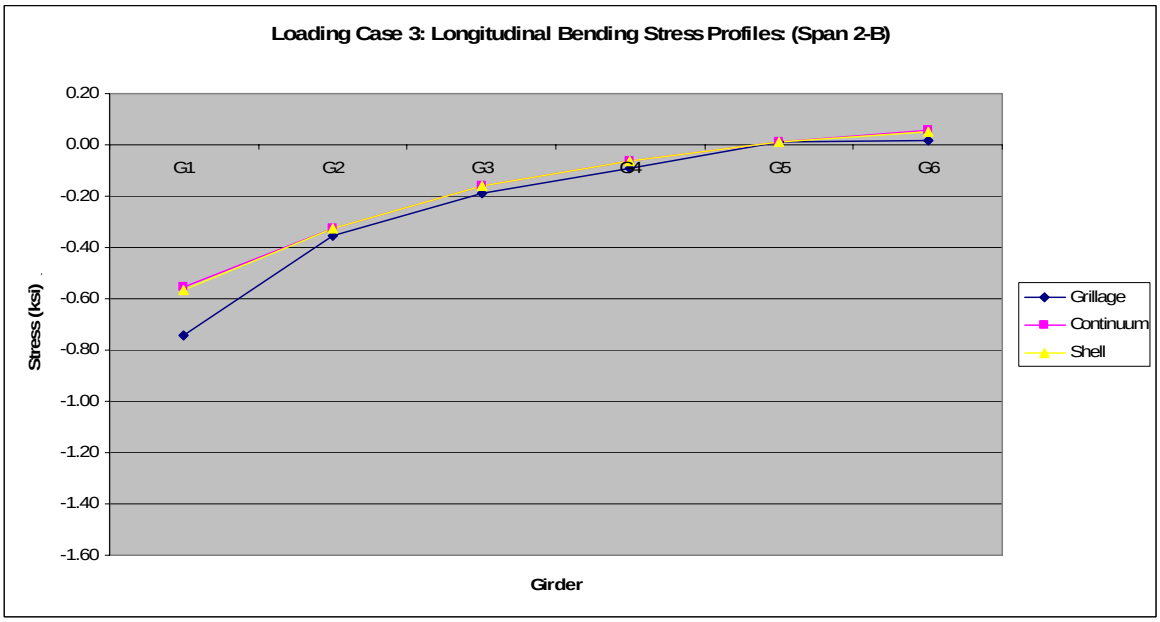

Figure 5.68 Loading Case 3: longitudinal bending stress profiles (Span 2-B).

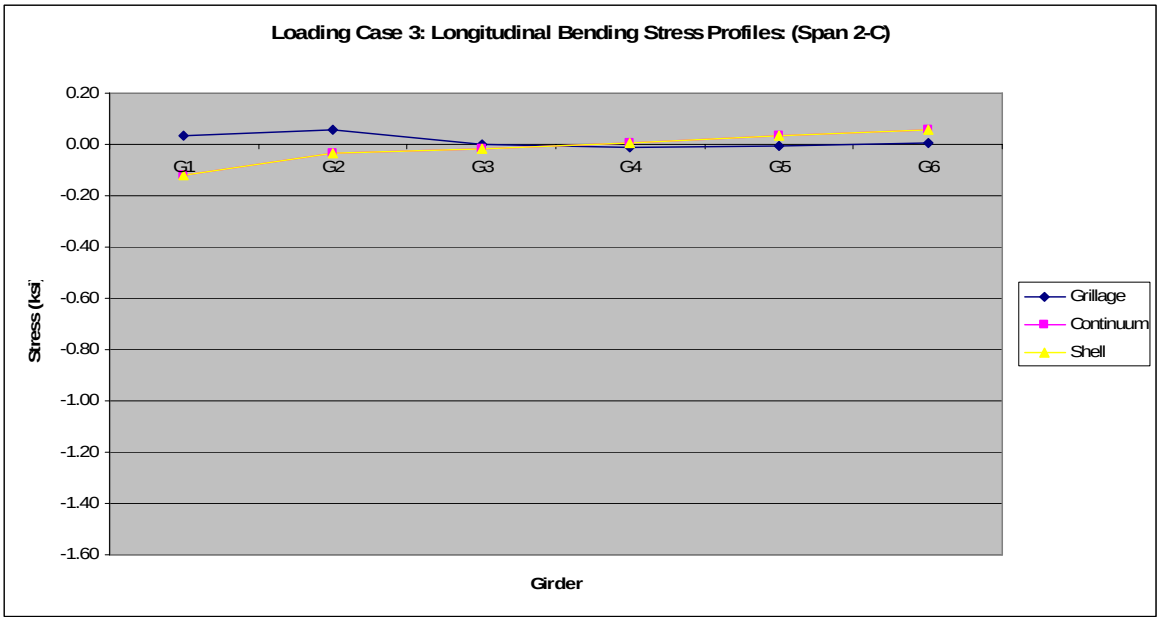

Figure 5.69 Loading Case 3: longitudinal bending stress profiles (Span 2-C).

A noticeable trend in Figures 5.64 and 5.65 is that of the distinct "jumps" in the longitudinal bending stresses between girders in the grillage finite element model. This behavior is relatively consistent throughout in that small variations in stresses between individual girders of the shell finite element models are substantially magnified in the grillage model.

5.5.2 Loading Case 13

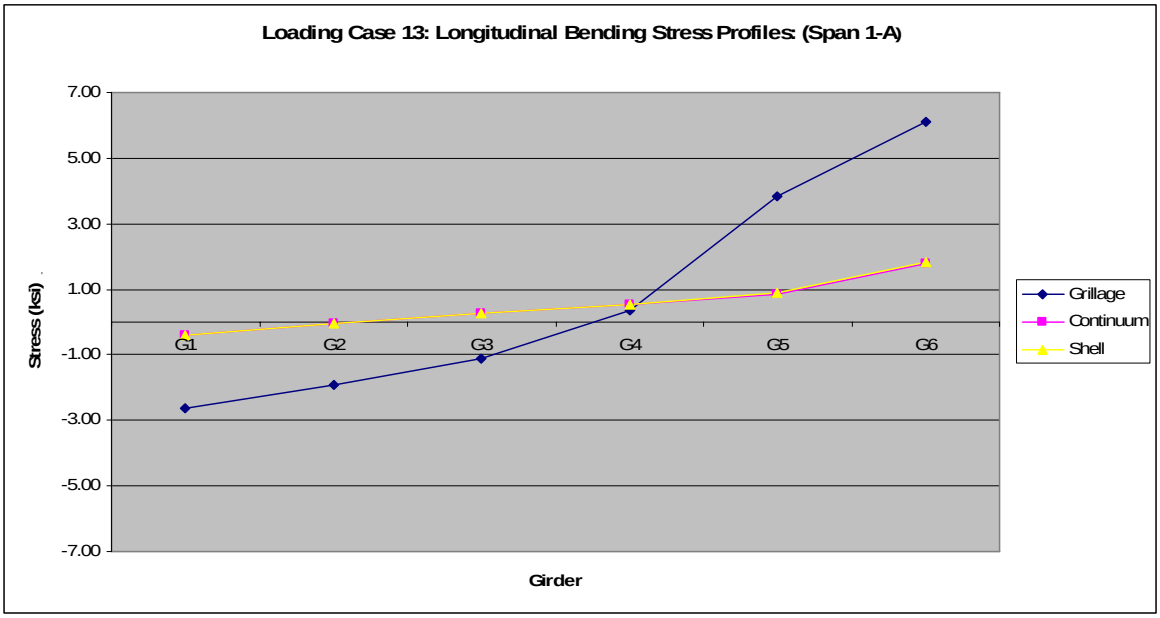

Figure 5.70 Loading Case 13: longitudinal bending stress profiles (Span 1-A).

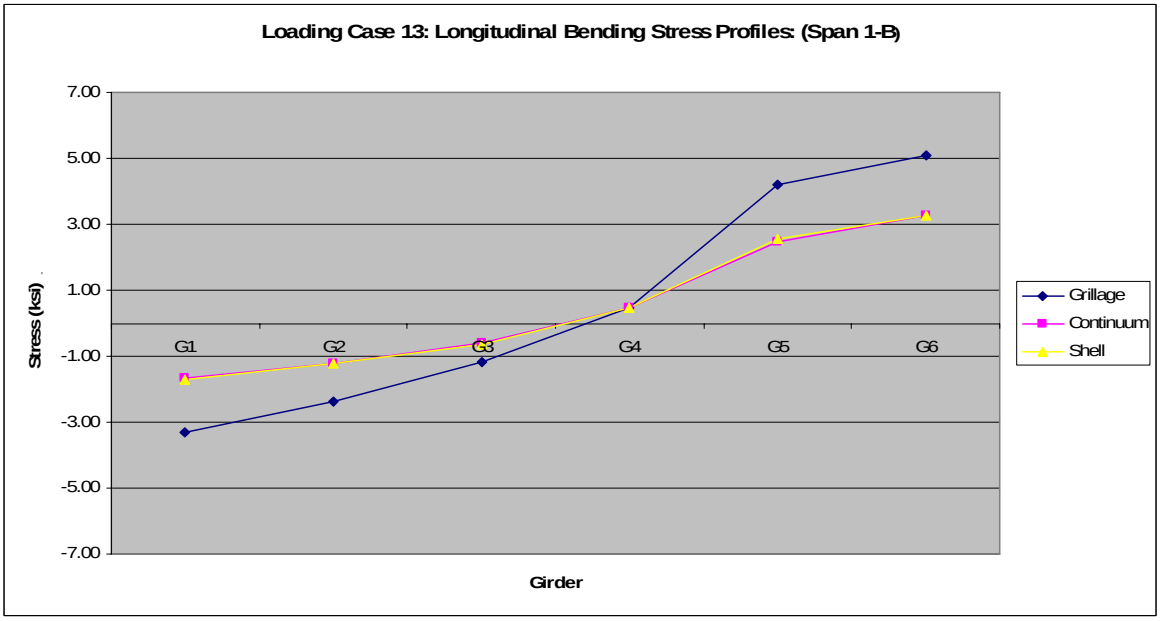

Figure 5.71 Loading Case 13: longitudinal bending stress profiles (Span 1-B).

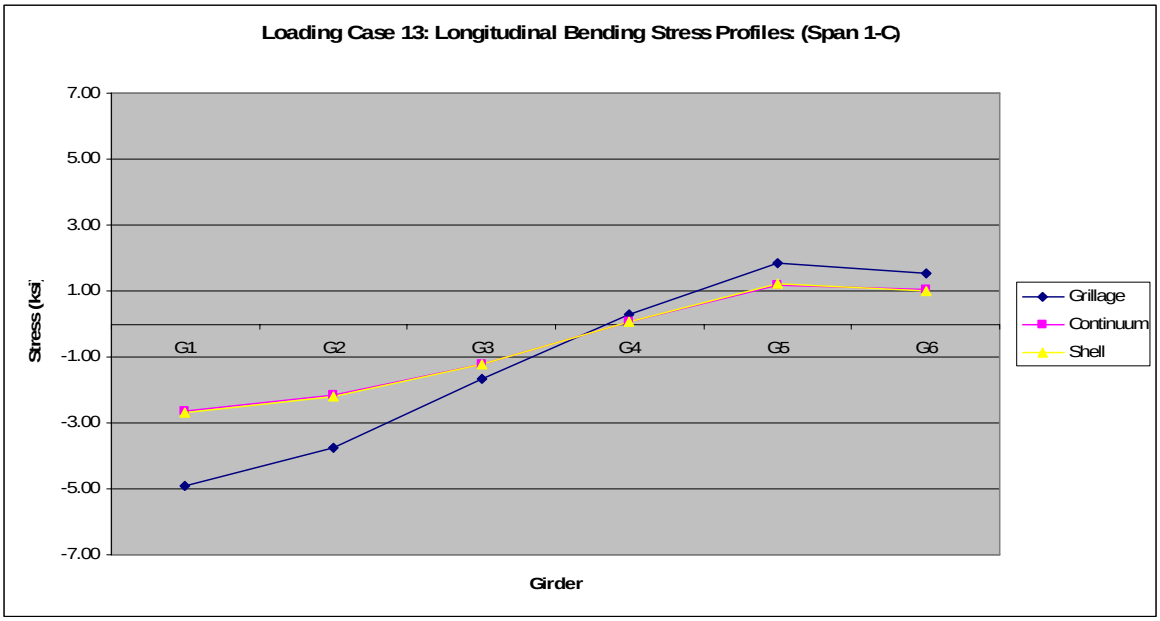

Figure 5.72 Loading Case 13: longitudinal bending stress profiles (Span 1-C).

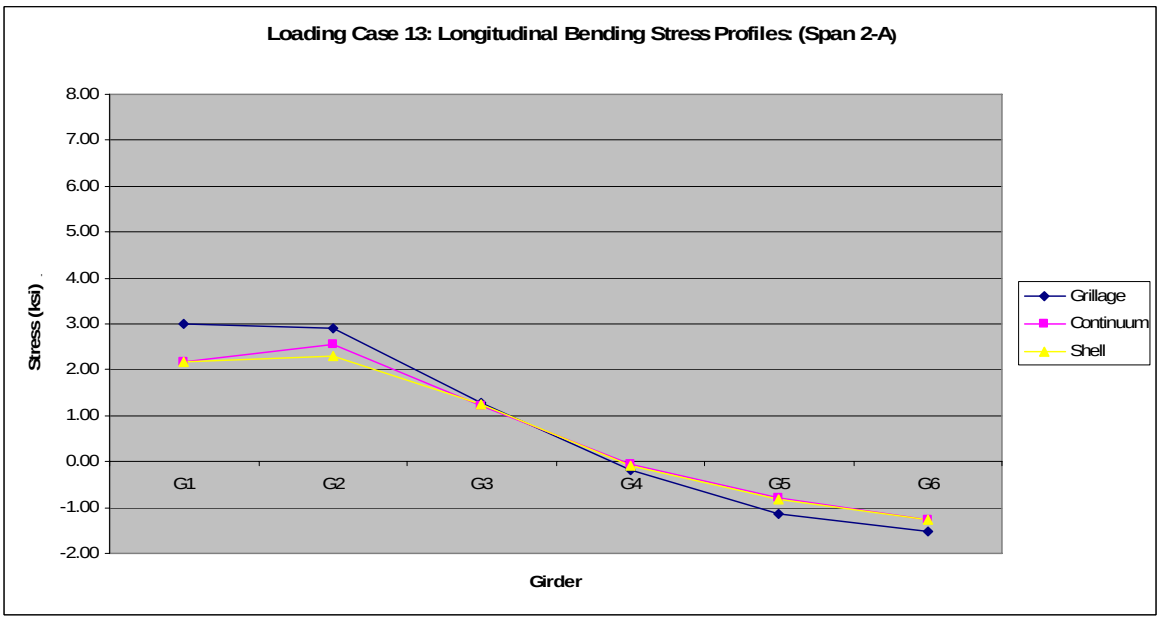

Figure 5.73 Loading Case 13: longitudinal bending stress profiles (Span 2-A).

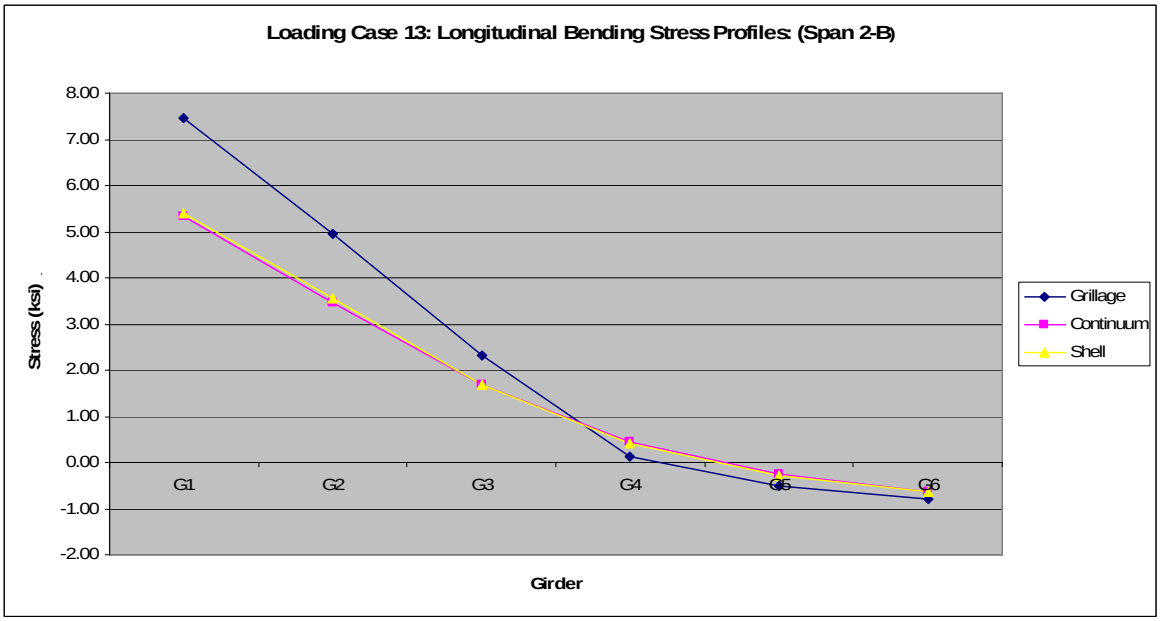

Figure 5.74 Loading Case 13: longitudinal bending stress profiles (Span 2-B).

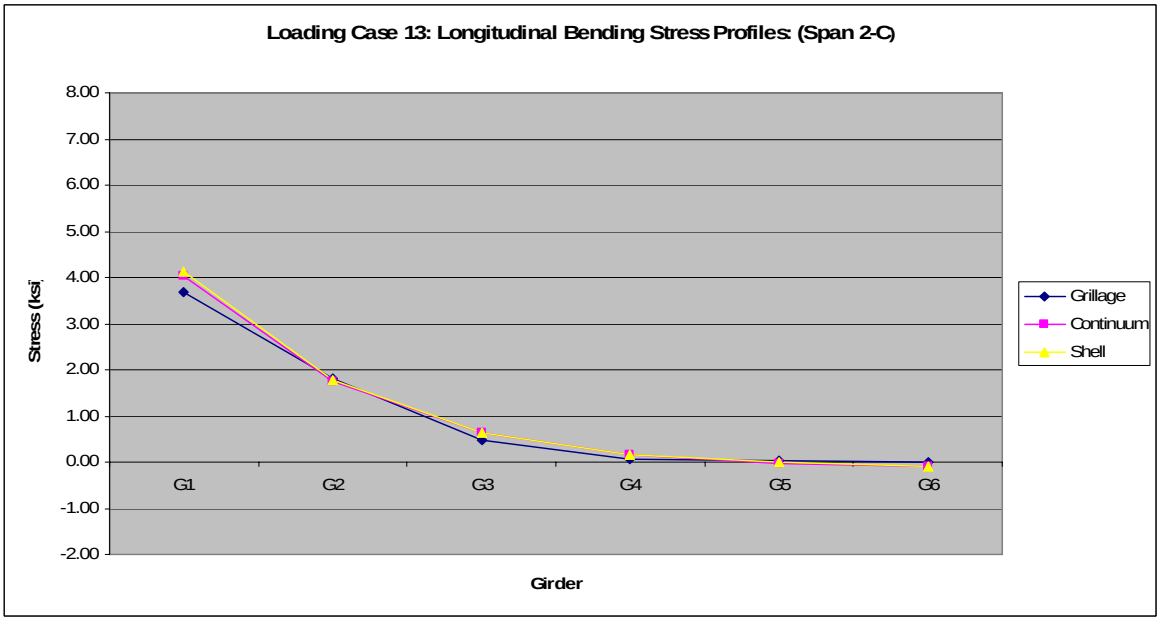

Figure 5.75 Loading Case 13: longitudinal bending stress profiles (Span 2-C).

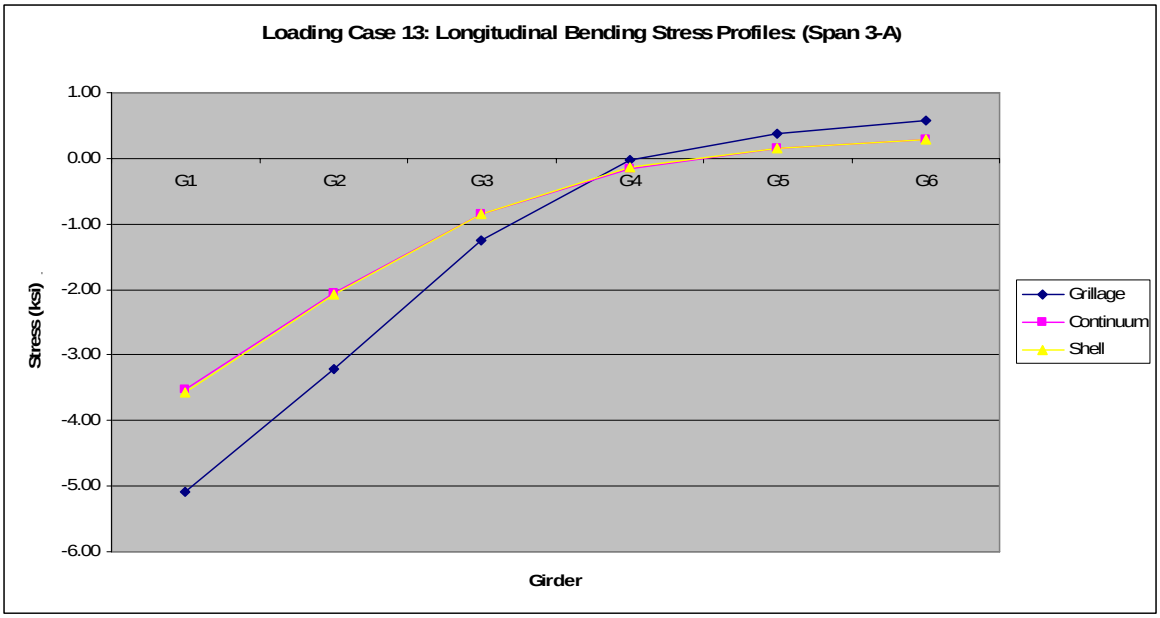

Figure 5.76 Loading Case 13: longitudinal bending stress profiles (Span 3-A).

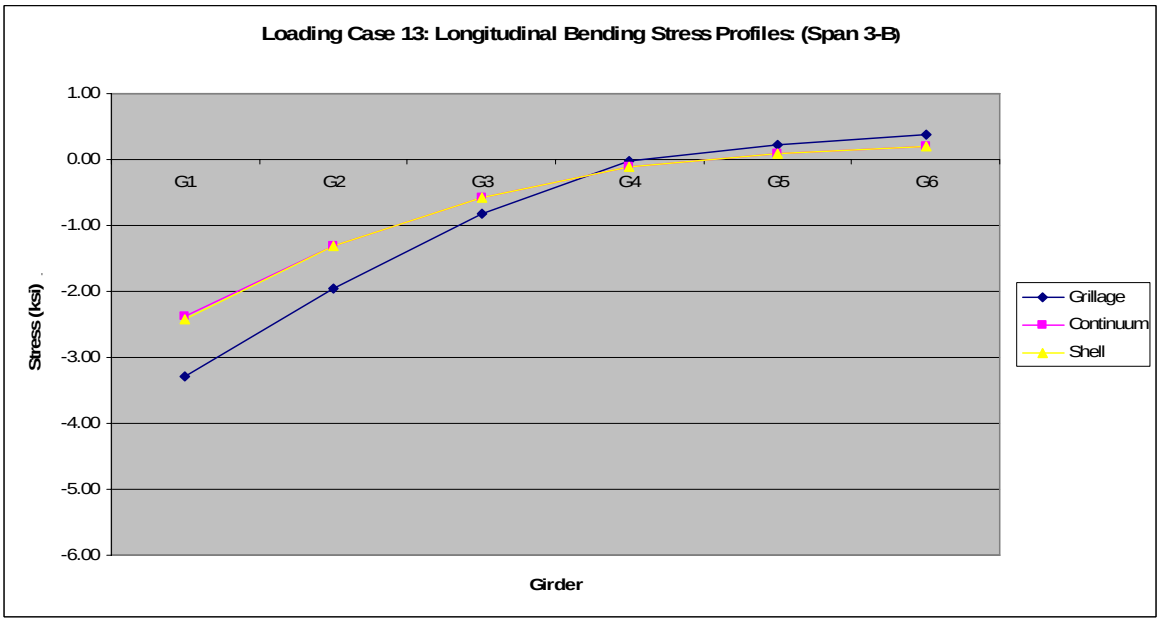

Figure 5.77 Loading Case 13: longitudinal bending stress profiles (Span 3-B).

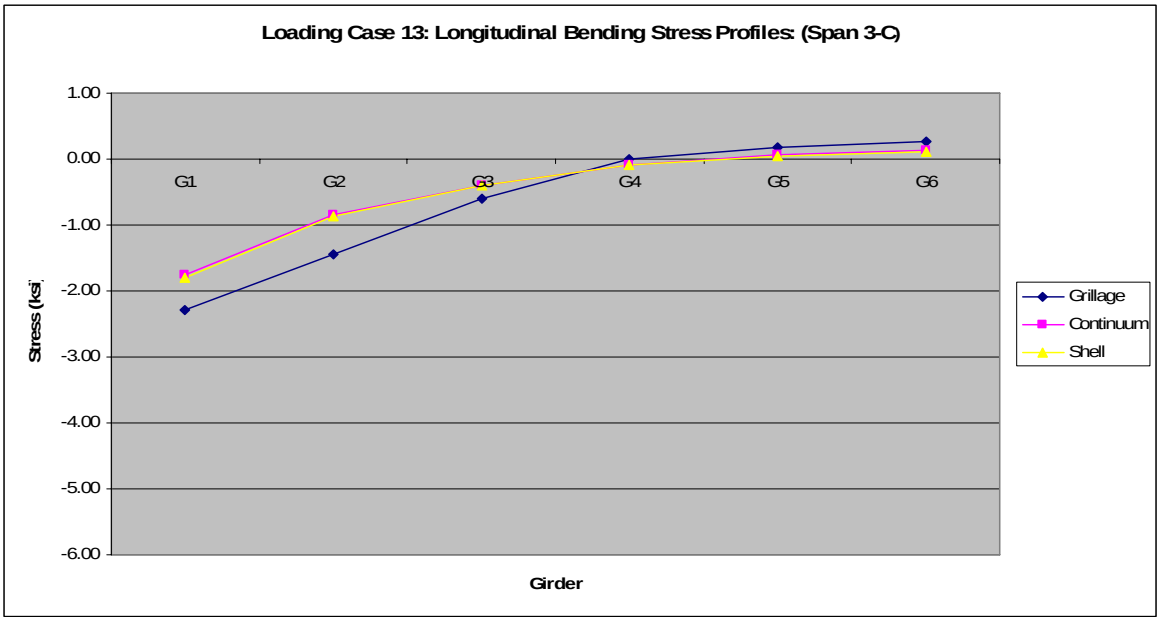

Figure 5.78 Loading Case 13: longitudinal bending stress profiles (Span 3-C).

Of interest with regard to Loading Case 13 is Figure 5.75 where the longitudinal bending stress profiles are approximately equal for *all three* finite element models. It has been demonstrated through the examination of a variety of structural response parameters that the grillage finite element modeling approach employed herein is deficient in its prediction of the behavior of the subject bridge described in Section 2.1. It appears that, such situations as are depicted in Figure 5.75, as well as those seen in Appendix E, relate to conditions in which the grillage model predicts an accurate *local* behavior. Furthermore, it is questionable whether these predictions are arrived at in the correct manner or purely coincidental in nature.

At the beginning of this thesis, it was clearly stated that a simplified model is required to accurately predict both local *and* global behaviors in order to be valid tool for the design office. The grillage modeling approach employed herein does not fulfill this requirement. Following, in Chapter 6, is a compilation of the conclusions drawn from the results presented herein; as well as

suggestions for future research on methods to improve the accuracy of the grillage modeling approach with little additional effort required.

6.0 CONCLUSIONS

The primary goal of this thesis was to provide insight into the accuracy of a more simplified modeling approach, based upon a grillage finite element model, as compared to a more refined shell finite element modeling approach; such that the validity of such a simplification may be confirmed (or in this case, denied). Through the presentation and discussion of results from a variety of loading cases, it has been shown that the grillage finite element model, as described in Section 3.2, is insufficient at accurately capturing the behavior of the subject bridge described in Section 2.1.

The governing characteristic which drives the inaccuracy of the grillage model, as pointed out in the previous chapter, comes from its treatment of the concrete deck. Clearly, the fundamental assumption of the grillage modeling approach employed herein (i.e. that of the transverse steel diaphragms being the primary load distribution mechanism of the bridge), is not a valid assumption to make in the present problem. While the prevailing characteristic of this modeling approach is that of a significant overestimation of local response, two points must be made and kept in mind, lest it be thought that grillage modeling is a conservative approach.

First, as it is that the accuracy of an analysis technique oftentimes can be rationalized into a measure of the economy of the subsequent design, it is important that in adopting a conservative approach to a problem, that this approach not be overly conservative. The grillage finite element model, as compared to the shell finite element models resulted in errors on the

order of 40% to 70% when considering longitudinal bending stresses; this magnitude of error is unacceptable by today's standards.

The second point comes from the actual examination of results from such a simplified approach. It is frequently pointed out throughout Chapter 5 that the results from the grillage finite model match those of the shell finite element models with reasonable accuracy. However, when considering the cumulative results from any single loading case, it is seen that such occurrences are local in nature, and could actually be simple coincidences as a result of the interaction of the applied loads. It is therefore important when approaching a problem such as that presented herein, that careful examination of the entire body of results commence prior to making a conclusion with regard to the validity of the assumption.

Furthermore, it must be pointed out that this thesis encompassed the examination of a grillage finite element model being applied to a longitudinally skewed, steel I-girder bridge. It is possible that this approach oversimplified the behavior inherent to such bridges; perhaps a non-skewed bridge would yield more favorable results. However, if a modeling approach does not accurately predict the structural response of more than one system, is it truly cost-effective to adopt such an approach?

Avenues for future research in this area include the iterative process of refining the grillage modeling approach until the behavior falls within reasonable bounds of the more refined shell finite element models. The concrete deck is noted throughout this thesis as being insufficiently represented in the grillage modeling approach (i.e. through modified beam section properties emanating from a transformed section, and through the inclusion of auxiliary members.

Another possible method to improve the accuracy of the grillage finite element model is to take a more three-dimensional approach to the problem by employing 2-node Hermitian beam finite elements for all of the steel members (longitudinal steel girders and transverse steel diaphragms) and MITC4 shell finite elements [Bathe, 1996] for the concrete deck; connection of these components necessitates the use of node-to-node rigid links. This would eliminate a significant portion of the computational demand imposed by the modeling of the longitudinal steel girders in the shell finite element models while still allowing for the accurate representation of the concrete deck.

As pointed out in Chapter 4, the additional benefit of employing two separate shell finite element modeling approaches lies in an examination of the relative differences between the results from both models. While not explicitly stated in Chapter 5, it is clear that both shell finite element models performed in a very consistent manner with regard to one another. If one considers the shell deck model to be correct, the continuum deck model actually regularly performed within 5% of the shell deck model. However, given the computational resources available during the analysis of these models, the savings afforded by the continuum deck model equated to roughly one-fourth of the time required for the shell deck model (recall that the continuum deck model employed approximately one million degrees of freedom where the shell deck model employed twice that amount).

Given a choice between these two distinct modeling approaches, it is clear that the continuum deck model provides the most time-efficient solution with an almost negligible loss in accuracy. Furthermore, the continuum deck model affords the opportunity to efficiently assign "real-world" behavior of concrete to be examined by employing the aforementioned concrete material model [Bathe, et al, 1989].

In closing, it is reiterated that a simplified modeling approach *must not* be presumed to provide a conservative solution to any and / or all problem domains. The assumptions inherent in the simplification of a given structural system must be thoroughly understood prior to the adoption of any simplified approach. Furthermore, it is noted the wide variety of computational tools available to the engineer, while being able to efficiently provide solutions to complicated problems, must be employed with a certain amount of discretion. This is not to say such tools are not to be trusted, but rather that they are thoroughly understood prior to use. It is therefore the *educated* implementation of both present and future computational tools which forms a vital component in the future advancement of the field of structural engineering.

APPENDIX A

SUPPLEMENTARY RESULTS (REACTIONS)

A.1 Loading Case 5

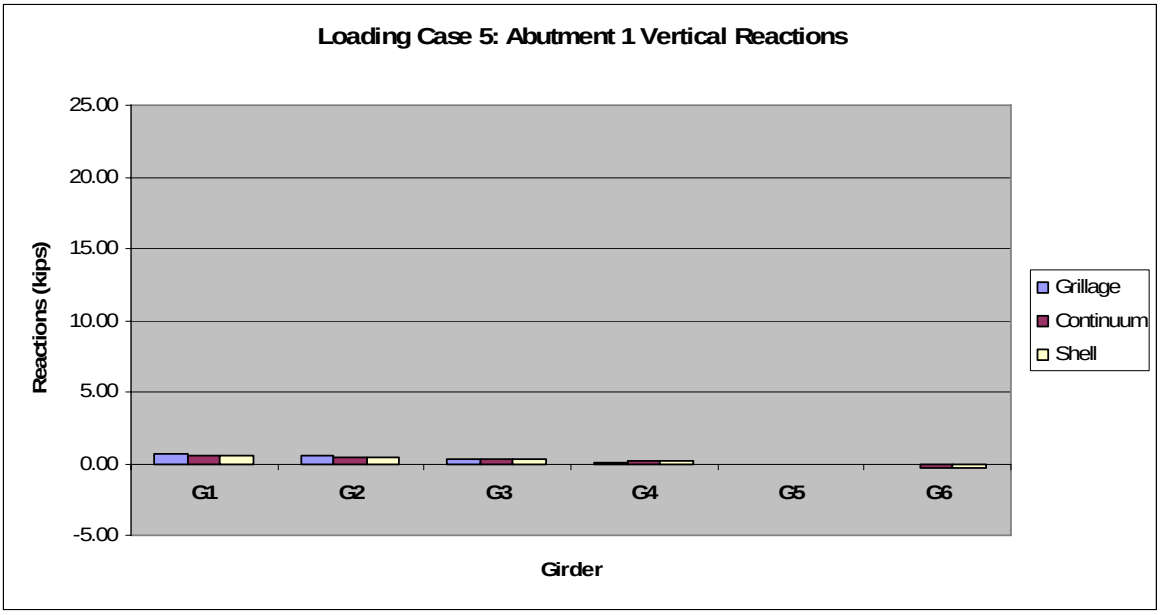

Figure A.1 Loading Case 5: Abutment 1 vertical reactions.

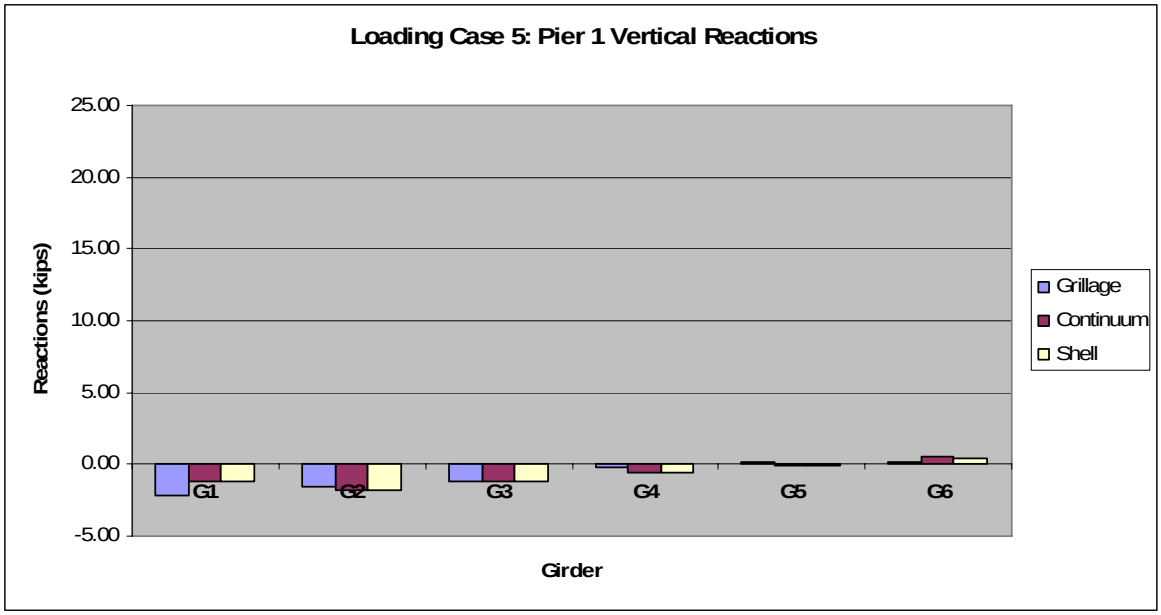

Figure A.2 Loading Case 5: Pier 1 vertical reactions.

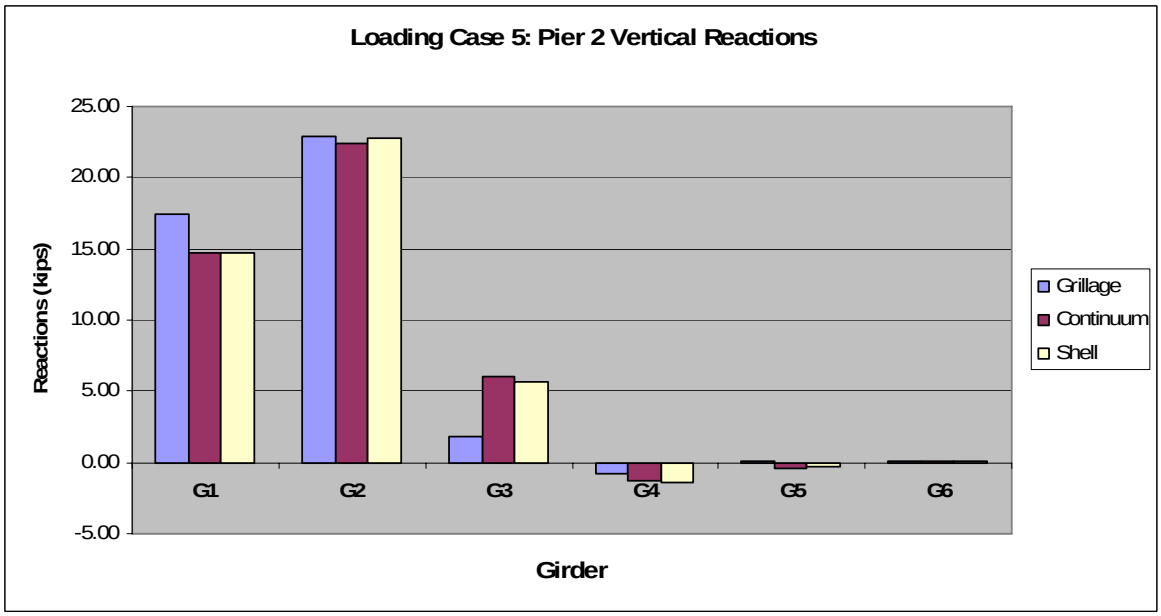

Figure A.3 Loading Case 5: Pier 2 vertical reactions.

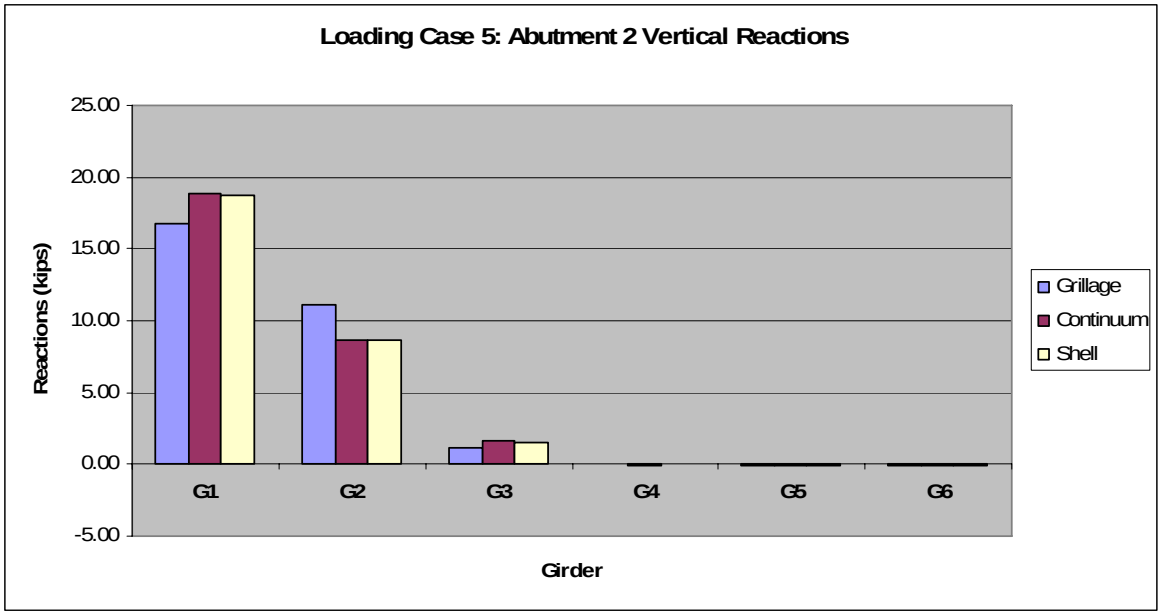

Figure A.4 Loading Case 5: Abutment 2 vertical reactions.

A.2 Loading Case 6

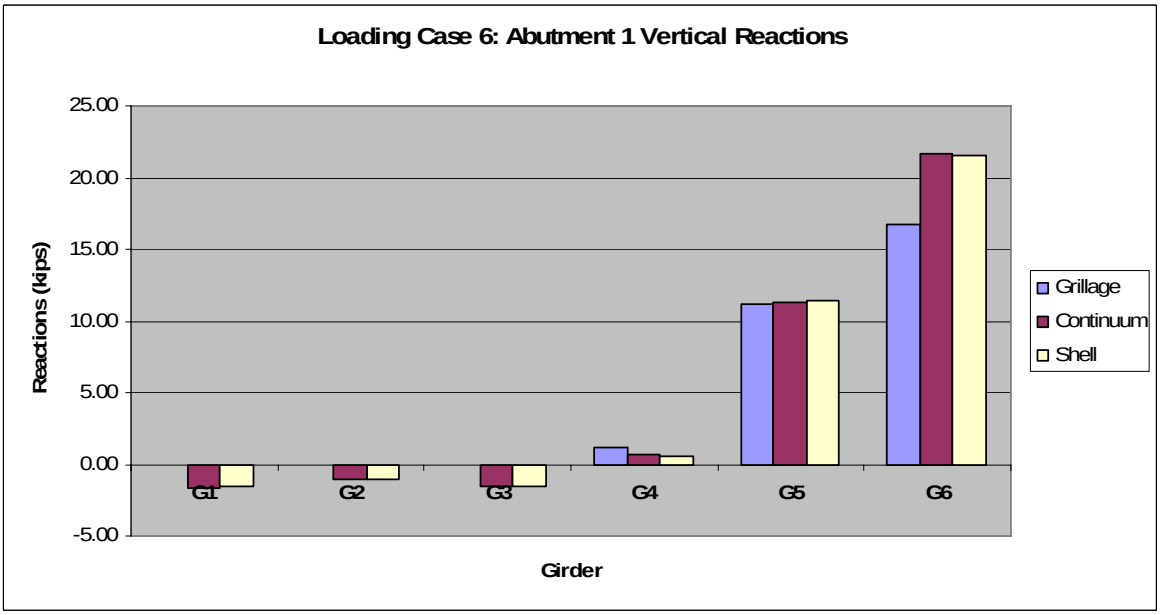

Figure A.5 Loading Case 6: Abutment 1 vertical reactions.

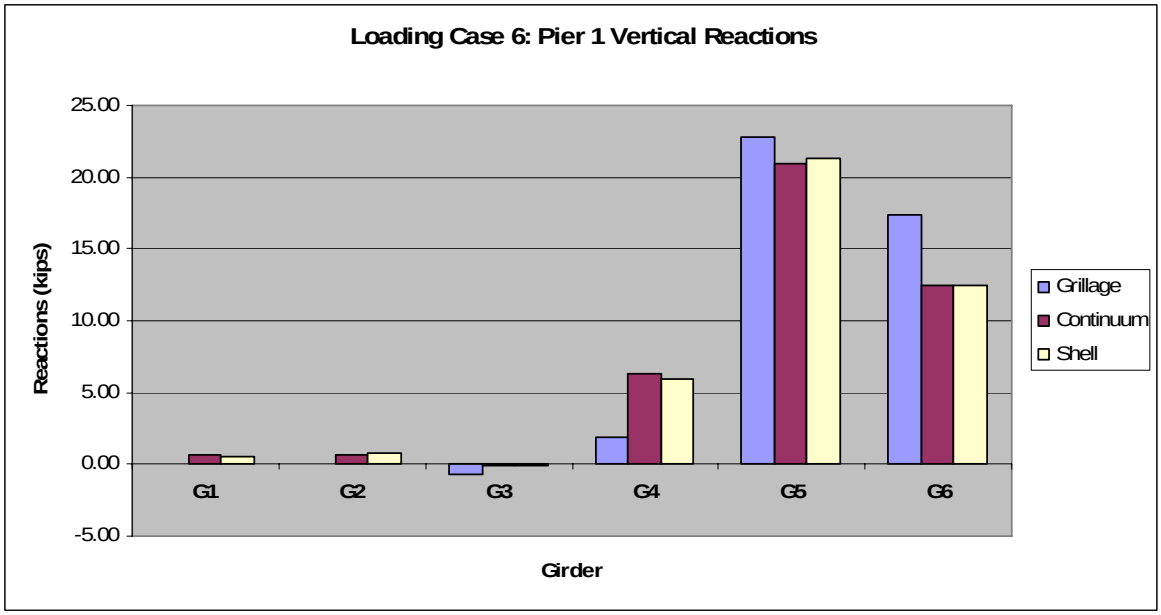

Figure A.6 Loading Case 6: Pier 1 vertical reactions.

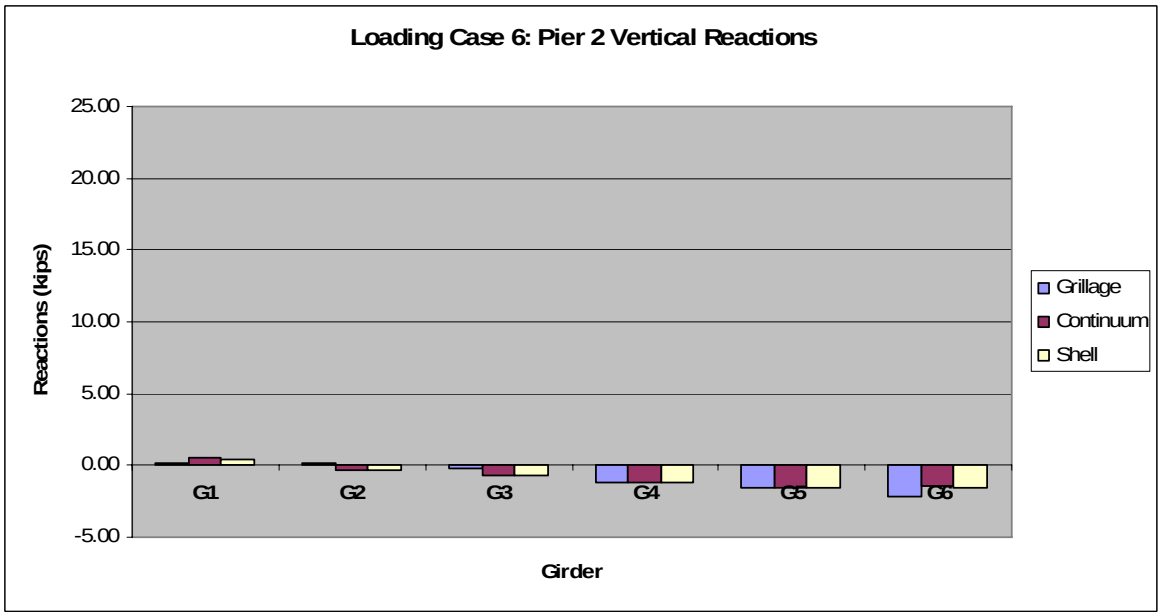

Figure A.7 Loading Case 6: Pier 2 vertical reactions.

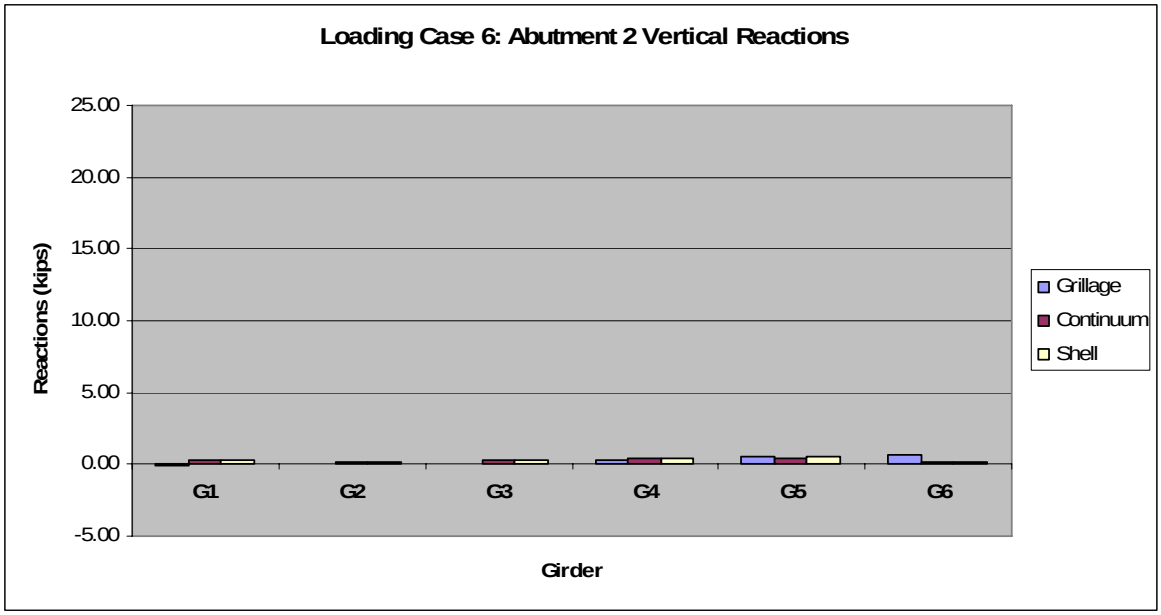

Figure A.8 Loading Case 6: Abutment 2 vertical reactions.

A.3 Loading Case 7

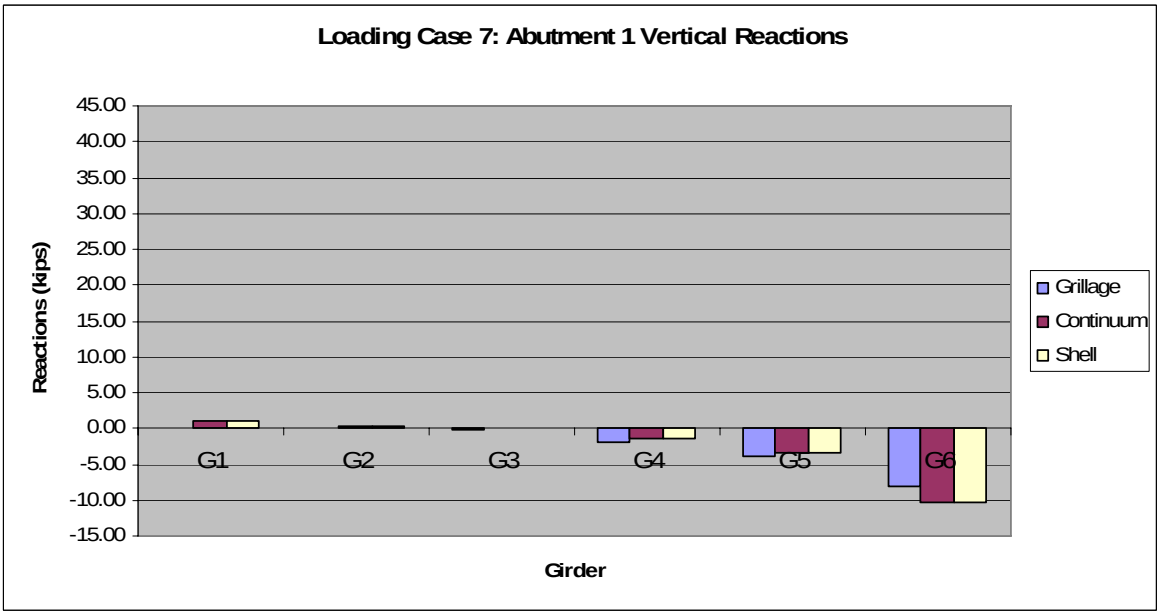

Figure A.9 Loading Case 7: Abutment 1 vertical reactions.

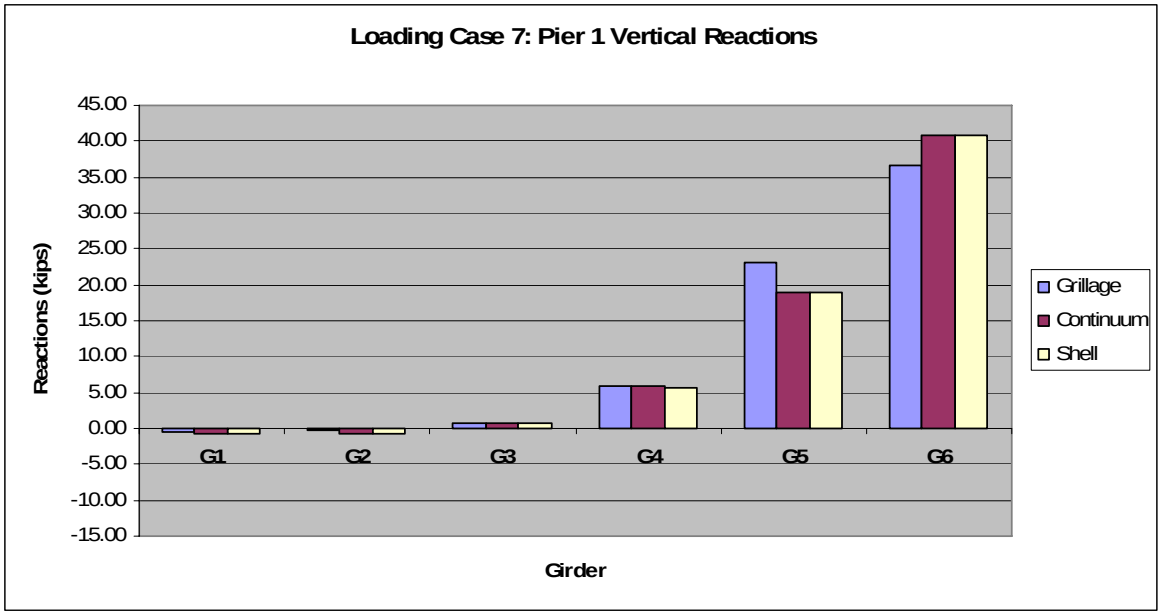

Figure A.10 Loading Case 7: Pier 1 vertical reactions.

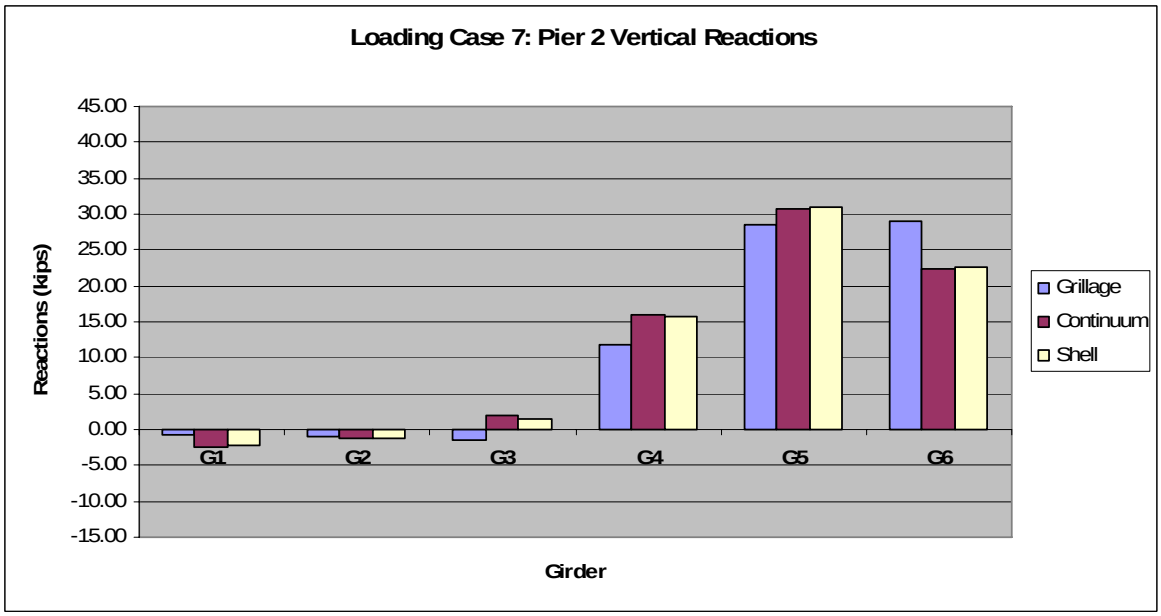

Figure A.11 Loading Case 7: Pier 2 vertical reactions.

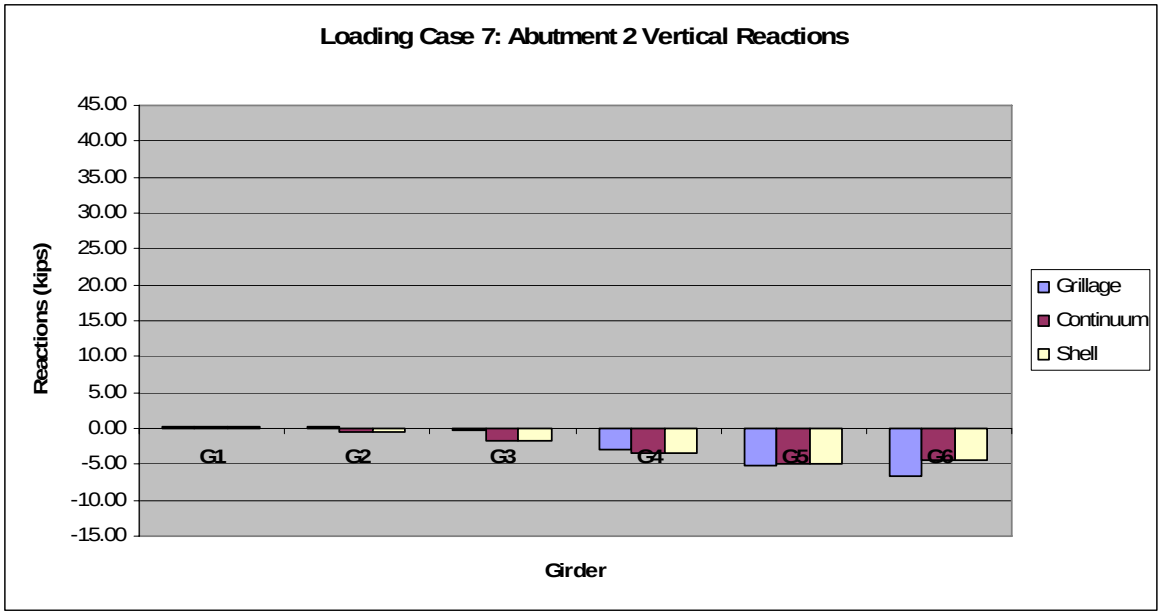

Figure A.12 Loading Case 7: Abutment 2 vertical reactions.

A.4 Loading Case 8

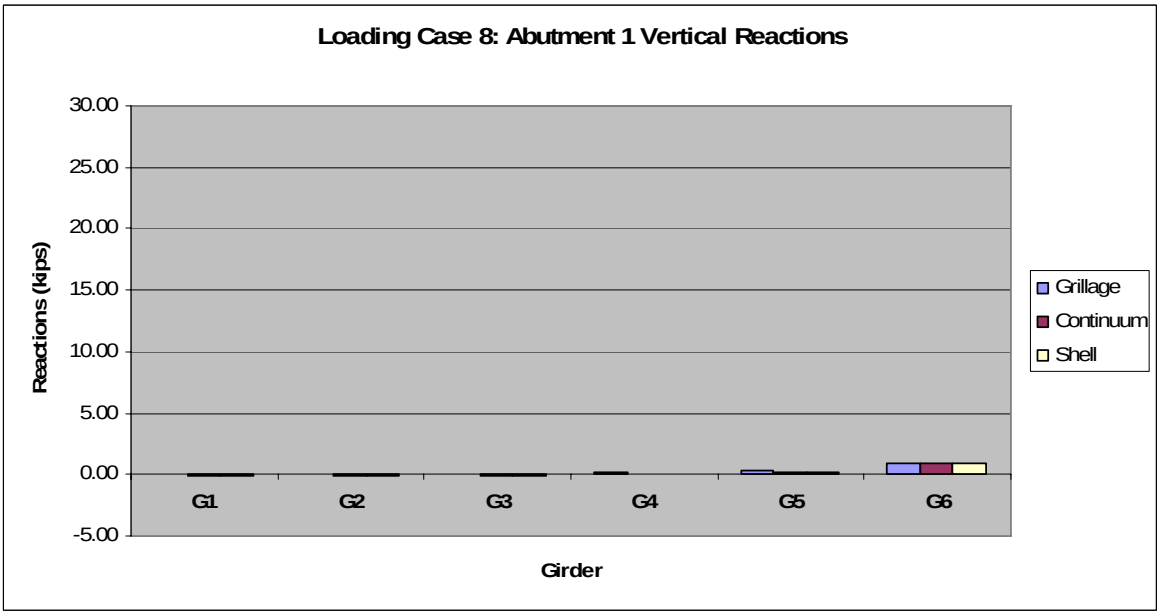

Figure A.13 Loading Case 8: Abutment 1 vertical reactions.

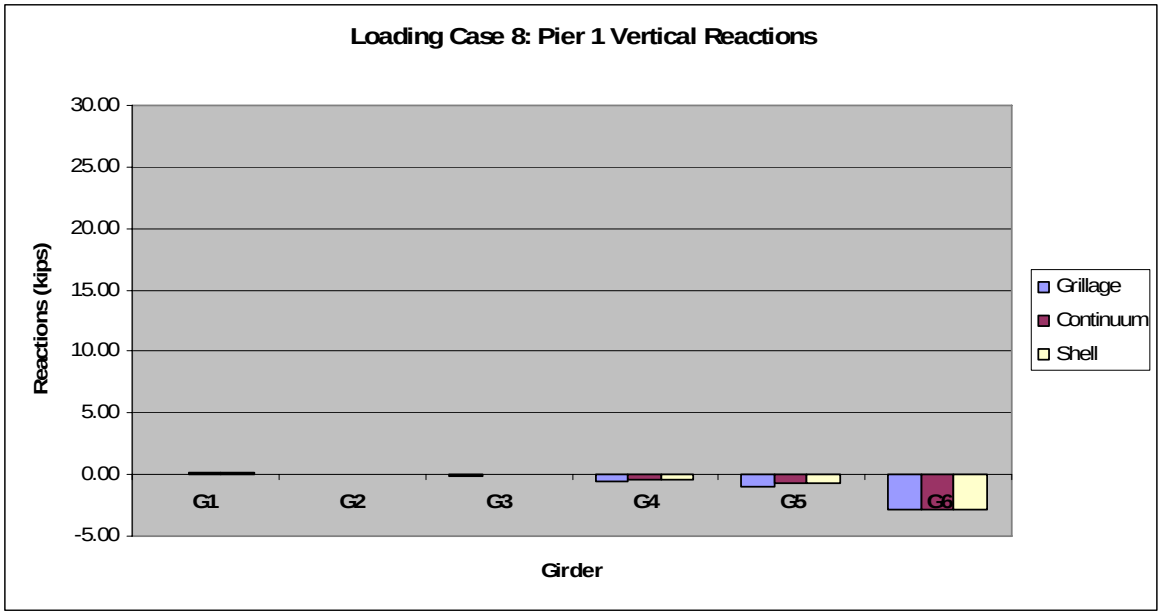

Figure A.14 Loading Case 8: Pier 1 vertical reactions.

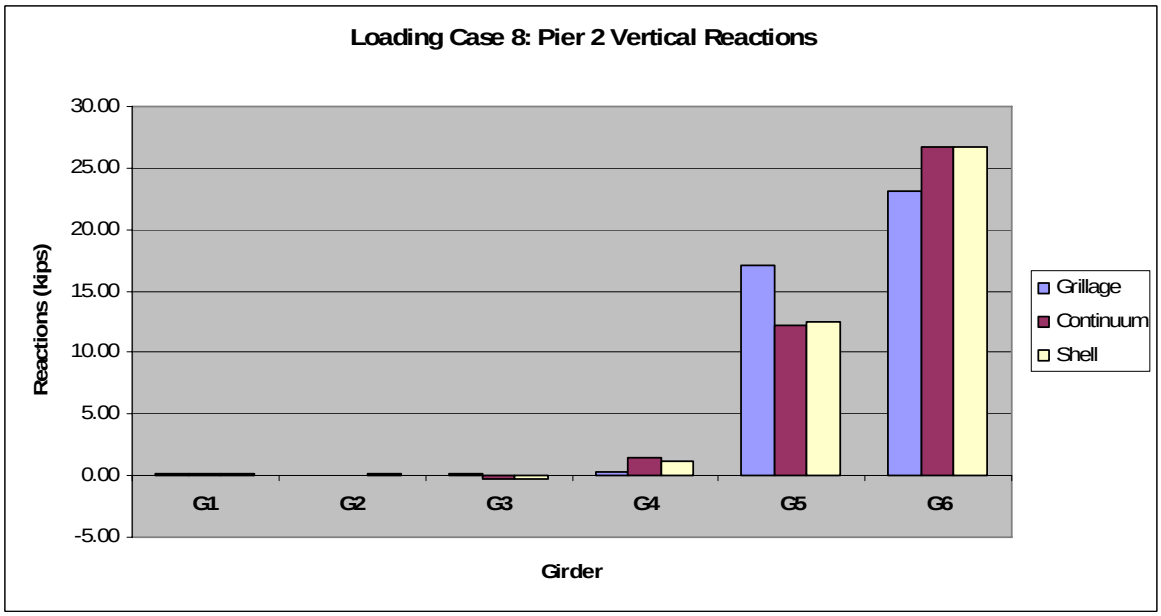

Figure A.15 Loading Case 8: Pier 2 vertical reactions.

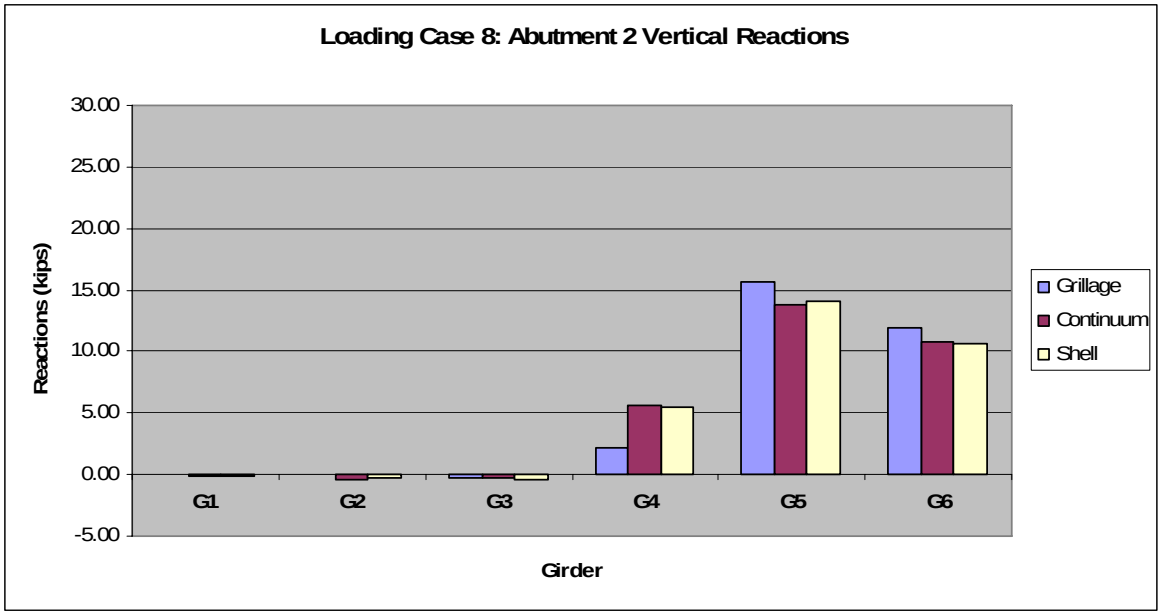

Figure A.16 Loading Case 8: Abutment 2 vertical reactions.

A.5 Loading Case 9

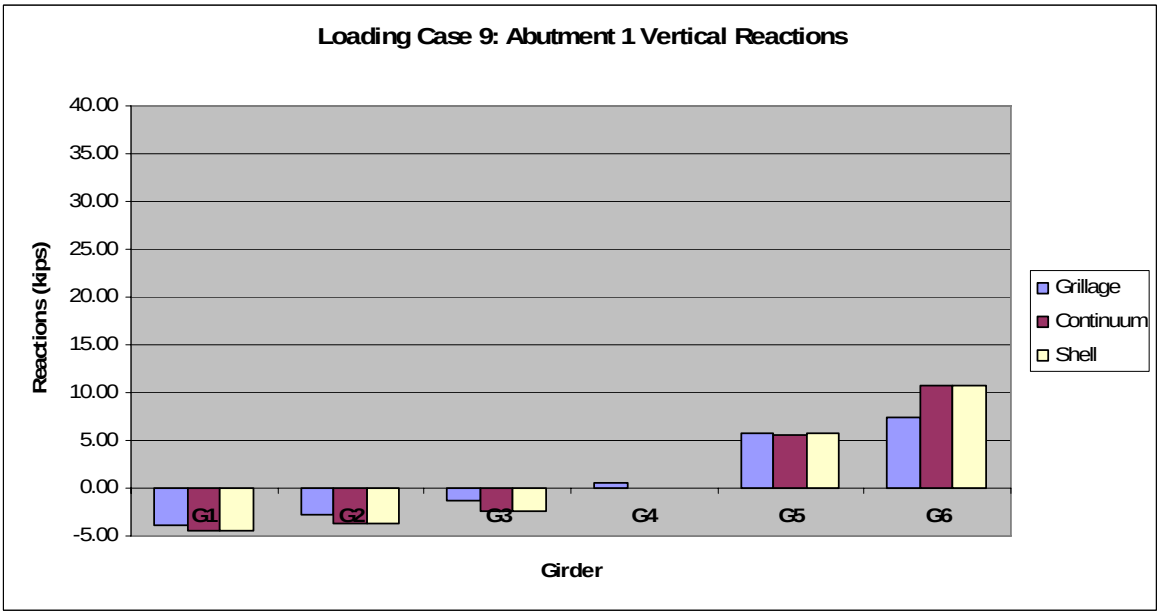

Figure A.17 Loading Case 9: Abutment 1 vertical reactions.

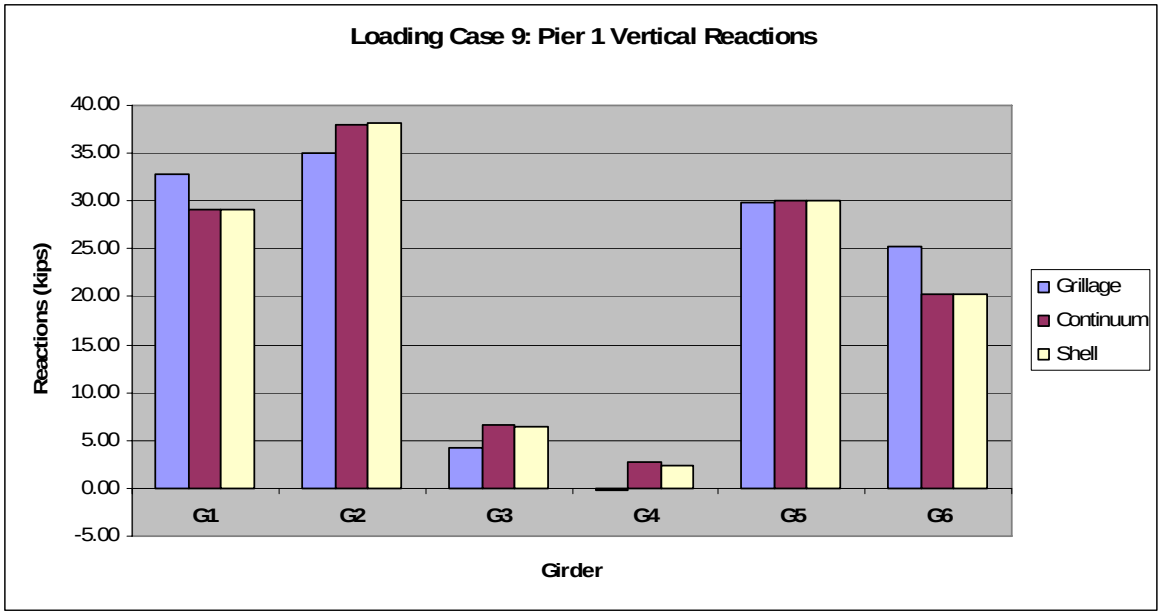

Figure A.18 Loading Case 9: Pier 1 vertical reactions.

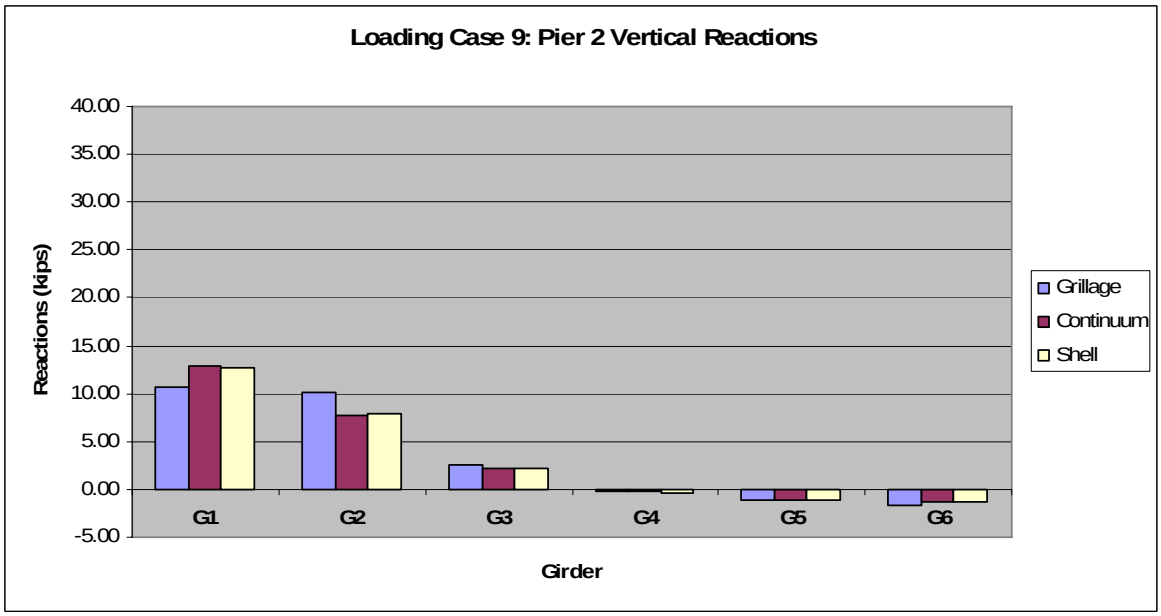

Figure A.19 Loading Case 9: Pier 2 vertical reactions.

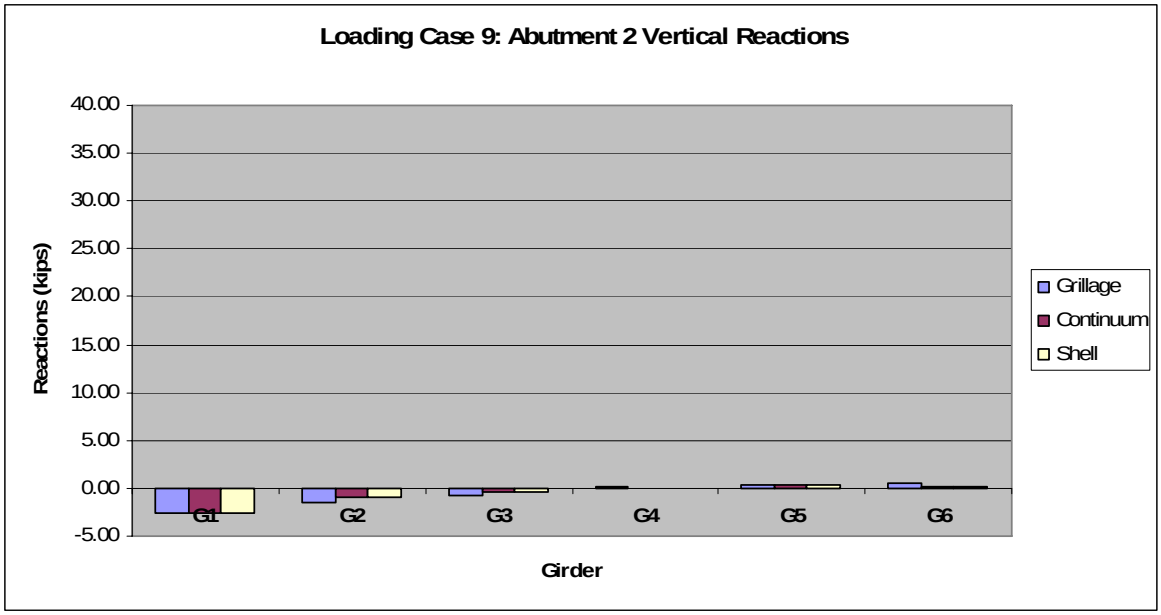

Figure A.20 Loading Case 9: Abutment 2 vertical reactions.

A.6 Loading Case 11

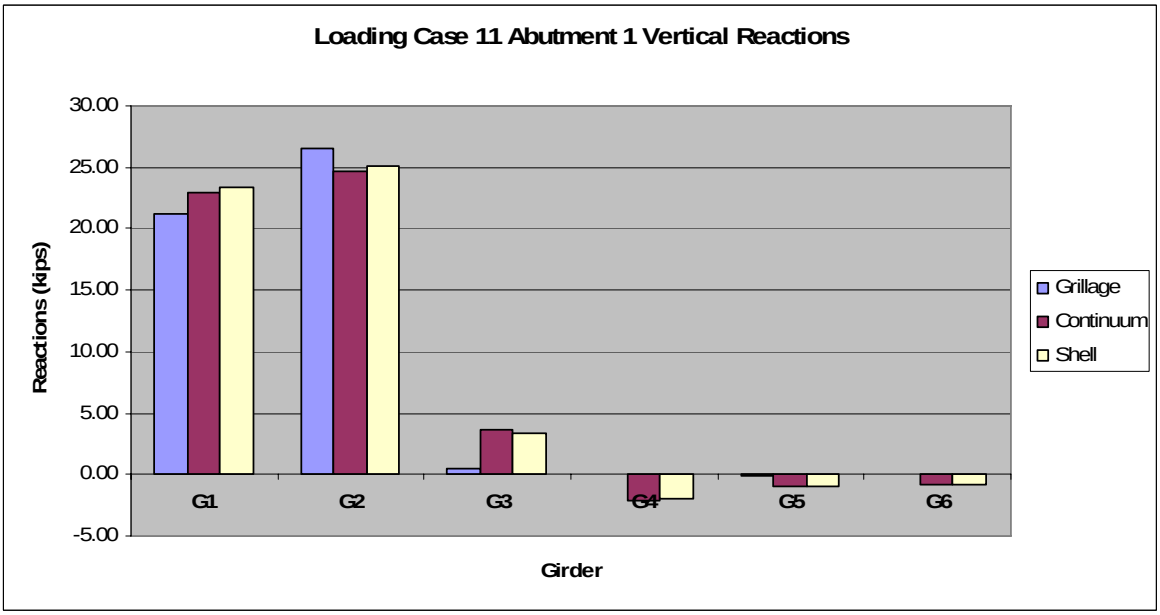

Figure A.21 Loading Case 11: Abutment 1 vertical reactions.

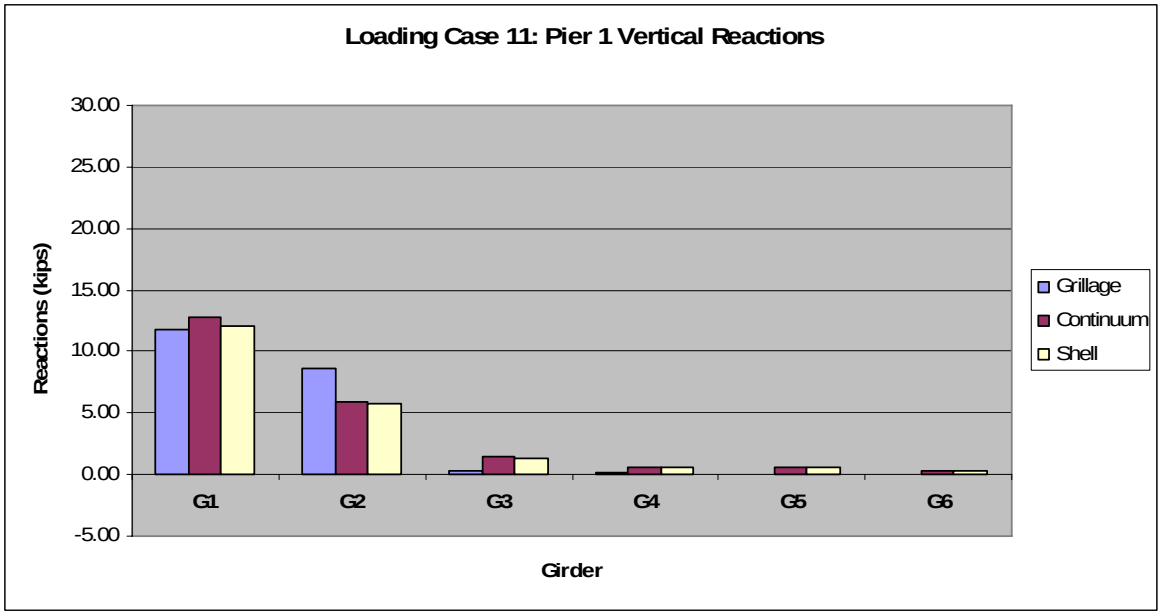

Figure A.22 Loading Case 11: Pier 1 vertical reactions.

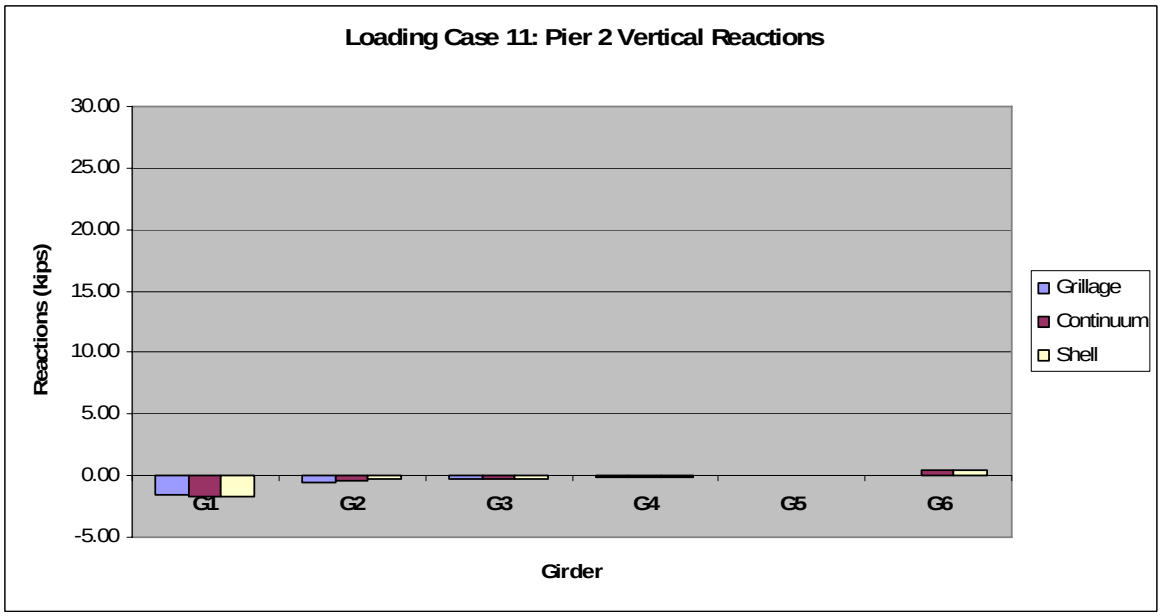

Figure A.23 Loading Case 11: Pier 2 vertical reactions.

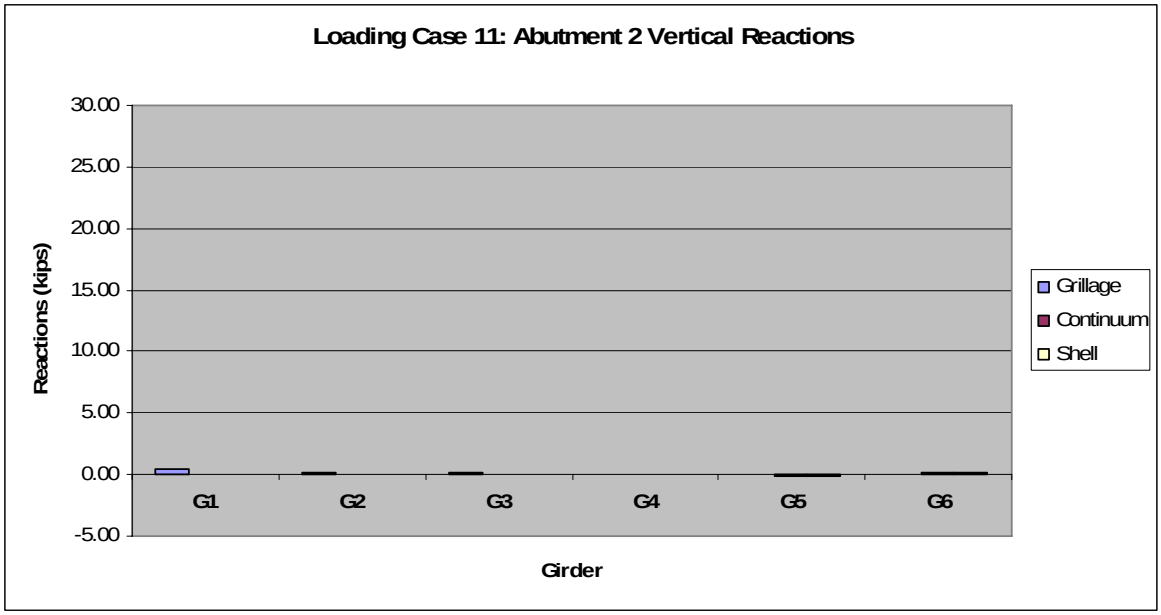

Figure A.24 Loading Case 11: Abutment 2 vertical reactions.

A.7 Loading Case 12

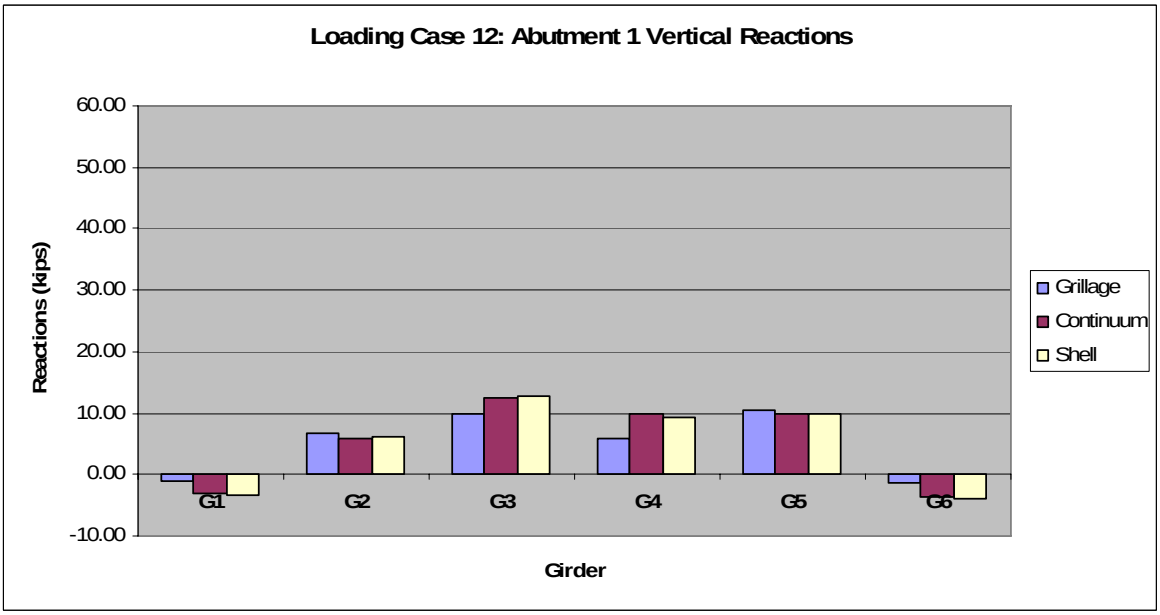

Figure A.25 Loading Case 12: Abutment 1 vertical reactions.

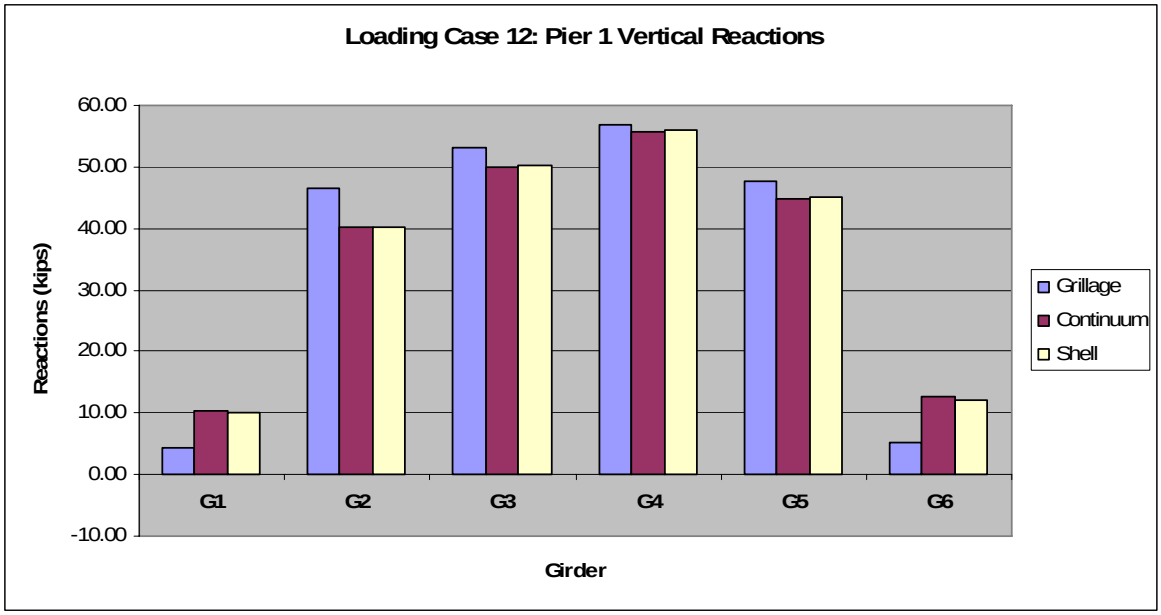

Figure A.26 Loading Case 12: Pier 1 vertical reactions.

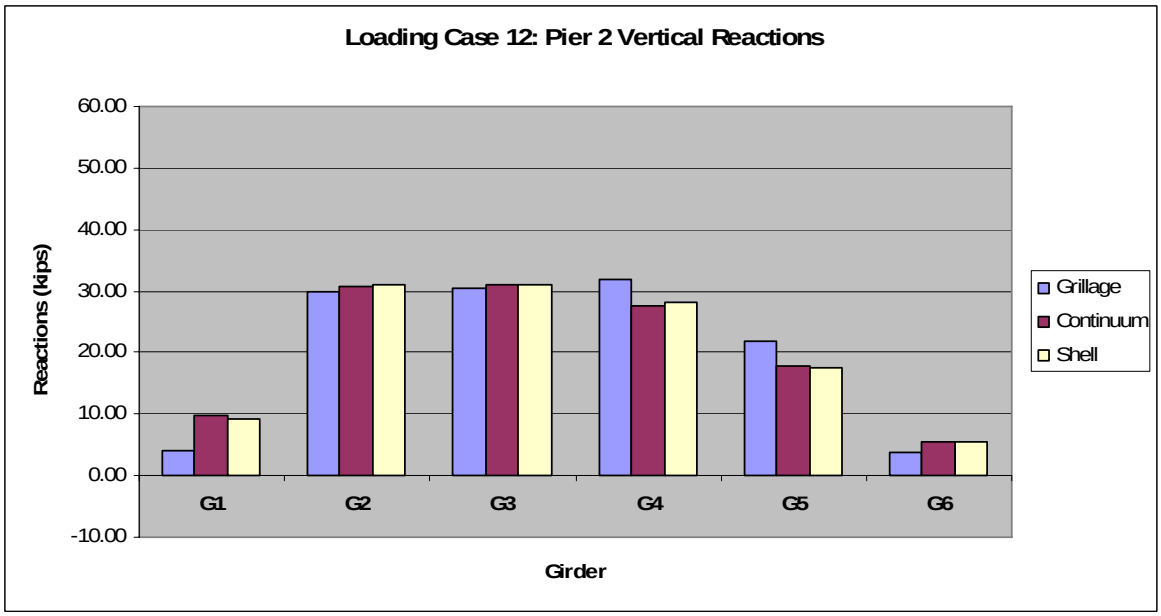

Figure A.27 Loading Case 12: Pier 2 vertical reactions.

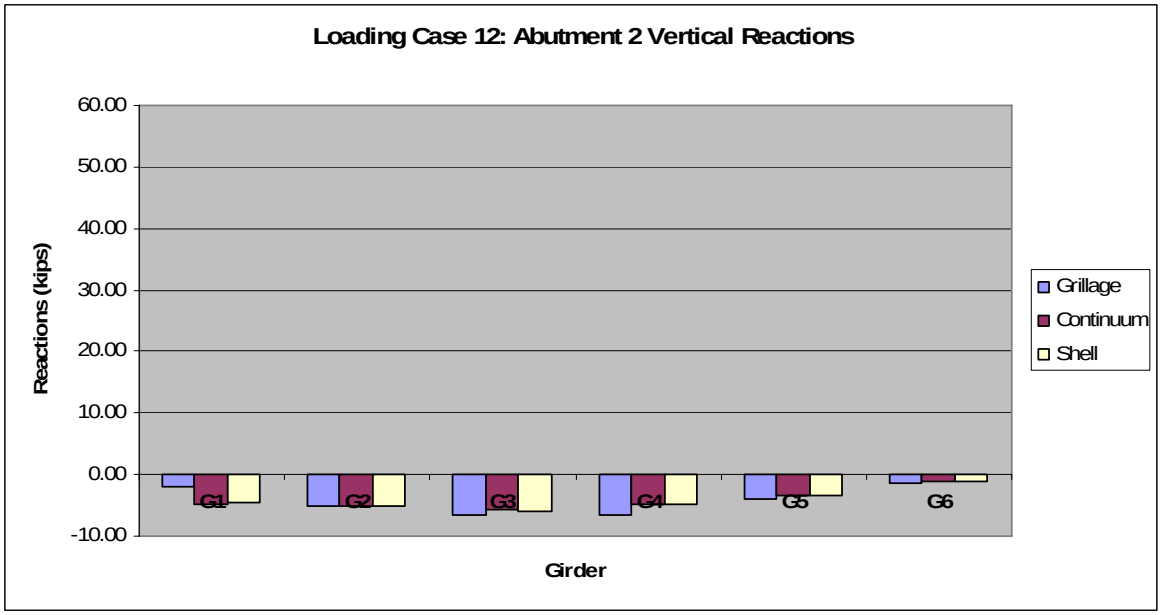

Figure A.28 Loading Case 12: Abutment 2 vertical reactions.

APPENDIX B

SUPPLEMENTARY RESULTS (MAXIMUM VERTICAL DEFLECTIONS)

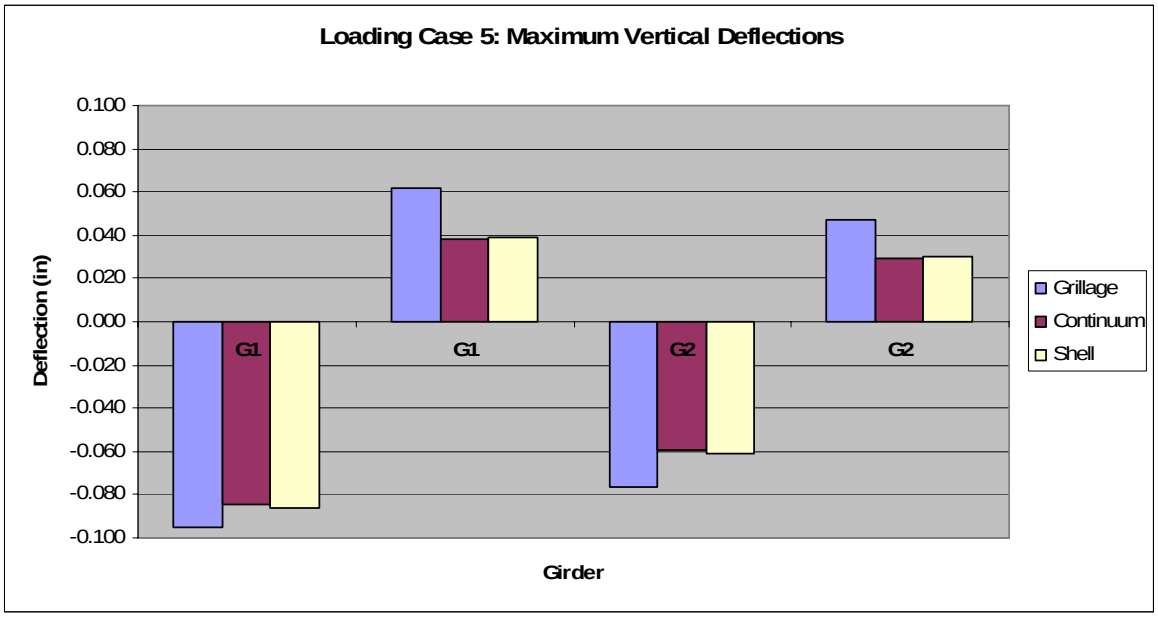

Figure B.1 Loading Case 5: maximum vertical deflections.

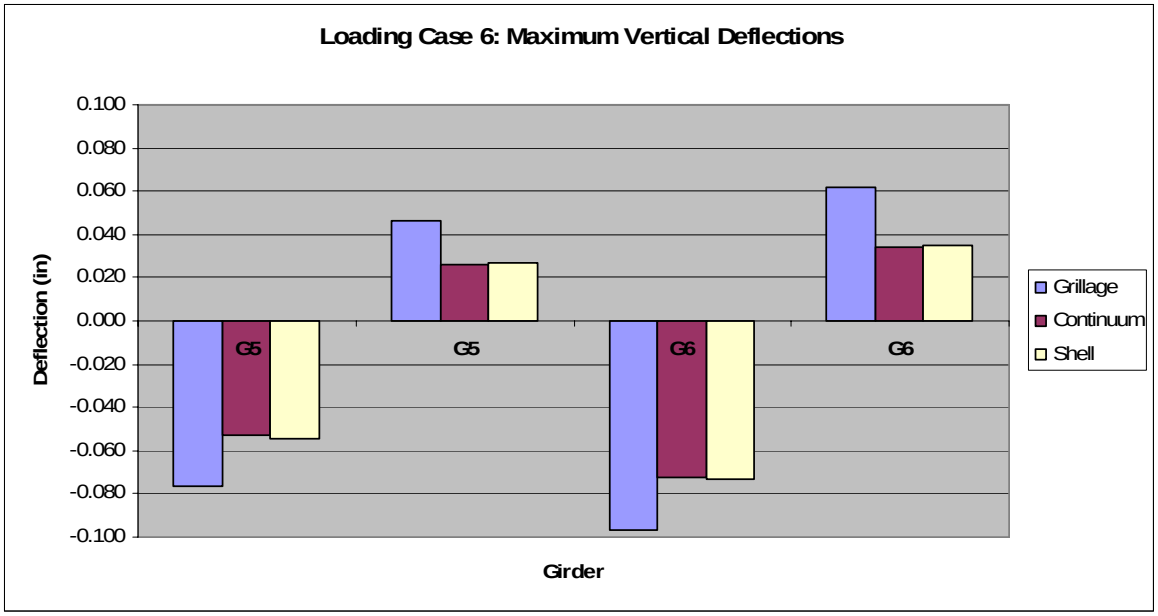

Figure B.2 Loading Case 6: maximum vertical deflections.

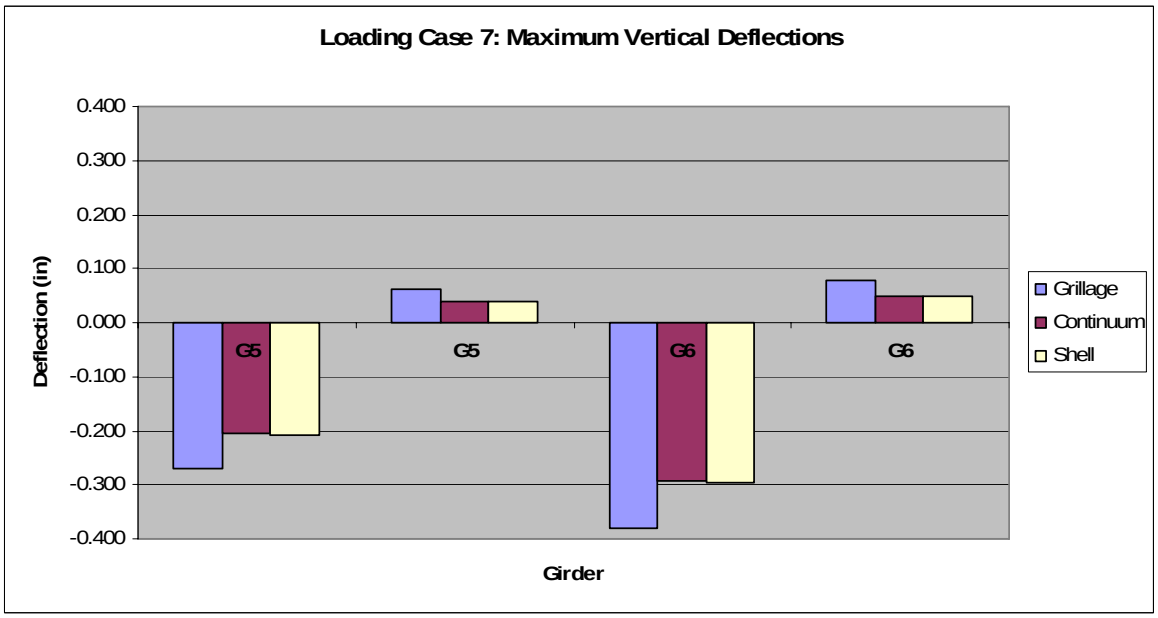

Figure B.3 Loading Case 7: maximum vertical deflections.

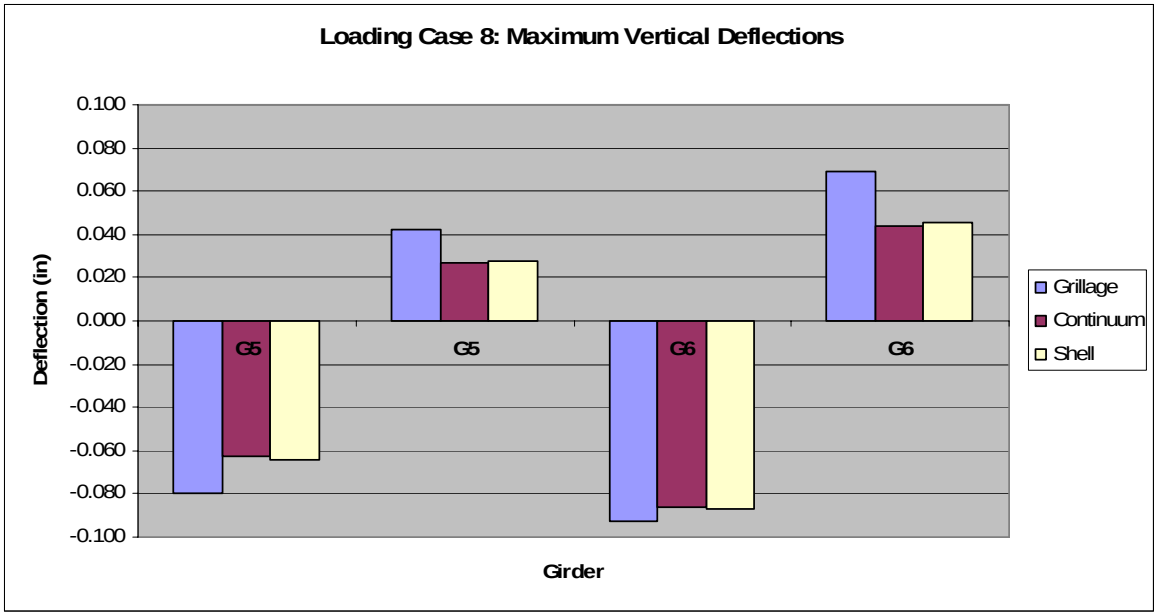

Figure B.4 Loading Case 8: maximum vertical deflections.

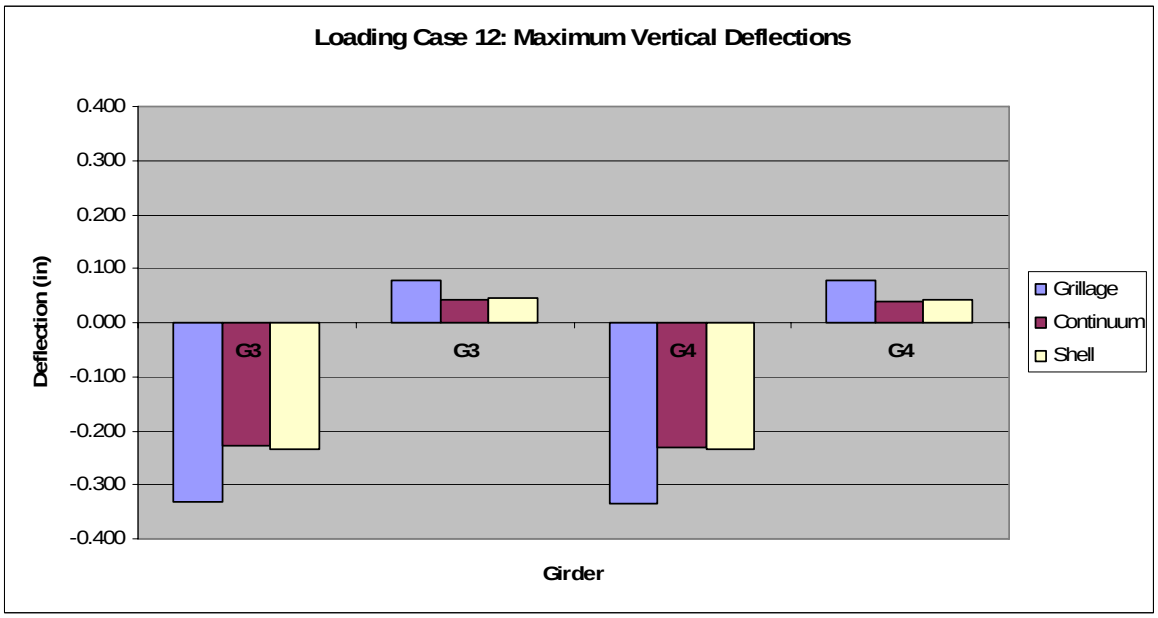

Figure B.5 Loading Case 12: maximum vertical deflections.

APPENDIX C

SUPPLEMENTARY RESULTS (VERTICAL DEFLECTION PROFILES)

C.1 Loading Case 2

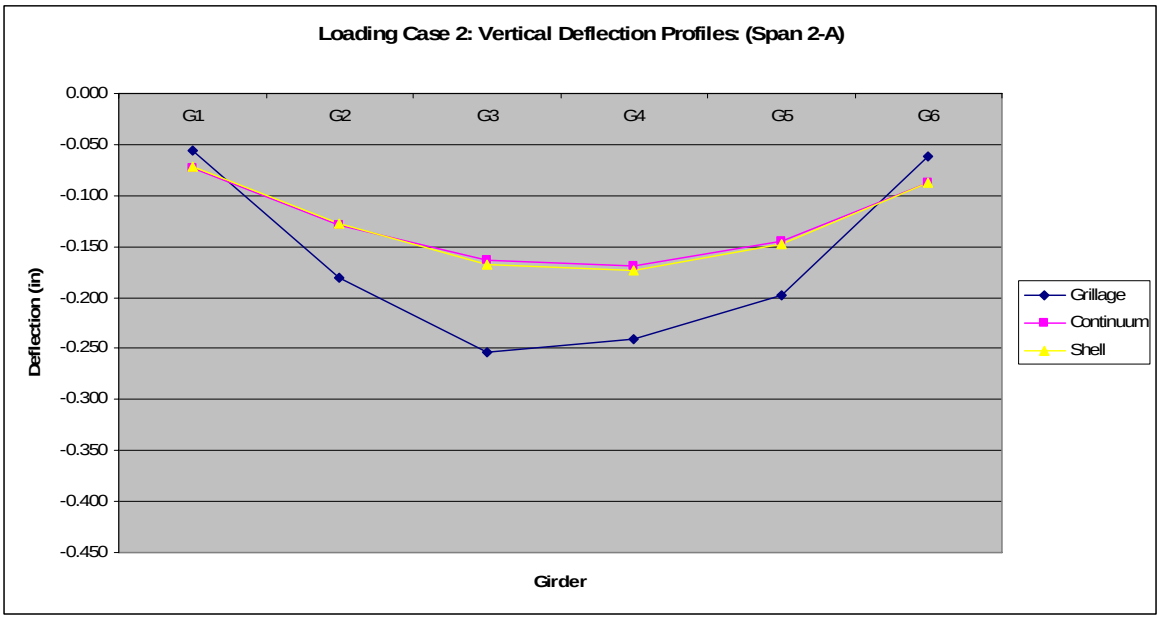

Figure C.1 Loading Case 2: vertical deflection profiles (Span 2-A).

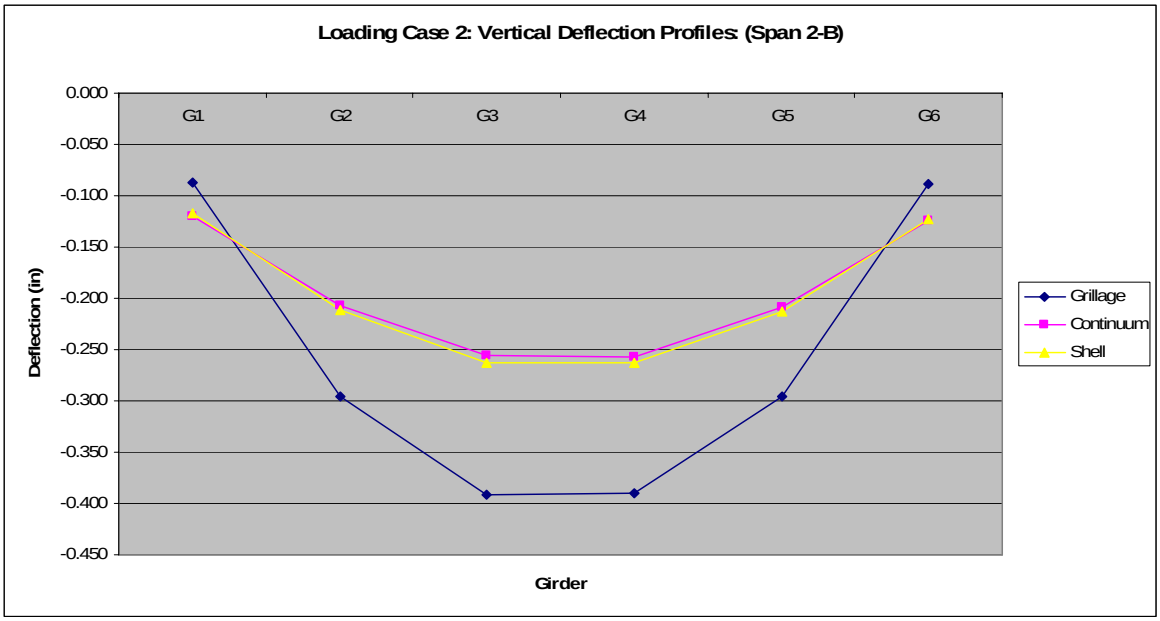

Figure C.2 Loading Case 2: vertical deflection profiles (Span 2-B).

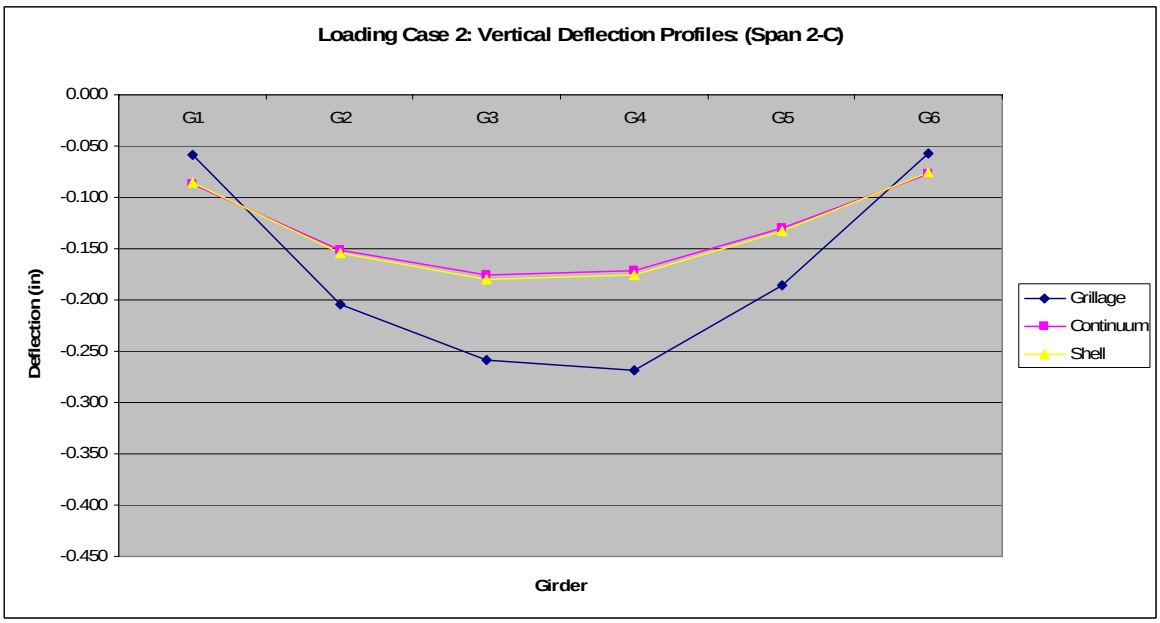

Figure C.3 Loading Case 2: vertical deflection profiles (Span 2-C).

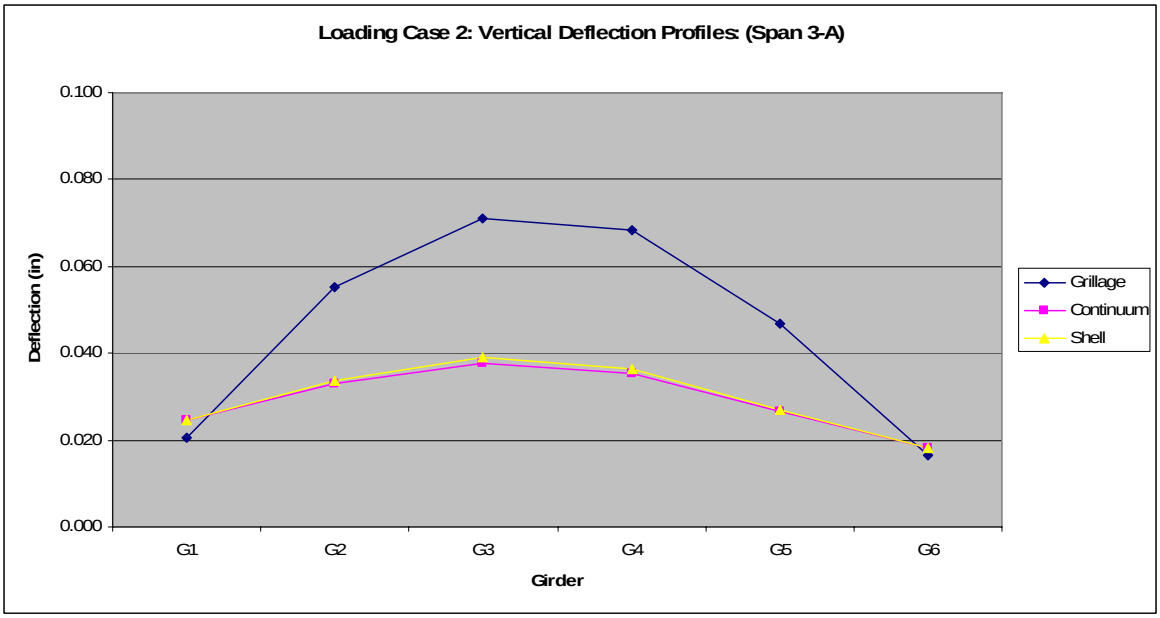

Figure C.4 Loading Case 2: vertical deflection profiles (Span 3-A).

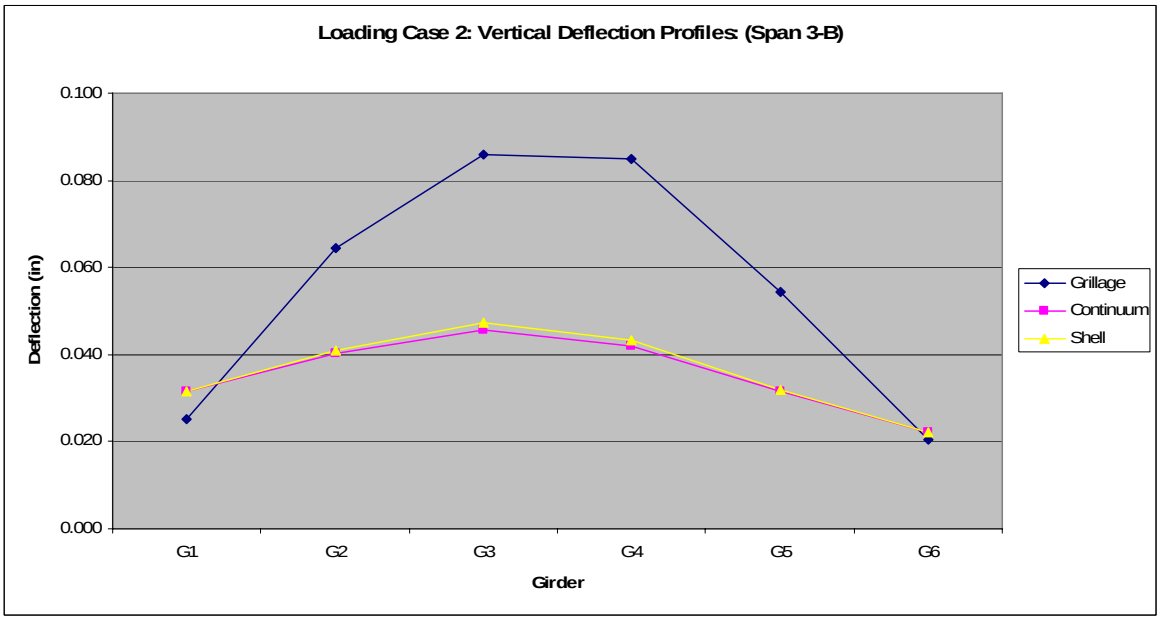

Figure C.5 Loading Case 2: vertical deflection profiles (Span 3-B).

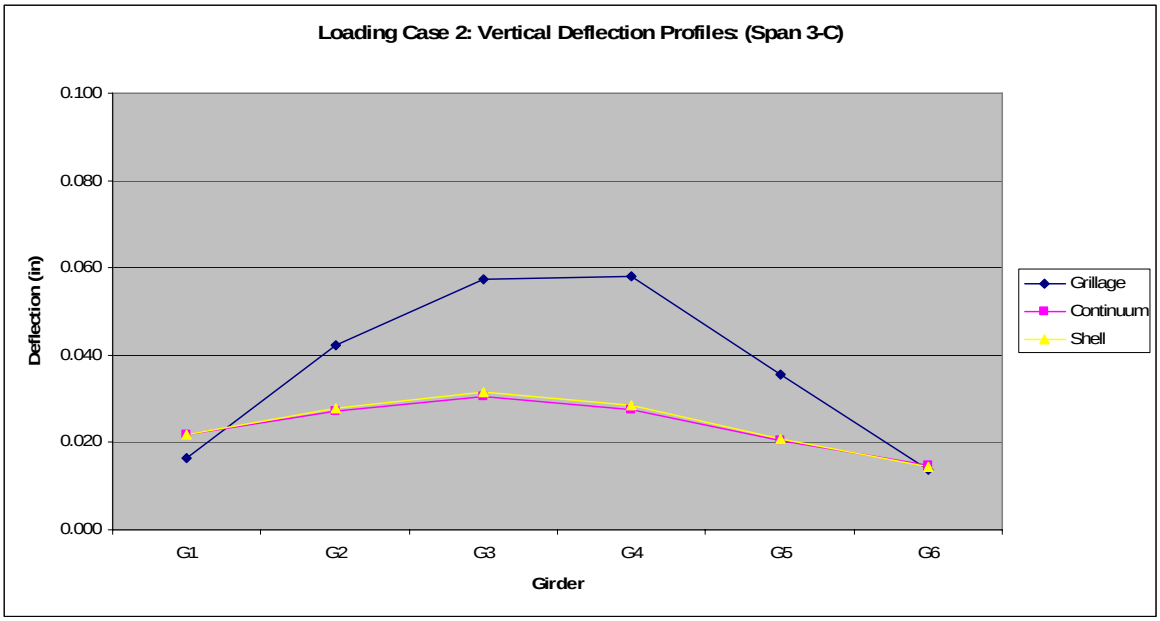

Figure C.6 Loading Case 2: vertical deflection profiles (Span 3-C).

C.2 Loading Case 4

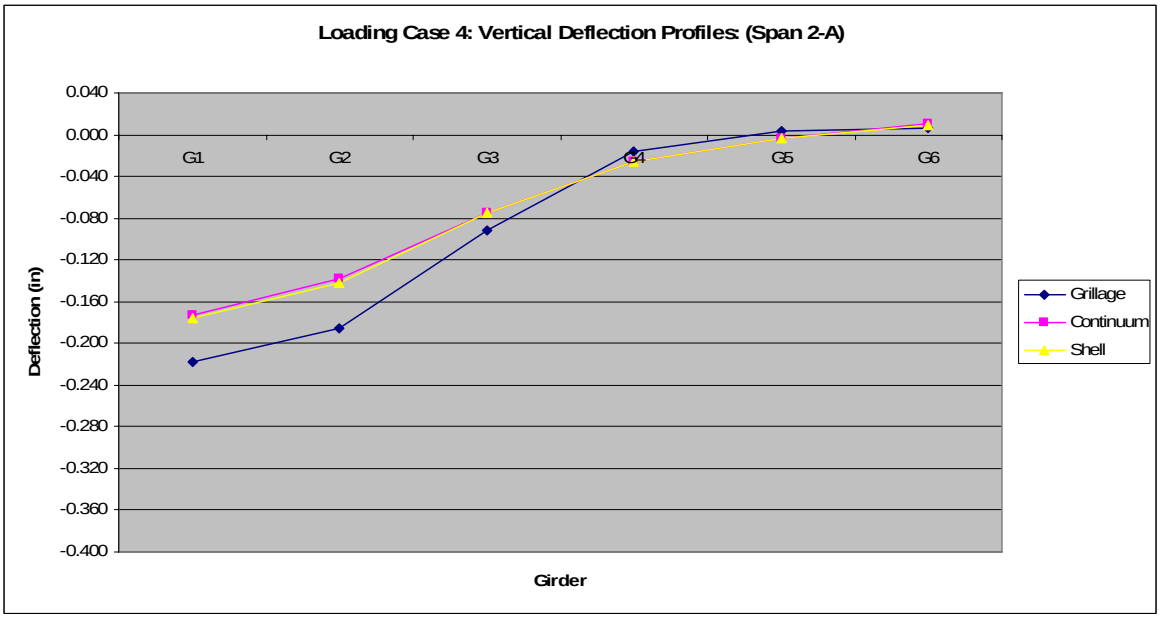

Figure C.7 Loading Case 4: vertical deflection profiles (Span 2-A).

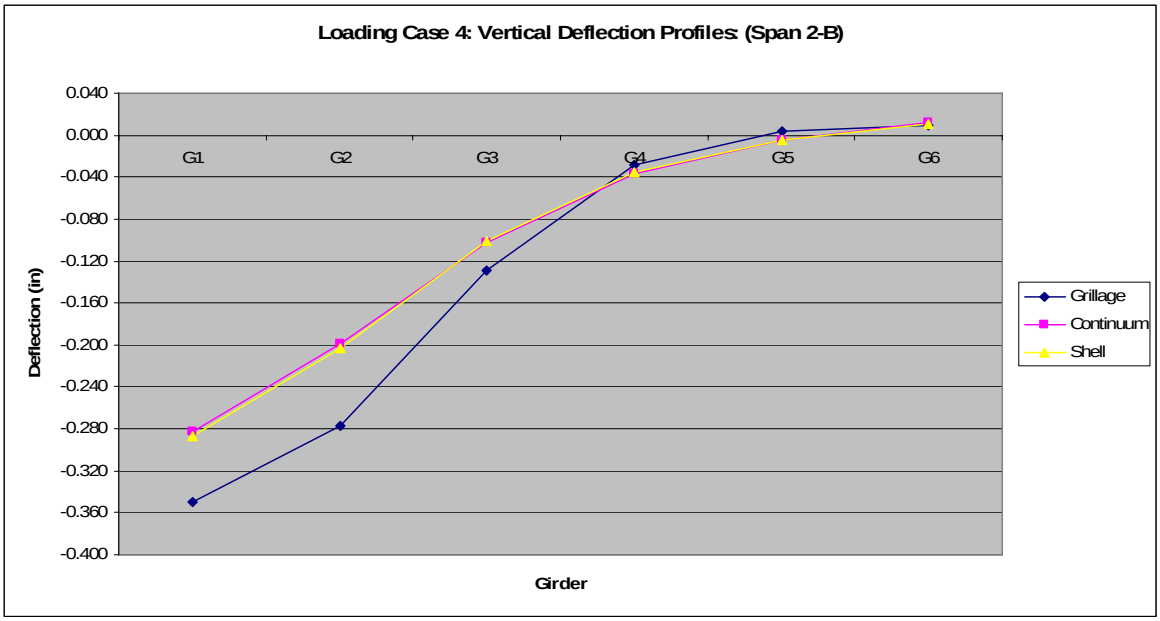

Figure C.8 Loading Case 4: vertical deflection profiles (Span 2-B).

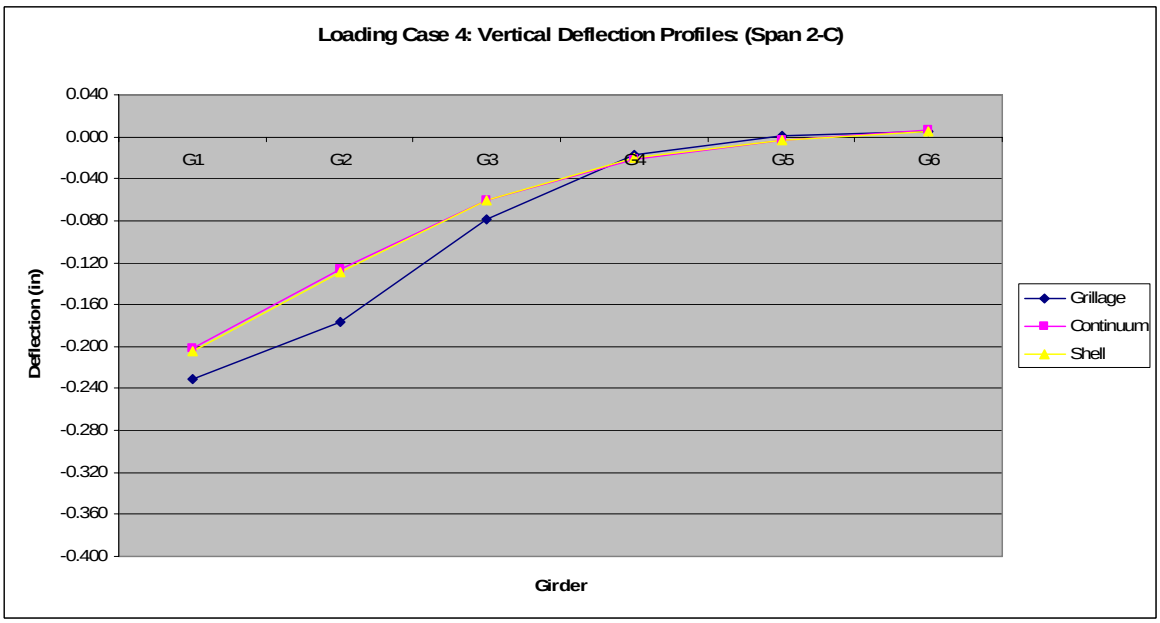

Figure C.9 Loading Case 4: vertical deflection profiles (Span 2-C).

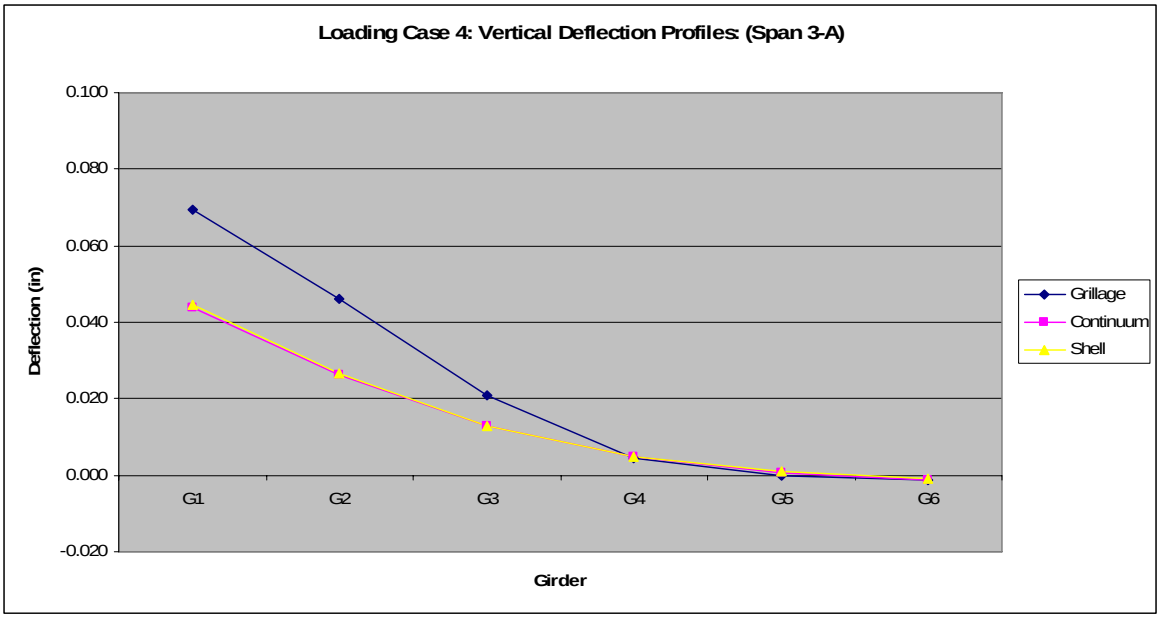

Figure C.10 Loading Case 4: vertical deflection profiles (Span 3-A).

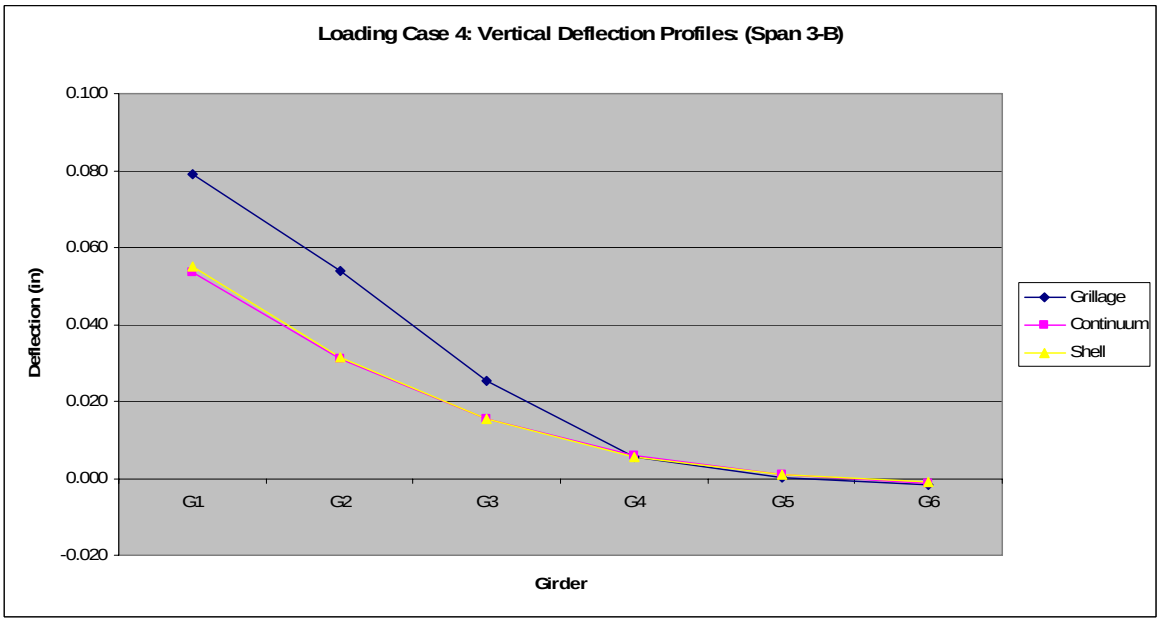

Figure C.11 Loading Case 4: vertical deflection profiles (Span 3-B).

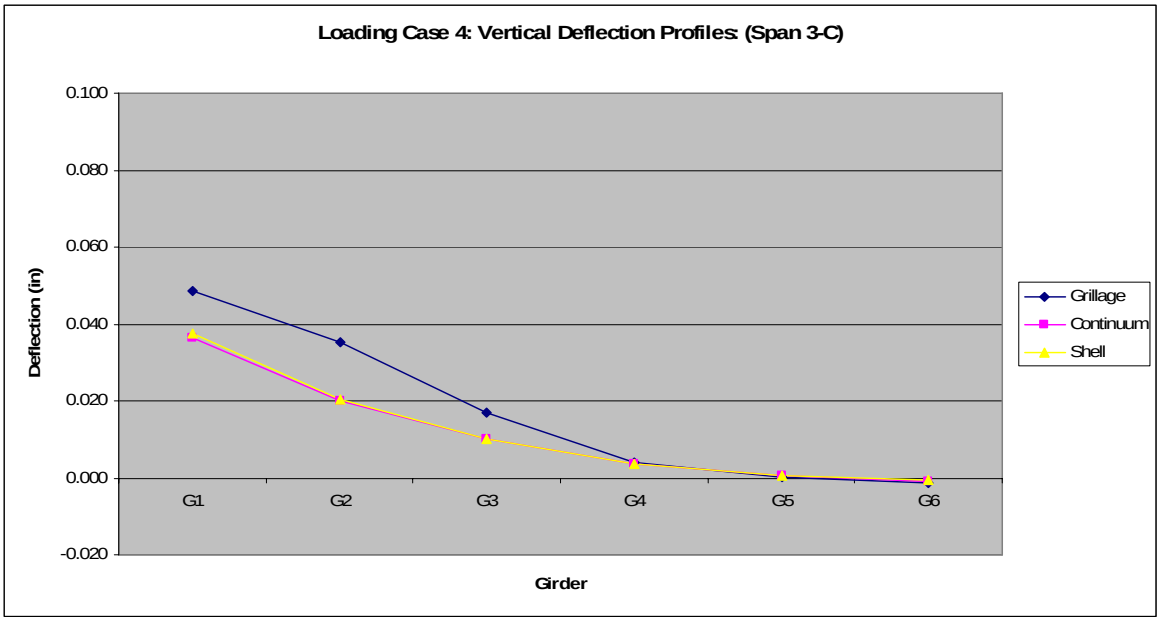

Figure C.12 Loading Case 4: vertical deflection profiles (Span 3-C).

C.3 Loading Case 5

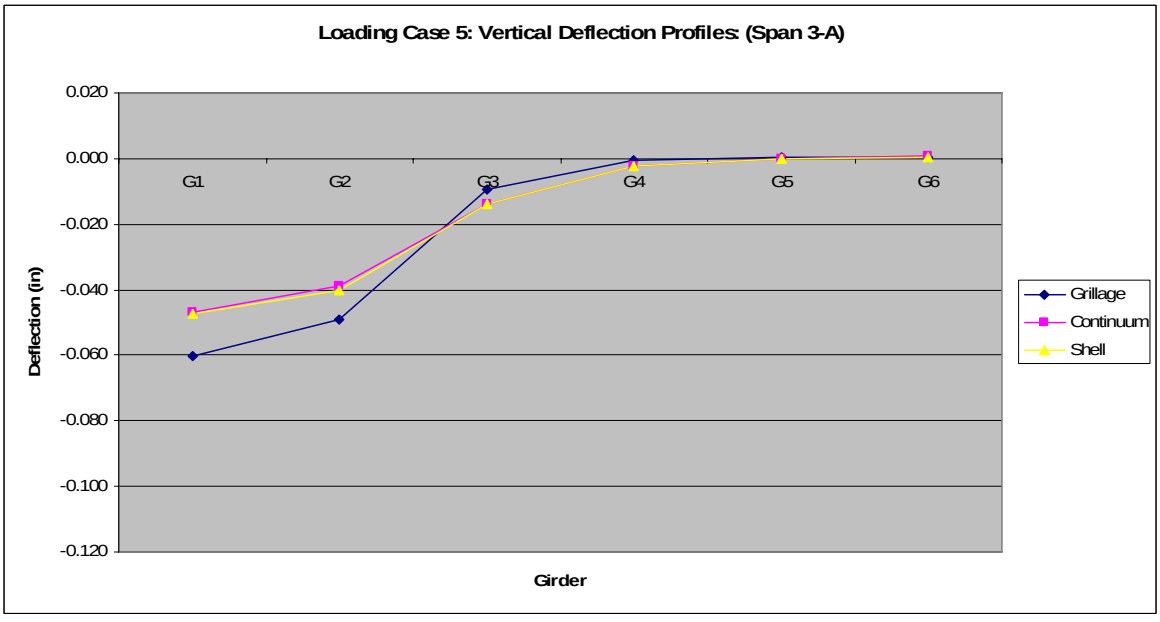

Figure C.13 Loading Case 5: vertical deflection profiles (Span 3-A).

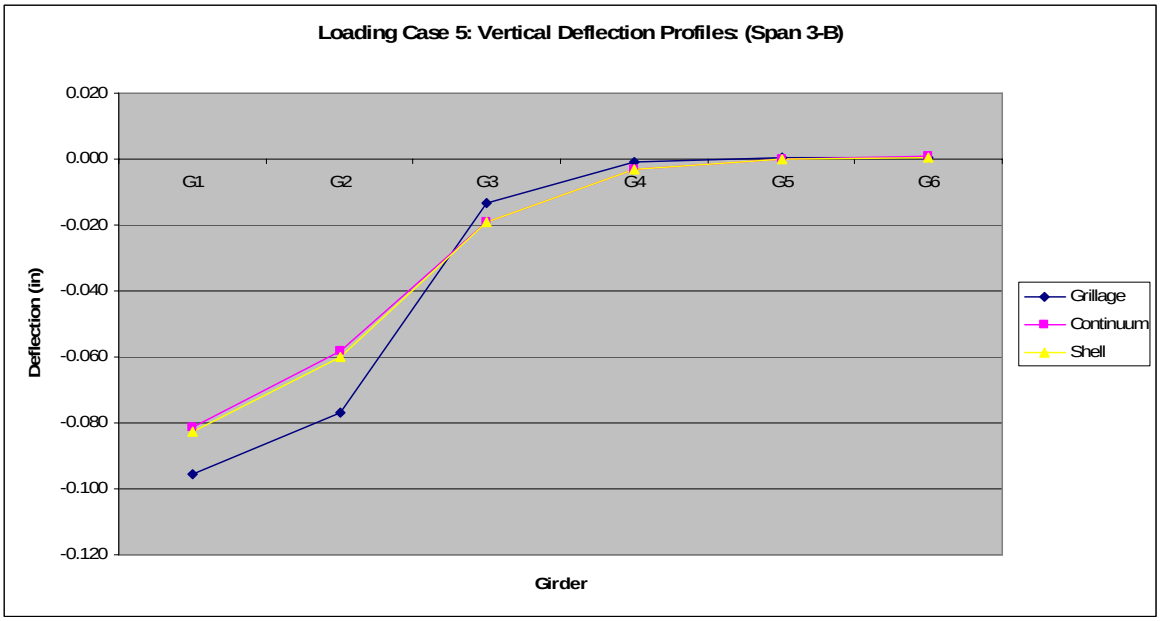

Figure C.14 Loading Case 5: vertical deflection profiles (Span 3-B).

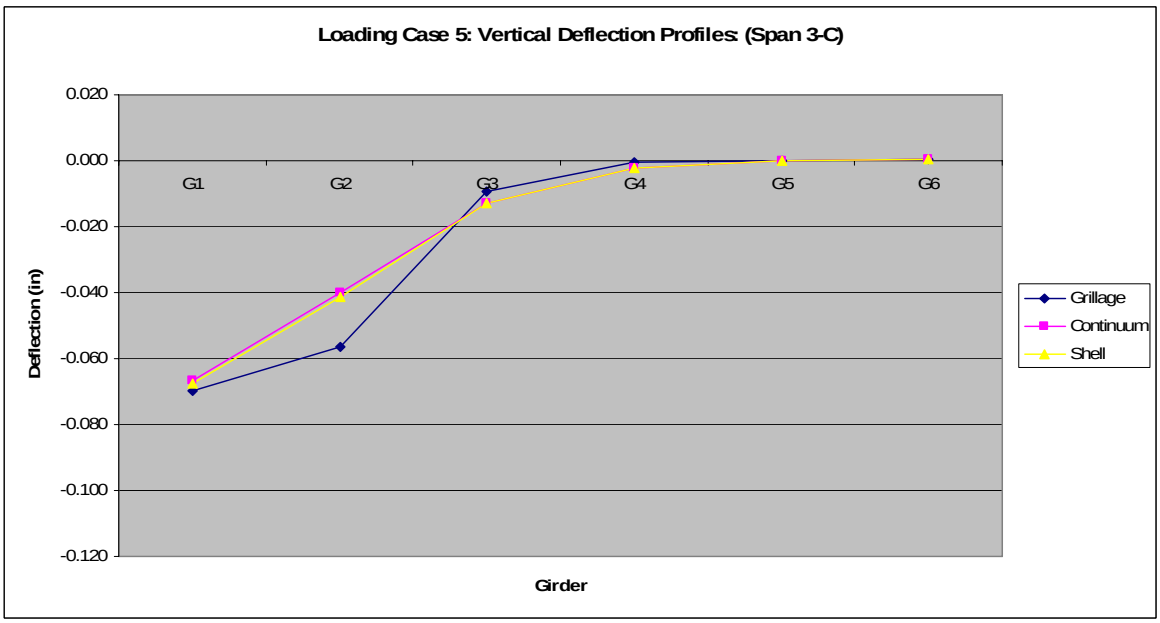

Figure C.15 Loading Case 5: vertical deflection profiles (Span 3-C).

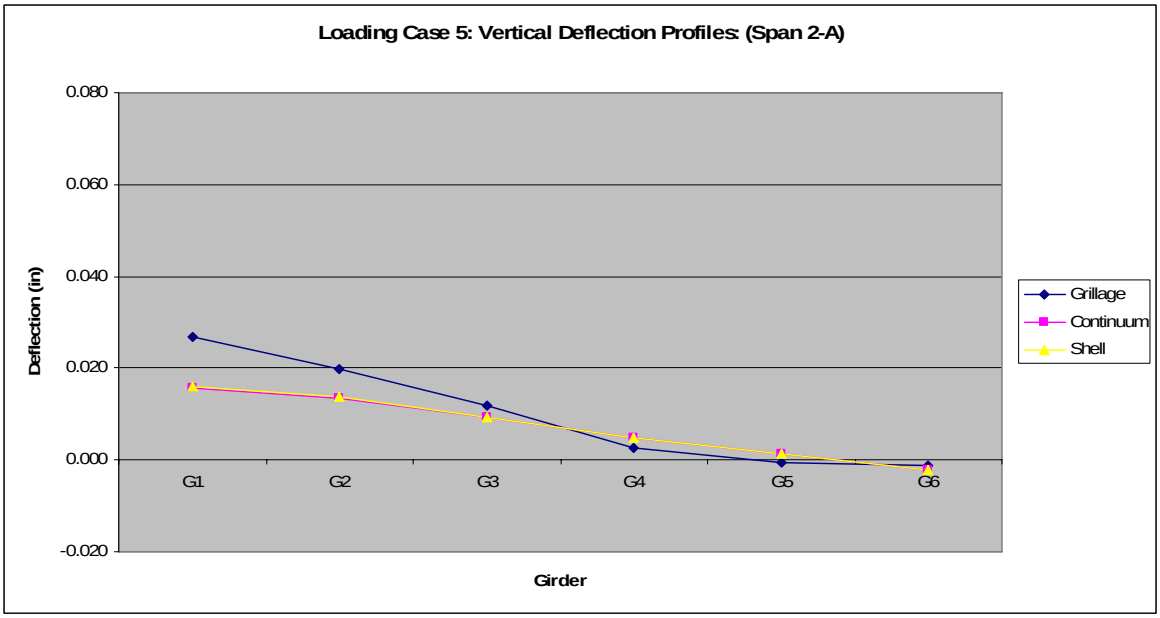

Figure C.16 Loading Case 5: vertical deflection profiles (Span 2-A).

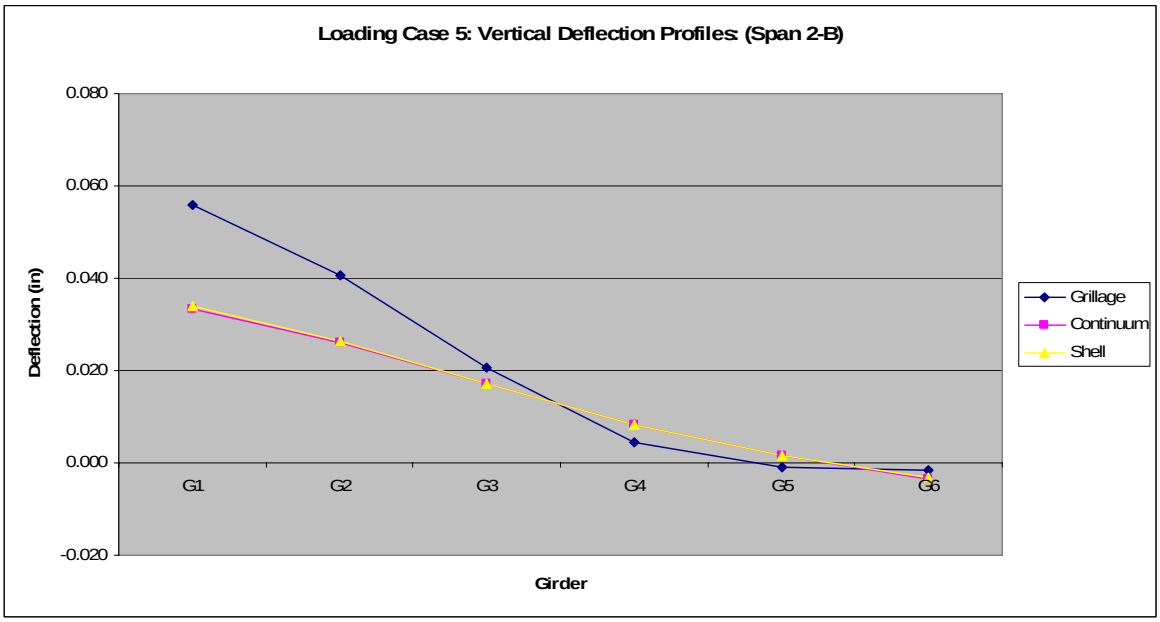

Figure C.17 Loading Case 5: vertical deflection profiles (Span 2-B).

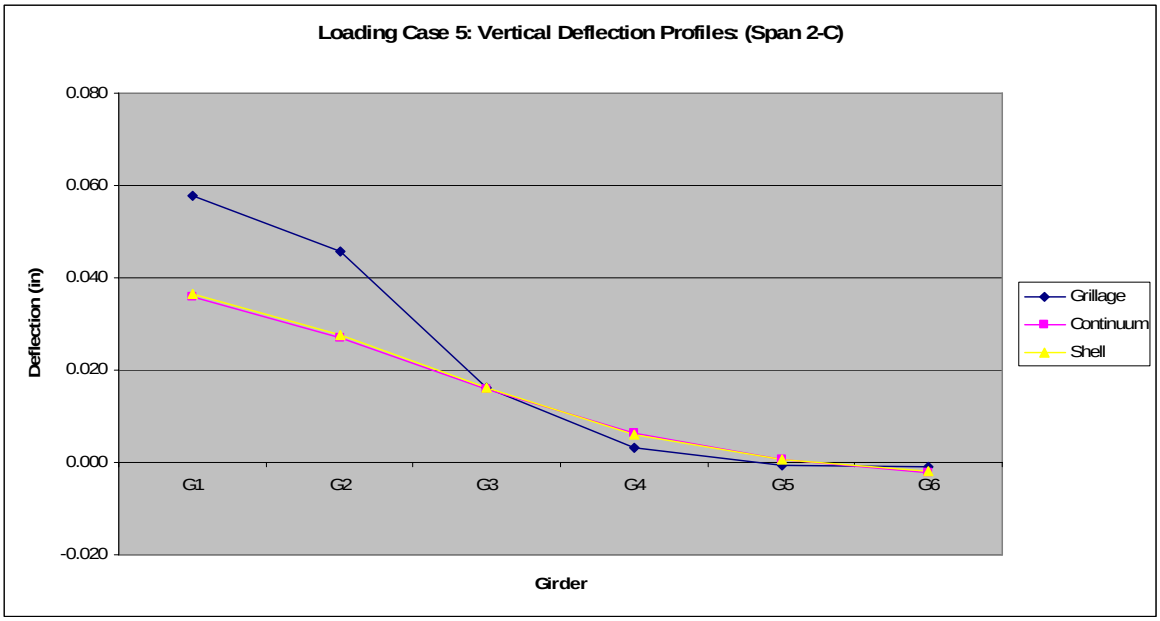

Figure C.18 Loading Case 5: vertical deflection profiles (Span 2-C).

C.4 Loading Case 6

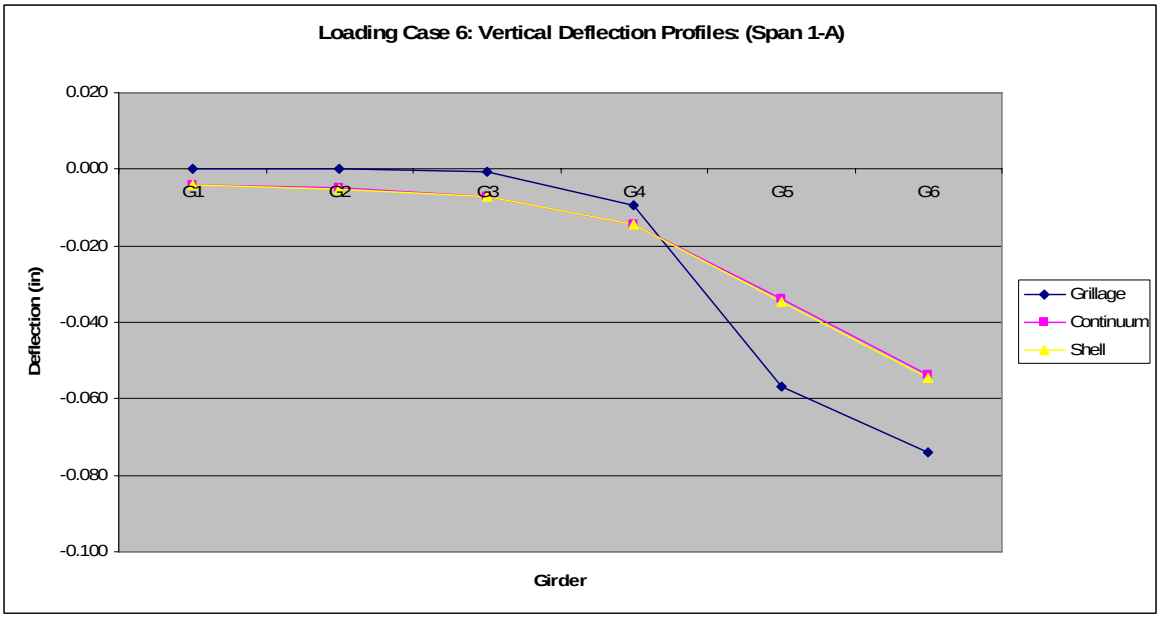

Figure C.19 Loading Case 6: vertical deflection profiles (Span 1-A).

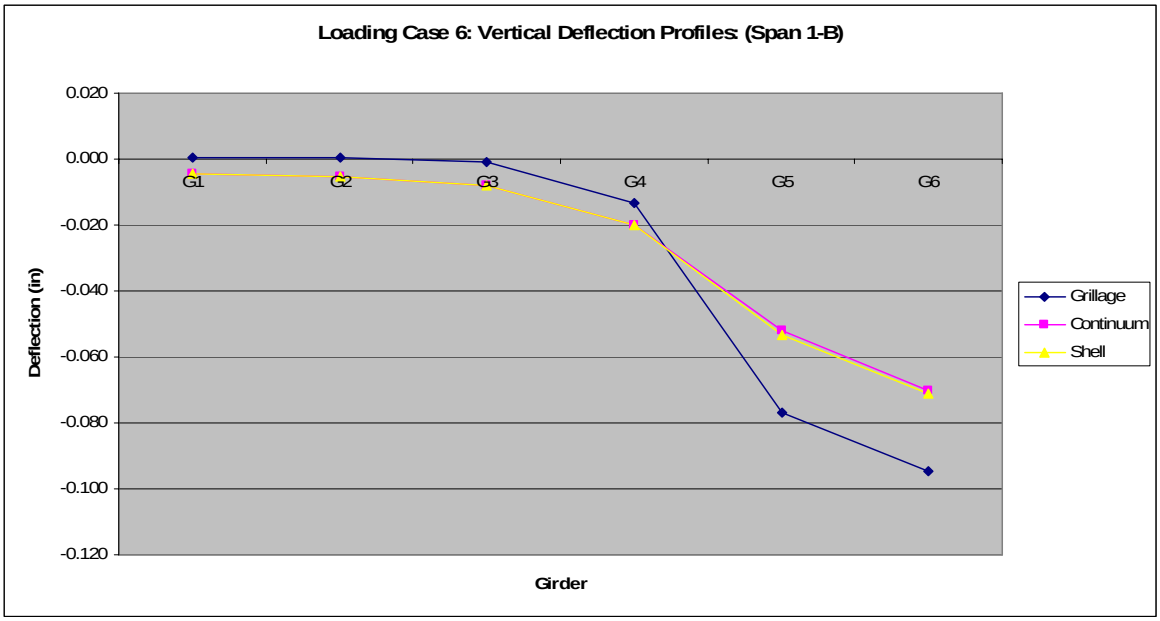

Figure C.20 Loading Case 6: vertical deflection profiles (Span 1-B).

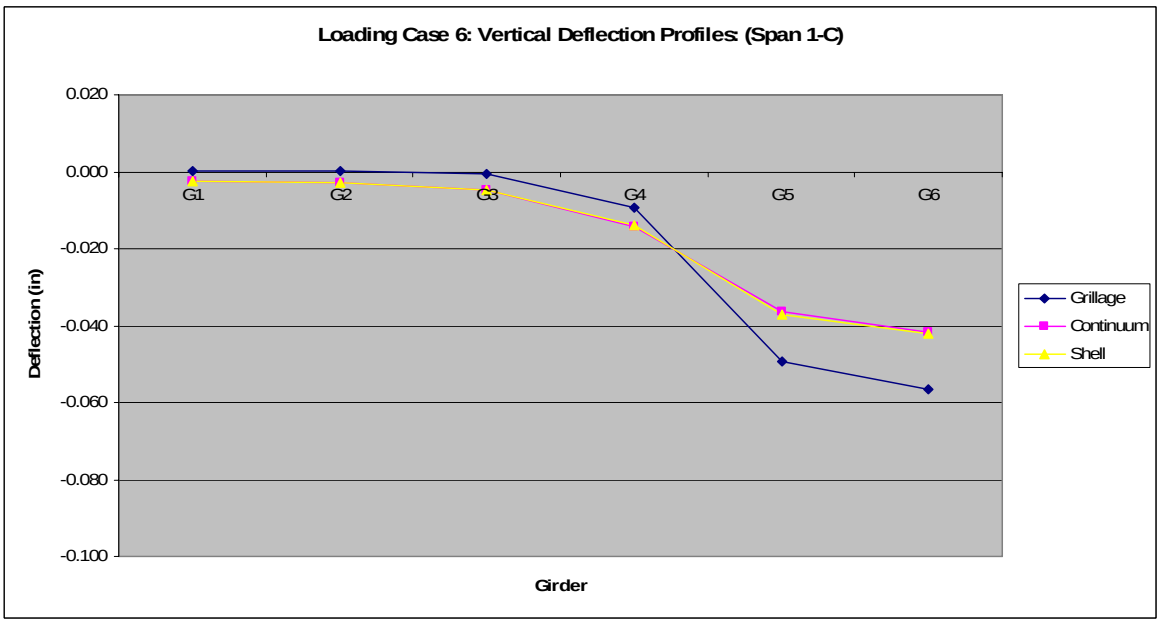

Figure C.21 Loading Case 6: vertical deflection profiles (Span 1-C).

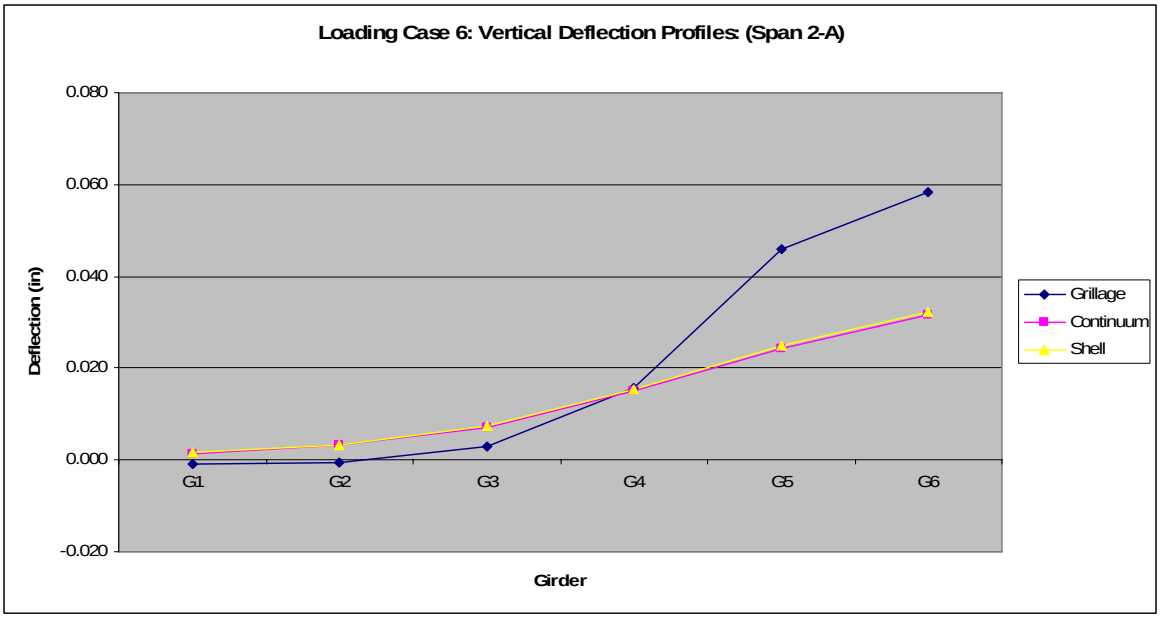

Figure C.22 Loading Case 6: vertical deflection profiles (Span 2-A).

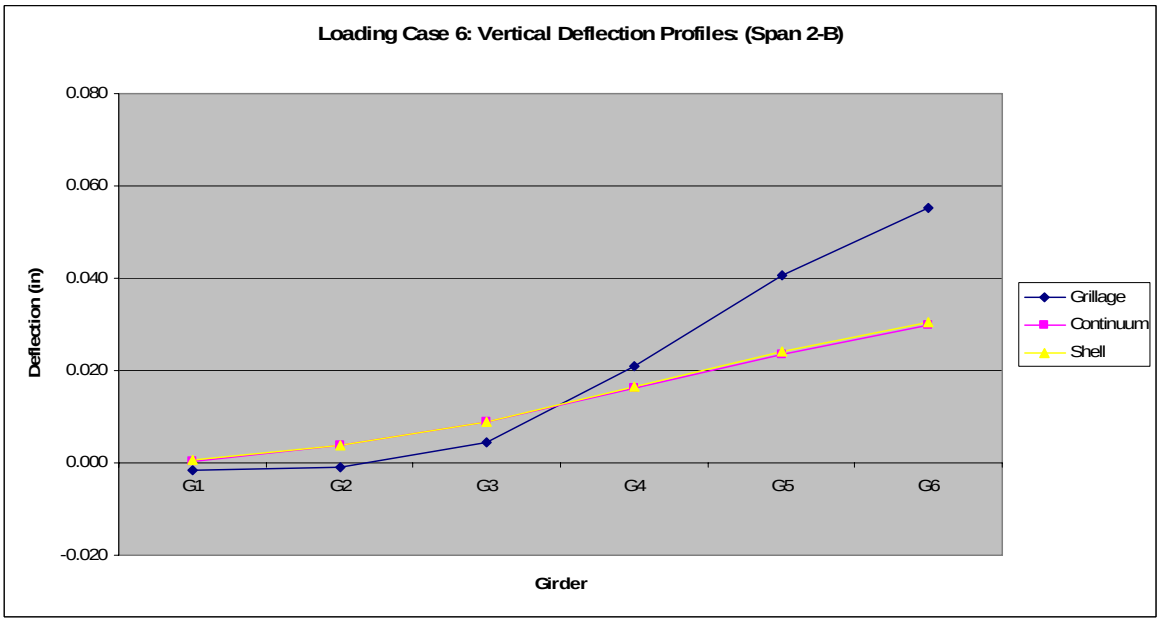

Figure C.23 Loading Case 6: vertical deflection profiles (Span 2-B).

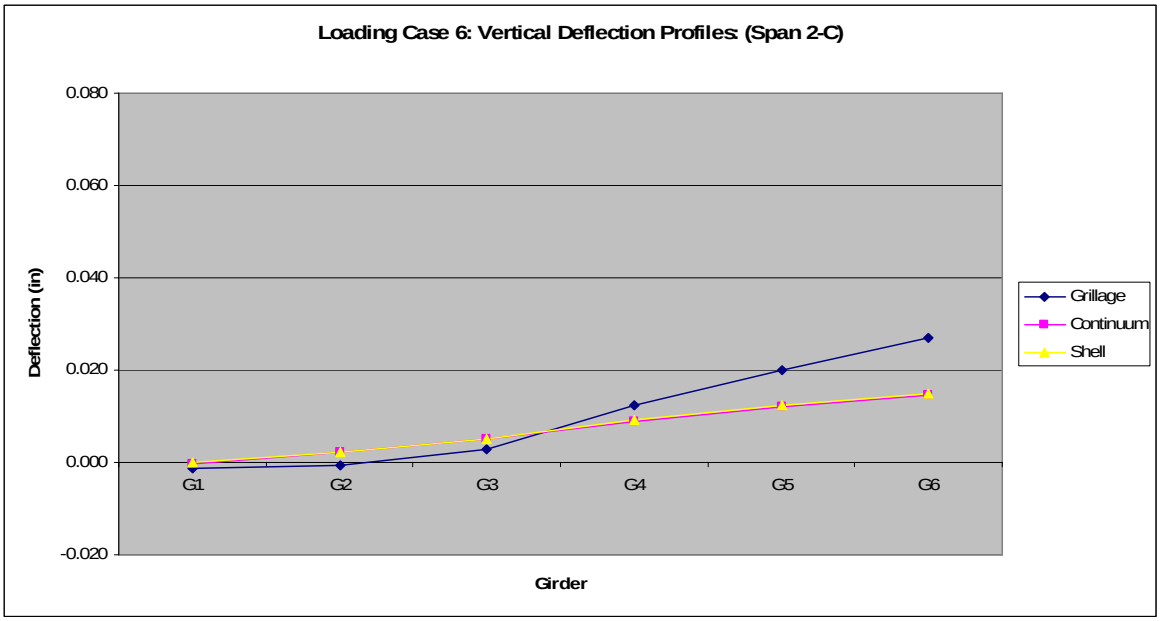

Figure C.24 Loading Case 6: vertical deflection profiles (Span 2-C).

C.5 Loading Case 7

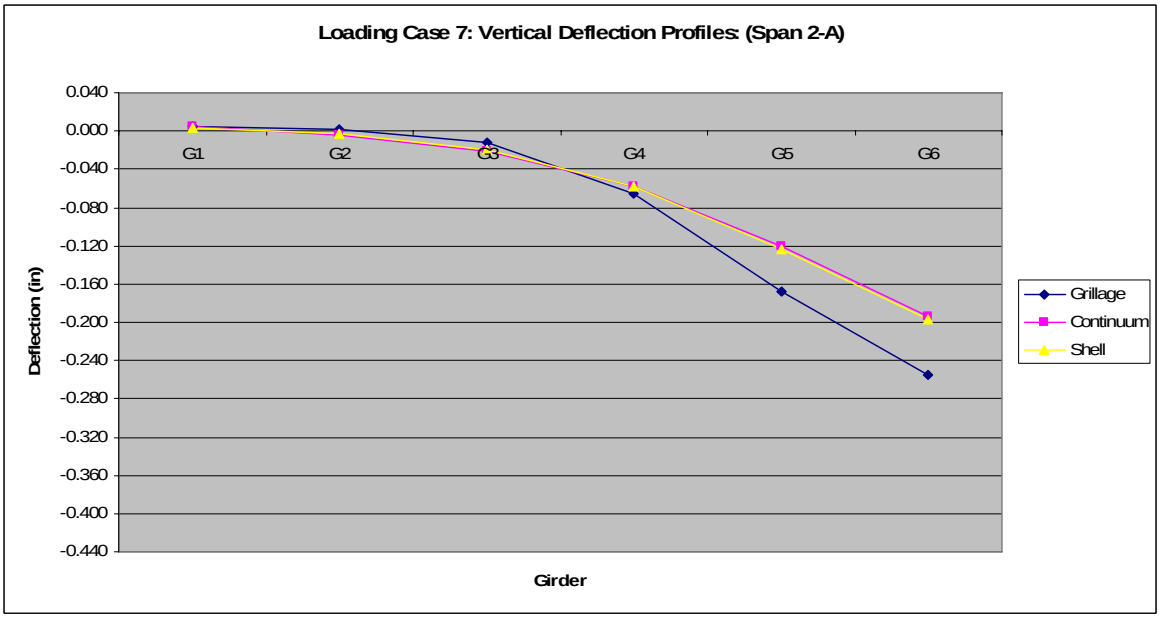

Figure C.25 Loading Case 7: vertical deflection profiles (Span 2-A).

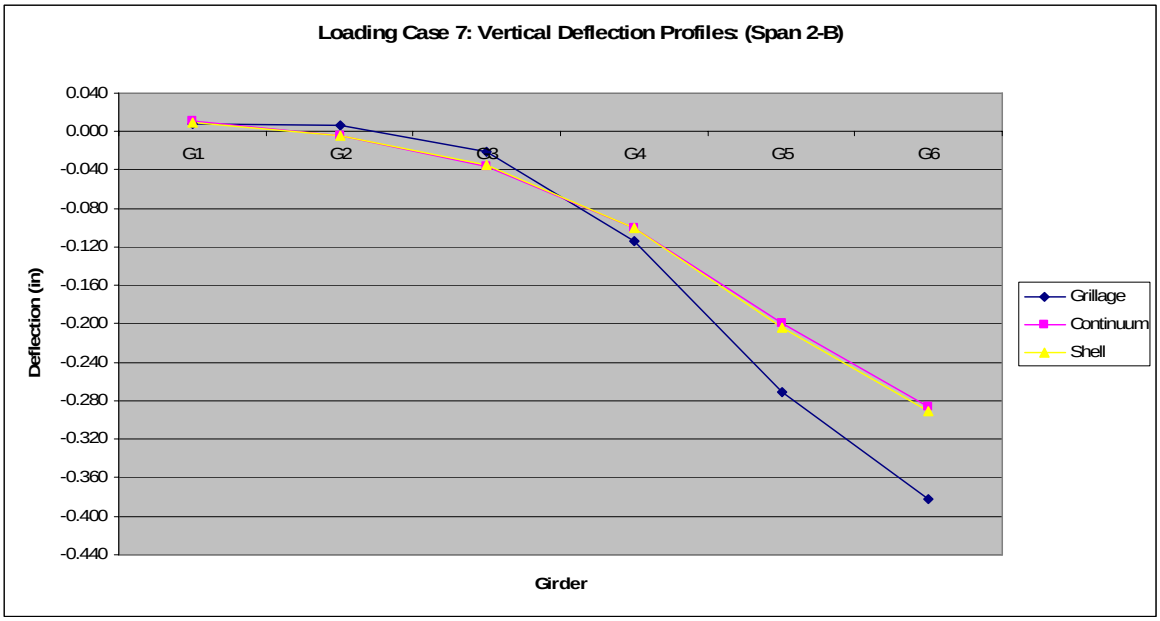

Figure C.26 Loading Case 7: vertical deflection profiles (Span 2-B).

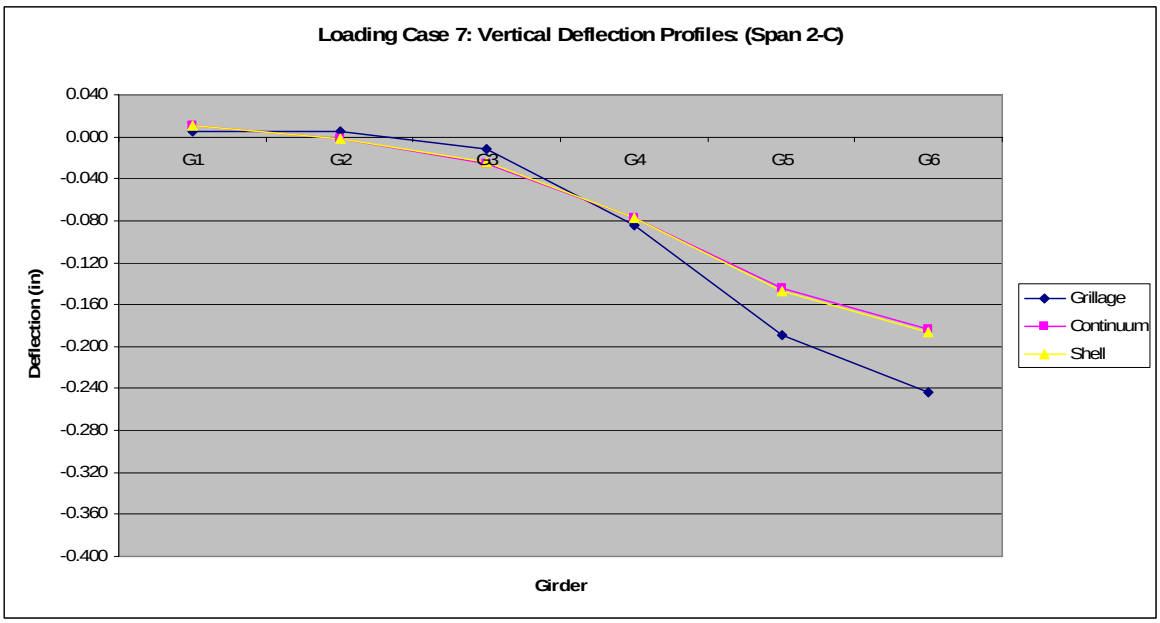

Figure C.27 Loading Case 7: vertical deflection profiles (Span 2-C).

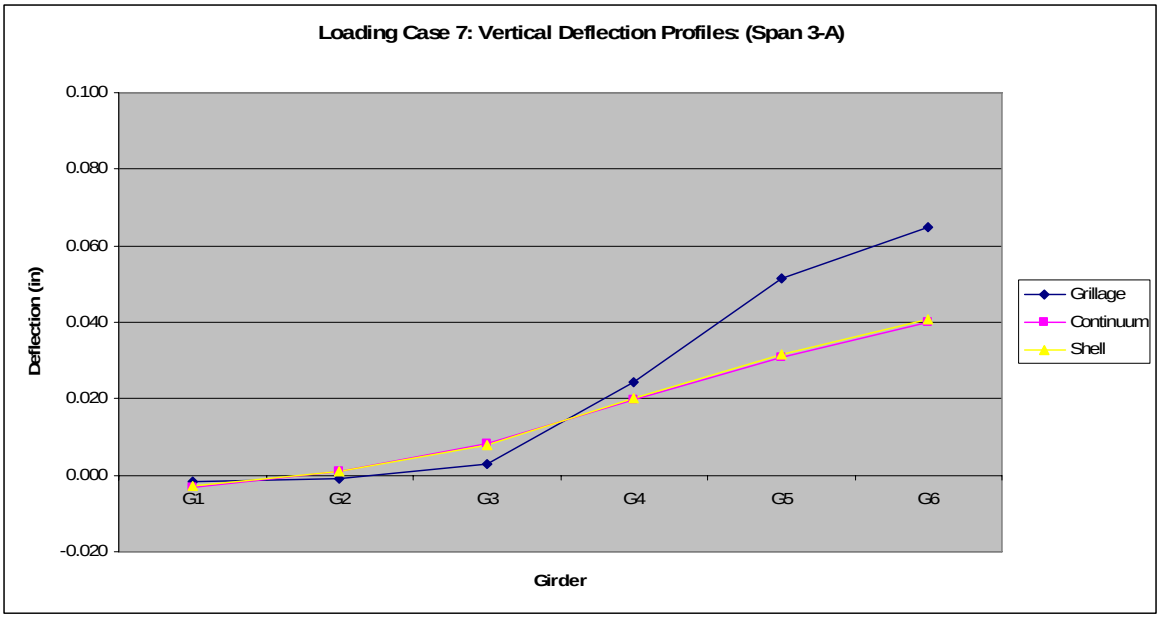

Figure C.28 Loading Case 7: vertical deflection profiles (Span 3-A).

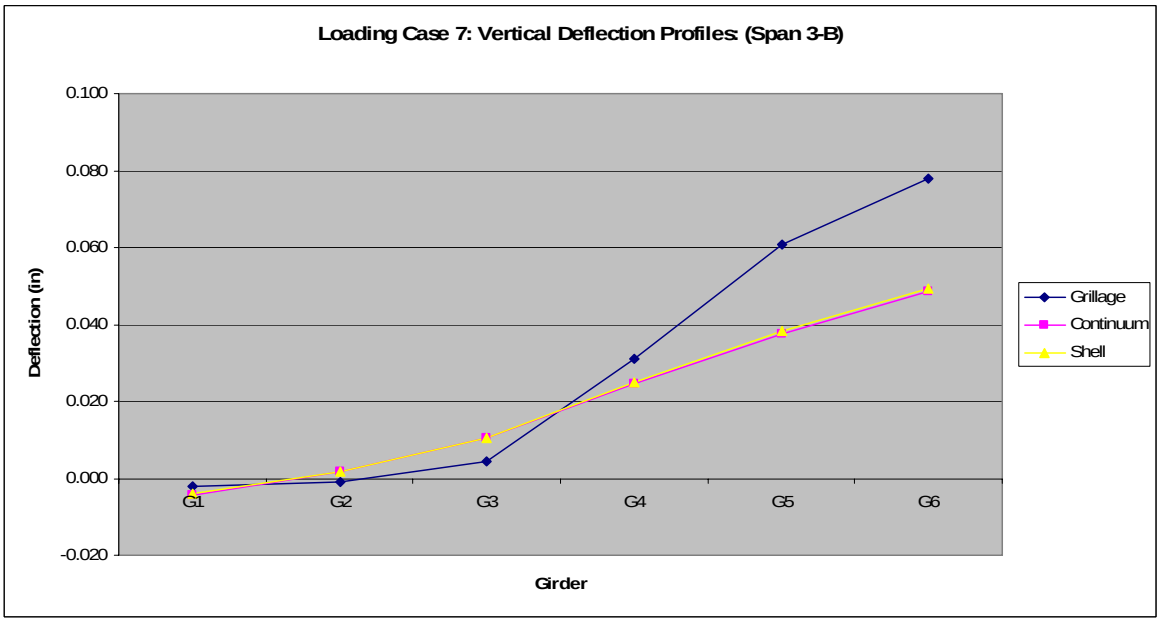

Figure C.29 Loading Case 7: vertical deflection profiles (Span 3-B).

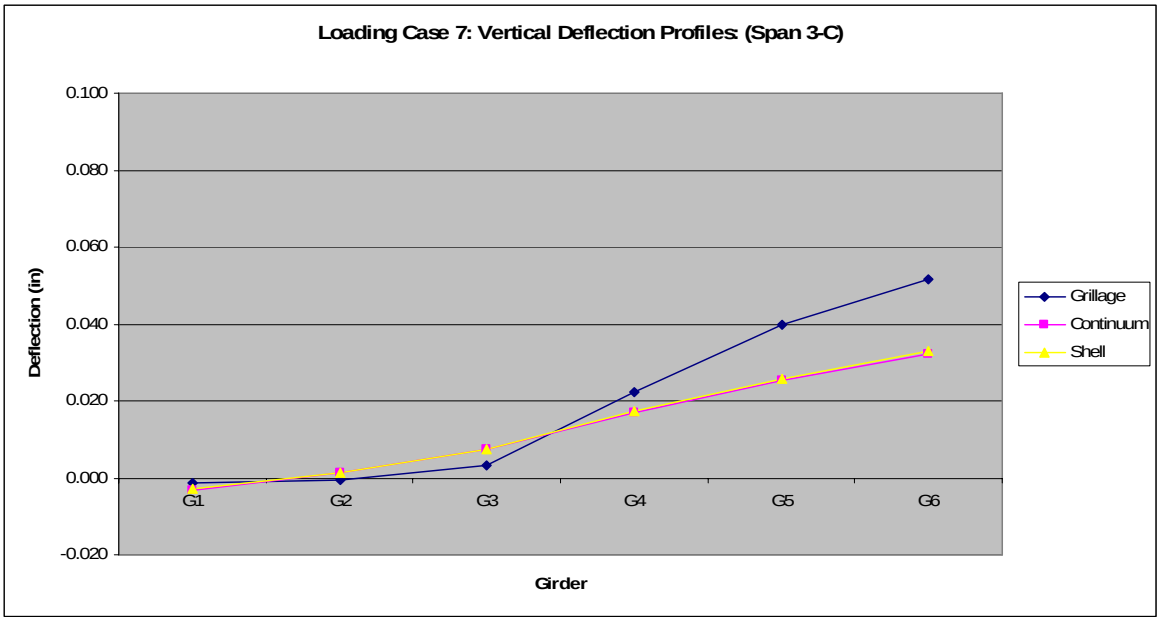

Figure C.30 Loading Case 4: vertical deflection profiles (Span 3-C).

C.6 Loading Case 8

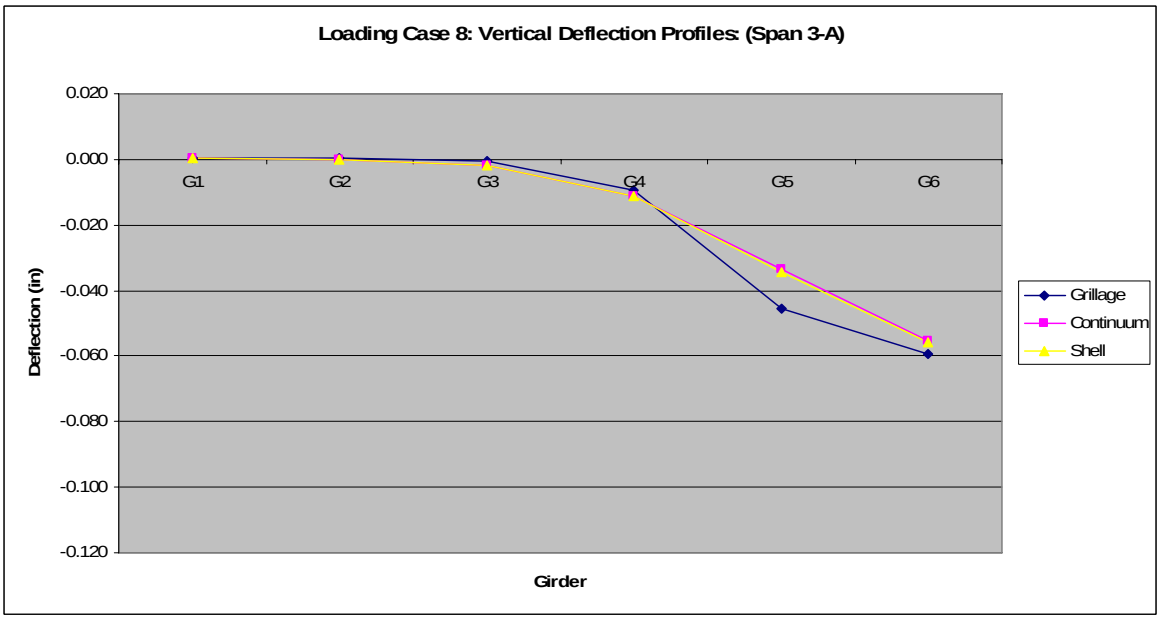

Figure C.31 Loading Case 8: vertical deflection profiles (Span 3-A).

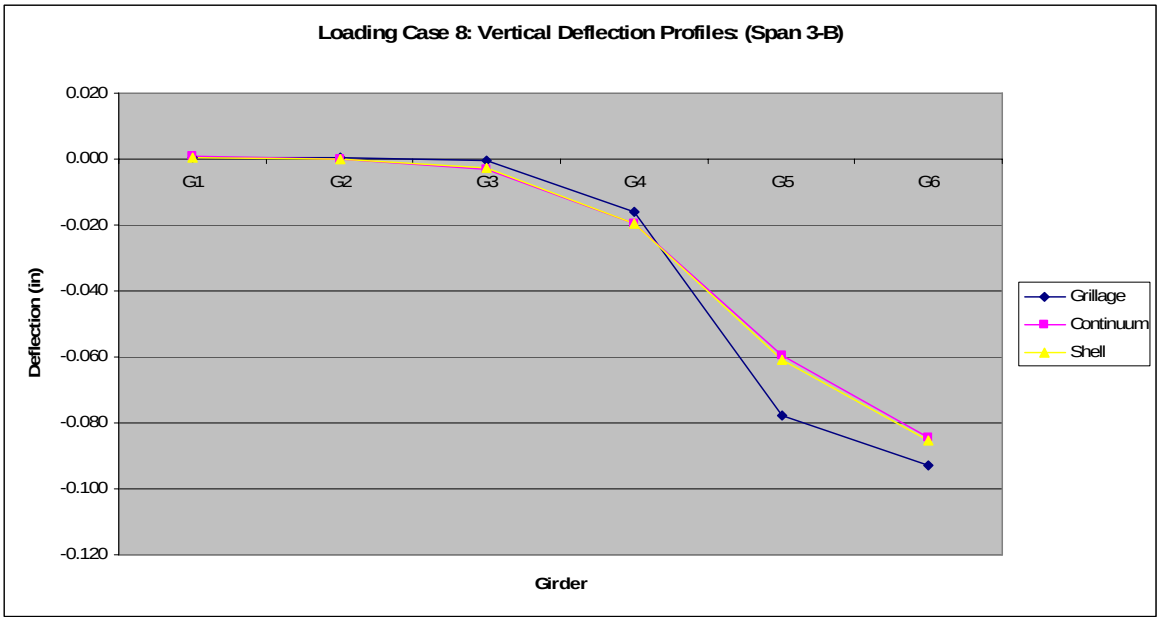

Figure C.32 Loading Case 8: vertical deflection profiles (Span 3-B).

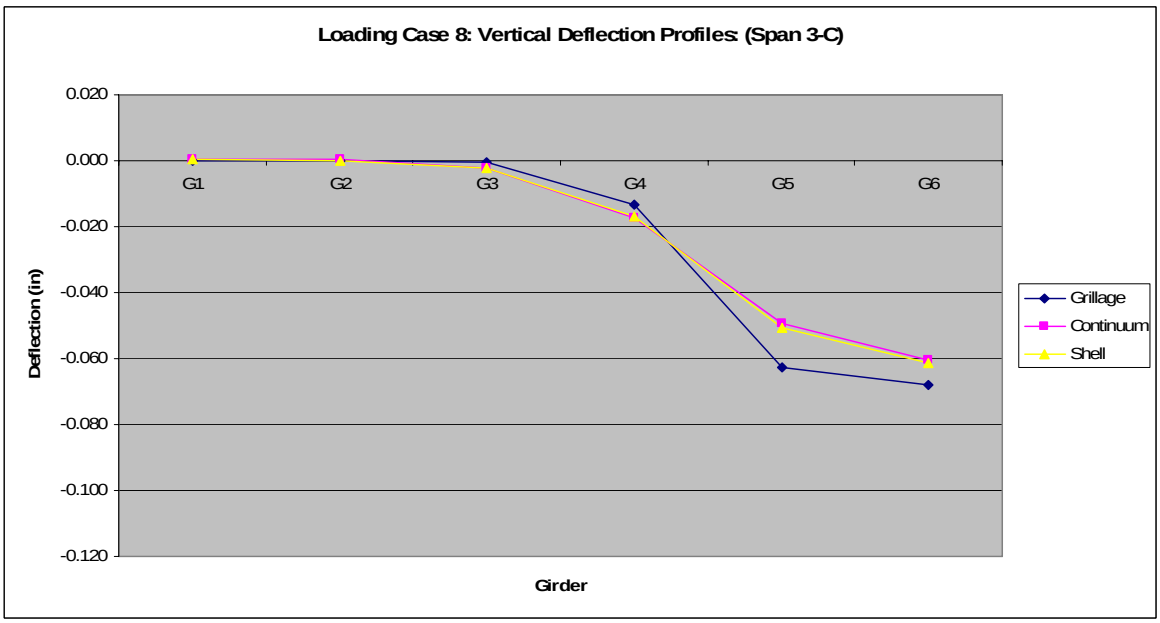

Figure C.33 Loading Case 8: vertical deflection profiles (Span 3-C).

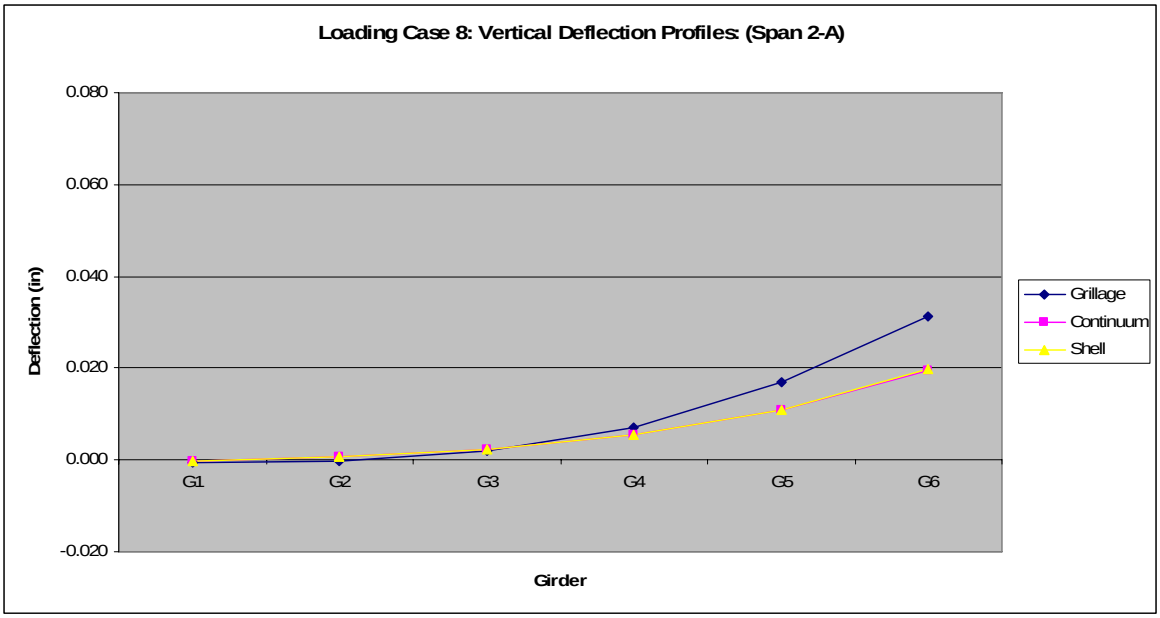

Figure C.34 Loading Case 8: vertical deflection profiles (Span 2-A).

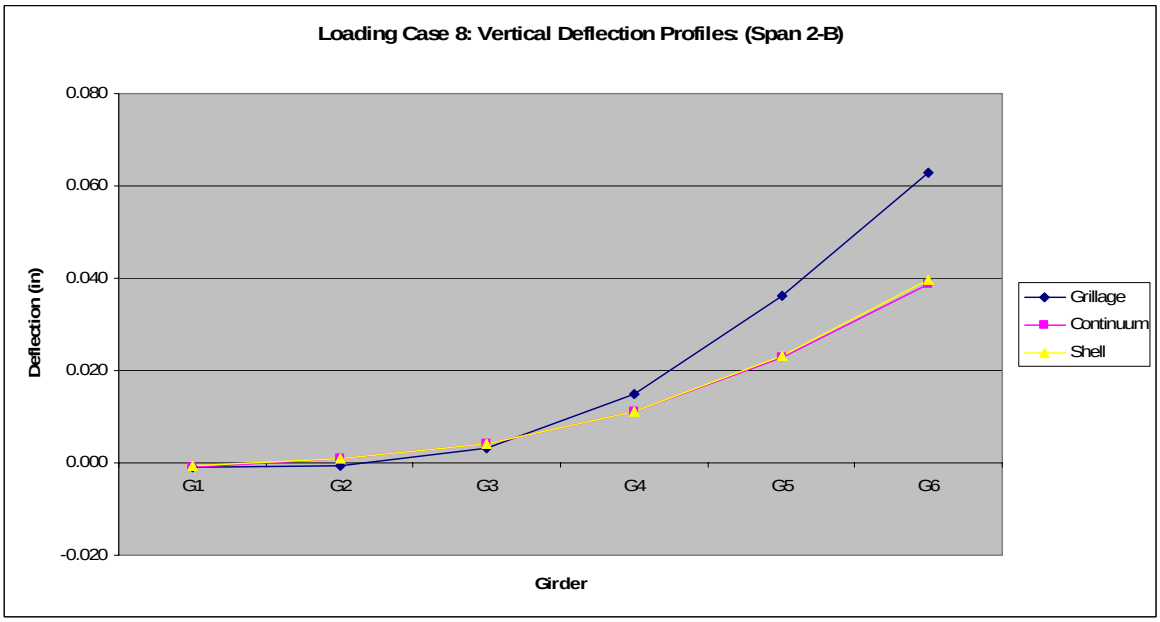

Figure C.35 Loading Case 8: vertical deflection profiles (Span 2-B).

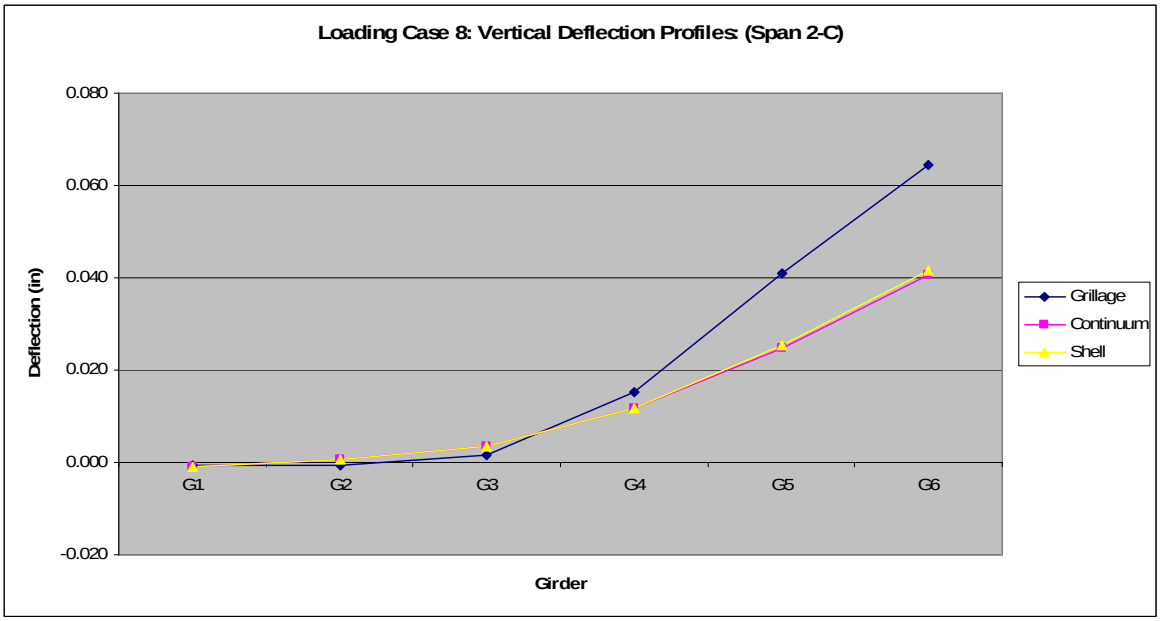

Figure C.36 Loading Case 8: vertical deflection profiles (Span 2-C).

C.7 Loading Case 12

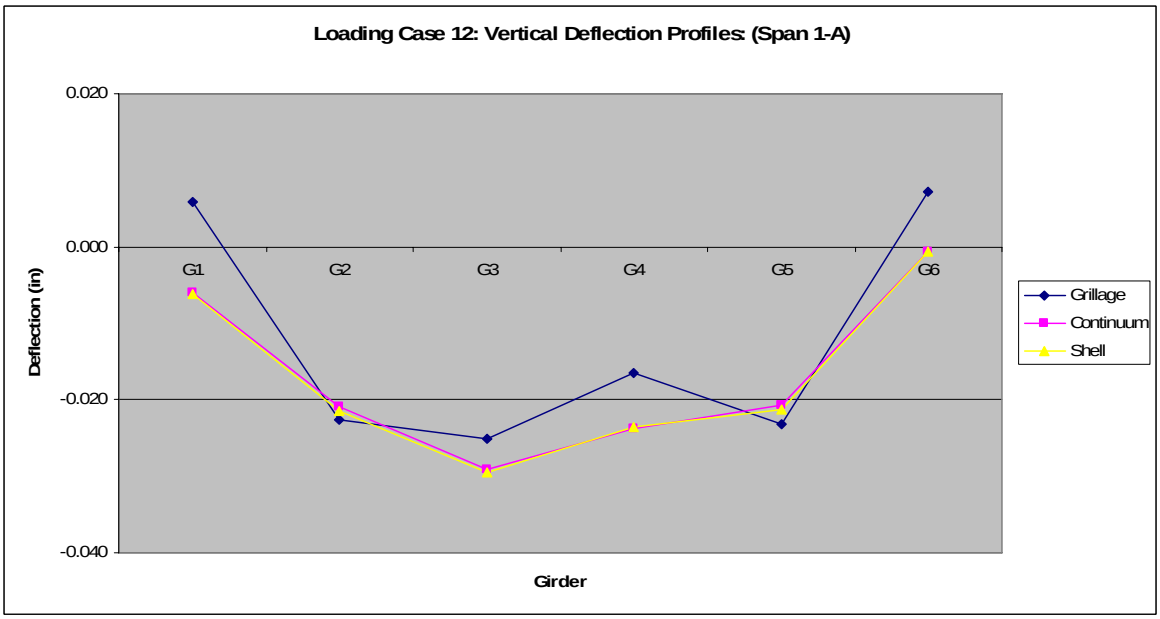

Figure C.37 Loading Case 12: vertical deflection profiles (Span 1-A).

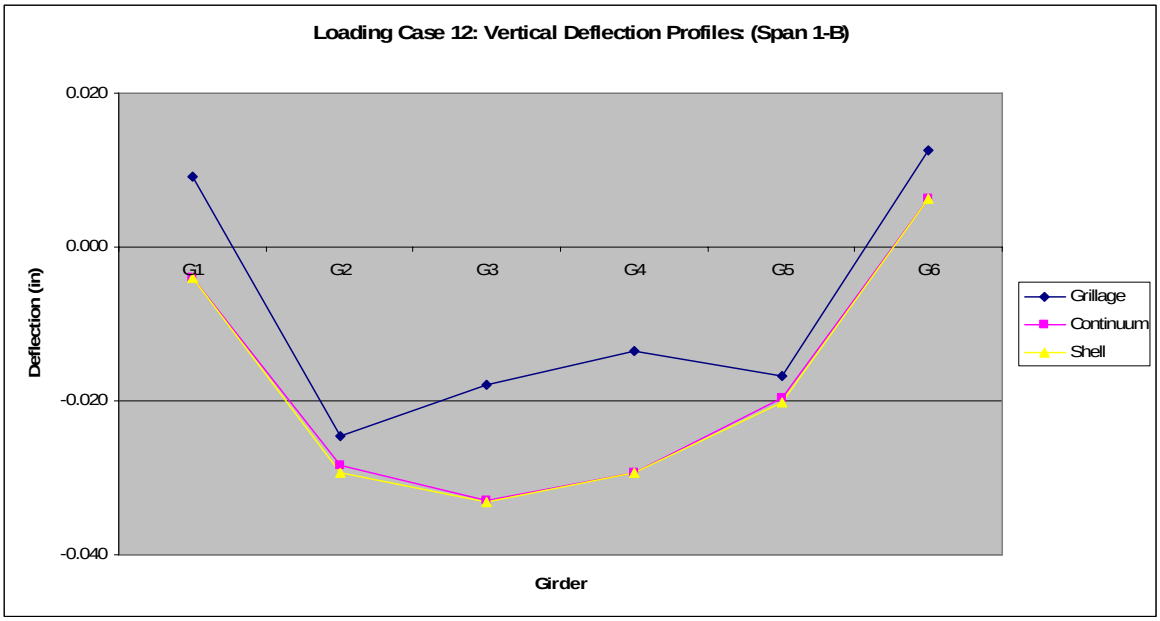

Figure C.38 Loading Case 12: vertical deflection profiles (Span 1-B).

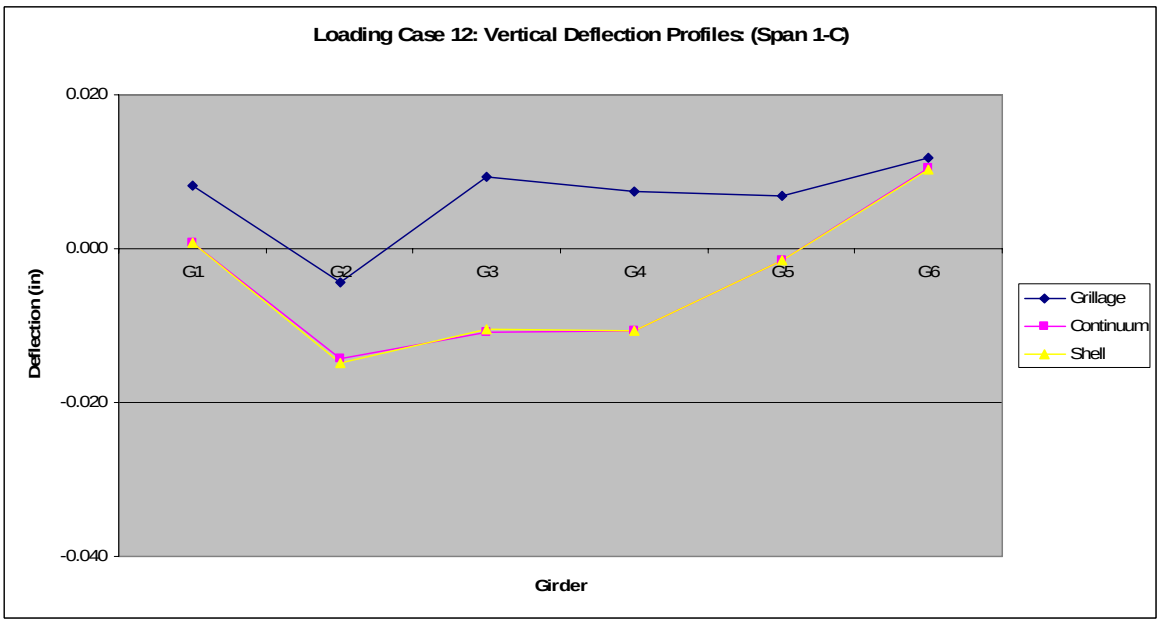

Figure C.39 Loading Case 12: vertical deflection profiles (Span 1-C).

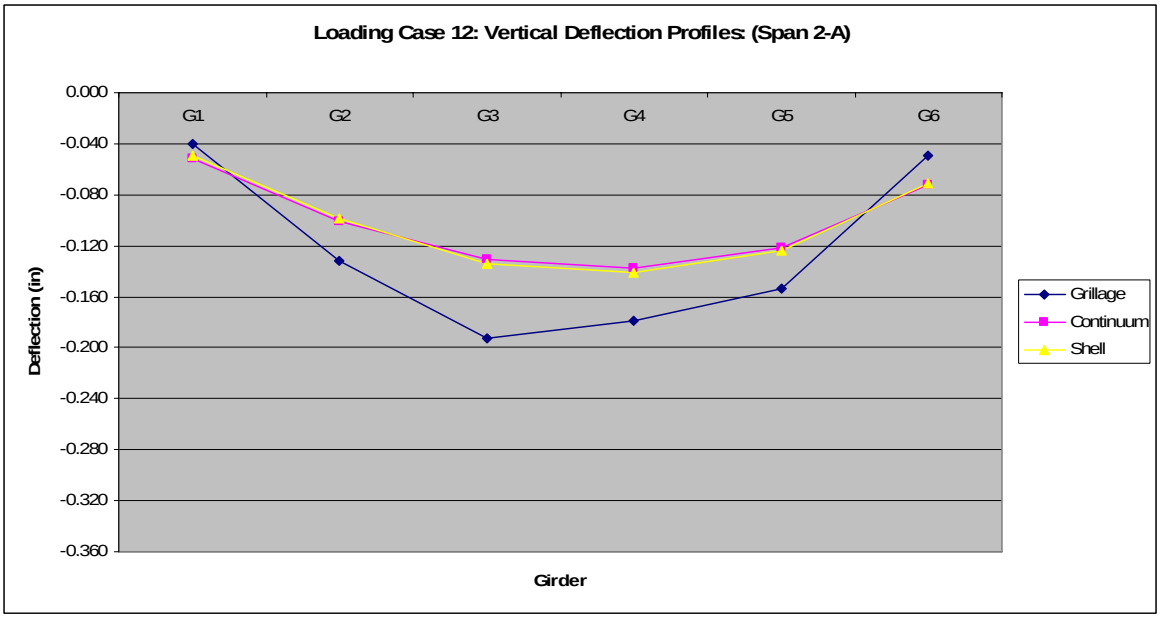

Figure C.40 Loading Case 12: vertical deflection profiles (Span 2-A).

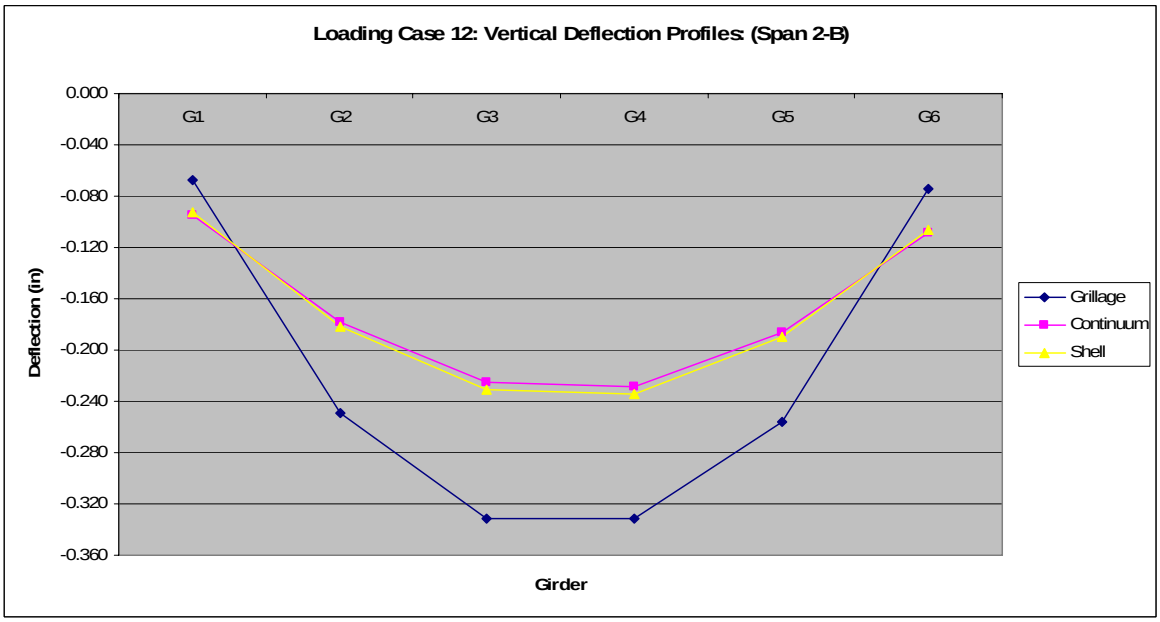

Figure C.41 Loading Case 12: vertical deflection profiles (Span 2-B).

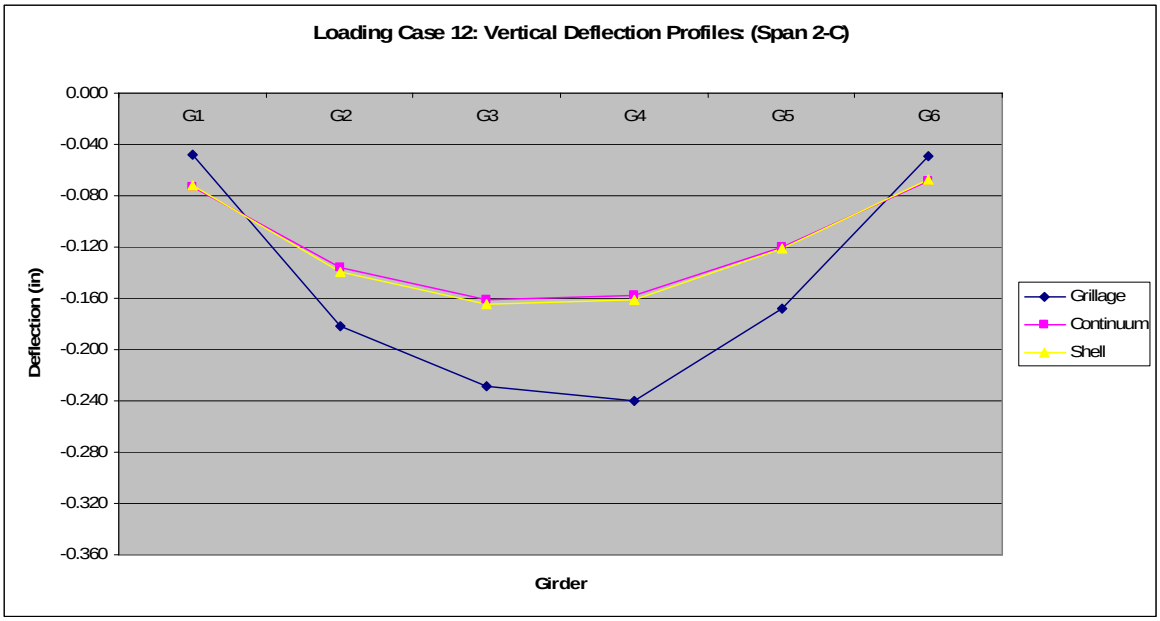

Figure C.42 Loading Case 12: vertical deflection profiles (Span 2-C).

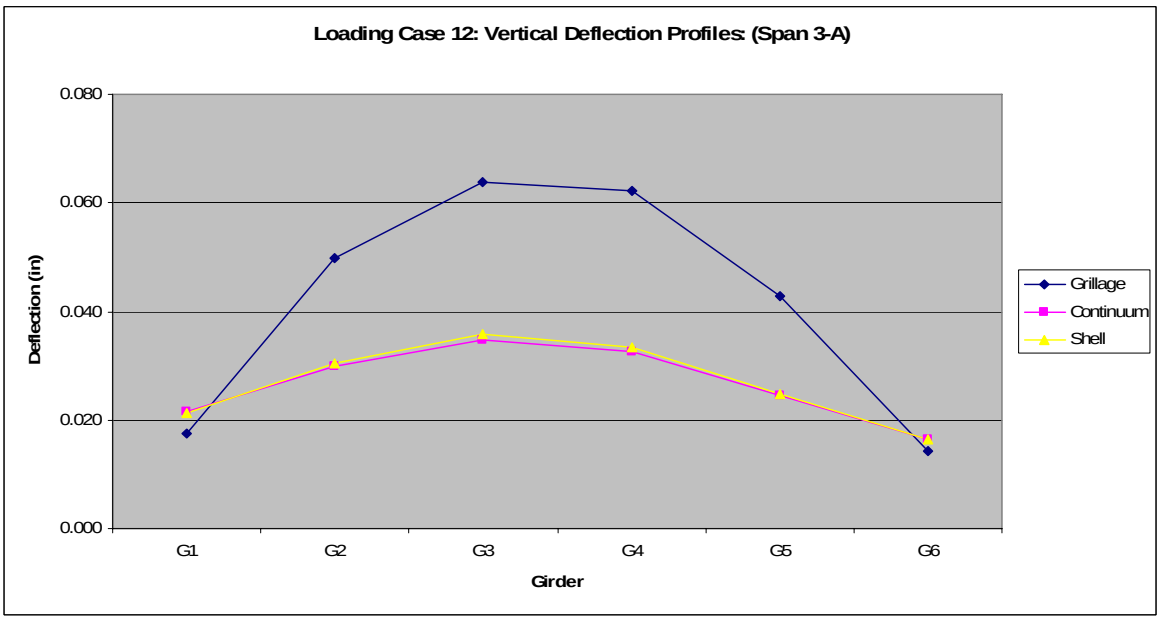

Figure C.43 Loading Case 12: vertical deflection profiles (Span 3-A).

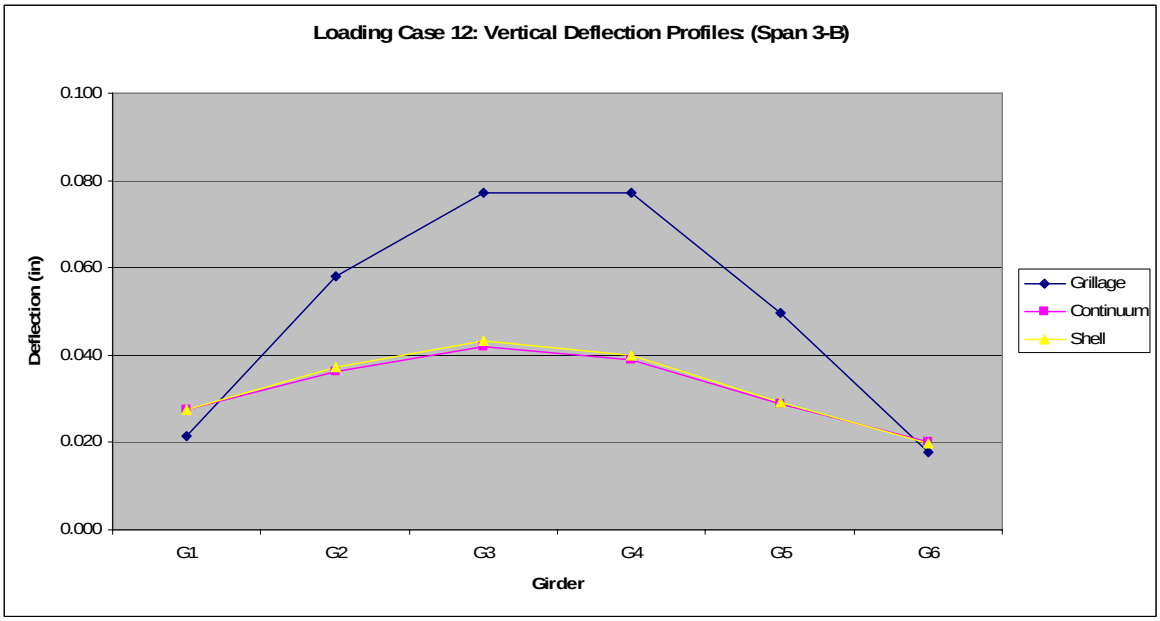

Figure C.44 Loading Case 12: vertical deflection profiles (Span 3-B).

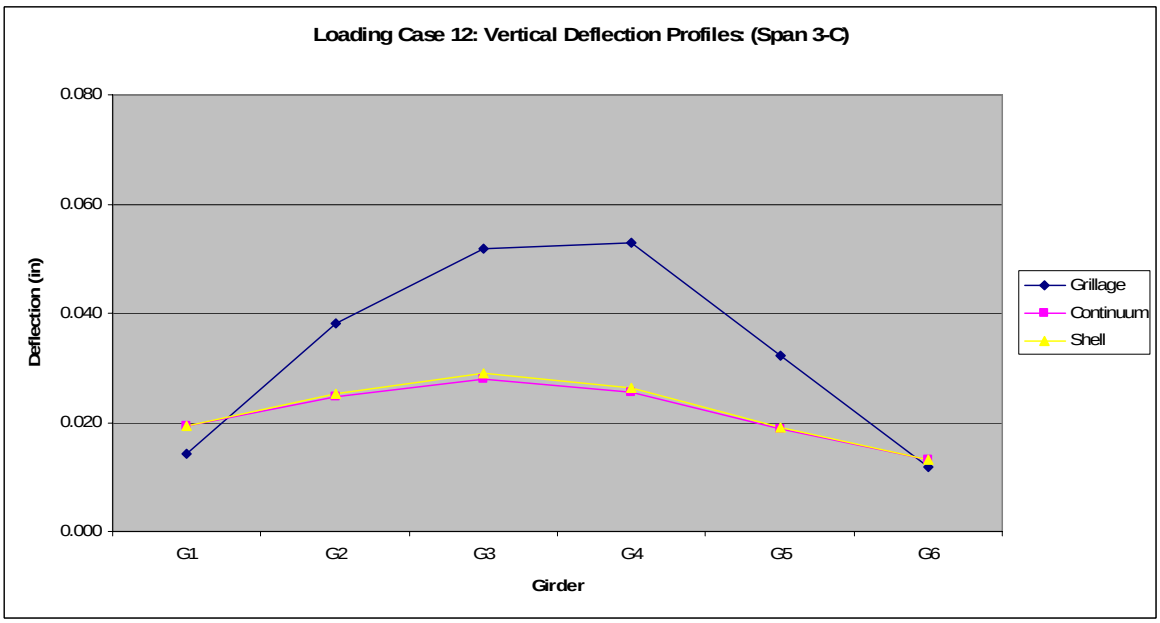

Figure C.45 Loading Case 12: vertical deflection profiles (Span 3-C).

APPENDIX D

SUPPLEMENTARY RESULTS (MAXIMUM LONGITUDINAL BENDING STRESSES)

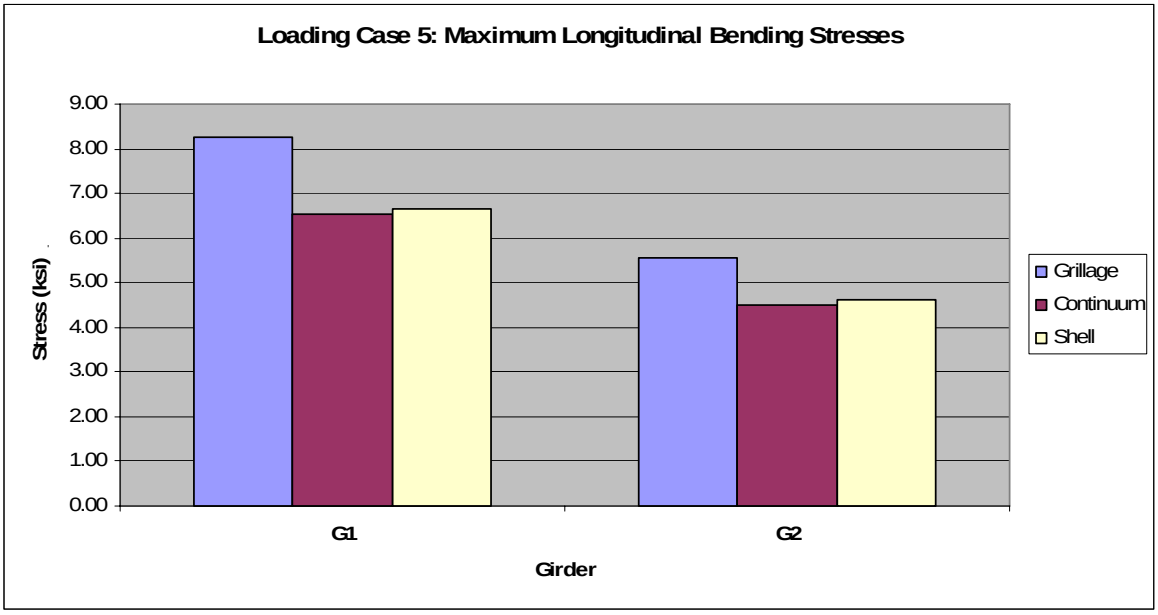

Figure D.1 Loading Case 5: maximum longitudinal bending stresses.

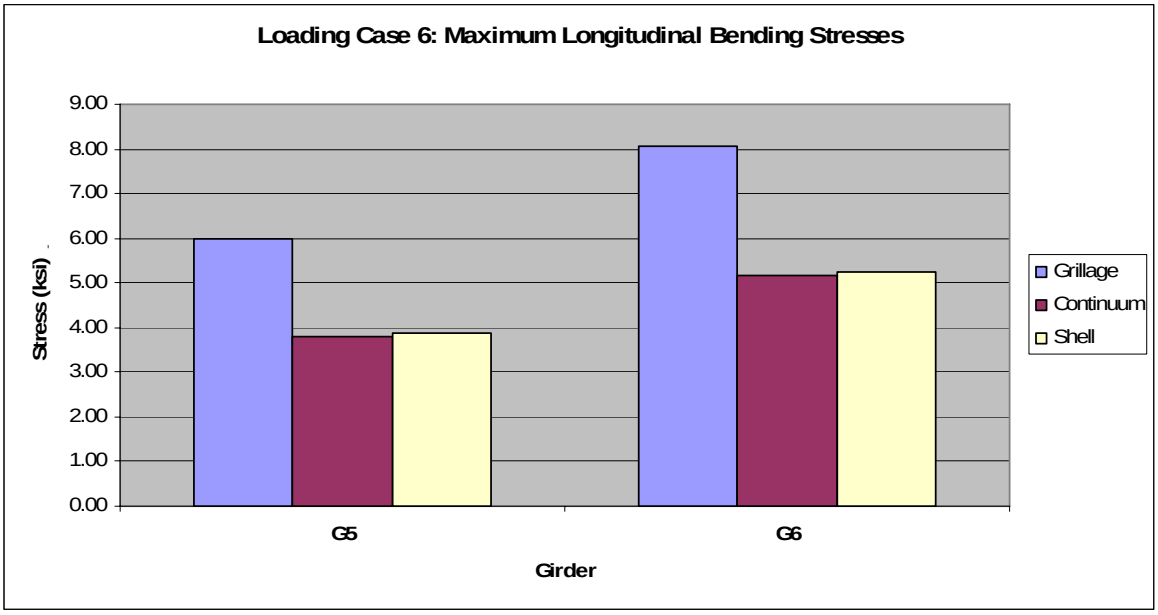

Figure D.2 Loading Case 6: maximum longitudinal bending stresses.

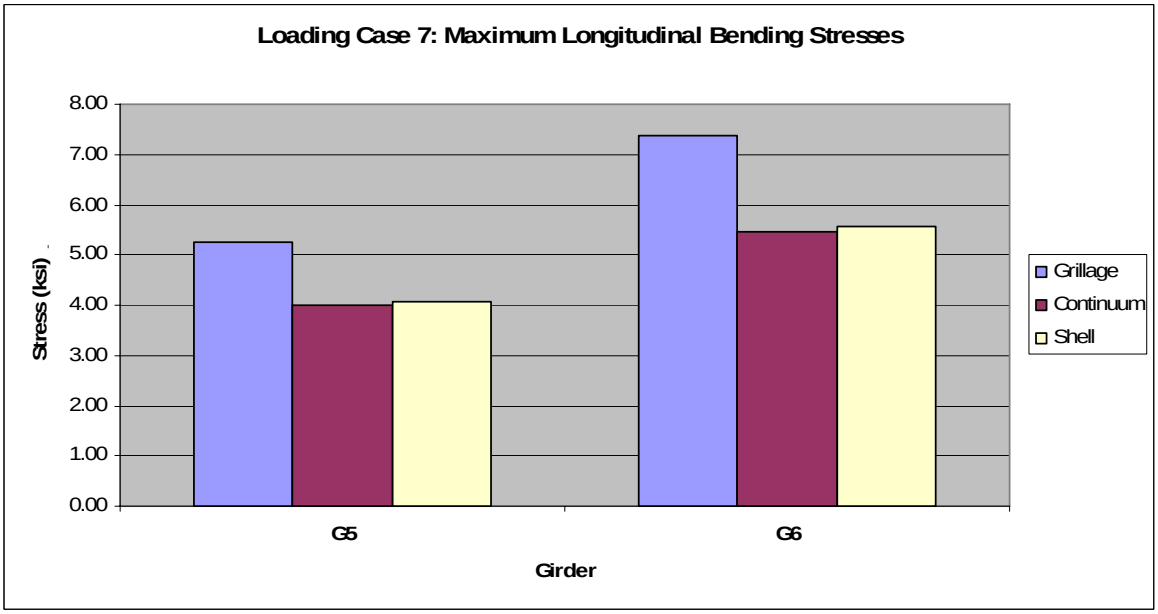

Figure D.3 Loading Case 7: maximum longitudinal bending stresses.

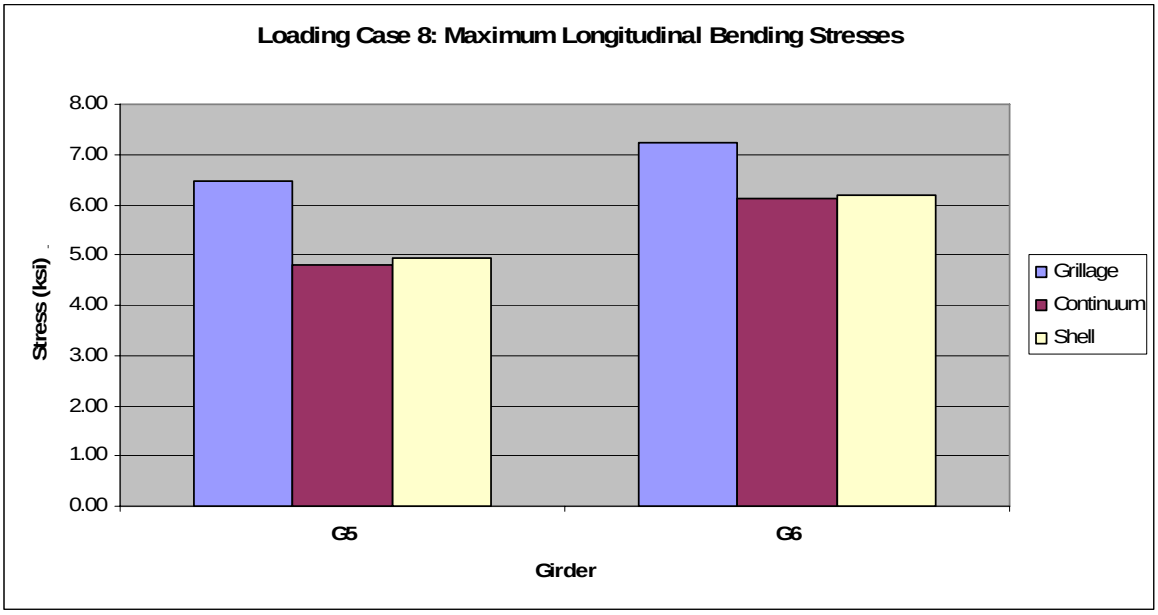

Figure D.4 Loading Case 8: maximum longitudinal bending stresses.

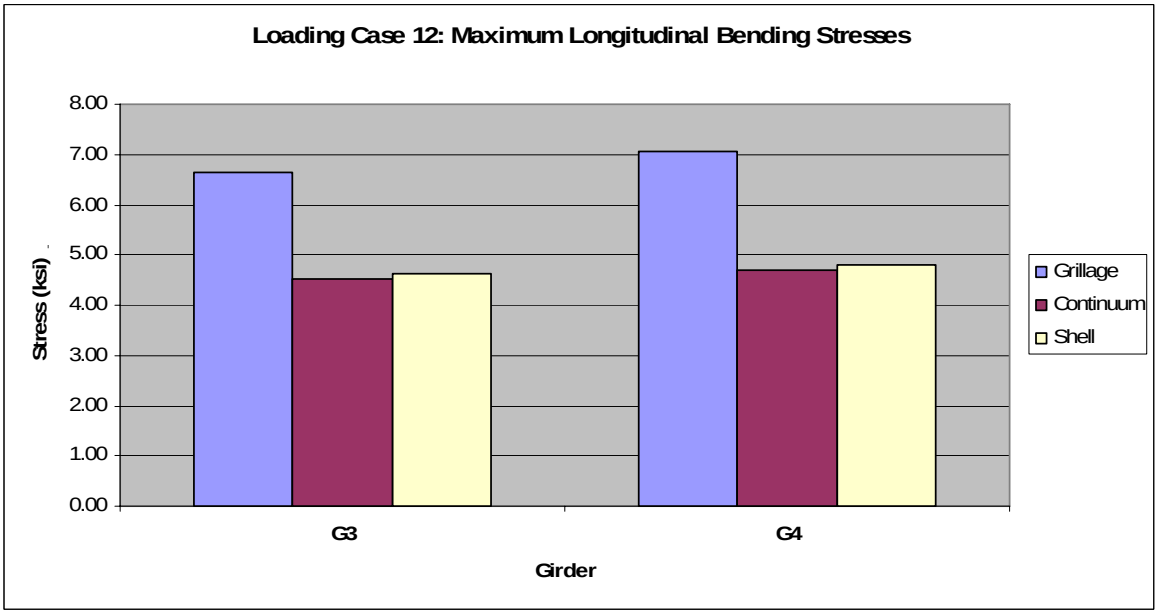

Figure D.5 Loading Case 12: maximum longitudinal bending stresses.

APPENDIX E

SUPPLEMENTARY RESULTS (LONGITUDINAL BENDING STRESS PROFILES)

E.1 Loading Case 1

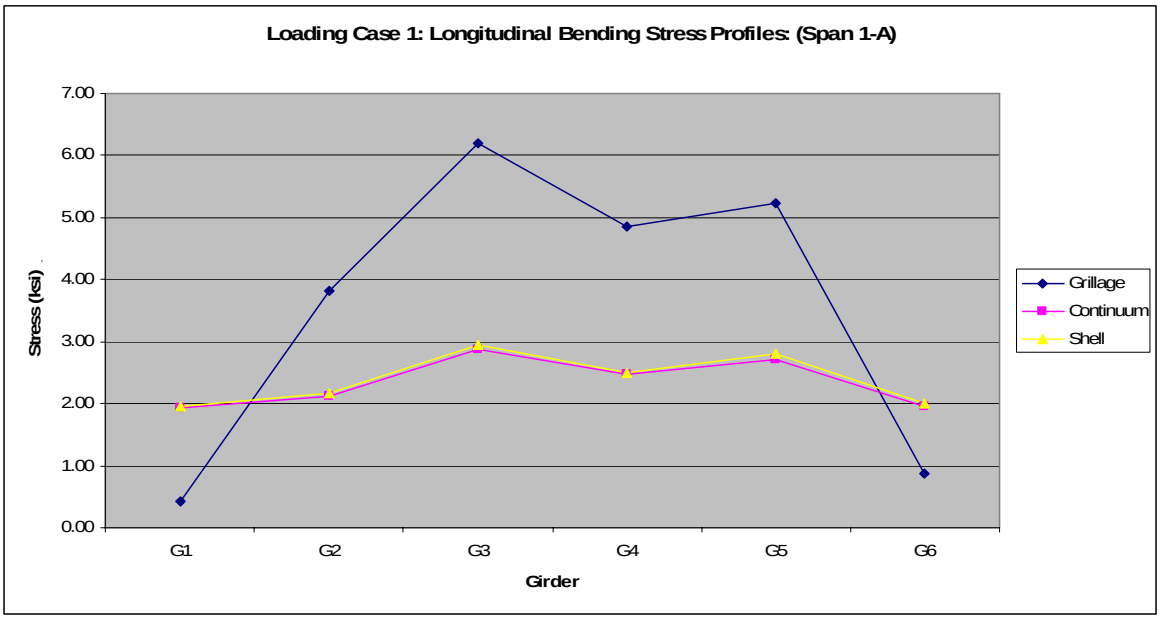

Figure E.1 Loading Case 1: longitudinal bending stress profiles (Span 1-A).

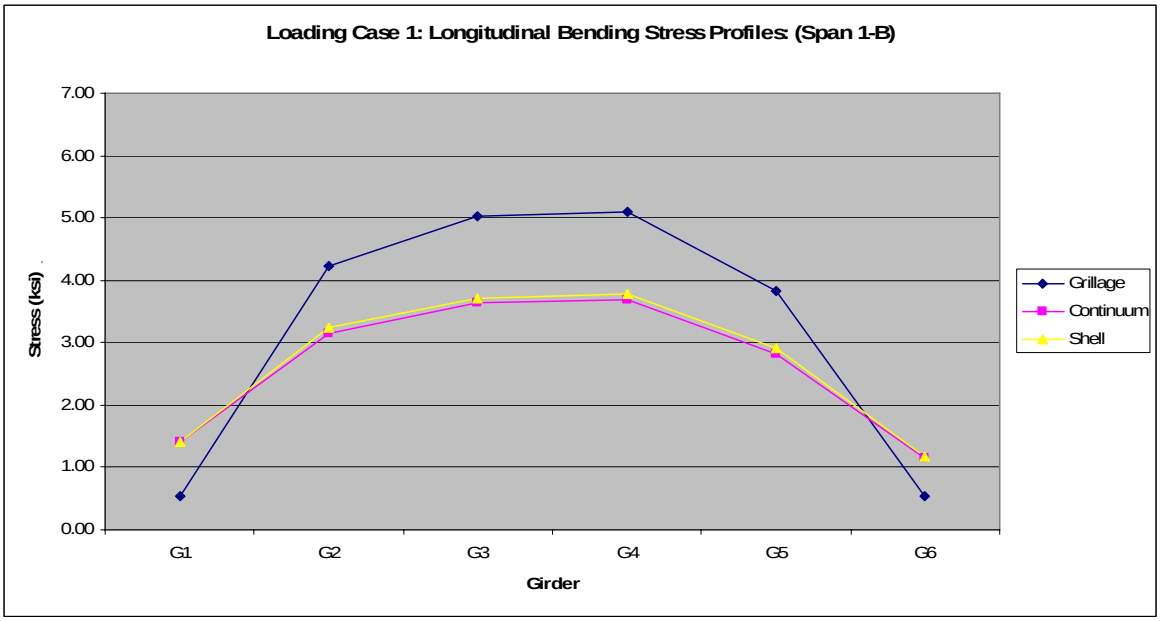

Figure E.2 Loading Case 1: longitudinal bending stress profiles (Span 1-B).

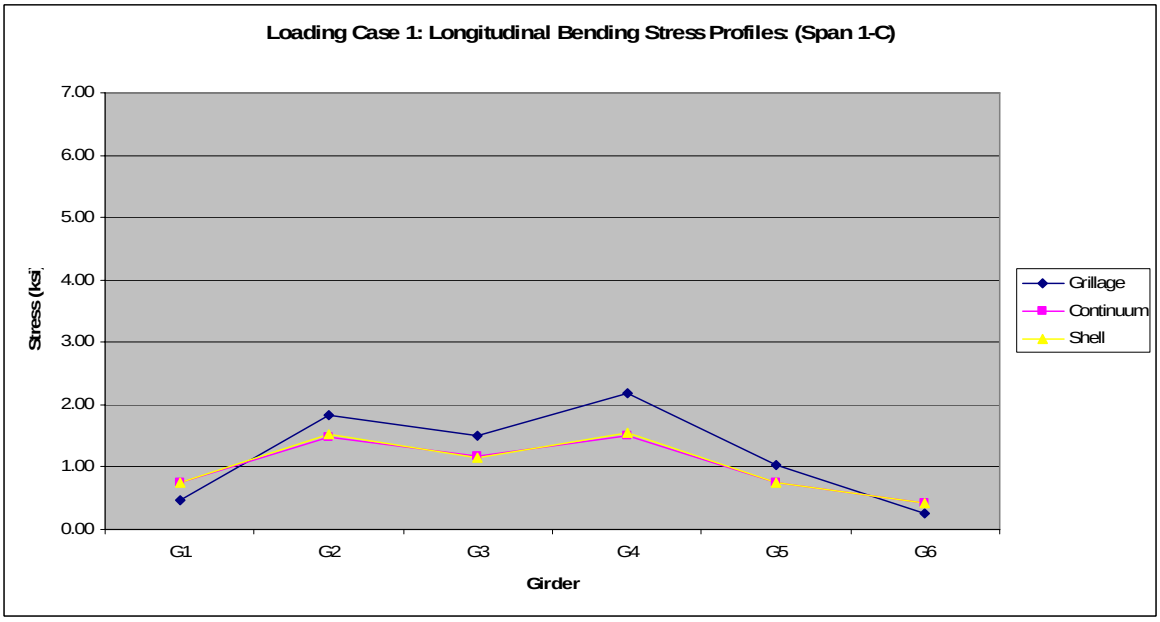

Figure E.3 Loading Case 1: longitudinal bending stress profiles (Span 1-C).

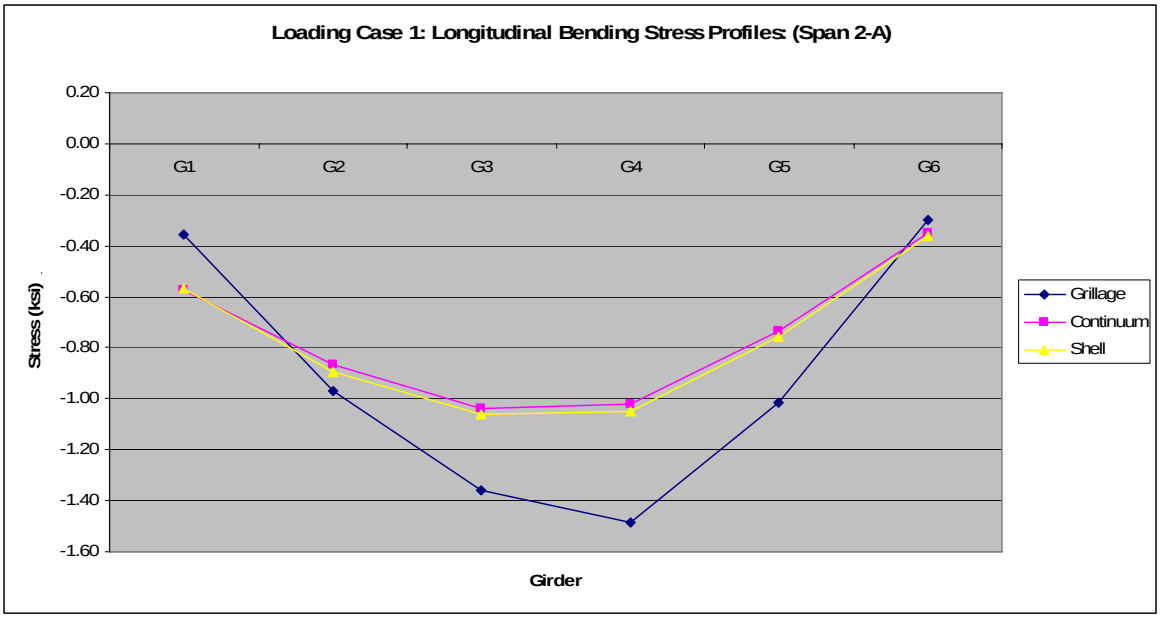

Figure E.4 Loading Case 1: longitudinal bending stress profiles (Span 2-A).

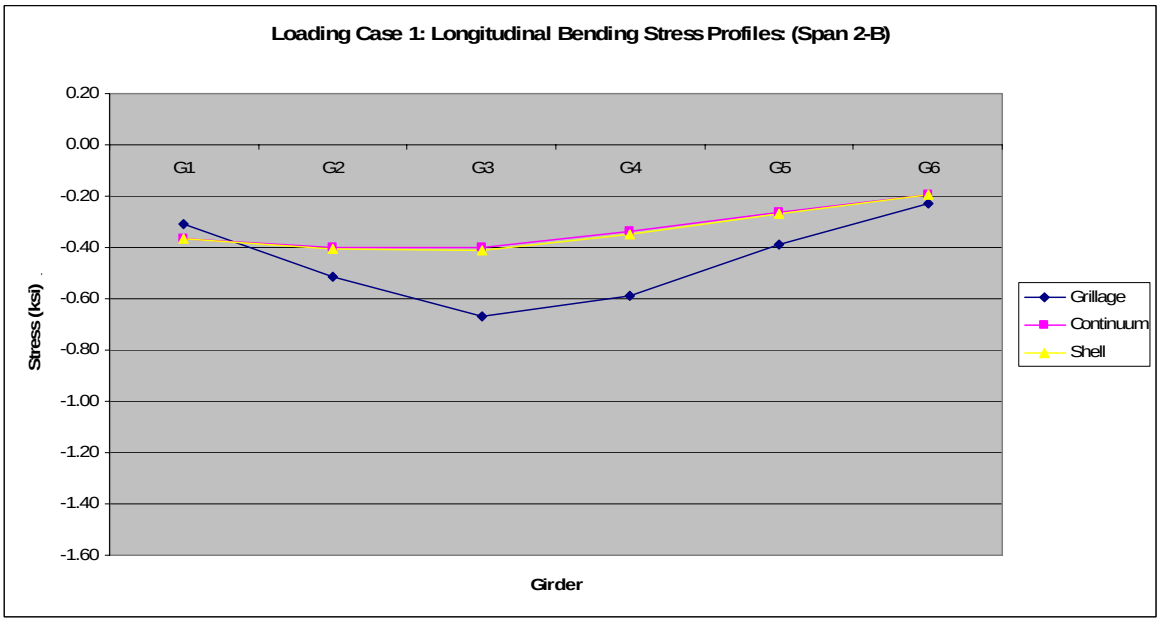

Figure E.5 Loading Case 1: longitudinal bending stress profiles (Span 2-B).

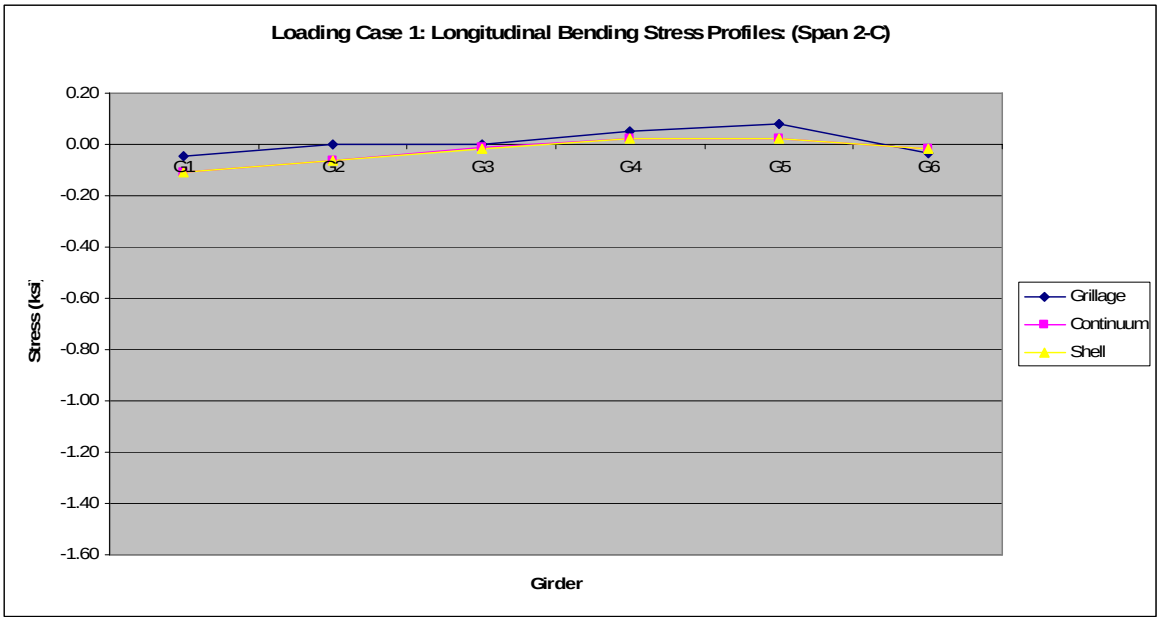

Figure E.6 Loading Case 1: longitudinal bending stress profiles (Span 2-C).

E.2 Loading Case 2

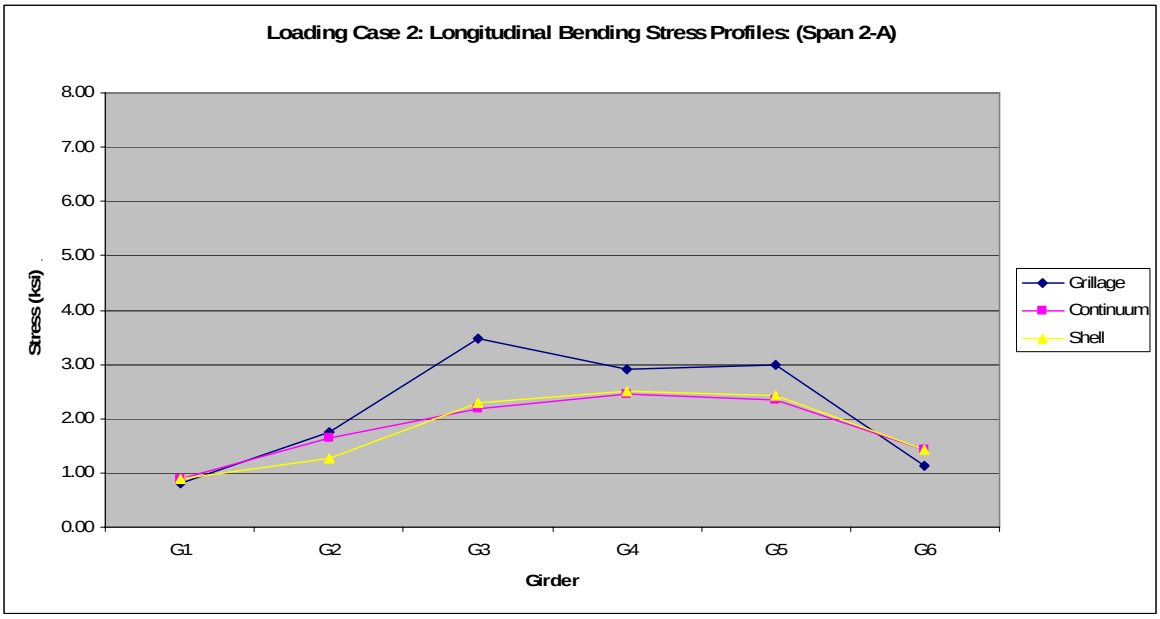

Figure E.7 Loading Case 2: longitudinal bending stress profiles (Span 2-A).

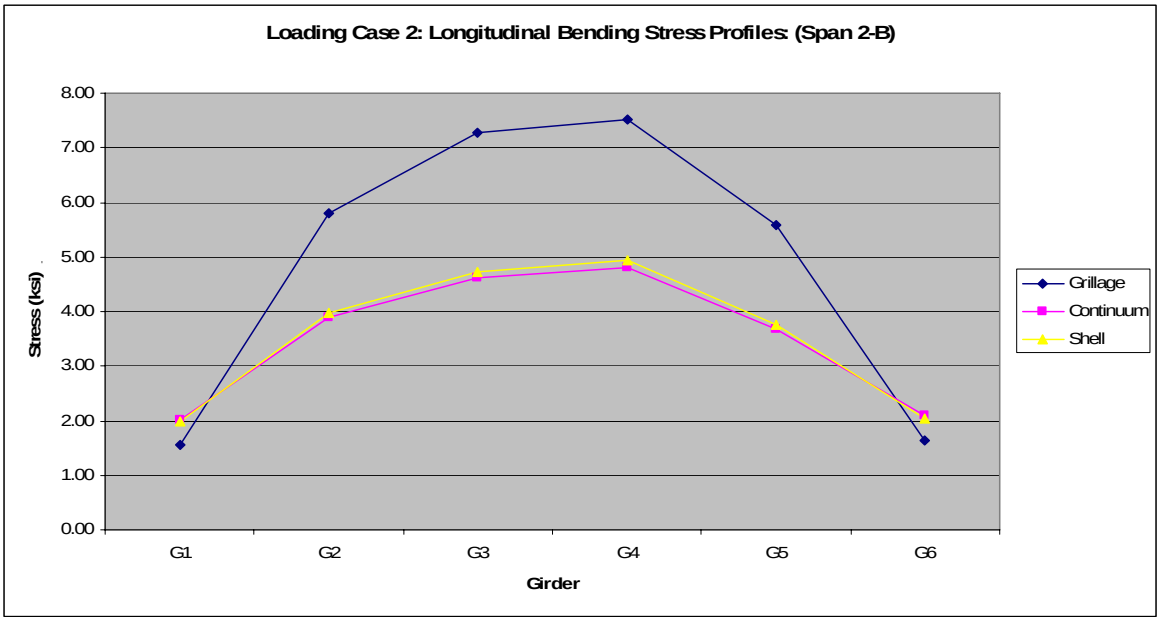

Figure E.8 Loading Case 2: longitudinal bending stress profiles (Span 2-B).

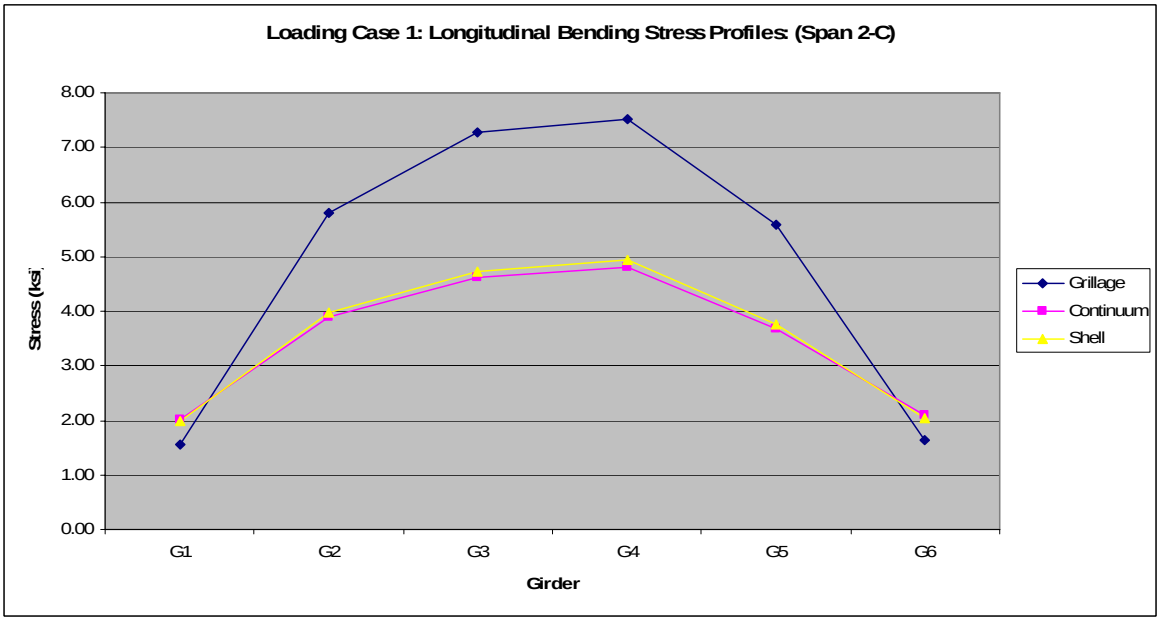

Figure E.9 Loading Case 2: longitudinal bending stress profiles (Span 2-C).

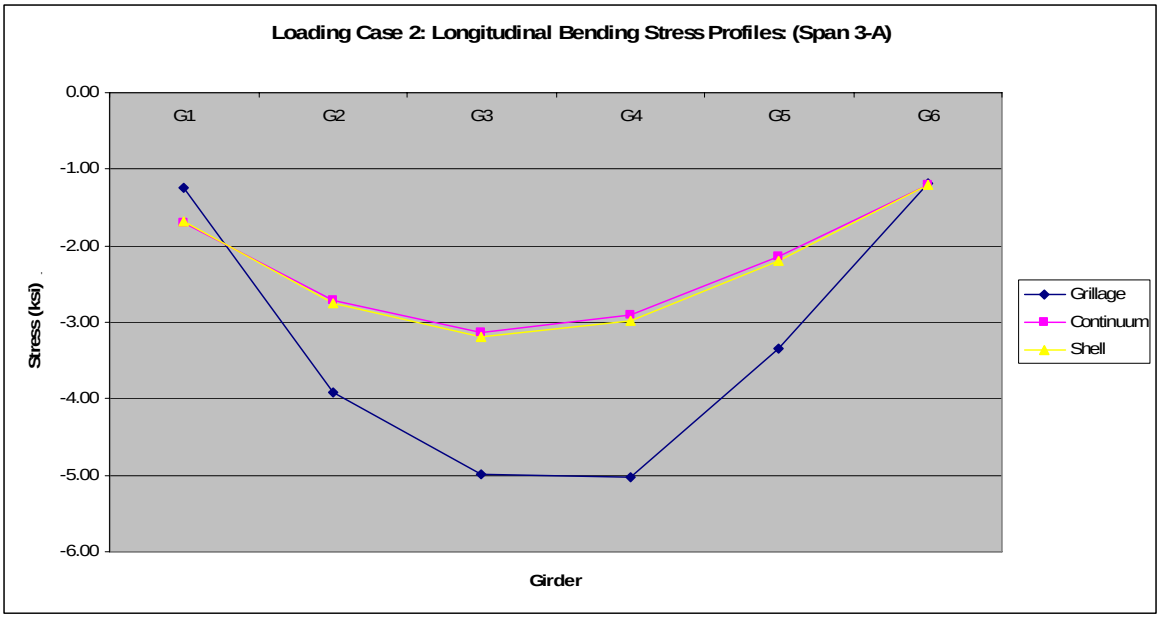

Figure E.10 Loading Case 2: longitudinal bending stress profiles (Span 3-A).

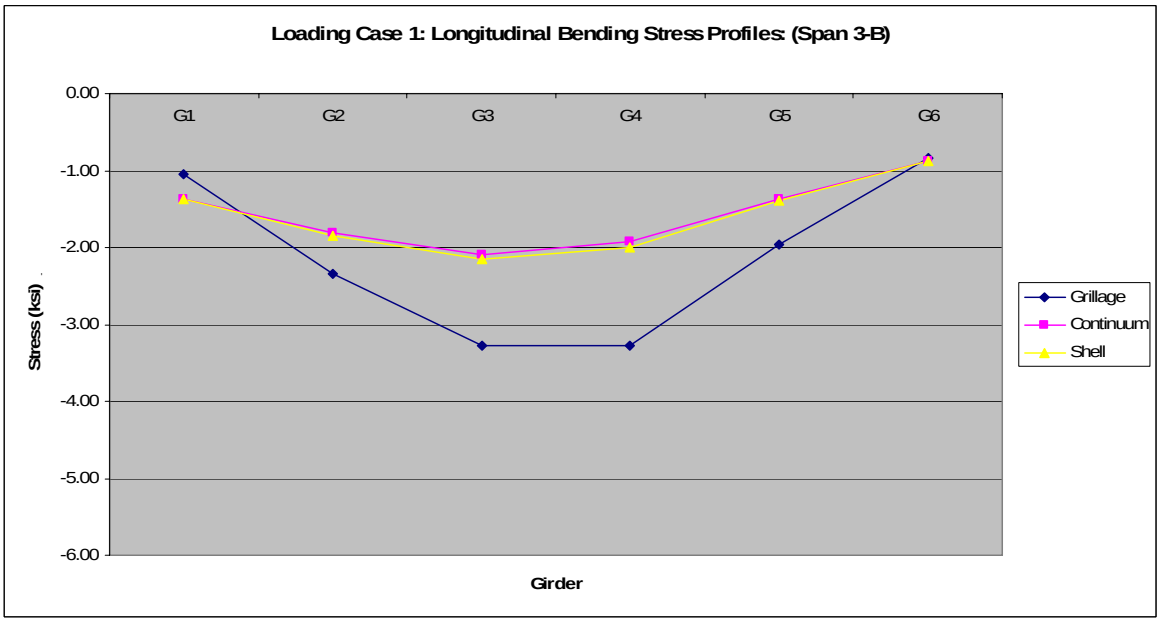

Figure E.11 Loading Case 2: longitudinal bending stress profiles (Span 3-B).

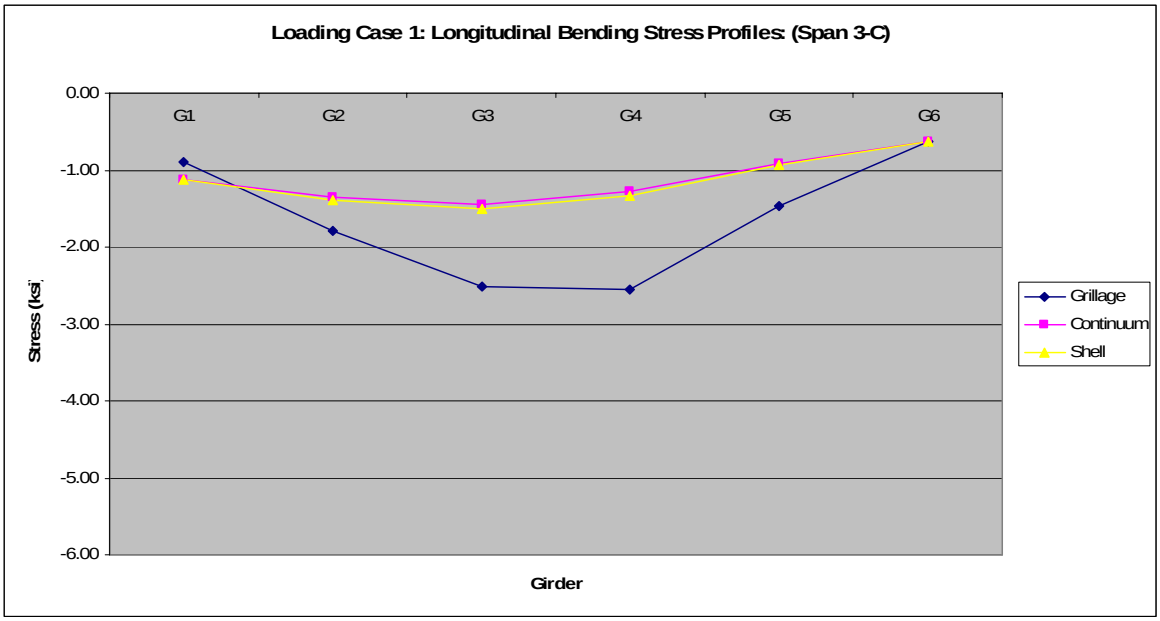

Figure E.12 Loading Case 2: longitudinal bending stress profiles (Span 3-C).

E.3 Loading Case 4

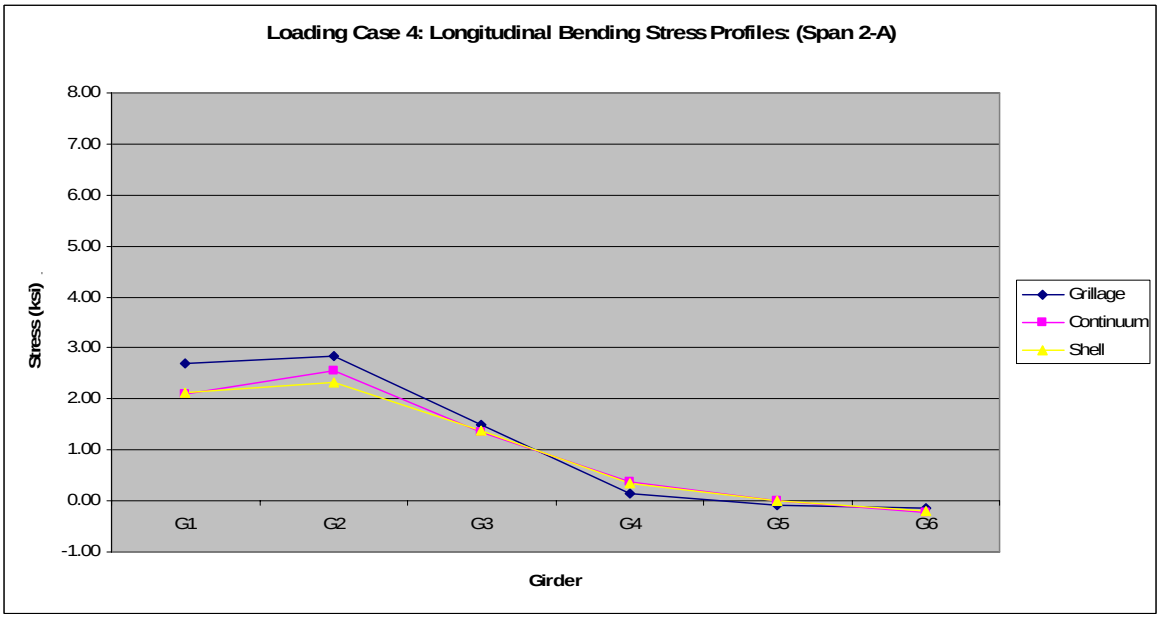

Figure E.13 Loading Case 4: longitudinal bending stress profiles (Span 2-A).

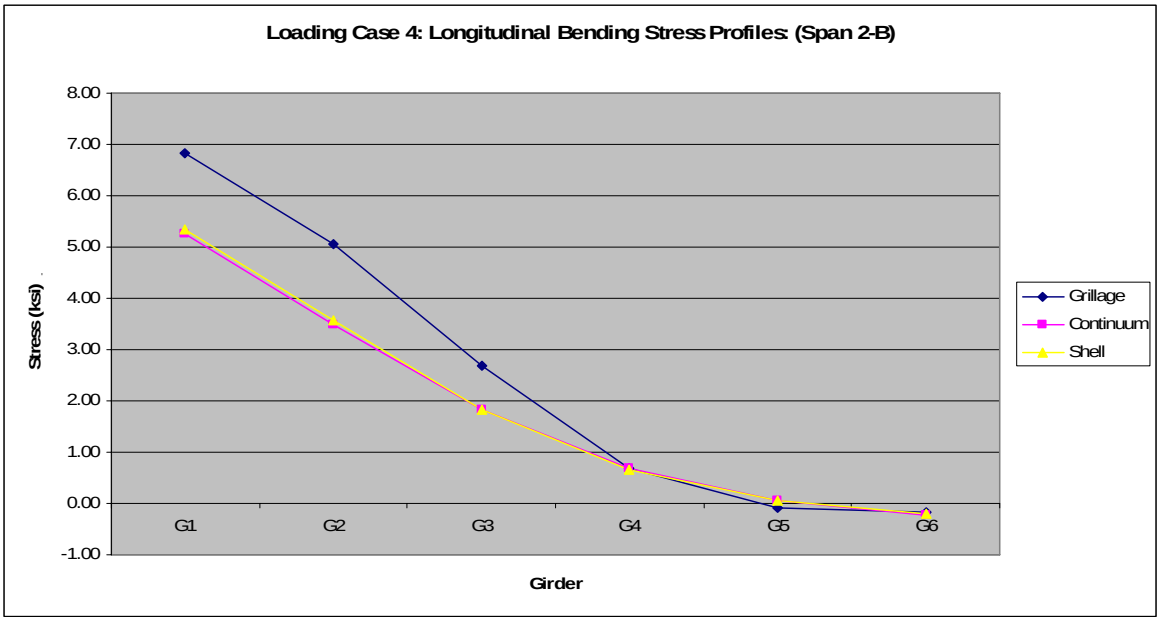

Figure E.14 Loading Case 4: longitudinal bending stress profiles (Span 2-B).

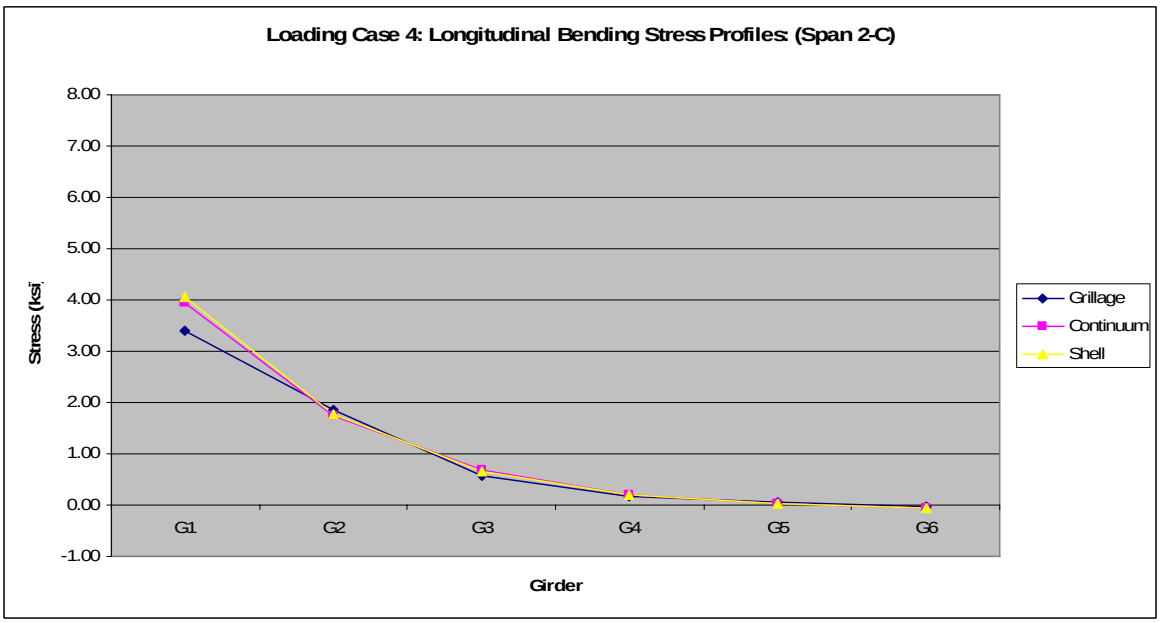

Figure E.15 Loading Case 4: longitudinal bending stress profiles (Span 2-C).

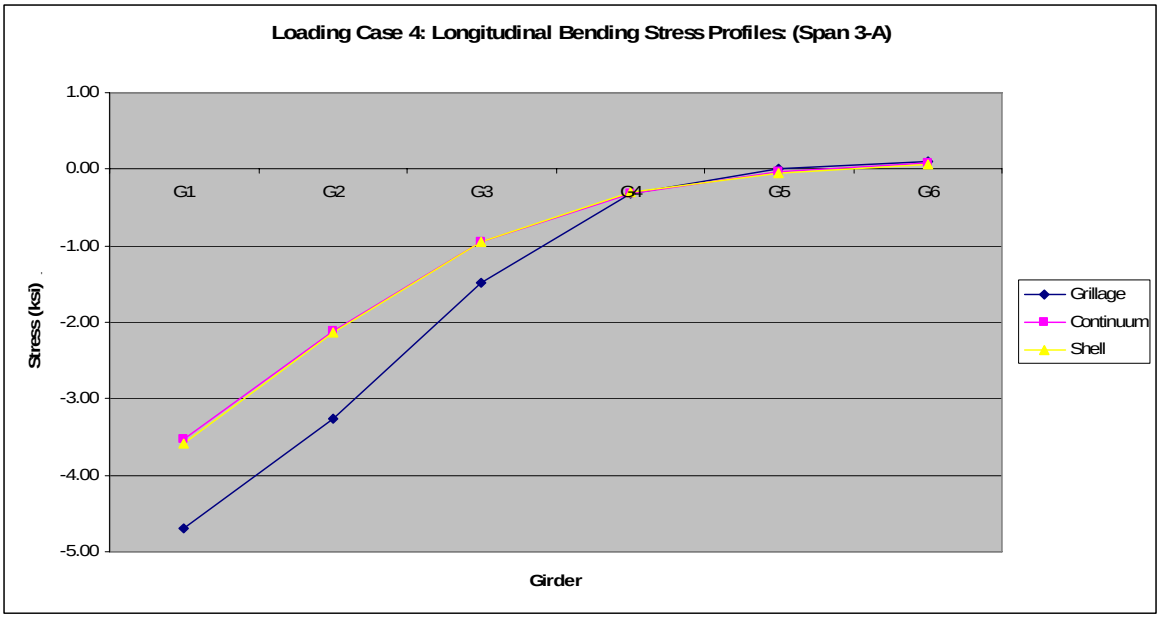

Figure E.16 Loading Case 4: longitudinal bending stress profiles (Span 3-A).

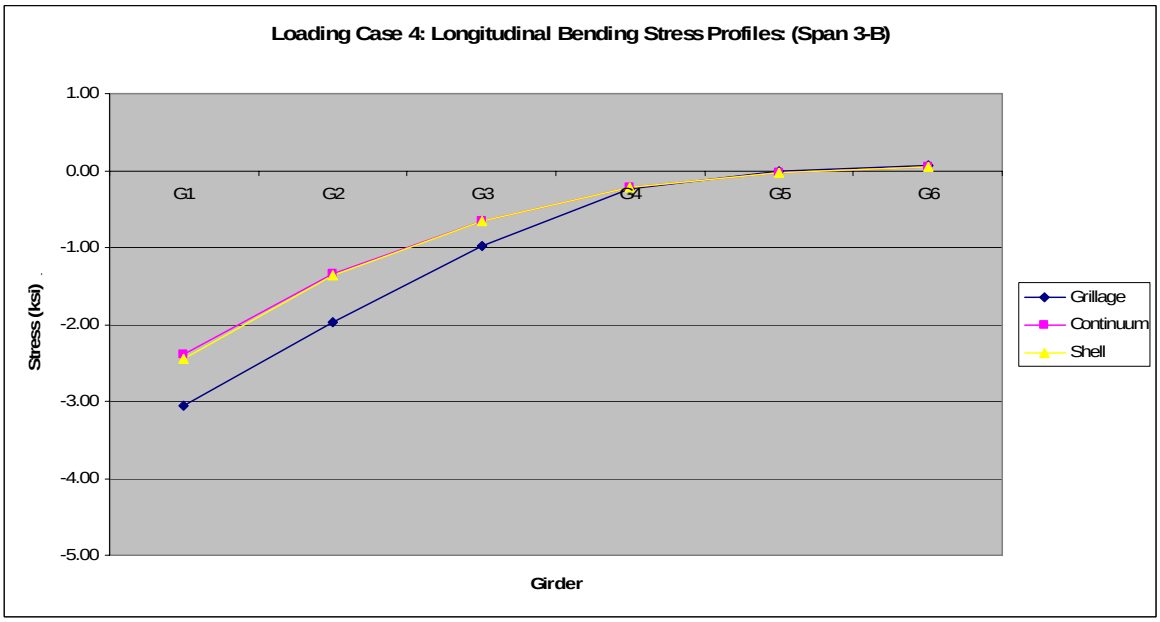

Figure E.17 Loading Case 4: longitudinal bending stress profiles (Span 3-B).

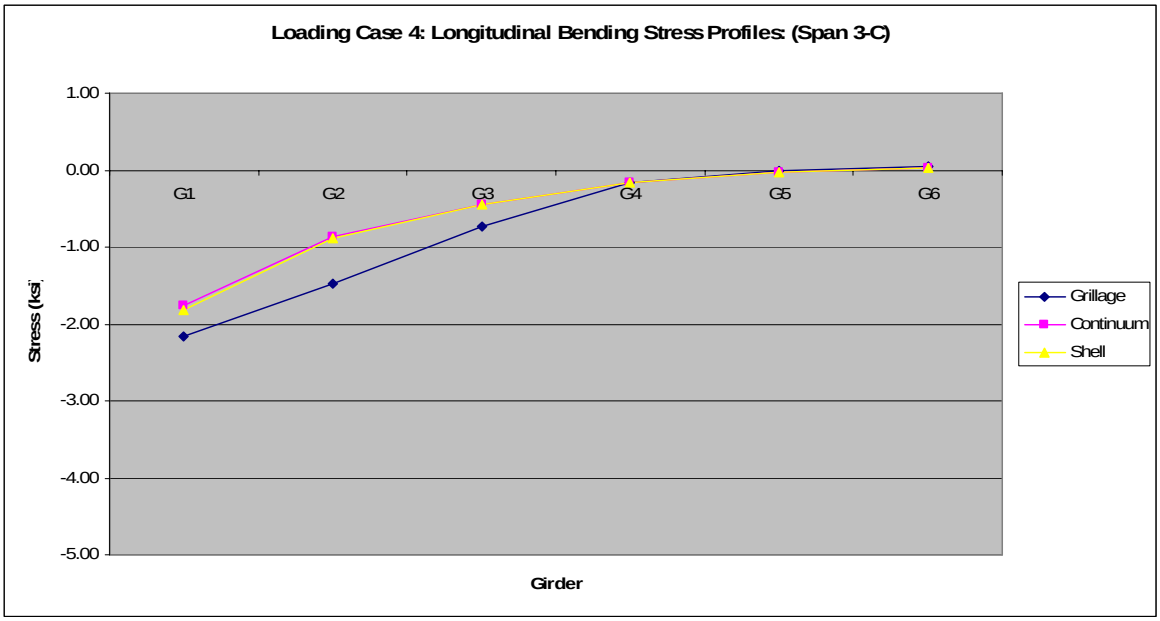

Figure E.18 Loading Case 4: longitudinal bending stress profiles (Span 3-C).

E.4 Loading Case 5

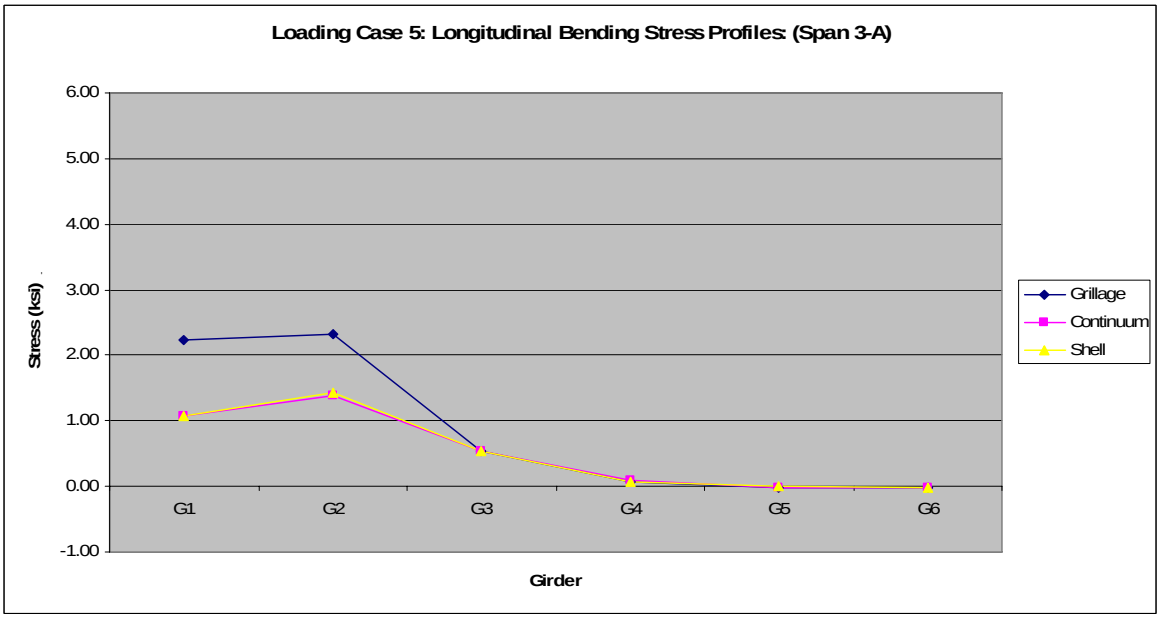

Figure E.19 Loading Case 5: longitudinal bending stress profiles (Span 3-A).

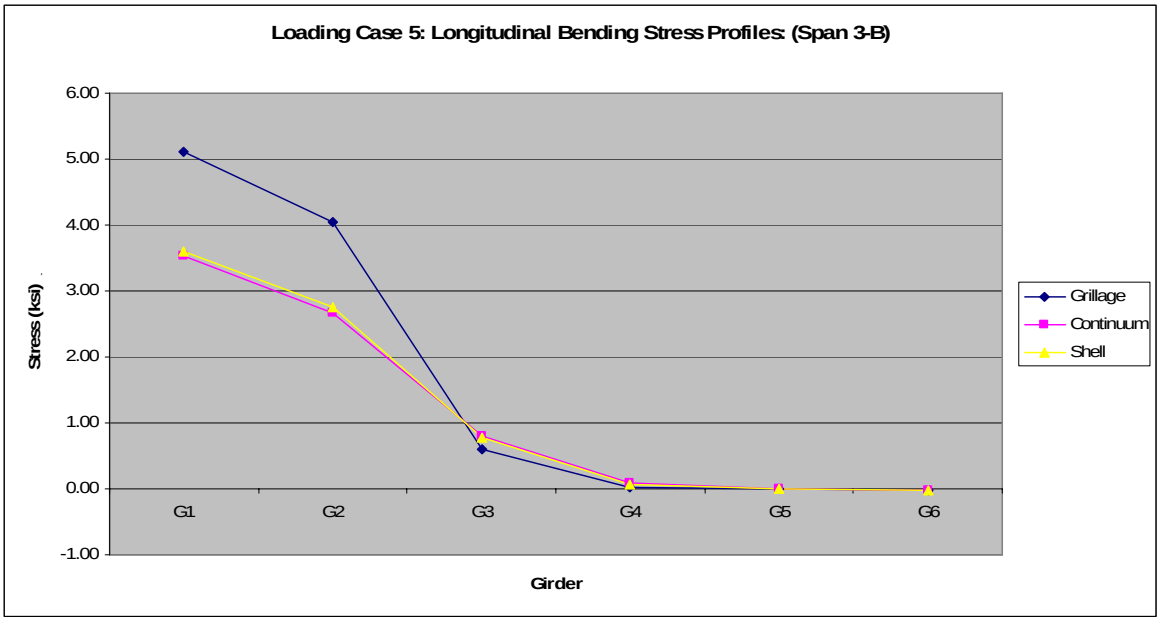

Figure E.20 Loading Case 5: longitudinal bending stress profiles (Span 3-B).

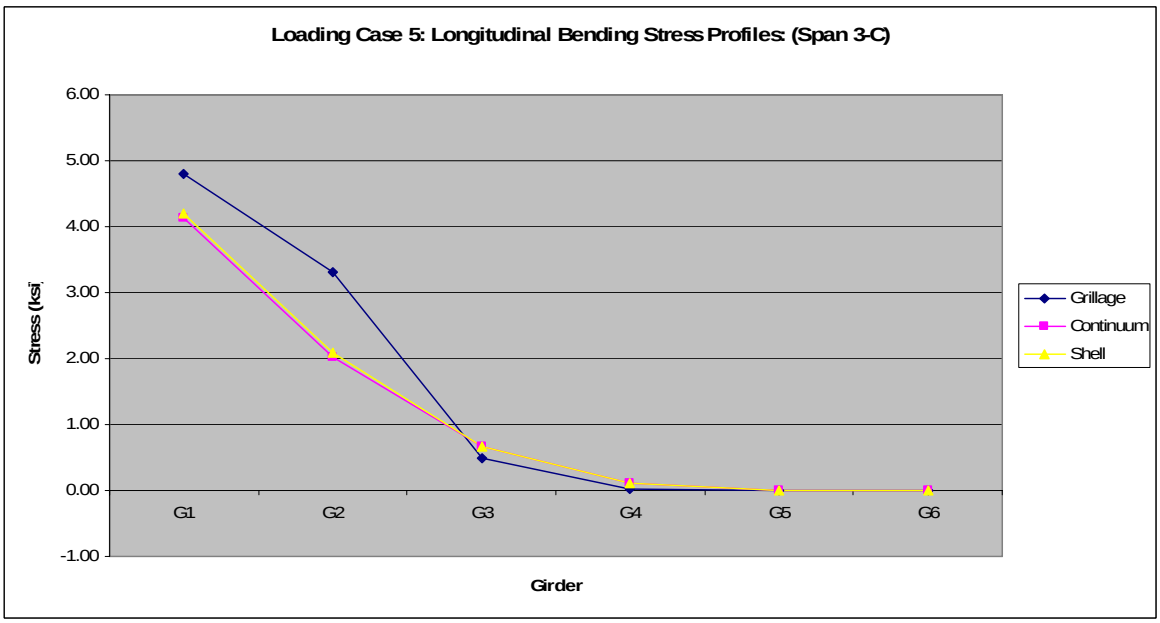

Figure E.21 Loading Case 5: longitudinal bending stress profiles (Span 3-C).

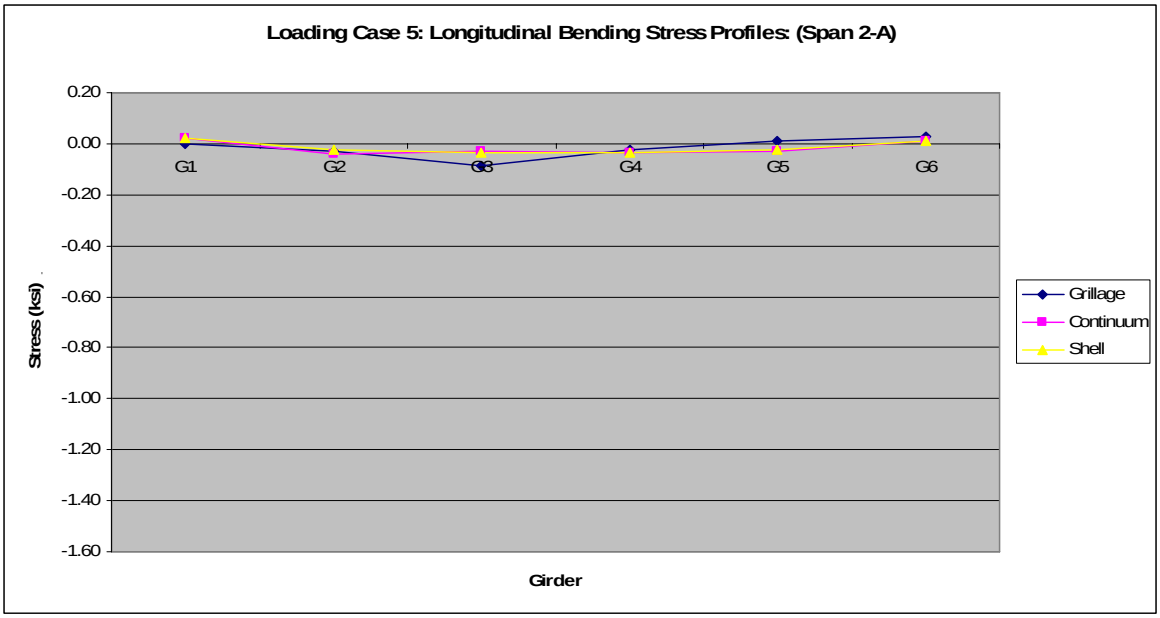

Figure E.22 Loading Case 5: longitudinal bending stress profiles (Span 2-A).

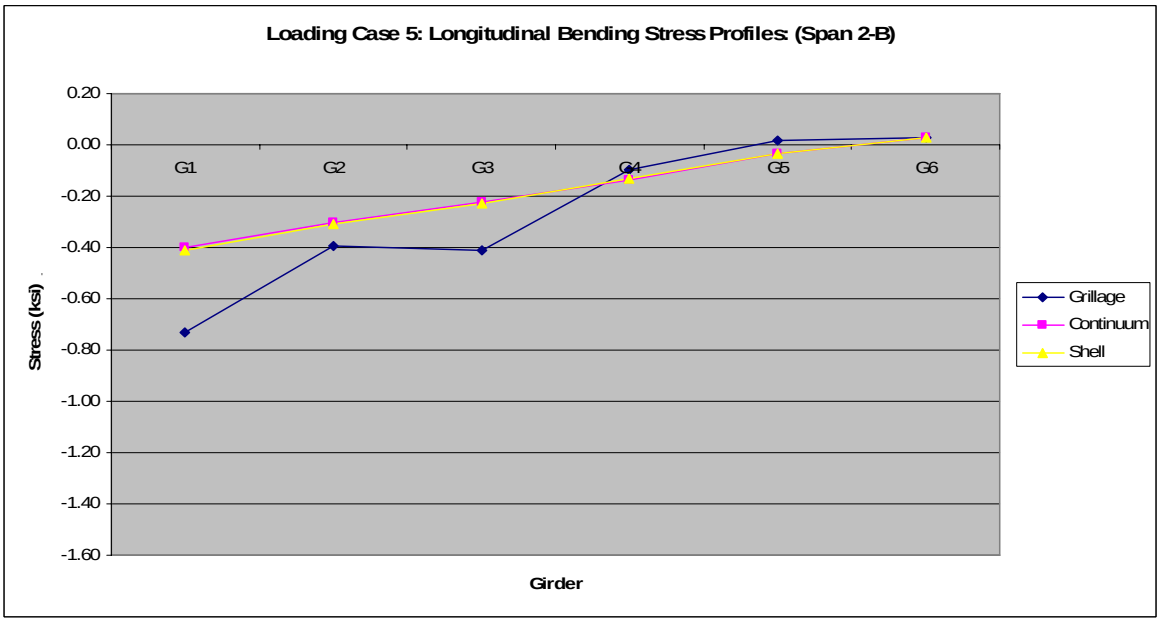

Figure E.23 Loading Case 5: longitudinal bending stress profiles (Span 2-B).

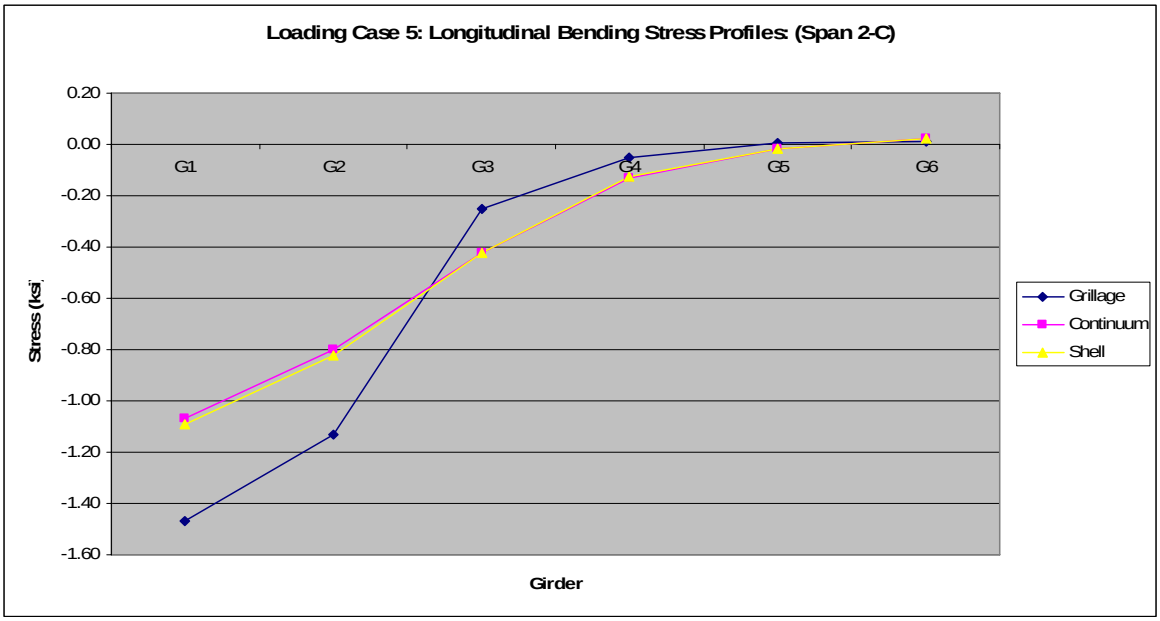

Figure E.24 Loading Case 5: longitudinal bending stress profiles (Span 2-C).

E.5 Loading Case 6

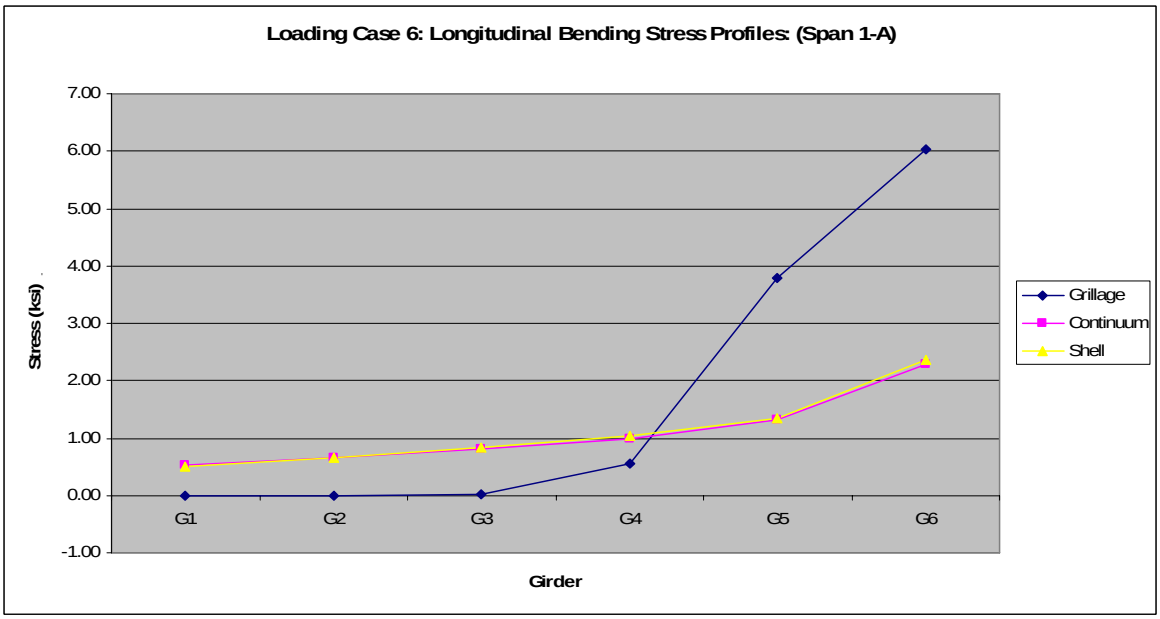

Figure E.25 Loading Case 6: longitudinal bending stress profiles (Span 1-A).

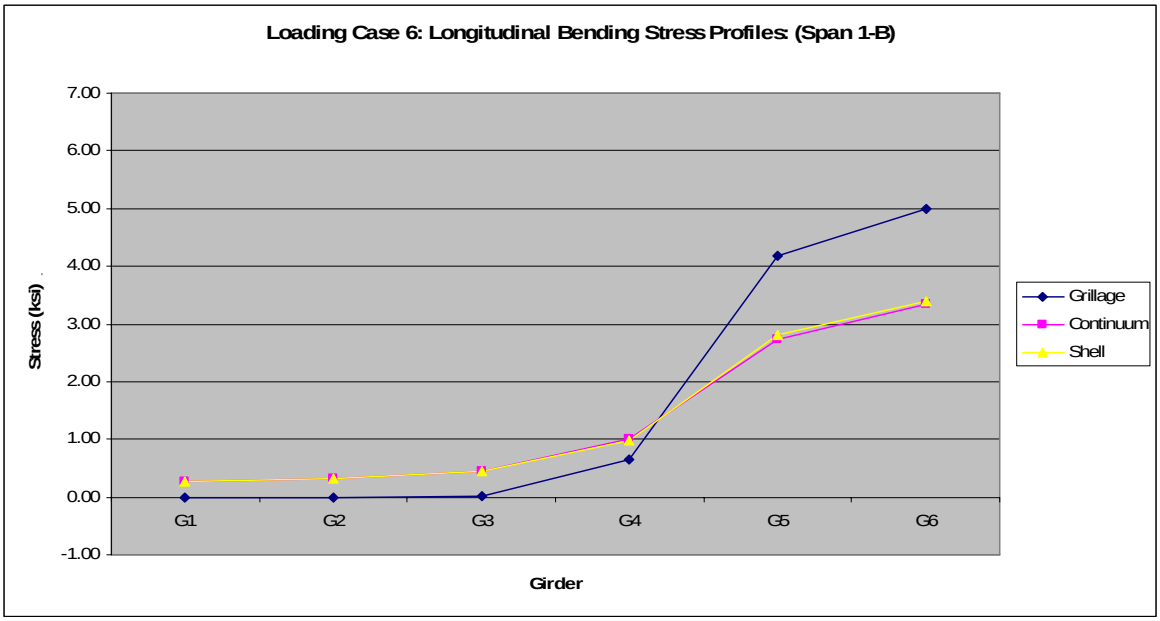

Figure E.26 Loading Case 6: longitudinal bending stress profiles (Span 1-B).

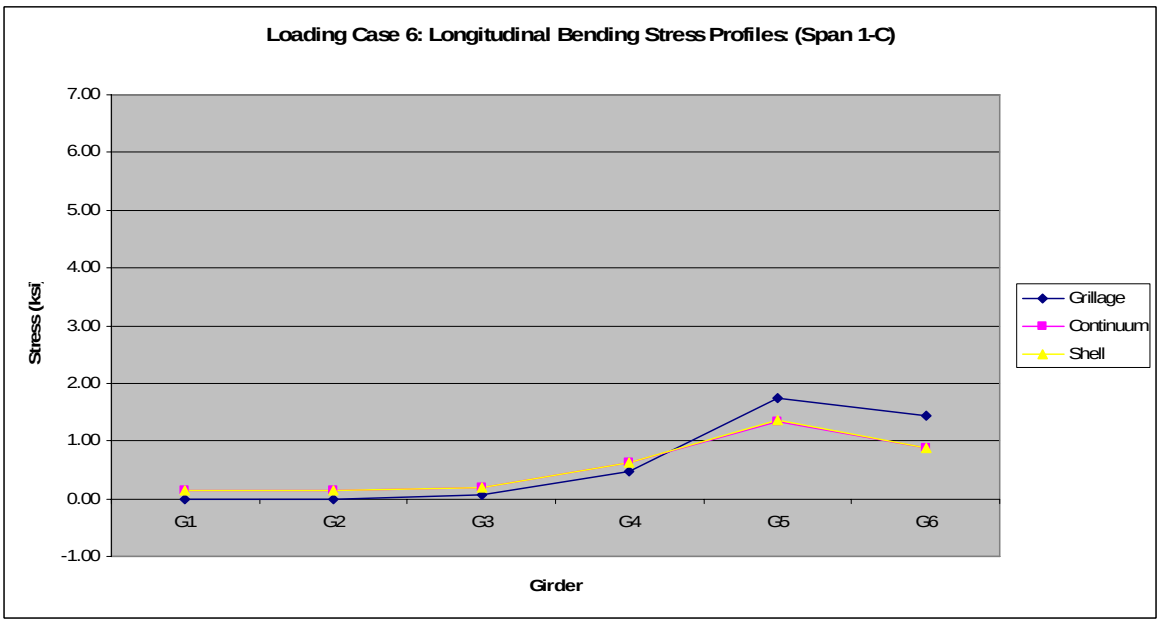

Figure E.27 Loading Case 6: longitudinal bending stress profiles (Span 1-C).

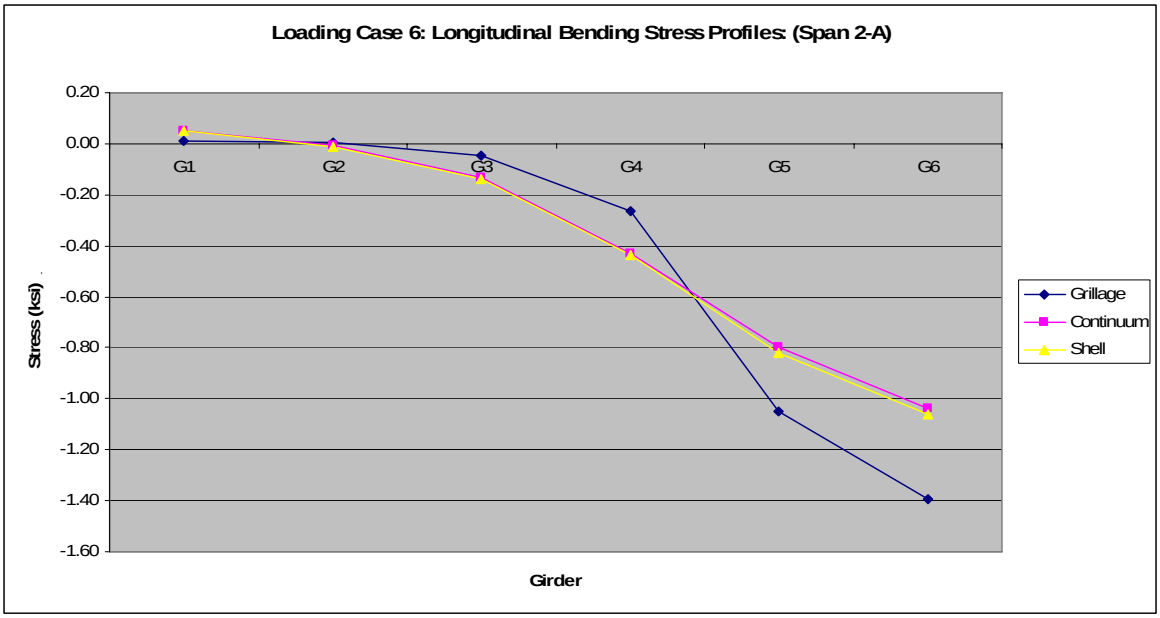

Figure E.28 Loading Case 6: longitudinal bending stress profiles (Span 2-A).

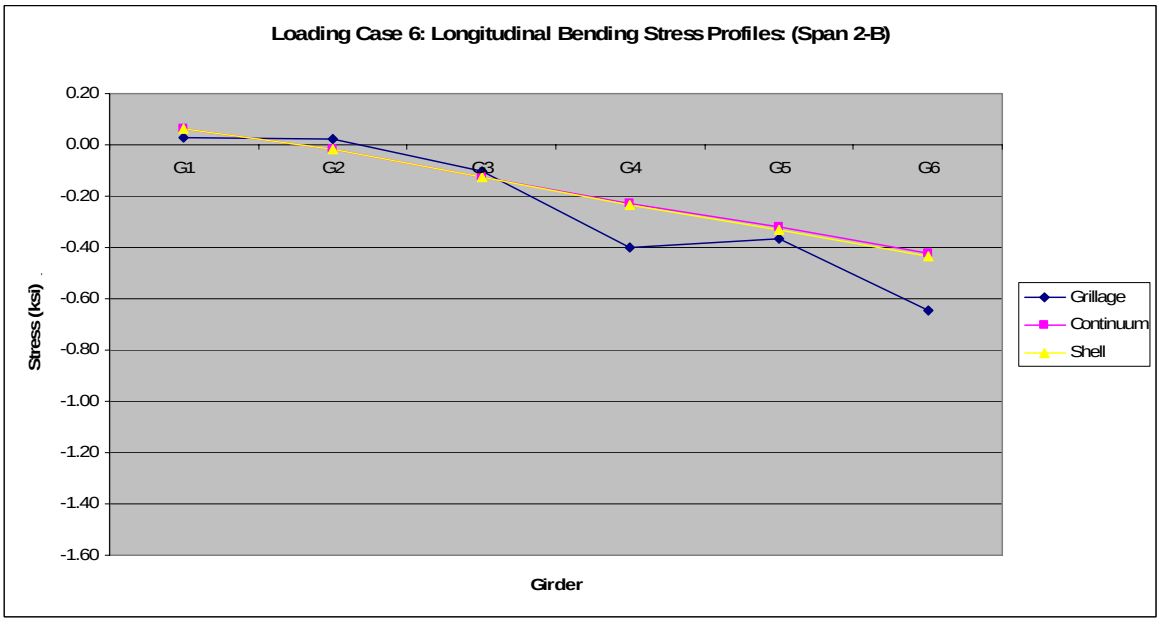

Figure E.29 Loading Case 6: longitudinal bending stress profiles (Span 2-B).

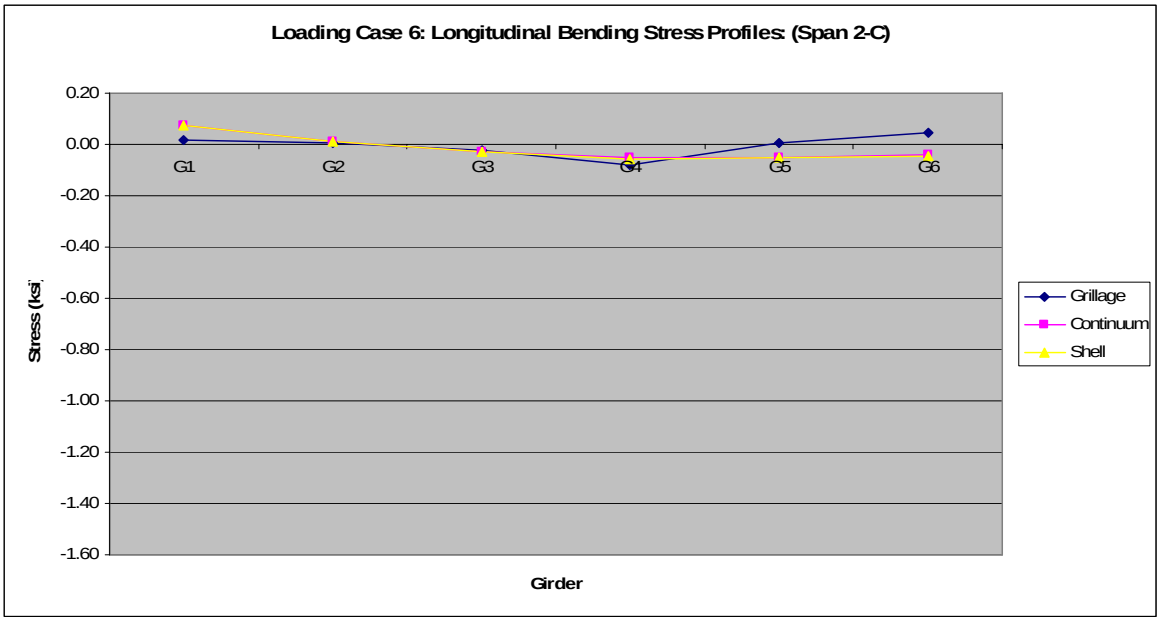

Figure E.30 Loading Case 6: longitudinal bending stress profiles (Span 2-C).

E.6 Loading Case 7

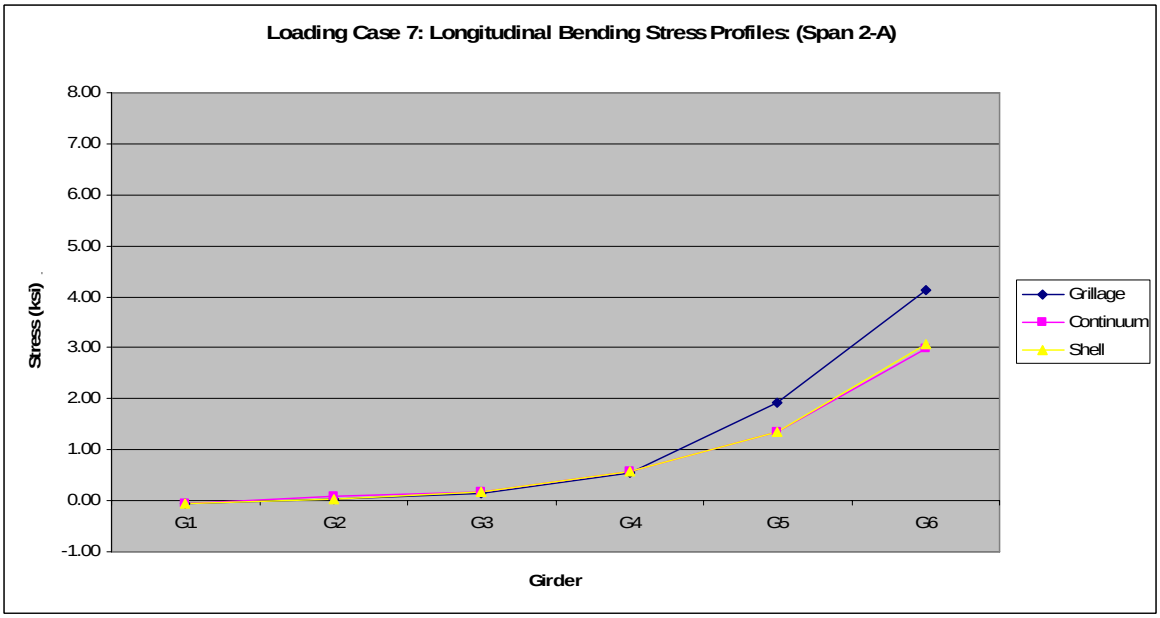

Figure E.31 Loading Case 7: longitudinal bending stress profiles (Span 2-A).

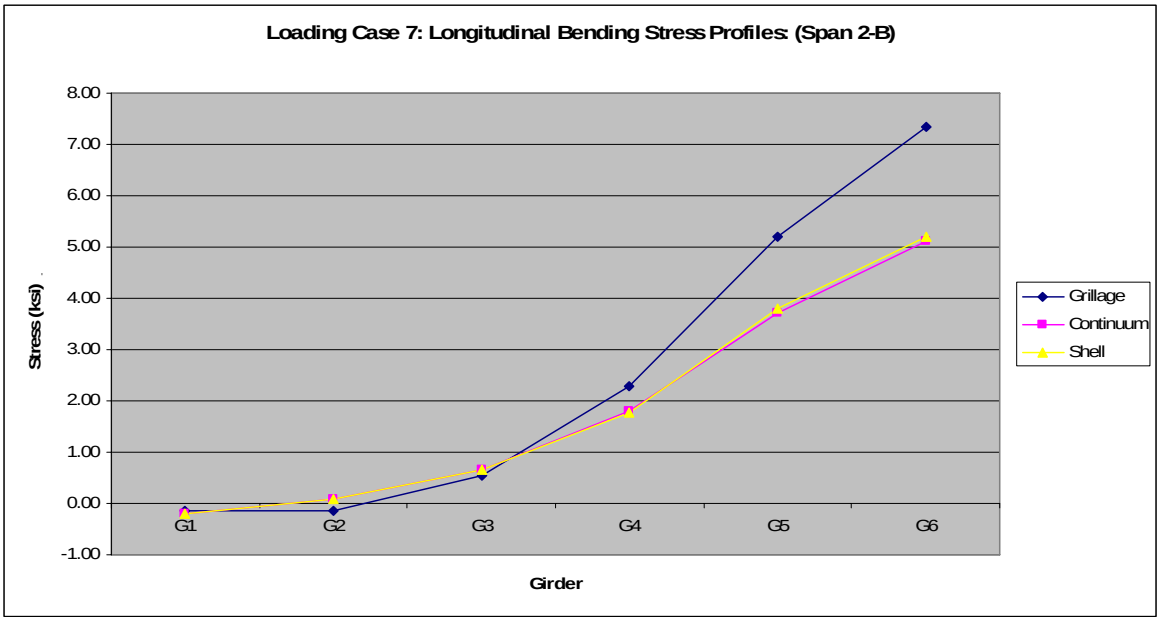

Figure E.32 Loading Case 7: longitudinal bending stress profiles (Span 2-B).

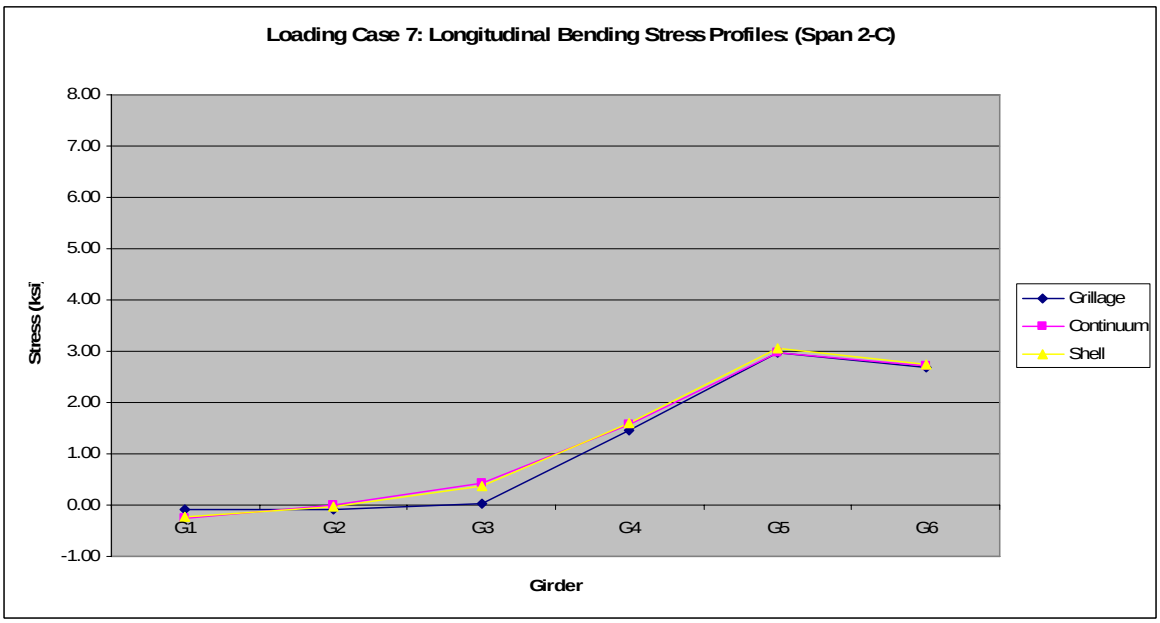

Figure E.33 Loading Case 7: longitudinal bending stress profiles (Span 2-C).

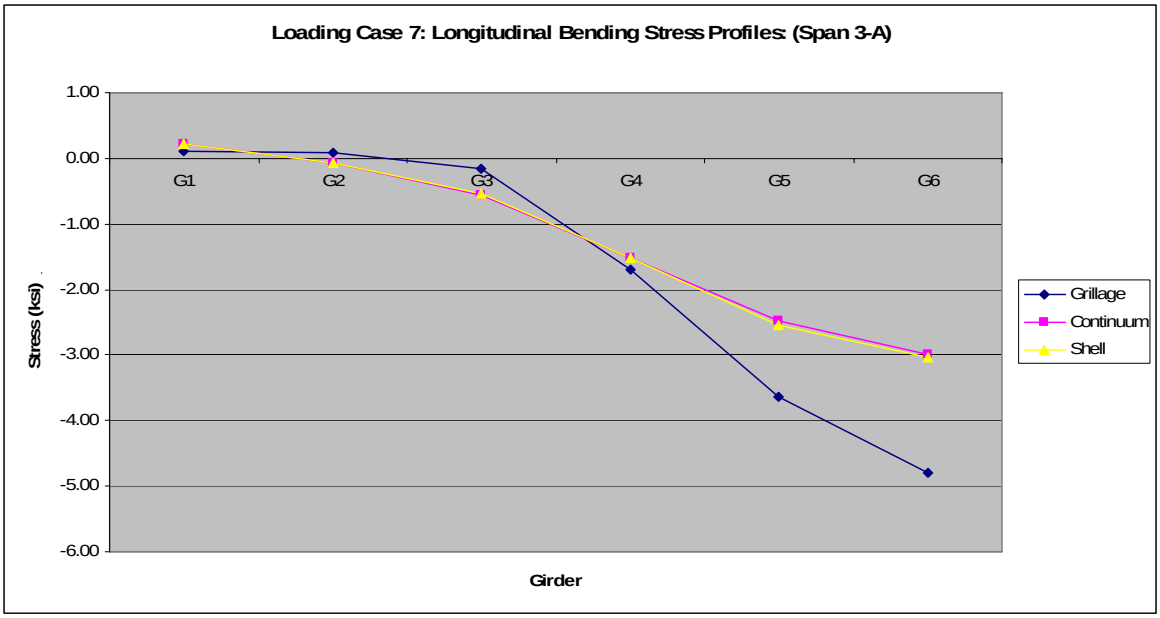

Figure E.34 Loading Case 7: longitudinal bending stress profiles (Span 3-A).

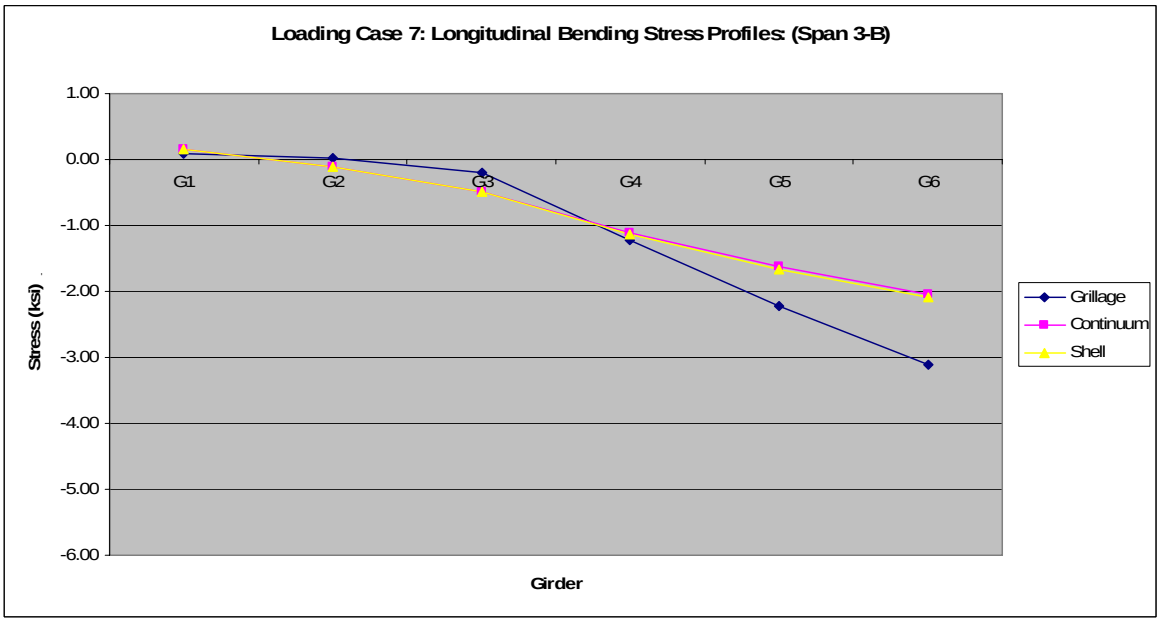

Figure E.35 Loading Case 7: longitudinal bending stress profiles (Span 3-B).

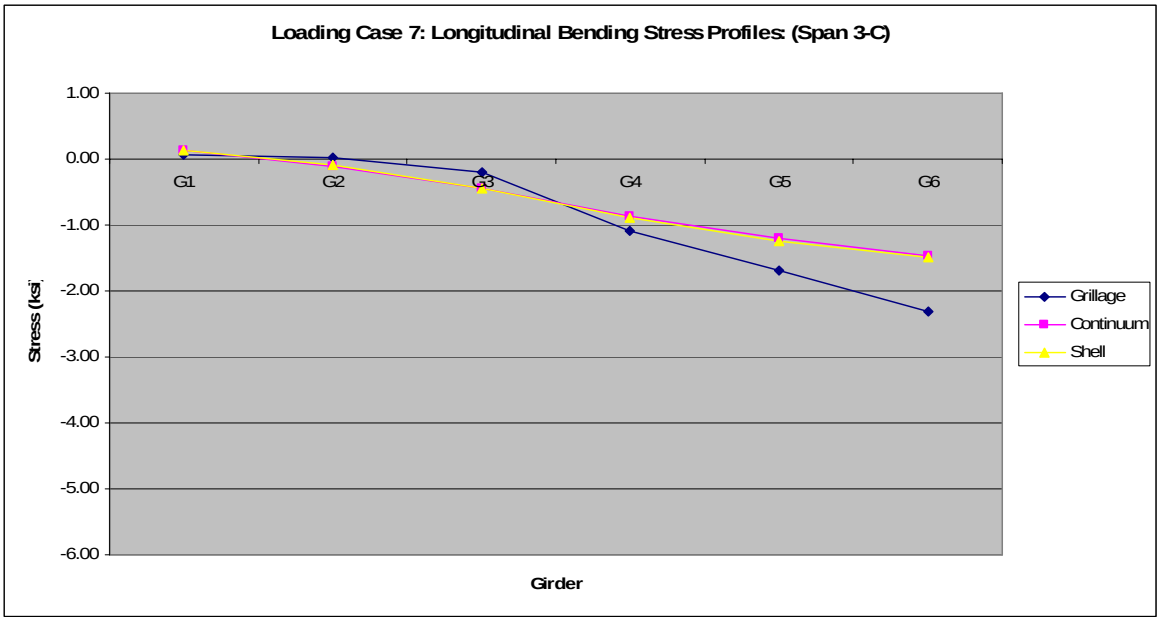

Figure E.36 Loading Case 7: longitudinal bending stress profiles (Span 3-C).

E.7 Loading Case 8

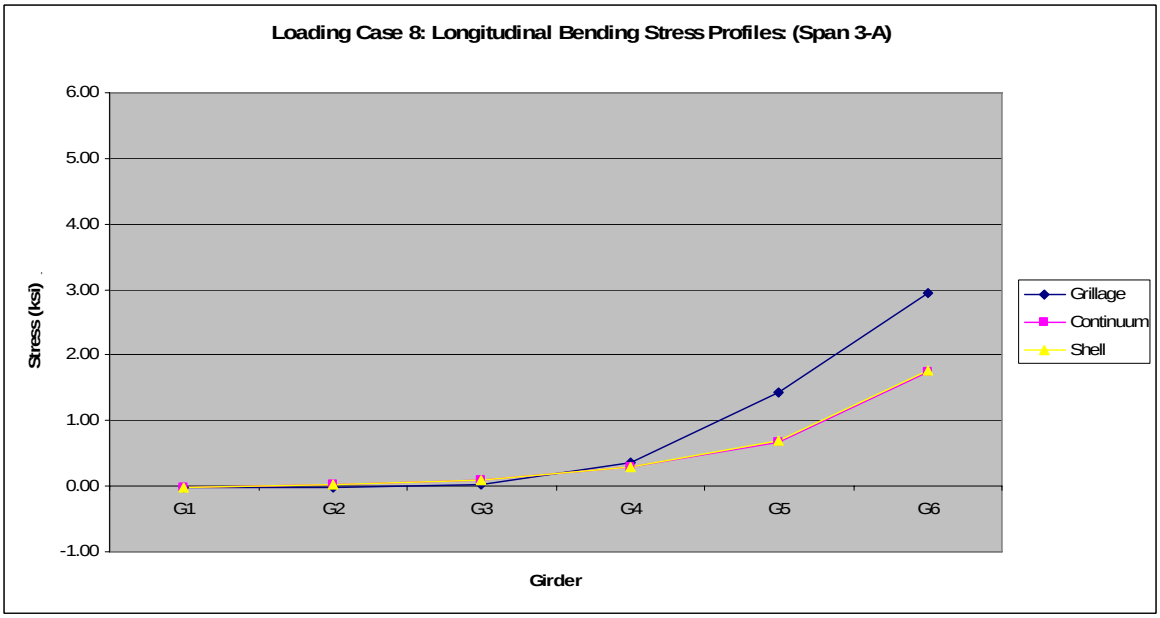

Figure E.37 Loading Case 8: longitudinal bending stress profiles (Span 3-A).

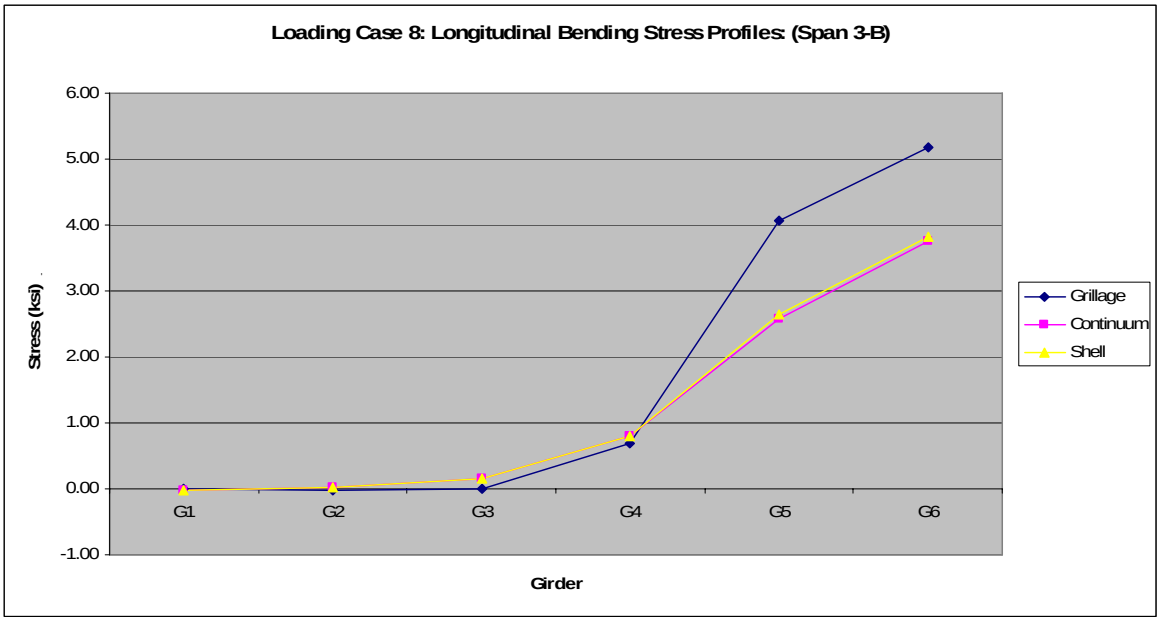

Figure E.38 Loading Case 8: longitudinal bending stress profiles (Span 3-B).

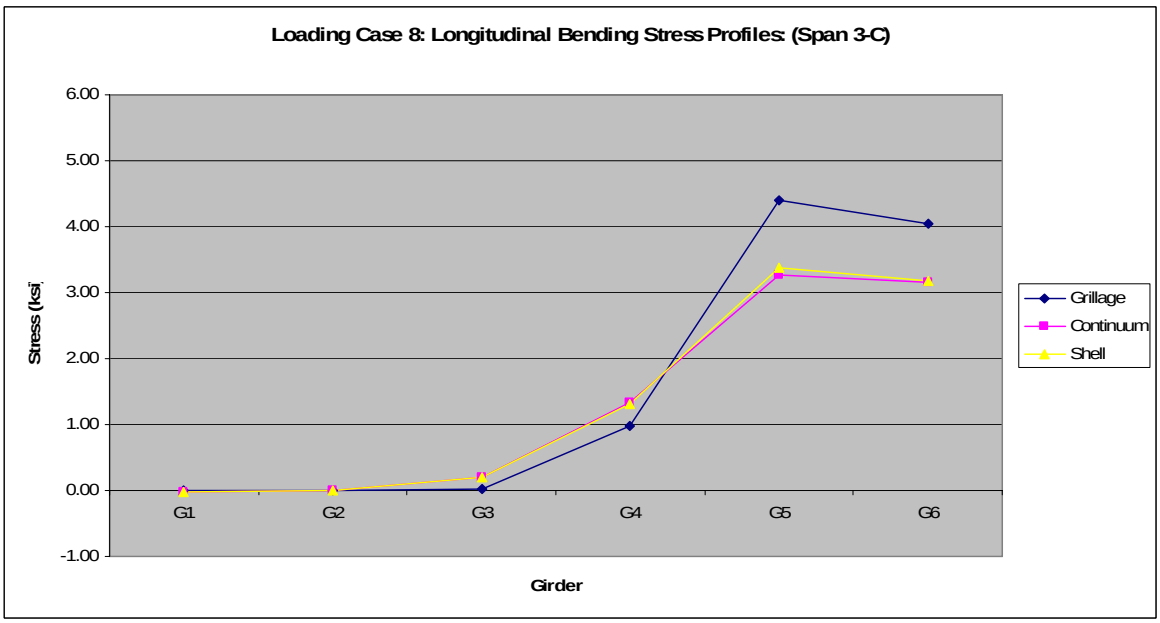

Figure E.39 Loading Case 8: longitudinal bending stress profiles (Span 3-C).

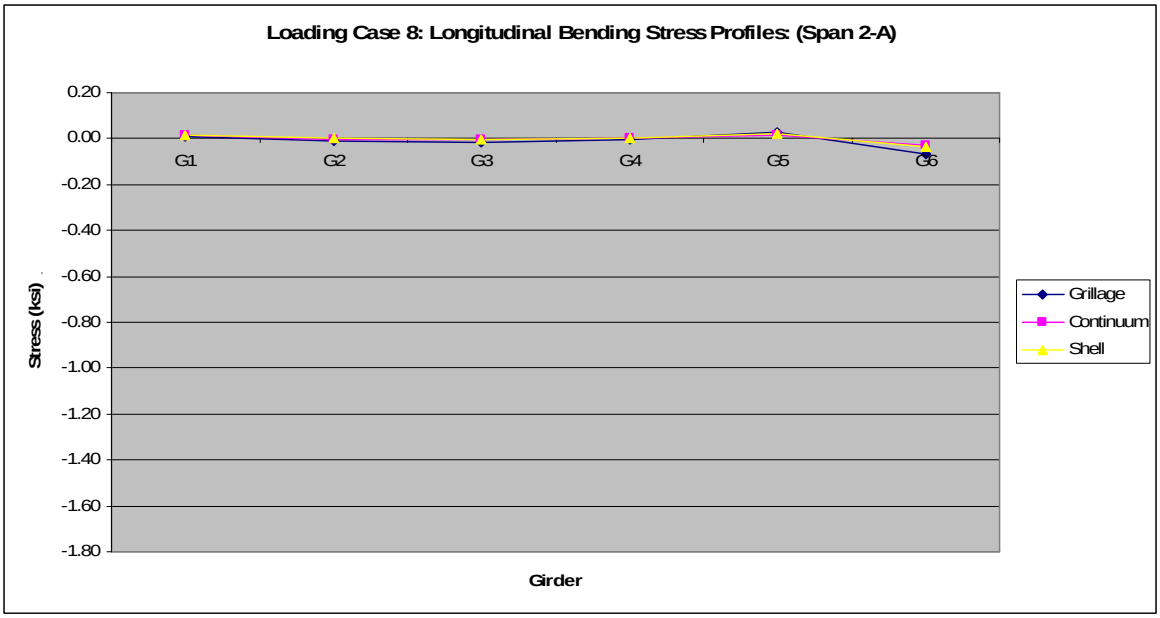

Figure E.40 Loading Case 8: longitudinal bending stress profiles (Span 2-A).

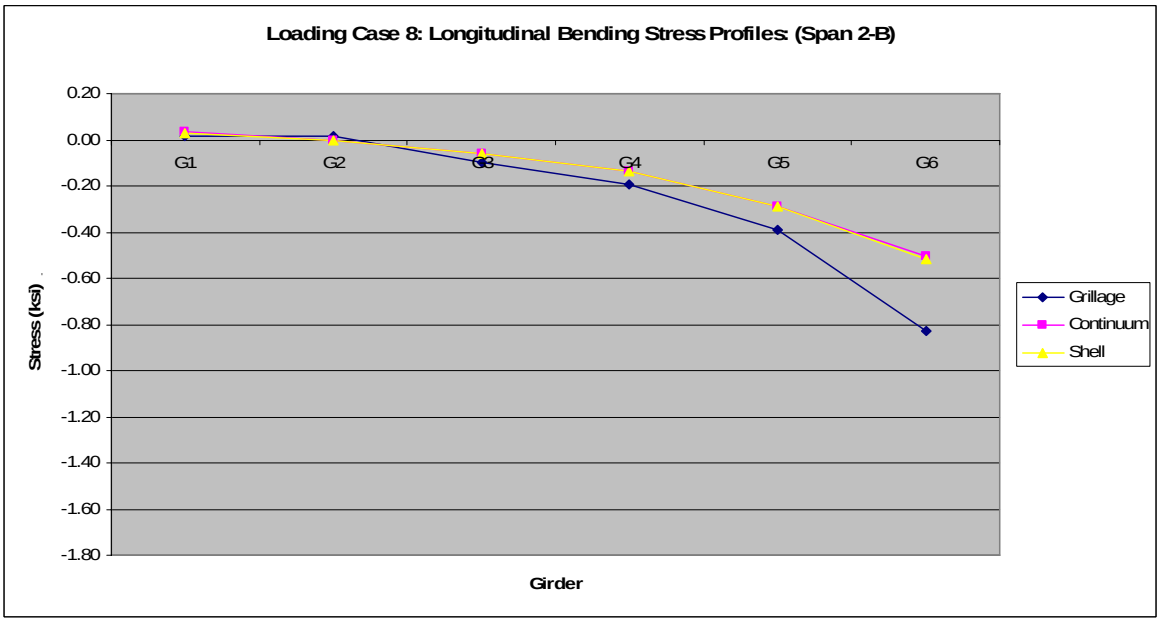

Figure E.41 Loading Case 8: longitudinal bending stress profiles (Span 2-B).

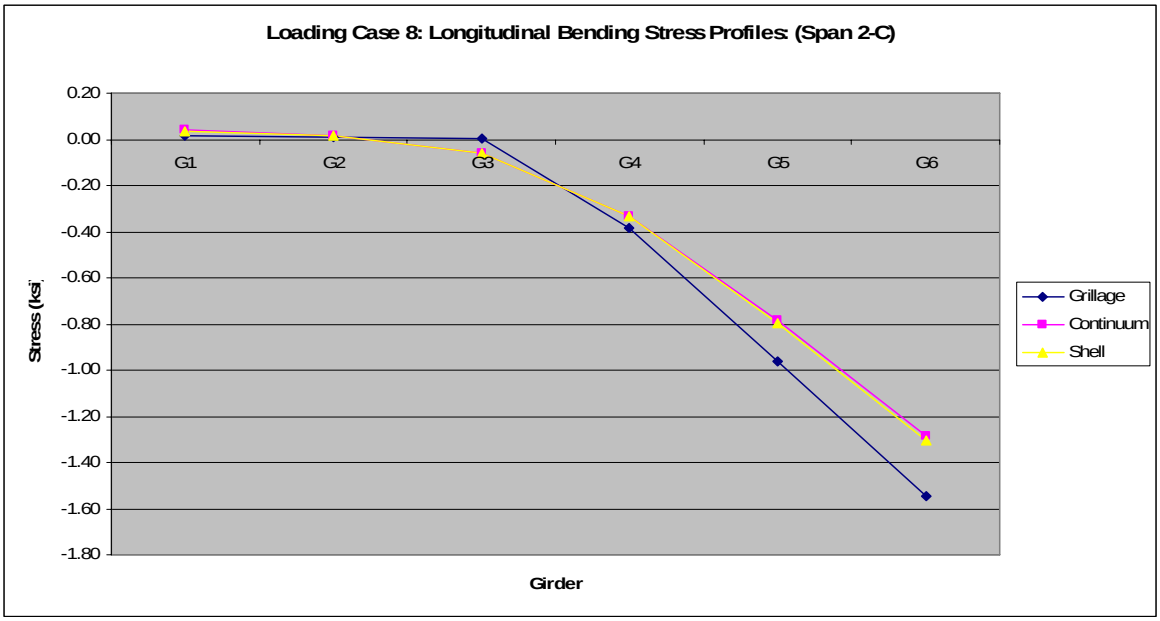

Figure E.42 Loading Case 8: longitudinal bending stress profiles (Span 2-C).

E.8 Loading Case 12

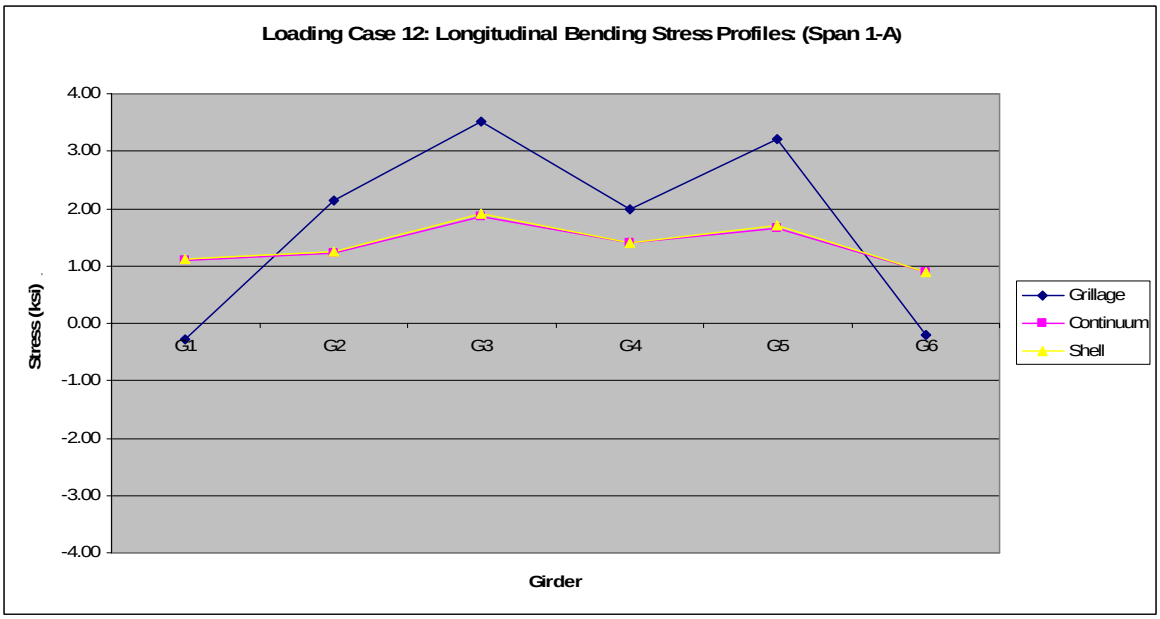

Figure E.43 Loading Case 12: longitudinal bending stress profiles (Span 1-A).

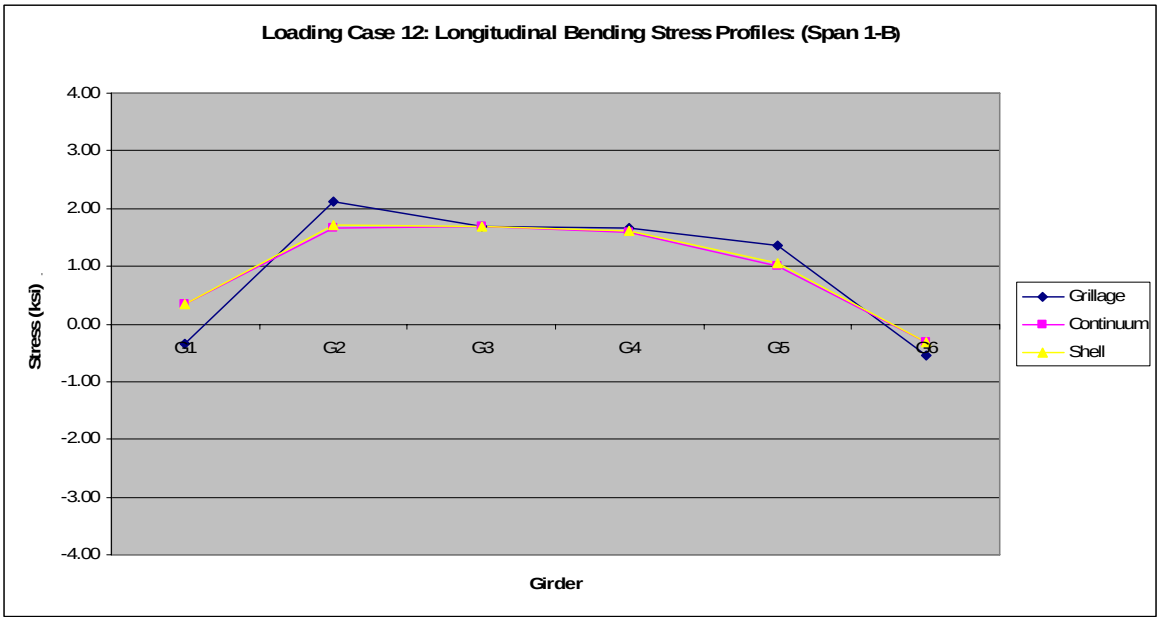

Figure E.44 Loading Case 12: longitudinal bending stress profiles (Span 1-B).

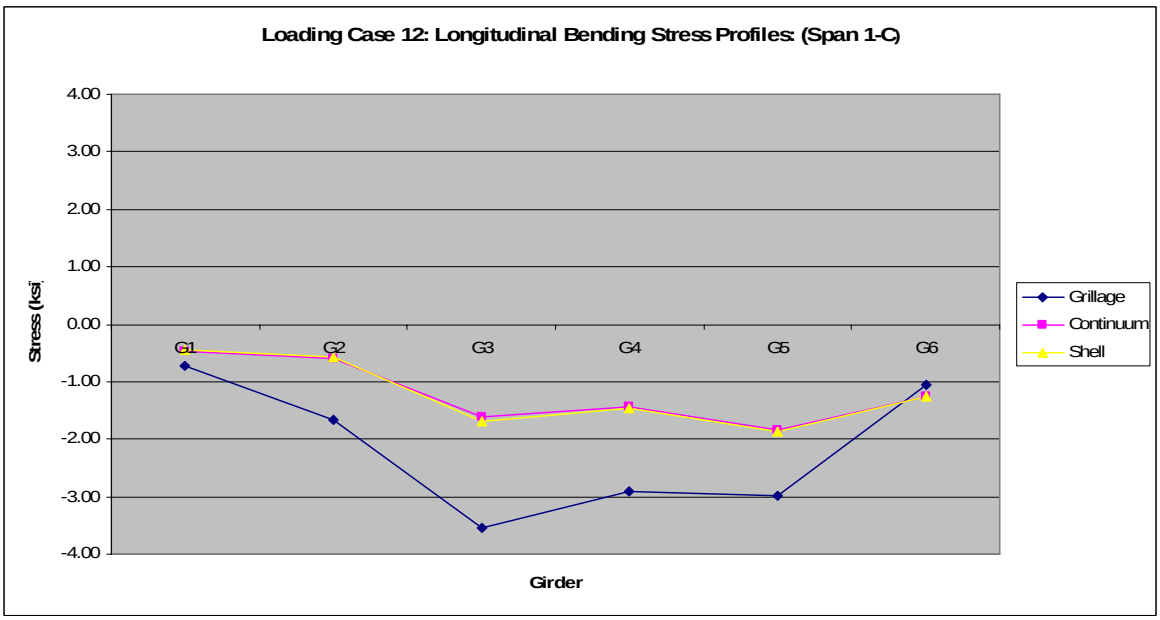

Figure E.45 Loading Case 12: longitudinal bending stress profiles (Span 1-C).

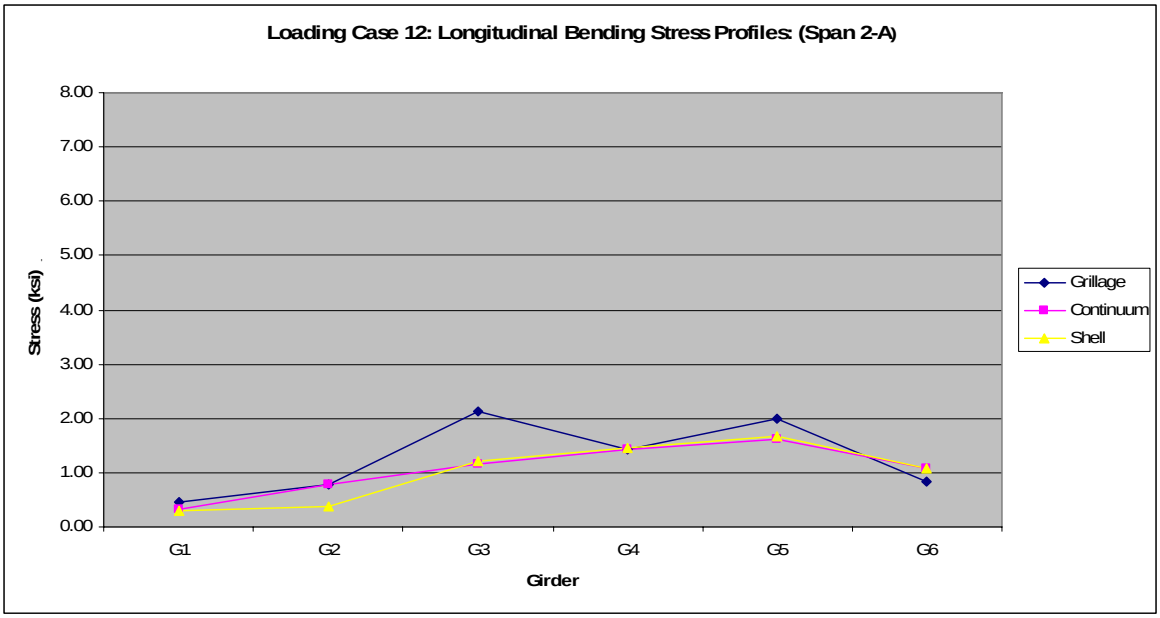

Figure E.46 Loading Case 12: longitudinal bending stress profiles (Span 2-A).

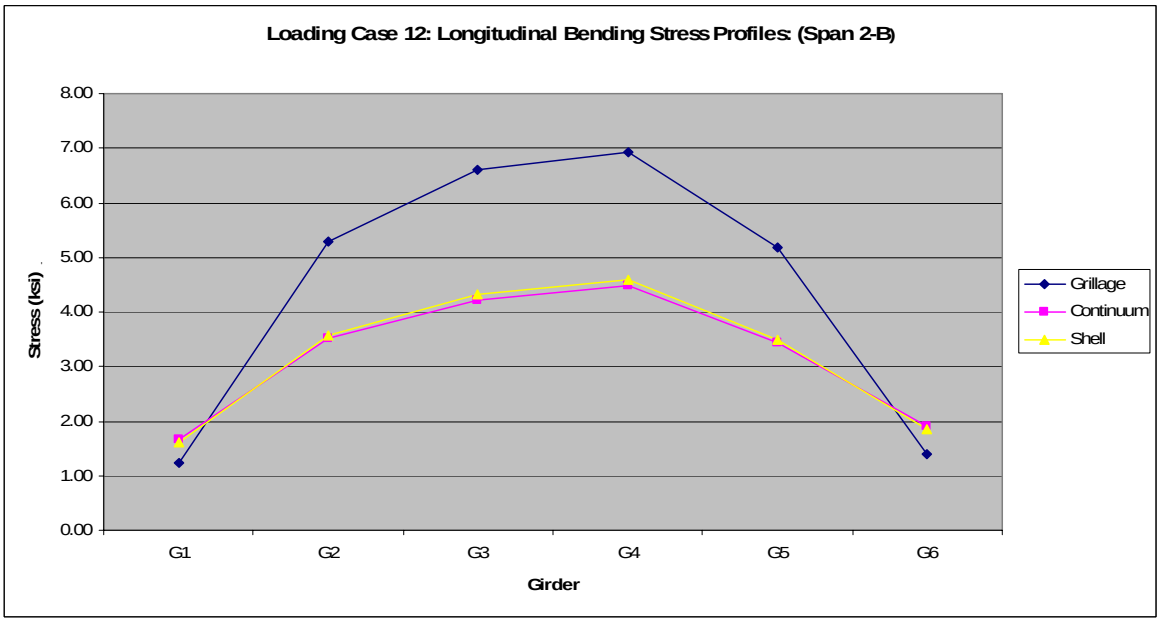

Figure E.47 Loading Case 12: longitudinal bending stress profiles (Span 2-B).

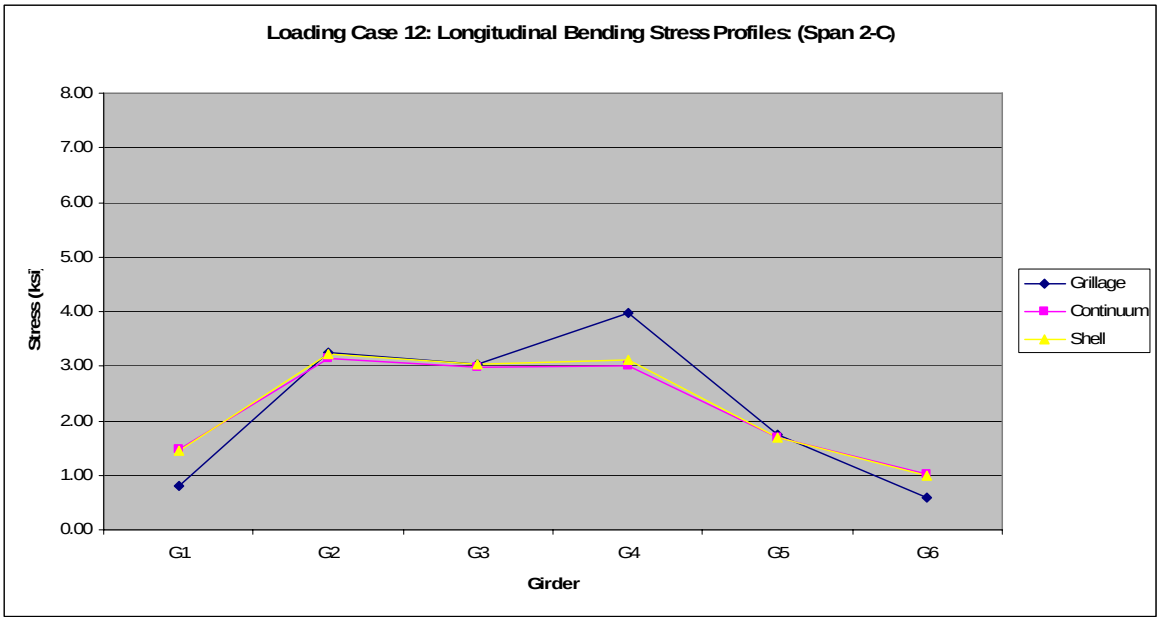

Figure E.48 Loading Case 12: longitudinal bending stress profiles (Span 2-C).

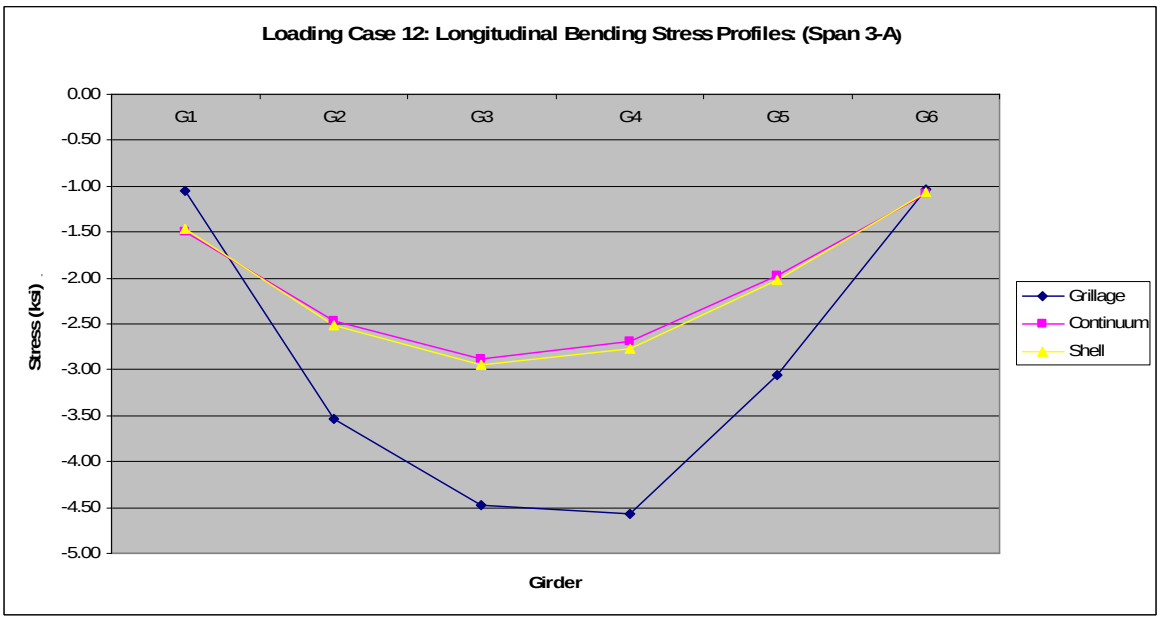

Figure E.49 Loading Case 12: longitudinal bending stress profiles (Span 2-A).

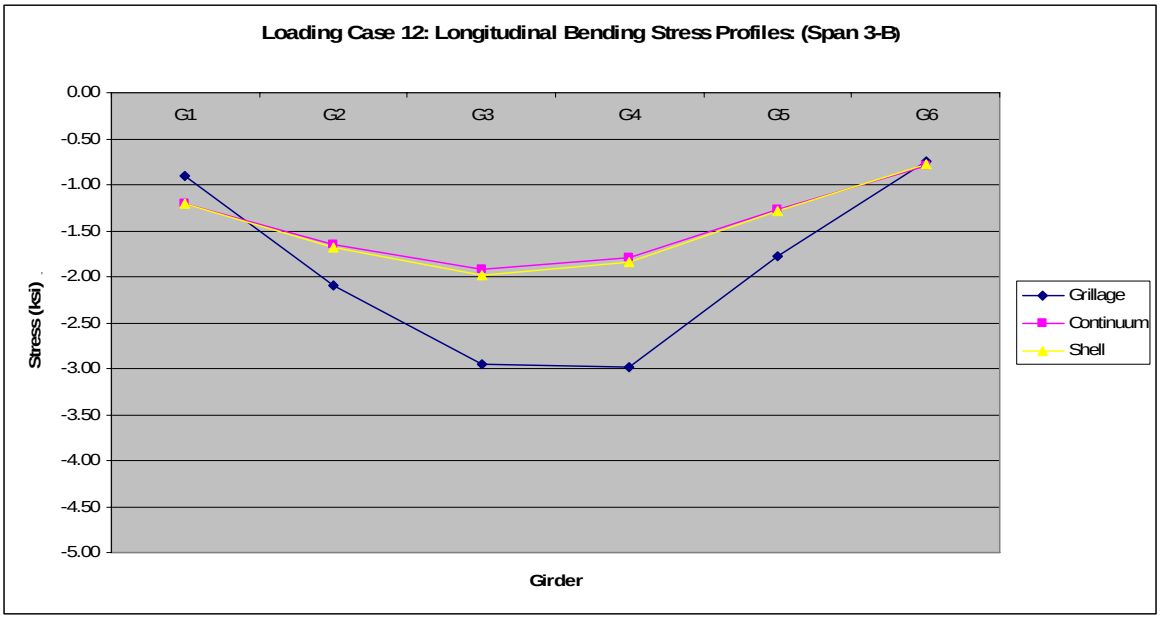

Figure E.50 Loading Case 12: longitudinal bending stress profiles (Span 3-B).

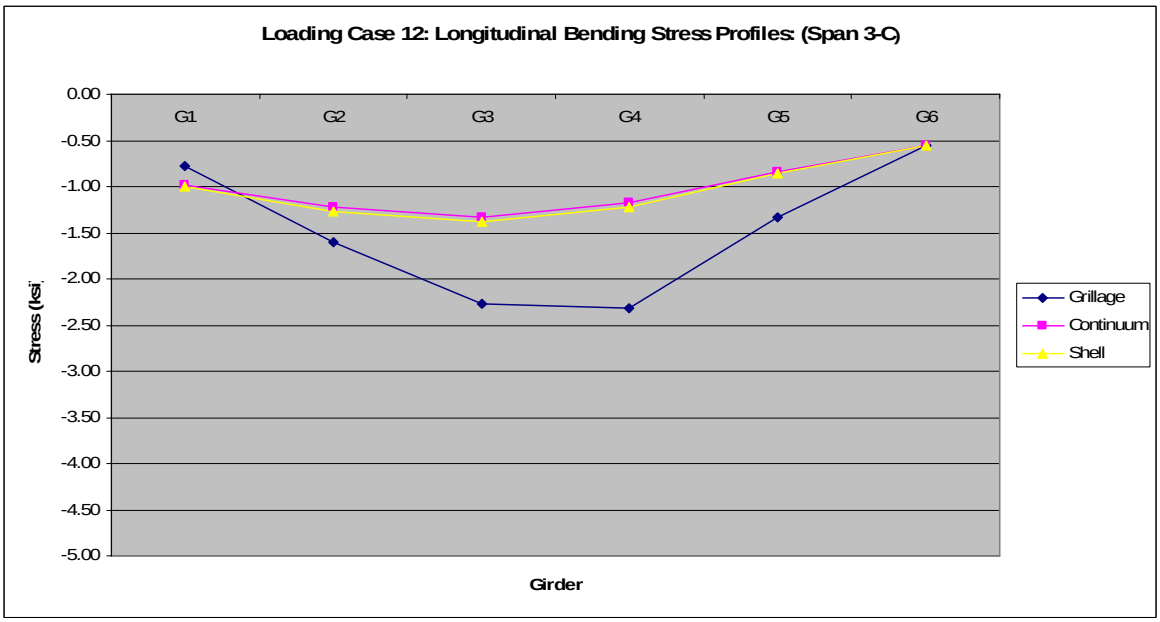

Figure E.51 Loading Case 12: longitudinal bending stress profiles (Span 3-C).

APPENDIX F

SAMPLE INPUT FILES

Tables given below represent lines of code which can be employed in the creation of the underlying geometry for a finite element model in ADINA. In a number of cases, a given function may occur on multiple items (e.g. applying a finite element mesh to multiple volumes). In ADINA, functions which allow this employ the ampersand followed by "CLEAR" (i.e. "@CLEAR") to signal the beginning of a list. Subsequently, a concluding ampersand finishes the list. An example of this is given in Table 6.1; future tables will only show the ampersand designations. It is noted throughout that the universal character for ending a command in ADINA is the asterisk.

Following are a number of commands with the associated syntaxes; when it is that the command syntax is particularly convoluted, parameters which were most commonly modified in these commands will be indicated in red. It will be worthwhile for the reader to modify the values given in order to better understand the function of the individual parameters within the command.

Table F.1 Line construction syntax; specifying endpoints.

```
LINE STRAIGHT NAME=1 P1=1 P2=2
*
LINE STRAIGHT NAME=2 P1=2 P2=3
*
LINE STRAIGHT NAME=3 P1=3 P2=4
*
.
.
.
LINE STRAIGHT NAME=17 P1=17 P2=18
*
LINE STRAIGHT NAME=18 P1=18 P2=19
*
LINE STRAIGHT NAME=19 P1=19 P2=20
*
LINE COMBINED NAME=20 COUPLED=YES RESTRICT=YES
@CLEAR
1
2
3
.
.
.
17
18
19
@
*
```

Table F.2 Line construction syntax; specifying starting point and vector path for extrusion (i.e. dx, dy, and dz).

```
LINE EXTRUDED NAME=1 POINT=1 DX=1.00000000000,
    DY=2.00000000000000 DZ=3.00000000000000 SYSTEM=0 PCOINCID=YES,
    PTOLERAN=1.00000000000000E-05
@CLEAR
@
*
```

Table F.3 Surface construction syntax; specifying points to define corners.

```
SURFACE VERTEX NAME=1 P1=1 P2=2 P3=3 P4=4
*
```

Table F.4 Surface construction syntax; specifying lines to define edges.

```
SURFACE PATCH NAME=1 EDGE1=1 EDGE2=2 EDGE3=3 EDGE4=4
*
```

Table F.5 Surface construction syntax; specifying starting line and vector path for extrusion (i.e. dx, dy, and dz).

```
SURFACE EXTRUDED NAME=1 LINE=1 DX=1.00000000000000,
    DY=2.00000000000000 DZ=3.00000000000000, SYSTEM=0 PCOINCID=YES,
    PTOLERAN=1.00000000000000E-05 NDIV=1 OPTION=VECTOR
@CLEAR
@
*
```

Table F.6 Volume construction syntax; specifying line for extrusion (i.e. the “extrusion line”).

```
VOLUME EXTRUDED NAME=1 SURFACE=1 PCOINCID=YES,
    PTOLERAN=1.00000000000000E-05 OPTION=LINE LINE=1
@CLEAR
@
*
```

Table F.7 Syntax to define point-to-point transformation (i.e. “Copy and Paste”).

```
TRANSFORMATI TRANSLATION NAME=1 MODE=POINTS P1=1 P2=2
*
```

Table F.8 Syntax to “Copy and Paste” lines and surfaces; specifying point-to-point transformation.

```
LINE TRANSFORMED NAME=2 PARENT=1 TRANSFOR=1 PCOINCID=NO,
    PTOLERAN=1.00000000000000E-05 COUPLED=YES NCOPY=1
@CLEAR
@
*
SURFACE TRANSFORMED NAME=2 PARENT=1 TRANSFOR=1 PCOINCID=NO,
    PTOLERAN=1.00000000000000E-05 COUPLED=YES NCOPY=1
@CLEAR
@
*
```

Table F.9 Syntax for line, surface, and volume subdivision; specifying element edge length.

```
SUBDIVIDE LINE NAME=1 MODE=LENGTH SIZE=1.00000000000000
@CLEAR
@
*
SUBDIVIDE SURFACE NAME=1 MODE=LENGTH SIZE=1.00000000000000
@CLEAR
@
*
SUBDIVIDE VOLUME NAME=1 MODE=LENGTH SIZE=1.00000000000000
@CLEAR
@
*
```

Table F.10 Syntax for line, surface, and volume subdivision; specifying number of elements per geometric entity.

```
SUBDIVIDE LINE NAME=1 MODE=DIVISIONS NDIV=10 RATIO=1.00000000000000,
    PROGRESS=ARITHMETIC CBIAS=NO
@CLEAR
@
*
SUBDIVIDE SURFACE NAME=1 MODE=DIVISIONS NDIV1=10 NDIV2=10,
    RATIO1=1.00000000000000 RATIO2=1.00000000000000,
    PROGRESS=GEOMETRIC EXTEND=NONE CBIAS1=NO CBIAS2=NO
@CLEAR
@
*
SUBDIVIDE VOLUME NAME=1 MODE=DIVISIONS NDIV1=10 NDIV2=10 NDIV3=10,
    RATIO1=1.00000000000000 RATIO2=1.00000000000000,
    RATIO3=1.00000000000000 PROGRESS=GEOMETRIC EXTEND=NONE CBIAS1=NO,
    CBIAS2=NO CBIAS3=NO
@CLEAR
@
*
```

Table F.11 Syntax to construct point-to-point (i.e. node-to-node) rigid link.

```
RIGIDLINK NAME=1 SLAVETYP=POINT SLAVENAM=2 MASTERTY=POINT,
    MASTERNA=1 DISPLACE=DEFAULT OPTION=0 SLAVEBOD=0 MASTERBO=0,
    DOF=ALL
@CLEAR
@
*
```

Table F.12 Syntax to construct surface-to-surface rigid link.

```
RIGIDLINK NAME=1 SLAVETYP=SURFACE SLAVENAM=2 MASTERTY=SURFACE,
    MASTERNA=1 DISPLACE=DEFAULT OPTION=1 SLAVEBOD=0 MASTERBO=0,
    DOF=ALL
@CLEAR
@
*
```

Table F.13 Syntax to define truss "finite element group."

```
EGROUP TRUSS NAME=2 SUBTYPE=GENERAL DISPLACE=DEFAULT MATERIAL=1,
    INT=DEFAULT GAPS=NO INITIALS=BOTH CMASS=DEFAULT,
    TIME-OFF=0.00000000000000 OPTION=REBAR RB-LINE=2 DESCRIPT='NONE'
*
```

Table F.14 Syntax to define beam "finite element group."

```
EGROUP BEAM NAME=1 SUBTYPE=THREE-D DISPLACE=DEFAULT MATERIAL=1
RINT=5,
    SINT=DEFAULT TINT=DEFAULT RESULTS=STRESSES INITIALS=NONE,
    CMASS=DEFAULT RIGIDEND=NONE MOMENT-C=NO RIGIDITY=1,
    MULTIPLY=1000000.00000000 RUPTURE=ADINA OPTION=NONE,
    BOLT-TOL=0.0100000000000000 DESCRIPT='NONE'
*
```

Table F.15 Syntax to define shell "finite element group."

```
EGROUP SHELL NAME=1 DISPLACE=DEFAULT MATERIAL=1 RINT=DEFAULT,
    SINT=DEFAULT TINT=2 RESULTS=STRESSES STRESSRE=GLOBAL PRINTVEC=0,
    NLAYERS=1 INITIALS=NONE FAILURE=0 SECTION=0 CMASS=DEFAULT,
    STRAINS=DEFAULT RUPTURE=ADINA TIME-OFF=0.00000000000000,
    OPTION=NONE DESCRIPT='NONE'
*
```

Table F.16 Syntax to define 3-D solid (i.e. continuum) “finite element group.”

```
EGROUP THREEDSOLID NAME=1 DISPLACE=DEFAULT STRAINS=DEFAULT
MATERIAL=1,
   RSINT=DEFAULT TINT=DEFAULT RESULTS=STRESSES DEGEN=NO
FORMULAT=0,
   STRESSRE=GLOBAL INITIALS=NONE FRACTUR=NO CMASS=DEFAULT,
   STRAIN-F=0 UL-FORMU=DEFAULT LVUS1=0 LVUS2=0 SED=NO
RUPTURE=ADINA,
   INCOMPAT=DEFAULT TIME-OFF=0.00000000000000 POROUS=NO,
   WTMC=1.00000000000000 OPTION=NONE DESCRIPT='NONE'
*
```

Table F.17 Syntax to generate 2-node truss finite elements on lines (“GROUP=1” in this case is a truss “finite element group”).

```
GLINE NODES=2 NCOINCID=ENDS NCENDS=12 NCTOLERA=1.00000000000000E-05,
    SUBSTRUC=0 GROUP=1 MIDNODES=CURVED
@CLEAR
@
*
```

Table F.18 Syntax to generate 2-node beam finite elements on lines (“GROUP=1” in this case is a beam “finite element group”).

```
GLINE NODES=2 AUXPOINT=1 NCOINCID=ALL,
   NCTOLERA=1.00000000000000E-05 SUBSTRUC=0 GROUP=1 MIDNODES=CURVED
@CLEAR
@
*
```

Table F.19 Syntax to generate MITC4 shell finite elements on surfaces ("GROUP=1" in this case is a shell "finite element group").

```
GSURFACE NODES=4 PATTERN=AUTOMATIC NCOINCID=ALL,
   NCTOLERA=1.00000000000000E-05 SUBSTRUC=0 GROUP=1,
   PREFSHAP=AUTOMATIC MESHING=MAPPED SMOOTHIN=NO DEGENERA=NO,
   COLLAPSE=NO MIDNODES=CURVED METHOD=ADVFRONT FLIP=NO
@CLEAR
```

Table F.20 Syntax to generate 8-node continuum finite elements within volumes ("GROUP=1" in this case is a 3-D solid "finite element group").

```
GVOLUME NODES=8 PATTERN=0 NCOINCID=ALL NCTOLERA=1.00000000000000E-
05,
   SUBSTRUC=0 GROUP=1 MESHING=MAPPED PREFSHAP=AUTOMATIC,
   DEGENERA=YES COLLAPSE=NO MIDNODES=CURVED METHOD=DELAUNAY,
   BOUNDARY=ADVFRONT
@CLEAR
```

BIBLIOGRAPHY

ADINA Research and Development. ADINA Theory and Modeling Guide, Volume I: ADINA, Report ARD 03-7. Watertown, Massachusetts: ADINA Research and Development, Inc., 2003.

American Association of State Highway and Transportation Officials (AASHTO), AASHTO LRFD Bridge Design Specifications, U.S. Customary Units. 3rd ed. Washington, D.C.: AASHTO, 2004.

American Concrete Institute (ACI), Building Code Requirements for Structural Concrete (ACI 318-02) and Commentary (ACI 318R-02), An ACI Standard. 2002 ed. Farmington Hills, Michigan: ACI, 2002.

American Institute of Steel Construction (AISC), Manual of Steel Construction: Load and Resistance Factor Design. 3rd ed. Chicago, Illinois: AISC, 2001.

Bathe, K.-J. Finite Element Procedures. Englewood Cliffs, New Jersey: Prentice Hall, 1996.

Bathe, K.-J., and E.N. Dvorkin. "On the Automated Solution of Nonlinear Finite Element Equations." *Computers & Structures*, Volume 17 (1983): 871-79.

Bathe, K.-J., J. Walczak, A. Welch, and N. Mistry. "Nonlinear Analysis of Concrete Structures." *Computers & Structures*, Volume 32 (1989): 563-90.

Chang, C.-J., D.W. White, F. Beshah, and W. Wright. "Design Analysis of Curved I-Girder Bridge Systems – An Assessment of Modeling Strategies." *Proceedings of the Structural Stability Research Council, 2005 Annual Stability Conference*, Montreal, Quebec, April 6-9, 2005. Rolla, Missouri: Structural Stability Research Council, 2005. 349-69.

Felippa, C.A. Introduction to Finite Element Methods. Boulder, Colorado: Aerospace Engineering Sciences Department, University of Colorado, 2004.

Hambly, E.C. Bridge Deck Behaviour. 2nd ed. London, England: E & FN Spon, 1991.

Jaeger, L.G., B. Bakht. "The grillage analogy in bridge analysis." *Canadian Journal of Civil Engineering*, Volume 9 (1982): 224-235.

Kostem, C.N. “Approximations and Errors in the Grillage Analysis of Multibeam Bridges.” *Proceedings of the 3rd Annual International Bridge Conference*, Pittsburgh, Pennsylvania, June 2-4, 1986. Pittsburgh, Pennsylvania: Engineers’ Society of Western Pennsylvania, 1986. 214-18.

Kostem, C.N. “Finite Element Analysis of Highway Bridges.” Proceedings of the 1st International Bridge Conference, Pittsburgh, Pennsylvania, June 4-6, 1984. Pittsburgh, Pennsylvania: Engineers’ Society of Western Pennsylvania, 1984. 239-46.

Kostem, C.N., S.C. Ragazzo. "Grillage Analogy for Multigirder Bridges." *Proceedings of the Fifth International Conference on Computing in Civil and Building Engineering*, Anaheim, CA, 7-9 June 1993. New York, New York: American Society of Civil Engineers, 1993. 188-92.

Logan, D.L. A First Course in the Finite Element Method. 3rd ed. Pacific Grove, California: Brooks/Cole, 2002.

O’Brien, E.J., and D.L. Keogh. Bridge Deck Analysis. London, England: E & FN Spon, 1999.

Panos, P., C.N. Kostem. “Structural Response of Simple Span Bridges to Nonstandard Vehicles.” *Proceedings of the 2nd Annual International Bridge Conference*, Pittsburgh, Pennsylvania, June 17-19, 1985. Pittsburgh, Pennsylvania: Engineers’ Society of Western Pennsylvania, 1985. 184-88.

Przemieniecki, J.S. Theory of Matrix Structural Analysis. New York, New York: McGraw-Hill Book Company, 1968.

Stull, C.J., C.J. Earls, B. Akinci. “On the strength and stability of slab on steel I-girder bridge systems damaged by truck strikes.” *Proceedings of the Structural Stability Research Council, 2006 Annual Stability Conference*, San Antonio, Texas, February 8-11, 2006. Rolla, Missouri: Structural Stability Research Council, 2005. 57-72.